

A Structural Database for Pharmaceutical Salt Selection

A thesis presented for the degree of
Doctor of Philosophy
in the Faculty of Science
of the University of Strathclyde

by

Gary James Miller

Strathclyde Institute of Pharmacy and Biomedical Sciences
University of Strathclyde
Glasgow

June 2010

This thesis is the result of the author's original research. It has been composed by the author and has not been previously submitted for an examination that has led to the award of a degree.

The copyright of this thesis belongs to the author under the terms of the United Kingdom Copyright Acts as qualified by University of Strathclyde Regulation 3.49. Due acknowledgement must always be made of the use of any material contained in, or derived from, this thesis.

Signed:

Date:

Abstract

Salt formation is an important technique used in preclinical pharmaceutical development to modulate and optimise the physicochemical properties of a drug molecule containing an ionisable functional group. The current approach to salt selection relies on semi-empirical screening of the pharmaceutical molecule in combination with different counterions for the formation of a crystalline salt. This approach is necessitated by the limited understanding of the relationships between molecular and supramolecular structure and properties and the stoichiometry and ionisation state of the resultant crystalline solid.

Presented in this work is a structural database containing 110 novel multi-component crystalline systems produced by the co-crystallisation of a library of pharmaceutically acceptable organic acid counterions with basic molecules that model the functional groups found on pharmaceutically active molecules. The structures were characterised by single crystal X-ray diffraction and their hydrogen bond interactions and molecular packing arrangements were examined using Mercury and XPac.

This enabled the identification of robust hydrogen bonded synthons and supramolecular constructs for salts of secondary or tertiary amine bases in combination with different types of counterion. These observations were correlated to the molecular structures of the salt formers and a series of “*salt selection rules*” that can be potentially used to guide counterion selection for a novel pharmaceutical molecule were established. The applicability of these rules was assessed by the crystallisation of a validation set of 29 novel fluoroquinolone structures.

Variable-temperature X-ray powder diffraction and structure determination from powder diffraction data were employed to generate four novel anhydrous salts from their corresponding hydrates. Comparison of the hydrogen bond interactions and molecular packing arrangements allowed the examination of the structural role of water in determining and stabilising the supramolecular structures of the hydrated systems.

Acknowledgements

My principal thanks go to my supervisors, Professor Alastair Florence and Dr Alan Kennedy, for their support and guidance throughout my studies. Their help and encouragement has been invaluable in making the last four years an enjoyable and educational experience and I consider myself fortunate to have been given the opportunity to work with them.

I also thank my industrial supervisors, Dr Caroline Roger and Dr James McCabe of AstraZeneca PAR&D Macclesfield for their help during my visit to their site and their input into this project.

I had the pleasure of working in two supportive and friendly research groups and their assistance and companionship was very much appreciated. Particular thanks go to Andrea Johnston, Jean-Baptiste Arlin, Julie Bardin, Philippe Fernandes, Ryan Taylor and Scott McKellar of the Solid State Research Group and Dr John Reglinski, Dr Mark Spicer, Dawn Wallace, Katherine Trotter and Paul Duckmanton of the late Royal College R5.20 lab.

The XPac method proved to be an invaluable resource and I thank Professor Michael Hursthouse and Dr Graham Tissard of the University of Southampton and Dr Thomas Gelbrich of the University of Innsbruck for training me in the technique and their help with the interpretation of the results.

Financial support from AstraZeneca and the Strathclyde Institute of Pharmacy and Biomedical Sciences is gratefully acknowledged. So too is the assistance of the EPSRC X-Ray Crystallography Service with data collections and sincere apologies for the quality of many of the samples are hereby offered.

My high school chemistry teacher, Mr Burns, always succeeded in making the subject interesting, understandable and relevant. His enthusiasm inspired me to pursue a further education in science and for this he has my sincere gratitude.

Finally, I would like to thank my family and friends for their constant support, encouragement and, above all, for their understanding over the last four years.

Table of Contents

Abstract	I
Acknowledgements	II
Table of Contents	III
List of Figures	VIII
List of Tables	XI
Abbreviations	XIV

1 Introduction

1.1	Background	1
1.2	Salt formation in pharmaceutical development	3
1.2.1	Counterion selection	3
1.2.2	Effect on physicochemical properties	5
1.2.3	Current approach to salt selection	6
1.3	The organic solid state	8
1.3.1	Binary systems- salts, cocrystals and solvates	9
1.3.2	Hydrates	9
1.3.2.1	Hydrate formation	9
1.3.2.2	Classification of hydrates	10
1.3.2.3	Structural consequences of salt hydration	11
1.3.2.4	Effect of hydration on aqueous solubility	11
1.3.2.5	Effect of hydration on dissolution rate	13
1.4	Supramolecular chemistry	16
1.4.1	Crystallisation	16
1.4.2	Intermolecular interactions	16
1.4.2.1	Hydrogen bonding	17
1.4.2.2	Etter's Rules	19
1.4.3	Dispersion and repulsion energies	19
1.4.3.1	Kitaigorodskii's Close Packing and Aufbau Principles	20
1.4.3.2	Application of KAP to crystal structure analysis	21
1.4.4	Other anisotropic interactions	22
1.5	pKa and ionisation state	23
1.6	Crystal engineering	24
1.6.1	Growth synthons and crystal nucleation	25
1.6.2	Crystal engineering and the design of pharmaceutical cocrystals	26
1.6.3	Issues confronting salt systems	27
1.7	Systematic structural analysis	28
1.7.1	The Cambridge Structural Database System	28
1.7.1.1	Associated software	29
1.7.2	XPac	30
1.7.2.1	Principle of the method	30

1.7.2.2	Case examples	33
1.7.3	Hirshfeld surface analysis: Crystal Explorer	34
1.7.3.1	Application in crystal structure analysis	36
2	Aims and Objectives	
2.1	Aims	37
2.2	Objectives	37
3	Materials and Methods	
3.1	Materials	38
3.2	Synthesis of salts and crystal growth	43
3.2.1	Evaporative crystallisation	43
3.2.2	Crystallisation by slow diffusion	43
3.2.3	Crystallisation of novel pharmaceutical salts	43
3.3	Single-crystal X-ray diffraction	44
3.3.1	University of Strathclyde data collection	44
3.3.2	EPSRC X-ray crystallography service data collections	44
3.3.3	Synchrotron data collection	44
3.4	X-ray powder diffraction (XRPD)	45
3.4.1	Fingerprint analysis	45
3.4.2	Variable temperature X-ray powder diffraction (VT-XRPD)	45
3.5	Thermal analysis	46
3.6	Structure analysis	46
3.6.1	Analysis of hydrogen bonding interactions	46
3.6.1.1	Quantitative analysis of hydrogen bond motif frequencies	46
3.6.1.2	Systematic analysis of hydrogen bond structures	47
3.6.2	XPac analysis	48
4	Structure correlation in salt structures	
4.1	Introduction	54
4.2	Method	56
4.2.1	Sample preparation and data collection	56
4.2.2	Data analysis	58
4.3	Results and discussion	59
4.3.1	Outcomes of crystallisation experiments	59
4.3.2	Salt formation and ΔpK_a	62
4.4	Crystal structure analysis of dicarboxylic acid systems	64
4.4.1	Intermolecular hydrogen bonding interactions	64
4.4.2	Hydrogen bond motifs	67
4.4.2.1	Structures featuring a C1,1(7) chain	71
4.4.2.2	Structures based on the C2,2(12) motif	74
4.4.2.3	Discrete structures	75

4.4.3	Structural rules for dicarboxylic acid counterions	77
4.5	Benzoic acid counterions	78
4.5.1	Intermolecular hydrogen bonds	78
4.5.2	Hydrogen bonded motifs	80
4.5.2.1	Structures based on the C2,2(6) motif	83
4.5.2.2	Structures based on the D1 motif	84
4.5.2.3	Structures based on the R4,4(12) motif	86
4.5.2.4	Solvent-separated structure	86
4.5.3	XPac analysis of the packing arrangements of the benzoate anions	87
4.5.3.1	Structures containing supramolecular construct A	89
4.5.3.2	Structures containing supramolecular construct B	91
4.5.3.3	Structures containing supramolecular construct C	92
4.5.3.4	Structures containing supramolecular construct D	93
4.5.3.5	Structures containing supramolecular construct E	96
4.5.3.6	Structures containing supramolecular construct F	97
4.5.3.7	Relationship between hydrogen bonding and supramolecular constructs	98
4.5.4	Structural rules for benzoic acid counterions	100
4.6	Sulfonic acid structures	101
4.6.1	Intermolecular hydrogen bonds	101
4.6.2	Hydrogen bonding motifs	102
4.6.2.1	Structures based on the C2,2(6) motif	105
4.6.2.2	Structures based on other motifs	106
4.6.2.3	Solvent-separated structures	106
4.6.3	Examination of supramolecular constructs using XPac	107
4.6.3.1	Structures containing supramolecular construct SA	108
4.6.3.2	Structures containing construct supramolecular SB	109
4.6.3.3	Structures containing construct SC	110
4.6.3.4	Structures containing construct SD	111
4.6.3.5	Relationship between hydrogen bonding and supramolecular constructs	112
4.6.4	Structural rules for benzenesulfonic acid counterions	113
4.7	Summary	114
4.7.1	Case example of the application of the structural rules	114
5 Hydration in salt structures		
5.1	Introduction	116
5.2	Method	117
5.3	Occurrence of hydrate formation by cation and anion type	119
5.3.1	Hydrate occurrence and number of H-bonding groups	120
5.3.1.1	Hydrate formation and basic nitrogens	120
5.3.1.2	Hydrate formation and carboxylic acid groups	121

5.4	Hydrogen bonding interactions of water	123
5.4.1	Hydrogen bonding interactions of water in dicarboxylic acid salts	124
5.4.2	Hydrogen bond interactions of water in substituted benzoate salts	125
5.4.3	Hydrogen bonding interactions of water in sulfonate salts	126
5.5	Guidelines for counterion selection to minimise hydrate formation	127
5.5.1.1	Tertiary amines	127
5.5.1.2	Secondary amines	127
5.5.1.3	General guidelines	127
5.6	Structural aspects of salt hydration	128
5.6.1	Extended motifs from water and functional groups	128
5.6.2	Extended motifs in dicarboxylic acid salts	129
5.6.3	Extended motifs in benzoic acid salts	129
5.6.4	Extended motifs in sulfonic acid salts	129
5.7	Comparison of Hydrated and Anhydrous Structures	130
5.7.1	Changes to hydrogen bond interactions	130
5.7.1.1	Hydrogen bond interactions in hydrogen tartrate salts	130
5.7.1.2	Hydrogen bond contacts in bitartrate salts	132
5.7.1.3	Hydrogen bond contacts in benzoate salts	132
5.7.1.4	Overall trends on dehydration	132
5.7.2	Comparison of hydrate and anhydrous hydrogen tartrate salts	133
5.7.2.1	Secondary amine hydrogen tartrate salts	133
5.7.2.2	Tertiary amine hydrogen tartrate salt	135
5.7.3	Secondary amine bitartrate salts	136
5.7.4	Secondary amine benzoate salts	137
5.7.4.1	Piperidinium and morpholinium 4-hydroxybenzoate	137
5.7.4.2	1-Methylpiperazinium 4-hydroxybenzoate monohydrate	138
5.7.5	Conclusions from the dehydration experiments	139
5.8	Summary	141
5.8.1	Case example of the application of the guidelines	141
6	Validation of the structural rules: application to novel fluoroquinolone salts	
6.1	Introduction	143
6.2	Materials and Methods	146
6.2.1	CSD Database Searches	146
6.2.2	Crystallisation of Novel Pharmaceutical Salts	146
6.3	Validation of hydrogen bonding motifs with CSD structures	147
6.3.1	Comparison of Pm and Pmo for motifs in dicarboxylic acid salts	147
6.3.2	Comparison of Pm and Pmo for motifs in benzoic acid salts	148
6.3.3	Comparison of Pm and Pmo for motifs in monosulfonic acid salts	148
6.3.4	Summary of comparisons of Pm and Pmo	149

6.4	Novel pharmaceutical salt systems	150
6.4.1	Novel dicarboxylic acid salts	150
6.4.2	Novel benzoic acid salts	150
6.4.3	Pharmaceutical salts with sulfonic acid counterions	151
6.5	Application of structural rules to novel pharmaceutical salts	152
6.5.1	Structural rules for dicarboxylic acid salts	152
6.5.1.1	Structural rules applicable to all dicarboxylic acid salts	152
6.5.1.2	Structural rules applicable to aliphatic dicarboxylic acid salts	153
6.5.1.3	Structural rules applicable to hydroxyacid salts	154
6.5.2	Structural rules for benzoic acid counterions	156
6.5.2.1	Structural rules applicable to tertiary amine salts	156
6.5.2.2	Structural rules applicable to secondary amine salts	156
6.5.3	Structural rules for sulfonic acid salts	158
6.5.3.1	Structural rules applicable to tertiary amine salts	158
6.5.3.2	Structural rules applicable to secondary amine salts	159
6.5.3.3	Structural rules applicable to 4-hydroxybesylate salts	160
6.5.4	Summary	161
6.6	Hydrate formation and structure in fluoroquinolone salts	162
6.6.1	Consistency with guidelines to minimise hydrate formation	162
6.6.2	Water contact environments in the fluoroquinolone salts	162
6.6.3	Consistency with guidelines established in Chapter 5	163
6.7	Study of Fluoroquinolone packing arrangements using XPac	164
6.7.1	General	164
6.7.2	Structures containing construct A_1	166
6.7.2.1	Structures containing supramolecular construct A_{21}	167
6.7.2.2	Structures containing supramolecular constructs A_{22} and A_{31}	168
6.7.2.3	Structures containing supramolecular constructs A_{23} , A_{24} and A_{32}	169
6.7.3	Structures containing supramolecular constructs A_{12} and A_{14}	170
6.7.4	Structures containing construct B_{11}	171
6.7.5	Structures containing construct B_{12}	172
6.7.6	Summary of the XPac analysis of the fluoroquinolone salts	173
6.8	Case example of the application of the structural rules	173
6.9	Summary	175
7	Conclusions and further work	
7.1	Conclusions	177
7.2	Further Work	180
	References	177

List of Figures

Figure 1.1 Pharmacokinetic process following the administration of a drug.	2
Figure 1.2 Salt selection process for a new pharmaceutical.	7
Figure 1.3 “Classic” dissolution profile.	14
Figure 1.4 Dissolution profile showing a phase change.	15
Figure 1.5 Examples of negative charge assisted hydrogen bonds.	18
Figure 1.6 Schematic representation of the four stages of supramolecular assembly as described by KAP for a finite molecular unit.	20
Figure 1.7 Hirshfeld surfaces for the L-tartrate anion in 1-methylpiperazinium L-tartrate monohydrate.	35
Figure 1.8 2-D fingerprint plot produced for the L-tartrate anion in 1-methylpiperazinium L-tartrate monohydrate from the <i>di</i> and <i>de</i> surfaces.	35
Figure 3.1 The modified Hasse plot used in Chapter 1.	47
Figure 3.2 Common Ordered Sets of Points selected for the comparison of the packing arrangements of similar molecular components.	48
Figure 4.1 Classification of multicomponent crystalline solids characterised in this work.	55
Figure 4.2 The carboxylic and sulfonic acids selected as counterions in this study.	56
Figure 4.3 Heterocyclic bases tested as salt formers in combination with the acid counterions shown in Figure 4.1.	57
Figure 4.4 Outcomes of the crystallisation experiments for each group of acid counterions as a percentage of the acid-base combinations examined.	59
Figure 4.5 Chart showing the individual experimental outcomes according to the pKa values of the acid and base species.	63
Figure 4.6 Hydrogen bond contacts with type number, seen in the dicarboxylic acid structures.	65
Figure 4.7 Amine-carboxylate hydrogen bond motifs identified in the dicarboxylic acid structures identified by their graph set notation.	67
Figure 4.8 <i>Syn-syn</i> and <i>anti-anti</i> hydrogen bonded acid molecules in the C1,1(7) and C1,1(9) hydrogen bonded chains in the dicarboxylic acid structures.	68
Figure 4.9 Acid to acid hydrogen bonded motifs formed in the malic and tartaric acid salt structures.	68
Figure 4.10 Dendrogram showing the hydrogen bond synthons in the dicarboxylic acid structures.	70
Figure 4.11 H-bonded arrays containing an $\text{NH}^+\cdots\text{CO}_2^-$ motif in addition to the C1,1(7/9) hydrogen acid chain from Figure 4.10.	71
Figure 4.12 H-bond arrays containing $\text{OH}\cdots\text{CO}_2^-/\text{CO}_2\text{H}$ motifs and the C1,1(7/9) base vector from Figure 4.10.	72
Figure 4.13 Dicarboxylic acid structures based on the C2,2(12) motif.	74
Figure 4.14 Hydrogen bonds involving only acid or base molecules in the dicarboxylic acid structures.	78
Figure 4.15 Amine-carboxylic acid hydrogen bonding motifs identified in the benzoic acid subset of structures.	80

Figure 4.16 The hydroxyl to carboxylate hydrogen bonded chain motif identified in the structures containing a <i>para</i> -hydroxyl group.	81
Figure 4.17 Dendrogram showing the hydrogen bond synthons present in the benzoic acid structures.	82
Figure 4.18 The H-bond arrays formed by structures containing the C2,2(6) NH ₂ ⁺ ...CO ₂ ⁻ motif.	83
Figure 4.19 The two H-bonded arrays formed by structures containing discrete acid-base hydrogen bonds.	85
Figure 4.20 Intermolecular hydrogen bonding arrangement in MMHB.	86
Figure 4.21 Packing arrangement of SC A in DBDM and DBMA1.	90
Figure 4.22 Packing arrangement of A constructs in SAMA and HBMA.	90
Figure 4.23 Packing of SC B in DBPA and HBMM.	91
Figure 4.24 Packing arrangements of SC C ₁ in BZPD, TUMA and DBMA.	92
Figure 4.25 Construct D in SADM1 overlaid with construct D in BZPA.	93
Figure 4.26 Packing arrangement of SC D in SADM1 and SAMR .	94
Figure 4.27 Packing arrangement of SC D ₁ in BZPA and HBPA .	95
Figure 4.28 Packing arrangement of SC E ₁ in DBMR and HBMR.	96
Figure 4.29 Packing arrangements of SC F in TUDM, BZMA and BZPP.	97
Figure 4.30 Number of structures based on each amine-carboxylate hydrogen bonding motif containinmg a supramolecular construct.	98
Figure 4.31 Dendrogram showing the similarity relationships between the SCs identified in the benzoic acid structures.	99
Figure 4.32 Hydrogen bond contacts involving only acid and/or base molecules in the sulfonic acid structures.	101
Figure 4.33 Amine-sulfonate hydrogen bond motifs identified in the sulfonic acid structures labelled by their graph set notation.	102
Figure 4.34 C1,1(8) and C1,1(5) hydrogen bonded chain motifs identified in the sulfonic acid structures.	103
Figure 4.35 Dendrogram showing the hydrogen bond synthons present in the sulfonic acid salts.	104
Figure 4.36 Schematic showing the relationships between the extended hydrogen bonded structures based on the C2,2(6) chain.	105
Figure 4.37 Schematic showing the structures based on the alternative amine-sulfonate hydrogen bonding motifs to the C2,2(6) chain.	106
Figure 4.38 Packing arrangements of supramolecular construct SA ₁ in HSPD, HSPP and BSPA .	108
Figure 4.39 Packing arrangement of supramolecular construct SB in HSPA, HSPP, and TSMA .	109
Figure 4.40 Packing arrangements of supramolecular construct SC in HSMR, TSDM, TSPA and TSMA.	110
Figure 4.41 Packing arrangement of supramolecular construct SD in BSPP and TSPP.	111
Figure 4.42 Dendrogram showing the similarity relationships between the supramolecular constructs identified in the benzenesulfonic acid structures.	112
Figure 4.43 Chemical structure of the tetracyclic antidepressant Amoxapine.	115

Figure 5.1 Variation of water affinity with the number, type and protonation states of amine nitrogens in the basic molecules across the experimental matrix.	120
Figure 5.2 Variation in water affinity with the number of neutral and ionized carboxylic acid groups present on the acid molecule.	121
Figure 5.3 Variation in water affinity with the number of hydroxyl groups present on the acid molecule.	122
Figure 5.4 The three hydrogen bonding environments for water molecules in the hydrate structures.	123
Figure 5.5 Changes in hydrogen bond contacts between the acid and base molecules upon dehydration of the hydrate structures to form the anhydrate structures.	131
Figure 5.6 Comparison of the molecular packing arrangements in MRLT and PDLT monohydrate with their corresponding anhydrous structures.	133
Figure 5.7 Layered packing arrangement of the anions and cations in piperidinium hydrogen fumarate and morpholinium hydrogen succinate. Both structures are viewed along the axis of the C1,1(7) hydrogen acid chains.	134
Figure 5.8 Packing arrangement in the dihydrated MDRT compared with the anhydrate structure.	135
Figure 5.9 Comparison of the molecular packing arrangement in MALT monohydrate with the anhydrous structure.	136
Figure 5.10 Comparison of the packing arrangements of the stacks of acid anions in piperidinium 4-hydroxybenzoate dihydrate and the layers in the anhydrate.	137
Figure 5.11 Rearrangement of the C1,1(8) acid chains on dehydration of MAHB monohydrate to the anhydrate.	138
Figure 6.1 Structures of the fluoroquinolone antibacterial compounds examined in this work.	144
Figure 6.2 Face and side views of the 0-dimensional primary supramolecular construct A, found in 27 of the 32 fluoroquinolone salt structures.	164
Figure 6.3 Six one-dimensional SCs identified in the fluoroquinolone structures.	164
Figure 6.4 The relationships between the 31 structures with the SCs listed in Table 6.16. .	165
Figure 6.5 The 11 unique packing arrangements of SC A ₁ .	166
Figure 6.6 Comparison of the stacking of the two-dimensional A ₂₁ construct in CPAD dihydrate and CPSA monohydrate .	167
Figure 6.7 Comparison of the stacking of the two-dimensional A ₂₂ construct in the pseudoisostructural TSCP and TSNR salts, TSEN and EDNR.	168
Figure 6.8 Packing arrangements of SCs A ₂₃ and A ₂₄ viewed along the <i>t</i> ₁ vector of the A ₁₁ stacks.	169
Figure 6.9 The eight unique packing arrangements of SC A ₂ .	170
Figure 6.10 The four unique packing arrangements of construct B ₁₁ .	171
Figure 6.11 The packing arrangements of supramolecular construct B ₁₂ in FUEN and SAEN.	172

List of Tables

Table 1.1 Prevalence of anionic counterions as percentage of marketed salts of basic drugs.	4
Table 1.2 Selected properties of strong, moderate and weak hydrogen bonds.	17
Table 1.3 Reliable and occasional hydrogen bond donors and acceptors.	19
Table 1.4 The 16 possible hydrogen-bonded vector types and subtypes as determined by the application of Kitaigorodskii's Aufbau Principle.	22
Table 1.5 The three tolerance limits for the filter parameters in the intermolecular angles, dihedral angles and torsion angles in XPac.	32
Table 3.1 The acidic counterions selected for examination in this work including their molecular weights (MW), melting points and calculated pKa s.	39
Table 3.2 The model bases crystallised with the acidic counterions in this work including their molecular weights (MW), melting points and calculated pKa s.	41
Table 3.3 The pharmaceutically active molecules crystallised with the acidic counterions in this work including their molecular weights (MW), melting points and calculated pKa s.	42
Table 3.4 Variable count time scheme used for the VT-XRPD data collections.	45
Table 3.5 Data for base vectors t in the supramolecular constructs identified in the benzoic acid systems.	49
Table 3.6 Data for base vectors t in the supramolecular constructs identified in the benzenesulfonic acid systems.	51
Table 3.7 Data for base vectors t in the supramolecular constructs identified in the fluroquinolone structures.	52
Table 4.1 Outcomes of crystallisation experiments for dicarboxylic acid counterions with model bases.	60
Table 4.2 Outcomes of crystallisation experiments for monocarboxylic acid counterions with model bases.	60
Table 4.3 Experimental outcomes for crystallisations of sulfonic acid counterions and model bases.	61
Table 4.4 Frequencies of occurrence of the 17 hydrogen bond interactions in Figure 4.6.	65
Table 4.5 Frequencies of occurrence for the 12 motifs in the structures containing dicarboxylic acids.	69
Table 4.6 Frequencies of occurrence for the hydrogen bond contacts identified in the structures containing benzoic acids.	79
Table 4.7 Frequencies of occurrence for motifs in the structures containing benzoic acids.	81
Table 4.8 Relative proportions of system types forming B1 ₀ arrays.	85
Table 4.9 SCs in the benzoate structures.	87
Table 4.10 Selected structural details for structures containing construct A.	89
Table 4.11 Selected structural details for structures containing construct B.	91
Table 4.12 Selected structural details for structures containing construct C.	92
Table 4.13 Selected structural details for structures containing construct D.	93
Table 4.14 Selected structural details for structures containing construct E ₁ .	96

Table 4.15 Selected structural details for structures containing construct F.	97
Table 4.16 Frequencies of occurrence of the six hydrogen bonded contacts in the sulfonate salt structures.	101
Table 4.17 Frequencies of occurrence for motifs in the structures containing sulfonic acids.	103
Table 4.18 SCs in the benzenesulfonate structures.	107
Table 4.19 Selected structural details for structures containing construct SA.	108
Table 4.20 Selected structural details for structures containing construct SB.	109
Table 4.21 Selected structural details for structures containing construct SC.	110
Table 4.22 Selected structural details for structures containing construct SD.	111
Table 5.1 Crystallographic data and SDPD refinement parameters for the anhydrous salts generated by VT-XRPD.	118
Table 5.2 Occurrence of hydrates in salts in experimental matrix as no. of hydrates / total structures; frequency as a percentage in parentheses.	119
Table 5.3 Comparison of the frequencies of occurrence of water environments in this work and the CSD survey.	123
Table 5.4 Structural details for the dicarboxylic acid hydrates.	124
Table 5.5 Structural details for the benzoic acid hydrates.	125
Table 5.6 Structural details for the benzenesulfonic acid hydrates.	126
Table 5.7 Common hydrogen bonding arrangements observed for secondary and tertiary amine salts of the major types of acid counterion examined in this work.	128
Table 6.1 Frequencies of occurrence for motifs (Pmo) in the CSD structures containing dicarboxylic acids compared with their frequencies in the database of model systems described in Chapter 4 (Pm).	147
Table 6.2 Frequencies of occurrence for motifs (Pmo) in the validation set of structures containing benzoic acids compared with their frequencies in the database of model systems described in Chapter 4 (Pm).	148
Table 6.3 Frequencies of observation for H-bond motifs in the CSD and pharmaceutical sulfonate salts (Pmo) and the database of model systems from Chapter 4 (Pm).	149
Table 6.4 Novel dicarboxylic acid salts of pharmaceutically active molecules characterised in this work.	150
Table 6.5 Novel benzoic acid salts of fluoroquinolones characterised in this work.	151
Table 6.6 Novel sulfonic acid salts of fluoroquinolones.	151
Table 6.7 Agreement of the novel dicarboxylic acid salts with structural rules D1 and D5.	152
Table 6.8 Structural features observed in the dicarboxylic acid salts in comparison to those expected from Rules D2 and D7.	154
Table 6.9 Structural features observed in the hydroxyacid acid salts in comparison to those expected from Rules D3 and D6.	155
Table 6.10 Occurrence of the structural features predicted for the dicarboxylic acid systems formed with pharmaceutically active molecules from structural rules D1 and D5.	157

Table 6.11 Hydrogen bond acceptor for the amine nitrogen in the six tertiary amine sulfonate salts.	158
Table 6.12 Consistency of the amine-sulfonate hydrogen bond motifs in the novel secondary amine pharmaceutical sulfonic acid salts with structural rules S2.	159
Table 6.13 Water coordination environments in the dicarboxylic acid salts of fluoroquinolones.	162
Table 6.14 Water coordination environments in the novel benzoate salts of pharmaceuticals characterised in this work.	163
Table 6.15 Water coordination environments in the novel fluoroquinolone sulfonate salts characterised in this work.	163
Table 6.16 Similarity relationships between the supramolecular constructs identified in the fluoroquinolone salt structures.	165

Abbreviations

AD	Adipic acid/ hydrogen adipate/ adipate
ADME	Absorption, Distribution, Metabolism and Excretion
AX	Amoxapine
BS	Benzenesulfonic acid/ benzenesulfonate (besylate)
BZ	Benzoic acid/ benzoate
COSPs	Corresponding Ordered Set of Points
CP	Ciprofloxacin
CSD	Cambridge Structural Database
DB	2,4-Dihydroxybenzoic acid/ 2,4-dihydroxybenzoate
DM	1,4-Dimethylpiperazine/ 1,4-dimethylpiperazinium
DMSO	Dimethylsulfoxide
DSC	Differential Scanning Calorimetry
ED	1,2-Ethanedisulfonic acid/ 1,2-ethanedisulfonate (edisylate)
EN	Enrofloxacin
FU	Fumaric acid/ fumarate
HB	4-Hydroxybenzoic acid/ 4-hydroxybenzoate
HS	4-Hydroxybenzenesulfonic acid/ 4-hydroxybenzenesulfonate (hydroxybesylate)
KAP	Kitaigorodskii's Aufbau Principle
LM	L-Malic acid/ hydrogen L-malate/ L-malate
LT	L-Tartaric acid/ hydrogen L-tartrate/ L-tartrate
LV	Levofloxacin
MA	1-Methylpiperazine/ 1-methylpiperazinium
MD	1-Methylpiperadine/ 1-methylpiperadinium
MM	4-Methylmorpholine/ 4-methylmorpholinium
MR	Morpholine/ morpholinium
ME	Maleic acid/ hydrogen maleate/ maleate
MS	Methanesulfonic acid/ methanesulfonate (mesylate)
NR	Norfloxacin
PA	Piperazine/ piperazinium
PD	Piperidine/ piperidinium
PP	4-Phenylpiperazine
OF	Ofloxacin
RM	DL-Malic acid/ hydrogen DL-malate/ DL-malate (<i>rac</i> -Malate)
RT	DL-Tartaric acid/ hydrogen DL-tartrate/ DL-tartrate (<i>rac</i> -Tartrate)
SA	Salicylic acid/ salicylate
SC	Supramolecular Construct
SDPD	Structure Determination from Powder Diffraction Data
SP	Sparfloxacin
SU	Succinic acid/ hydrogen succinate/ succinate
SXRD	Single-Crystal X-Ray Diffraction
TS	4-Toluenesulfonic acid/ 4-toluenesulfonate (tosylate)
TU	4-Toluic acid/ 4-toluate (4-methylbenzoate)
VT-XRPD	Variable-Temperature X-Ray Powder Diffraction
XRPD	X-Ray Powder Diffraction

Chapter 1

Introduction

1.1 Background

In order to be effective a pharmaceutical must have the molecular structure required to produce the desired pharmacological effect. However, the efficacy of a pharmaceutical is also determined by its pharmacokinetic properties and consequent ability to reach the site of action. A set of guidelines, the “*rule of five*”, established by Lipinski (Lipinski, *et al.*, 1997) predict that poor solubility and membrane permeability is likely when the drug molecule has:

- (i) A molecular weight greater than 500 Da.
- (ii) A calculated $\log P$ value of greater than +5.
- (iii) More than 5 hydrogen bond donor groups.
- (iv) More than 10 hydrogen bond acceptor groups.

Solid dosage forms are preferred for pharmaceuticals due to their flexibility in design, reduced aseptic requirements and improved patient compliance in comparison with liquid oral and injectable formulations (Verma, *et al.*, 2002, Abdul and Poddar, 2004). However, the molecular structure of the drug frequently results in sub-optimal physicochemical and mechanical properties in solid formulations (Forbes, *et al.*, 1995). Properties including melting point, solubility, dissolution rate, stability, particle size, shape and permeability consequently affect the pharmacokinetic process of the drug *in vivo* (Huang and Tong, 2004). The pharmacokinetic process relates to the bioavailability and elimination of the drug *in vivo* as determined by its absorption, distribution, metabolism and excretion (ADME) profile shown in Figure 1.1.

Poor ADME profiles are a frequent problem for the high molecular weight and lipophilic molecules frequently isolated from high-throughput screens in DMSO (Bastin, *et al.*, 2000). This has led to a significant reduction in the aqueous solubility of pharmaceutical new chemical entities (NCEs). Prior to 1980 this rarely fell below 20 $\mu\text{g}/\text{mL}$ whilst currently solubilities in the region of 1 $\mu\text{g}/\text{mL}$ are frequently encountered (Serajuddin, 2007) with ca. 80% of NCEs suffering from poor solubility (Amidon *et al.* 1995). The dissolution rate of the drug is related to its solubility and is frequently the rate limiting step in drug absorption (Berge, *et al.*, 1977).

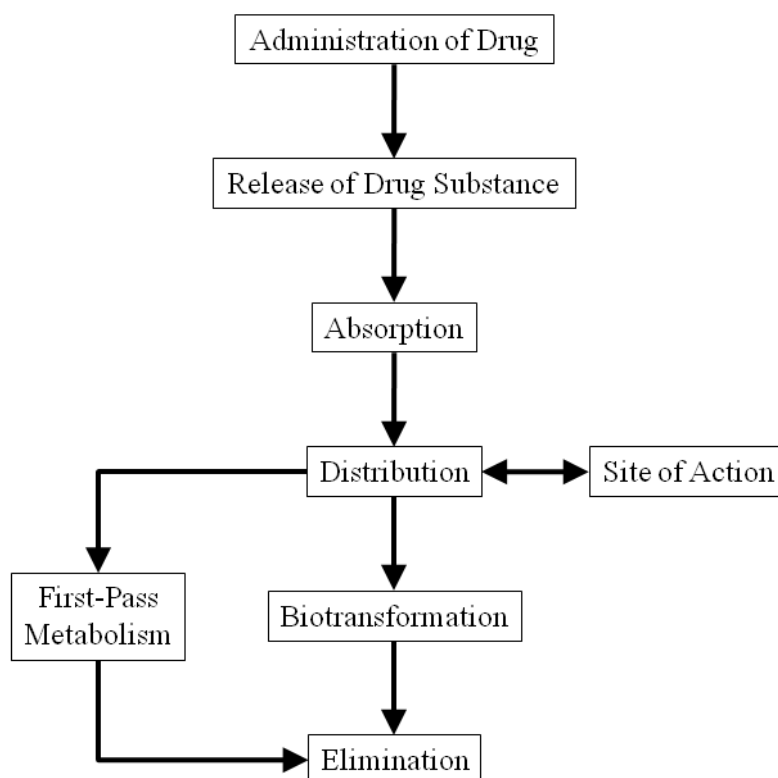


Figure 1.1 Pharmacokinetic process following the administration of a drug (Stahl and Vermuth, 2002).

The chemical and physical properties of the drug will affect the manufacturing, storage and shelf-life of the product. Low melting solids are problematic from a manufacturing and formulation standpoint as they can melt during processing or fail to bind effectively to substrates during tableting. The particle size and morphology determines the flowability of the powder during processing and its compatibility with stages in the synthetic process including filtration. Additionally, a homogenous solid is required to avoid variation in the bioavailability of the drug due to differences in particle size (Florence and Attwood, 2006) .

A number of formulation techniques can improve the physicochemical properties of a drug. The properties of a solid drug can be adjusted by exploring alternative solid forms including polymorphs, salts, cocrystals, solvates, and amorphous phases or by particle size reduction. The development of a suitable solid form commences early in the drug development process and is a critical stage in preclinical pharmaceutical development (Morissette, *et al.*, 2004).

1.2 Salt formation in pharmaceutical development

1.2.1 Counterion selection

When the active molecule possesses an acidic or basic functional group formulation as a salt allows its physicochemical properties to be optimised without altering the molecular structure of the drug molecule (Gould, 1986). The choice of counterion used to form a salt is dependent on the physicochemical properties of the candidate molecule, the toxicology and safety of the counterion, the intended route of administration and the desired dosage form. In order to form a stable salt it is generally the case that there should be a difference of at least 3 units between the pKa of the ionisable group on the drug molecule and the counterion (the “*rule of three*”), which can limit the range of available counterions (Bastin, *et al.*, 2000). The choice of counterion must also consider its effect on the crystalline lattice energy of the salt formed and consequently on its solubility and other physicochemical properties that influence its stability and manufacturability (Hammond, 2006).

The efficiency and cost-effectiveness of a salt screen can be maximised by selecting salt formers that satisfy the following criteria (Black, *et al.*, 2007):

- Low cost.
- Widely available.
- Low melting point.
- Molecular weight < 300 Da.
- Analytical data available.
- Crystalline, ideally with previously reported crystal structure(s).
- pKa that satisfies the “*rule of three*” (*vide supra*).
- Variety in charge distribution and stereochemistry across the screening set.

Counterions include polysaccharides, inorganic acids, sulfonic acids, amino acids, carboxylic acids and hydroxyacids for basic drug molecules and organic amines, metallic cations and cationic amino acids for acidic drugs. The anionic counterions currently used in salt formulations of basic drugs and their relative prevalence as a percentage of marketed salt forms are summarised in Table 1.1.

Table 1.1 Prevalence of anionic counterions as percentage of marketed salts of basic drugs (Stahl and Vermuth, 2002).

Anion	%	Anion	%	Anion	%
Aceglumate	0.07	Fosfatex	0.07	Nicotinate	0.13
Acephyllinate	0.26	Fumarate	0.92	Nitrate	1.18
Acetamidobenzoate	0.07	Gluceptate	0.13	Oleate	0.13
Acetate	2.09	Gluconate	0.52	Orotate	0.26
Acetylasparaginate	0.07	Glucoronate	0.13	Oxalate	0.26
Acetylaspartate	0.07	Glutamate	0.07	Oxoglutrate	0.13
Adipate	0.13	Glycerophosphate	0.52	Pamoate	1.37
Aminosalicylate	0.13	Glycinate	0.13	Pantothenate	0.07
Anhydro-methylenecitrate	0.07	Glycollyarsinilate	0.07	Pectinate	0.07
Ascorbate	0.13	Glycyrrhizate	0.07	Phenylethyl-barbiturate	0.13
Asparate	0.33	Hippurate	0.07	Phosphate	2.48
Benzoate	0.20	Hemisulphate	0.13	Picrate	0.07
Besylate	0.26	Hexylresorcinate	0.07	Policrillix	0.07
Bicarbonate	0.07	Hybenzate	0.20	Polistirex	0.85
Bisulfate	0.13	Hydrobromide	5.16	Pyridoxyl-phosphate	0.07
Bitartrate	0.52	Hydrochloride	47.5	Poly-galacturonate	0.20
Borate	0.26	Hydroiodide	1.18	Propionate	0.13
Butylbromide	0.07	Hydroxy-benzenesulfonate	0.07	Saccharinate	0.20
Camphorate	0.01	Hydroxybenzoate	0.07	Salicylate	0.78
Camsylate	0.59	Hydroxynapthoate	0.07	Stearate	0.20
Carbonate	0.46	Isethionate	0.52	Stearylsulfate	0.07
Chlorophenoxyacetate	0.07	Lactate	0.98	Subacetate	0.07
Citrate	2.81	Lactobionate	0.07	Succinate	0.52
Closylate	0.07	Lysine	0.65	Sulfate	5.82
Cromesilate	0.07	Malate	0.26	Sulfosalicylate	0.07
Cyclamate	0.13	Maleate	3.14	Tannate	0.85
Dehydrocholate	0.07	Mandelate	0.13	Tartrate	2.68
Dihydrochloride	1.37	Mesylate	3.20	Teprosiliate	0.07
Dimalonate	0.07	Methylbromide	0.39	Terephthalate	0.07
Edetate	0.07	Methyliodide	0.20	Teoclate	0.33
Edisylate	0.20	Methylnitrate	0.13	Thiocyanate	0.20
Estolate	0.13	Methylsulfate	0.98	Tidiacicate	0.07
Esylate	0.13	Monophosphadenine	0.07	Timonaciate	0.07
Ethylbromide	0.07	Mucate	0.07	Tosylate	0.39
Ethylsulfate	0.07	Napadisylate	0.13	Triethiodide	0.07
Fendizoate	0.07	Napsylate	0.20	Undecanoate	0.13
Formate	0.07			Xinafoate	0.07

During initial screening hydrochloride salts are one of the first formulated as the strongly acidic hydrochloride anion forms salts with very weak bases and is relatively non-toxic due to its occurrence in gastric fluid (Bastin, *et al.*, 2000). However, dissolution of the salt *in vivo* can be impaired by the common ion effect, as the equilibrium will lie towards the non-dissociated solid due to the excess of hydrochloride ions naturally present in the gastric solution. This effect frequently leads to hydrochloride salts having poorer solubility and dissolution characteristics than the free base (Miyazaki, *et al.*, 1981). Coupled with the increasing lipophilicity of new pharmaceutical molecules this has led to an increase in the diversity of the types of counterions employed in salt formation (Paulekuhn, *et al.*, 2007).

1.2.2 Effect on physicochemical properties

High aqueous solubility is desirable for both oral and intravenous administration to ensure adequate bioavailability and rapid onset of action. Also, the increased clearance by the kidneys of water-soluble drugs makes them less prone to accumulate in the body, thereby reducing their toxicity (Stahl and Vermuth, 2002). Dissolution is usually the rate-limiting step in the absorption process thereby determining the intensity, duration and onset time of the pharmacological effect. For example, due to its increased dissolution rate the absorption of the potassium salt of the antibiotic ampicillin was 17% higher four hours after oral administration than the trihydrate and subsequently demonstrated higher clearance rates (Berge, *et al.*, 1977).

The choice of counterion will also affect other physicochemical properties including melting point. The melting point and enthalpy of fusion of a salt is generally higher when the counterion has a high charge density, for example, a hydrochloride salt will have a higher melting point than the corresponding free base. This criteria is of particular importance for particle size reduction and distribution as solids with melting points of less than 100°C generally melt during milling (Gould, 1986). The crystals' size and habit will also have implications for milling and processing, with flat, plate-like crystals being prone to block filtration apparatus (Wong and Pilpel, 1990).

Other considerations include preventing the decomposition of the drug when it is exposed to moisture during processing and storage (Carstensen, *et al.*, 1985). The stability of the crystalline form must also be assessed in terms of its potential to undergo polymorphic transformations, its hygroscopicity and its stability towards hydrate formation (Stahl and Vermuth, 2002). These latter aspects are intimately related to the intermolecular interactions in the solid state and will be discussed more fully later.

Due to the significant differences in bioavailability, pharmacokinetic profile, toxicity and chemical stability each salt form of a drug requires regulatory approval prior to marketing (Davies, 2001). Changing the salt form of a drug subsequent to approval requires clinical testing to be repeated and regulatory re-approval, making it essential to identify the optimum salt form prior to the commencement of manufacture.

1.2.3 Current approach to salt selection

It is currently impossible to predict the effect that the structure of a pharmaceutical salt has on its physical properties, however some general relationships are accepted:

- (i) There is usually an inverse relationship between the melting point of a crystalline drug form and its aqueous solubility (Gould, 1986).
- (ii) Hydrates generally have lower aqueous solubilities than their corresponding anhydrates (Khankari and Grant, 1995) .
- (iii) Increasing the hydrophobicity of the counterion will decrease the solubility of the salt (Jones, *et al.*, 1969) and, conversely, a more hydrophilic counterion will form a more soluble salt (Agharkar, *et al.*, 1976).

Due to the limited understanding of the relationships between salt form, crystalline structure and physicochemical properties, the current industrial approach to salt selection is semi-empirical, employing high-throughput screening of different salt forms. This is a time-consuming and resource-intensive process and is summarised overleaf in Figure 1.2 (Stahl and Vermuth, 2002).

The initial selection of counterions is based on the calculated pKa of the ionisable groups on the pharmaceutical, with counterions selected based on the “rule of three” that there must be at difference of at least 3 pKa units between the ionisable group and counterion to ensure salt formation. In order to increase throughput and reduce the consumption of materials automated screening procedures are employed (Remenar, *et al.*, 2003). The efficiency of the process can also be improved by performing the least time consuming evaluations to rule out unsuitable candidates first followed by progressively lengthier evaluations (Morris, *et al.*, 1994). Molecular modelling techniques are being explored as a method of reducing the number of salts selected for initial screening, with some success. Currently this has only been applied to simple, rigid structures and further development is required before the technique can be applied to complex species and solvated systems (Hammond, 2006).

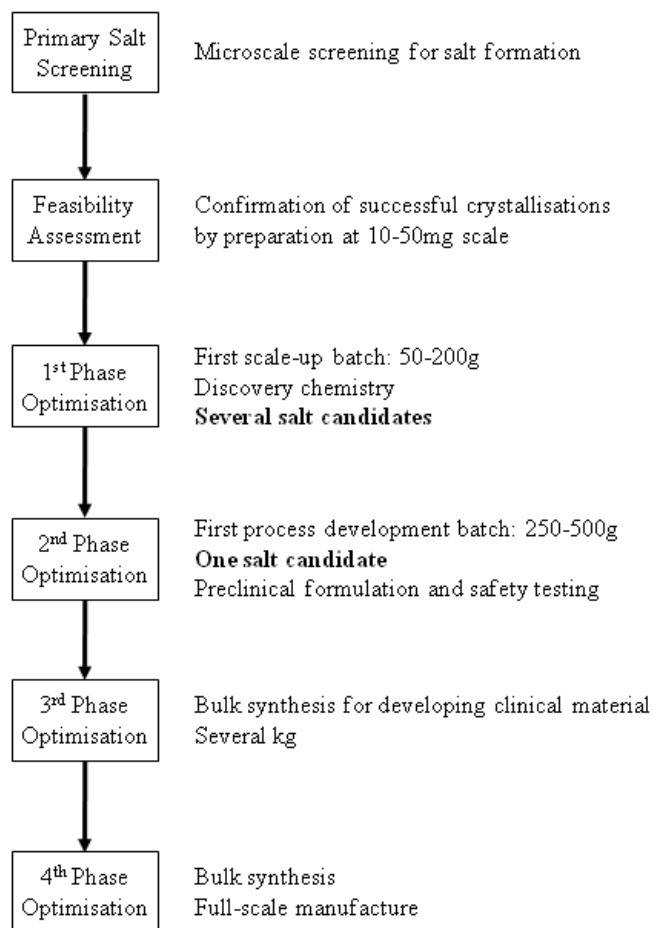


Figure 1.2 Salt selection process for a new pharmaceutical (Stahl and Vermuth, 2002).

The small quantity of active material typically available for preformulation studies has led to the development of semi-microscale techniques to allow the largest number of salt forms to be synthesised. Concentrated solutions of the counterions are added to wells containing approximately 5 mg of the candidate drug dissolved in a volatile solvent. The formation of crystals is monitored by microscopy to identify successful combinations of solvents and counterions that are repeated on a 10-50mg scale and their crystallinity, hygroscopicity, melting points and tendencies to form polymorphs and solvates are assessed. Viable formulations are then scaled up to gram quantities for comparison with the free acidic or basic drug in pharmacokinetic studies and for the investigation of suitable dosage forms, culminating in the selection of the most suitable salt form (Bastin, *et al.*, 2000).

1.3 The organic solid state

An organic crystal is a supramolecular assembly of molecules held in a periodic arrangement by a variety of directional and non-directional interactions of varying strengths and ranges. In addition to determining supramolecular structure these interactions also have a significant influence on the physical properties of the crystalline solid, including its melting point, aqueous solubility and crystal habit (Florence and Attwood, 2006). The importance of supramolecular interactions in this regard is most clearly demonstrated by polymorphism and is of particular importance to the pharmaceutical industry. For example the anti-inflammatory drug nabumetone has been isolated in two polymorphs, one melts at 65°C while the other melts at 80°C (Price, *et al.*, 2002) while an infamous example of polymorphism resulting in reduced solubility is the case of the HIV protease inhibitor Ritonavir (Bauer, *et al.*, 2001).

1.3.1 Binary systems- salts, cocrystals and solvates

Multi-component systems are those that contain more than one type of molecule in the crystal structure and include salts, cocrystals and solvates. A salt is an ionic product usually formed by the neutralisation reaction of an acid and base with proton transfer from the acid to the base as the defining characteristic. In contrast, cocrystals are systems in which no proton transfer has occurred and both species crystallise in their neutral state. There is some debate regarding the correct definition of a cocrystal, one viewpoint advanced by Aakeroy is that a cocrystal contains components that are solid at room temperature (Aakeroy and Salmon, 2005) in order to differentiate them from solvates and hydrates. As such this definition excludes systems where one component is a gas or one or both are liquid at ambient temperature (Bond, 2007). Opposing viewpoints are that the definition should be based on the nature of the multicomponent crystalline systems without reference to the properties of the starting materials (Stahly, 2007) or the intent or “element of design” in crystallising the system (Dunitz, 2003).

1.3.2 Hydrates

1.3.2.1 Hydrate formation

As stated previously the behaviour of a crystalline pharmaceutical material upon exposure to water is a critical parameter in the selection of a solid form due to the ubiquity of water in the atmosphere (Stahl and Vermuth, 2002). Due to its small size and versatile hydrogen bonding capabilities water is readily incorporated into crystalline lattices (Gillon, *et al.*, 2003). Water molecules can donate two hydrogen bonds through their hydrogen atoms and either form two covalent bonds or accept two more hydrogen bonds through the lone pairs of electrons on the oxygen atoms (Khankari and Grant, 1995).

1.3.2.2 Classification of hydrates

Hydrates can be classified according to their thermal properties determined by the onset temperature of dehydration and the shape of the desorption isotherms (Authelin, 2005). Two main types are defined by their sorption isotherms on formation (Vippagunta, *et al.*, 2001):

- Stoichiometric hydrates: well-defined water content with a different crystal structure to the corresponding anhydrate forms or other hydrates. Step-shaped sorption isotherms are observed and the pressure of the hydration/dehydration step is a function of temperature.
- Non-stoichiometric hydrates: variable water content without corresponding changes in crystal structure beyond anisotropic expansion to accommodate the water molecules. However, loss of crystallinity is possible on complete desorption of the water (Mimura, *et al.*, 2002). Their sorption isotherms have various shapes corresponding to one of five possible types of isotherm.

Hydrates can also be classified according to their structures, giving the three classes of pharmaceutical hydrates described by Morris (Morris, 1999):

- Class 1: isolated site hydrates- water molecules are located at well-defined and isolated crystallographic sites.
- Class 2: channel or planar hydrates- water molecules are located next to each other in the crystal structure forming channels or planar networks.
- Class 3: ion coordinated hydrates.

As this thesis focuses on organic molecular crystals the two classes of hydrates most relevant to this work are the class 1 and class 2 hydrates. In both cases, the incorporation of water is an important determinant of the supramolecular structure of the crystalline system.

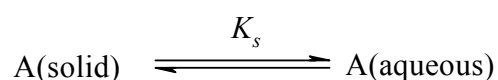
1.3.2.3 Structural consequences of salt hydration

For class 2 hydrates the most frequent changes in crystalline structure on dehydration are anisotropic and result from the escape of water through channels in the structure (Byrn and Lin, 1976) or changes in interlayer spacing of a common two-dimensional hydrogen bonded framework (Kiang, *et al.*, 2009). In class 1 hydrates the outcomes of hydration and dehydration do not appear to be readily predictable (Clarke, *et al.*, 2010).

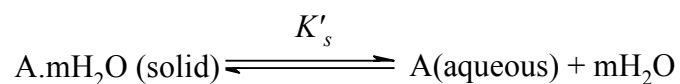
Hydrate formation has major implications for crystal engineering and the structures of crystalline systems. A recent examination of the structure and stability of organic cocrystal hydrates by Clarke *et al.* (Clarke, *et al.*, 2010) noted that, as of the May 2009 update, the CSD contained a low incidence of polymorphism in single-component molecular crystals (2.0%), cocrystals (2.0%) and hydrates (1.0%). However, a comparative analysis showed that in 35 of the 38 polymorphic cocrystals, the polymorphism was a result of conformational and packing changes and the hydrogen-bonded interactions persist between the polymorphs. In contrast, 28 of the 44 hydrate polymorphs exhibit changes in the hydrogen bonding arrangements of the water molecules. Clearly, due to its small size and flexibility in forming a diverse range of intermolecular hydrogen bonds water will have significant and unpredictable effects on the structure of a molecular crystal.

1.3.2.4 Effect of hydration on aqueous solubility

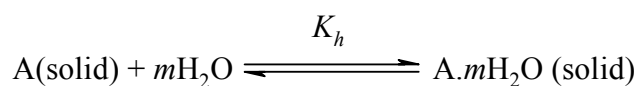
In addition to the structural effects of hydrate formation the interactions formed by the water molecules alter the lattice energy of the crystal (Desiraju, 1991). This affects the physicochemical properties of the supramolecular assembly, including its solubility, determined by the equilibrium constant K_s in the equilibrium:



The solubility of crystalline material A depends on several parameters including temperature, pressure and the thermodynamic activity of the solid. In the case of a hydrate the thermodynamic activity changes and the equilibrium constant, K'_s , will be different:



In systems where the hydrated form is thermodynamically more stable than the anhydrous form it is possible for anhydrous crystals to convert to the hydrated form:



The equilibrium constant K_h for the process is dependent on the thermodynamic activities, a , of the anhydrous and hydrated crystals and free water:

$$K_h = \frac{a[A.mH_2O \text{ (solid)}]}{a[A \text{ (solid)}]a[H_2O]^m}$$

The anhydrous form is more soluble than the hydrate as the hydrate is already interacting with water in the solid state, lowering the free energy change on dissolution (Khankari and Grant, 1995). This is sometimes expanded to infer that higher hydrates are less soluble in water than low hydrates, for example the solubility of the calcium salt of 4-aminosalicylic acid with a hydration state of 0.8 is greater than that of the calcium salt with a hydration state of 3 and of the tetrahydrate magnesium salt (Forbes, *et al.*, 1995).

1.3.2.5 Effect of hydration on dissolution rate

Dissolution is the process by which a solid dissolves in a liquid medium. The dissolution rate is a kinetic description of the rate at which this takes place. There are several theories regarding the precise mechanism by which this occurs, the simplest being the diffusion layer model. In this model, a thin film of saturated solution of concentration C_s known as the static layer exists at the interface of the solid and the bulk solution of concentration C . The diffusion of the molecules across this static layer is the rate-determining step. In the static layer, the solution in contact with the solid surface is saturated as molecules are dissociating from the solid into the layer at a greater rate than they diffuse from the static layer into the bulk solution. Fick's first law of diffusion gives the rate of diffusion across this static layer (Fick, 1855):

$$J = -DA \frac{\partial C}{\partial \chi}$$

J is the flux, defined as the net amount of solute that diffuses through area A per unit time. As this is the rate-limiting step, J is effectively the rate of dissolution of the solid and is proportional to the concentration gradient within the static layer. The concentration gradient across the static layer of thickness h is determined by the difference between C_s and the concentration of the stirred bulk solution C at time t :

$$\frac{\partial C}{\partial \chi} = \frac{C - C_s}{h}$$

Therefore the rate of dissolution can be defined by the Noyes-Whitney dissolution equation (Noyes and Whitney, 1897):

$$J = DA \frac{C_s - C}{h}$$

The diffusion coefficient D is constant for a constant temperature and the thickness of the static layer h is constant for a set stirring speed. If the solid is in sufficient excess to saturate the solution then the surface area A of the solid will be effectively constant allowing the simplification of the above term:

$$J = k(C_s - C)$$

The constant k is dependent on a number of factors including temperature, particle size, agitation rate and exposed surface area (Shefter and Higuchi, 1963). The general form of the Noyes-Whitney equation allows the interpretation of a classic dissolution profile as shown in Figure 1.3:

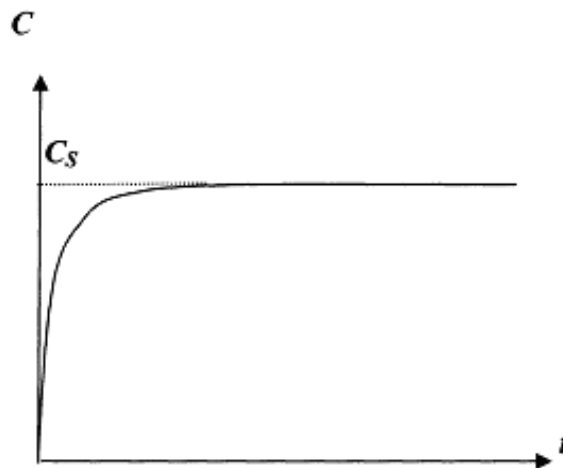


Figure 1.3 “Classic” dissolution profile (Pudipeddi *et al.*, 2002).

The dissolution rate J at time t is given by the gradient of a tangent to the curve at that time and decreases as the concentration C of the bulk solution increases. This is due to the decrease in the concentration gradient across the static layer. When $C = C_s$ the concentration gradient is zero and no further dissolution occurs. At this point the solution is saturated (Pudipeddi, *et al.*, 2002).

The saturation solubility C_s is determined by the relative free energy G of a molecule of the solid compound X in solid and in solution. As the solid dissolves to increase the concentration of X in solution the free energy $G_{X(solution)}$ will increase. The solid will continue to dissolve until the free energy of the solid and solution are the same (Pudipeddi, *et al.*, 2002). If the solid undergoes a solution-mediated transformation to a more stable form, for example transformation from the anhydrous form to a hydrate, C_s will be reduced leading to a characteristic reduction from maximum solubility to a lower equilibrium value as shown in Figure 1.4.

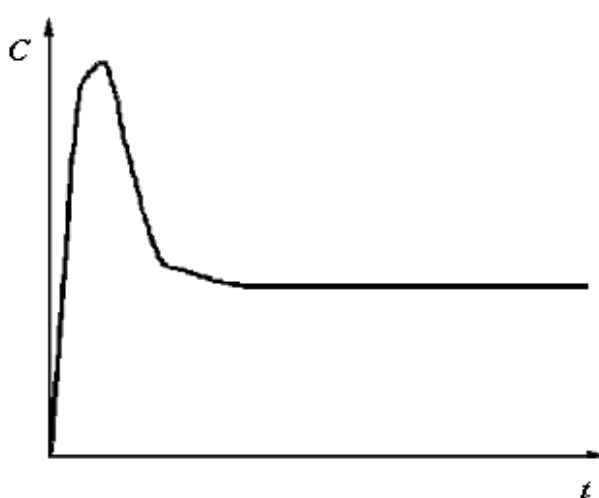


Figure 1.4 Dissolution profile showing a phase change (Florence and Johnston, 2006).

Provided its pharmacokinetic profile is suitable, the increased stability towards hydration over the anhydrous form can result in a hydrate being selected as the preferred form of an API. For example the monohydrate form of the antiplatelet agent picotamide is more stable than the anhydrate (Bettinetti, *et al.*, 1999). Other classes of pharmaceuticals currently marketed or under development as hydrates include the antibiotics ampicillin (Khankari, *et al.*, 1992) and cephalexin (Stephenson, *et al.*, 1998), the sodium salt of the antihistamine cromolyn (disodium cromoglycate) (Chen, *et al.*, 1999) and sildenafil citrate (Apperley, *et al.*, 2005).

1.4 Supramolecular Chemistry

1.4.1 Crystallisation

Crystallisation is the formation of a solid consisting of a periodic arrangement of molecules held together by a variety of intermolecular forces and interactions. Some interactions such as hydrogen bonds are short-range and directional whilst others are formally non-directional and act over longer ranges. The process of crystallisation involves the successive growth of the solid from a nucleation centre to form a crystal, with the final form determined by the manner of crystal growth resulting from the conditions of the crystallisation system (Desiraju, 1989).

Supersaturation of a solution is required for crystal growth and can be achieved by a number of methods including the evaporation of a solvent, cooling, addition of an antisolvent, chemical reaction of two or more species or by variation in the pH of the solution. Successful nucleation requires a critical number of ordered molecules to form an assembly and prevent subsequent dissolution, based on the principle that the surface area of a spherical body increases as the square of the radius whilst the internal volume increases as the cube of the radius. Therefore, as the size of the nucleus increases the disruptive surface forces (solute-solvent interactions) become less significant than the adhesive internal forces.

1.4.2 Intermolecular interactions

Various intermolecular and interionic interactions are responsible for determining the supramolecular structure of a crystalline entity and its resultant physicochemical properties. The supramolecular structure of a crystal is an equilibrium arrangement of molecules where the attractive forces that bring the molecules from infinite separation into contact are maximised and the repulsive forces are minimised. The attractive interactions can be broadly classified as medium-range isotropic interactions that define the close packing of molecules and anisotropic interactions that are more directional.

1.4.2.1 Hydrogen bonding

Hydrogen bonds are the highest energy interactions in molecular crystals after monopoles and are particularly prevalent in organic molecular crystals, where their strength and high directionality makes them important in supramolecular recognition and defining molecular packing. In particular, the directionality of the interaction allows control of molecular topologies and its selectivity leads to reproducible interactions that have been used as a basis for crystal structure prediction and the design of specific molecular crystal architectures.

A hydrogen bond consists of a hydrogen atom that is bonded to two or more heteroatoms in the arrangement $DH\cdots A$ where D is the donor atom and A is the acceptor, both of which are more electronegative than H. Different bonds can be classified according to their length or energy, topology, connectivity, chemical symmetry, proton position and D-H-A angle. The geometry of the hydrogen bond is defined by the length of the covalent D-H bond; the $D\cdots A$ and $H\cdots A$ contact distances and the D-H-A angle θ . Bent bonds are entropically favoured as the number of positions for A that make an angle θ with the D-H bond increases with $\sin \theta$. However, as the $D^{\delta-}-H^{\delta+}\cdots A^{\delta-}$ ion-dipole attraction reaches a maximum for $\theta = 180^\circ$ such bonds are enthalpically less favoured in comparison to linear bonds. The pertinent properties of strong, moderate and weak hydrogen bonds as summarised by Jeffrey are shown in Table 1.2.

Table 1.2 Selected properties of strong, moderate and weak hydrogen bonds (Jeffrey, 1997).

	Strong	Moderate	Weak
H-Bond nature	Mostly covalent	Mostly electrostatic	Electrostatic
Bond lengths	$D-H \approx H\cdots A$	$D-H < H\cdots A$	$D-H \ll H\cdots A$
$H\cdots A$ (Å)	1.2-1.5	1.5-2.2	2.2-3.2
$D\cdots A$ (Å)	2.2-2.5	2.5-3.2	3.2-4.0
D-H-A angle θ ($^\circ$)	165-180	130-180	90-150
Energy (kcal mol ⁻¹)	15-45	4-15	< 4
Typical donors	$[=O-H]^+$, $[\equiv N-H]^+$	-O-H, =N-H, P-O-H	C-H, Si-H
Typical acceptors	$[F]^-$, $[-O]^-$, $[P-O]^-$	=O, $\equiv N$, P=O	$C\equiv C$, phenyl
Examples	Charge-assisted $R_3N^+-H\cdots OOCR$	$-O-H\cdots O=$; $-O-H\cdots N\equiv$; $-N-H\cdots O=$; $-N-H\cdots N\equiv$	$C-H\cdots O$; $C-H\cdots N$; $O/N-H\cdots \pi$ -bonds

Two other factors affect the strength of hydrogen bonds: the difference in the energy of association of a proton with the atoms in the gas phase, known as the proton affinities (PA), of the donor and acceptor ($\Delta\text{PA} = \text{PA}_{\text{acceptor}} - \text{PA}_{\text{donor}}$) and by extension their acidity constants ($\Delta\text{pK}_a = \text{pK}_a_{\text{acceptor}} - \text{pK}_a_{\text{donor}}$) (Gilli and Gilli, 2000).

The effect of $\Delta\text{PA}/\Delta\text{pK}_a$ on bond strength can be demonstrated by consideration of homonuclear hydrogen bonds where ΔPA is zero and heteronuclear bonds where ΔPA is variable. Homonuclear $[\text{O}\cdots\text{H}\cdots\text{O}]^+$ and $[\text{O}\cdots\text{H}\cdots\text{O}]^-$ bonds are strong with energies of up to 30-32 kcal mol⁻¹ for $\Delta\text{PA} = 0$ but bond strength decreases significantly to 14 kcal mol⁻¹ when $\Delta\text{PA} = 5$ kcal mol⁻¹ (Meotner and Sieck, 1986). For acid-base hydrogen bonds between organic acids and nitrogen bases the large ΔpK_a s result in generally weak hydrogen bonds with a maximum energy of 25 kcal mol⁻¹ when the pK_a values of the acid and base match (Malarski, *et al.*, 1982).

Strong hydrogen bonds are associated with a small number of chemical arrangements (chemical leitmotifs). Five classes of homonuclear O-H \cdots O hydrogen bonds have been identified: strong positive- and negative-charge-assisted hydrogen bonds, strong resonance assisted (π -cooperative) hydrogen bonds, moderate polarization-assisted (σ -cooperative) hydrogen bonds and weak isolated hydrogen bonds (Gilli, *et al.*, 1994). These classifications appear to be applicable to all homonuclear bonds except resonance-assisted hydrogen bonds that cannot form with non-double-bonding atoms such as halogens (Gilli and Gilli, 2000). Some examples of negative-charge-assisted hydrogen bonds are shown in Figure 1.5. These bonds are strong, linear proton-centred contacts with $d(\text{O}\cdots\text{O}) = 2.38\text{-}2.50$ Å and bond energies of up to 30-31 kcal mol⁻¹.

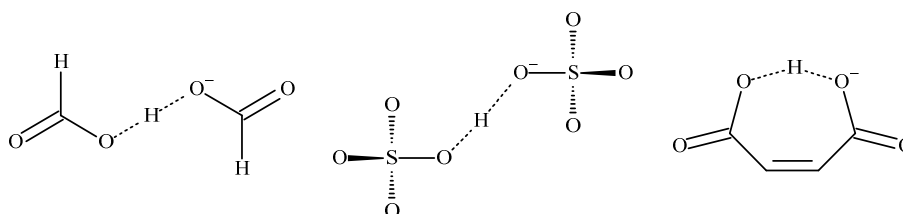


Figure 1.5 Examples of negative charge assisted hydrogen bonds, from left to right hydrogen diformate, hydrogen (bis)sulfate and hydrogen maleate.

1.4.2.2 Etter's Rules

A set of general rules for the packing of hydrogen bonded molecules in crystals were developed by Etter (Etter, 1982, 1990, 1991) as an expansion of Donohue's rule that all acidic hydrogen atoms participate in hydrogen bonding in the solid state (Donohue, 1952). Three of these rules are generally applicable:

- (i) All good acceptors will be used in hydrogen bonding where there are available hydrogen bond donors.
- (ii) If six-membered ring intramolecular hydrogen bonds can form, they will usually do so in preference to forming intermolecular hydrogen bonds.
- (iii) The best proton donors and acceptors remaining after intramolecular hydrogen bond formation form hydrogen bonds to each other.

The rules necessitate the classification of functional groups into reliable and occasional hydrogen bond donors/acceptors as shown in Table 1.3 (Byrn, *et al.*, 1994). These rules are generally regarded as reliable in the case of small molecular systems, however in systems containing larger molecules steric factors can prevent the formation of hydrogen bonds by all the available donor groups (Byrn, *et al.*, 1994).

Table 1.3 Reliable and occasional hydrogen bond donors and acceptors.

Classification	Functional Group
Reliable Donor	-OH (except alcohol), -NH ₂ , -NHR, -CONH ₂ , -CONHR, -COOH
Occasional Donor	-COH, -XH, -SH, -CH (X = halogen)
Reliable Acceptor	-COOH, -CONHCO-, NHCONH-, -CON< (1-3°), >P=O, >S=O, -OH
Occasional Acceptor	>O, -NO ₂ , -CN, -CO, -COOR, -N<, -Cl

1.4.3 Dispersion and repulsion energies

Dispersion or London forces are attractive forces between molecules resulting from the distortion of the electron clouds of the constituent atoms of the molecules. Polarisability increases with molecular volume and the number of π bonds in the molecules and result in stronger intermolecular interactions. The opposing repulsive forces are derived from the Pauli principle that closed-shell molecules cannot accept additional electrons into their doubly occupied molecular orbitals (Gilli, 2006).

1.4.3.1 Kitaigorodskii's Close Packing and Aufbau Principles

Kitaigorodskii's close-packing principle is based on the atom-atom potential method that approximates the total interaction energy between two molecules as sum of those between the constituent atoms. The molecules in a crystal will arrange to minimise the potential energy of the system by packing as tightly as possible in order to maximise the number of attractive intermolecular contacts. The majority of crystal structures therefore belong to space groups with second-order symmetry elements such as glide planes and screw axes as these allow the molecules to pack with the highest coordination number (Gilli, 2006). The complementarity of molecular surfaces where the 'bumps' of one molecules fit the 'hollows' of the adjacent molecules to allow the closest possible molecular packing has long been recognised as a key determinant of the stability of crystal structures (Brock and Dunitz, 1994).

This has led to a quantitative and qualitative approach to examining crystal structures as products of the sequential packing of molecules in favourable one, two and three-dimensional arrangements that has been dubbed Kitaigorodskii's Aufbau Principle (KAP). KAP is considered as a sequence of four stages (Perlstein, 1994), these are shown schematically in Figure 1.6.

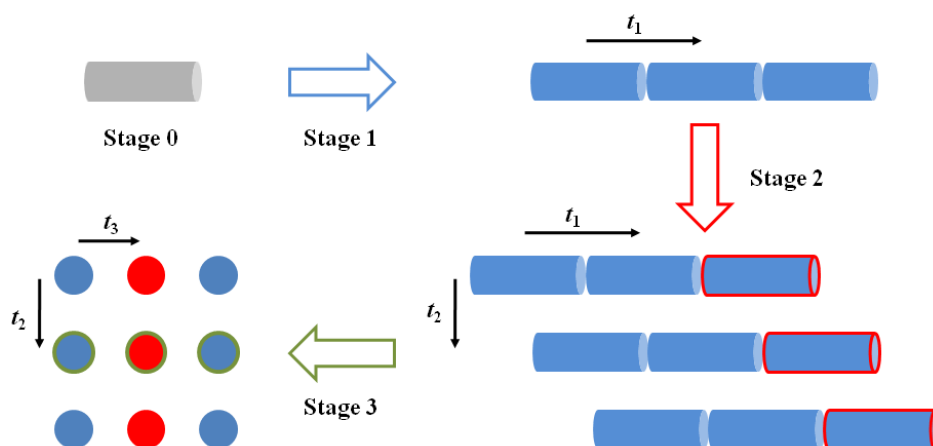


Figure 1.6 Schematic representation of the four stages of supramolecular assembly as described by Kitaigorodskii's Aufbau Principle (KAP) for a finite molecular unit, represented here by a cylinder. The directions of the three translation vectors of the assembly are indicated, after stage 3 t_1 is perpendicular to the plane of the page.

Stage 0: This stage considers single molecules or finite groups of molecules, for example asymmetric units or arrangements with internal symmetry such as cyclic trimers or hexamers.

Stage 1: The stage 0 molecules are arranged into an infinite one-dimensional stack with a single translational repeat distance (t_1). The most significant arrangements are the four that allow close packing: translation, glide, 2_1 screw and inversion stacks.

Stage 2: Stage 1 stacks are brought together to form a 2-dimensional monolayer with two translational repeat distances (t_1 and t_2). The first translation is along the direction of the stage 1 stacks while the second is along a direction determined by the relative coupling of the stacks.

Stage 3: The assembly of the full 3-dimensional crystal structure by the combination of stage 2 monolayers to generate a third translation repeat vector (t_3).

1.4.3.2 Application of KAP to crystal structure analysis

Gavezzotti demonstrated that KAP and Etter's first rule are not mutually exclusive as KAP is obeyed in the majority of organic molecular crystals that feature intermolecular hydrogen bonds (Gavezzotti and Filippini, 1994). It is therefore possible to utilise KAP in qualitative analyses of the hydrogen-bonded structures formed in organic molecular crystals and the relative importance of H-bond and packing effects in determining the supramolecular structure adopted.

An analysis of the vector properties of hydrogen bonding in crystal engineering by Perlstein *et al* compared the number of stages of KAP applied to the supramolecular assemblies that included hydrogen bonds along the stage vector across structures deposited in the CSD. The majority of the structures could be described by one of the 16 subtypes of the four hydrogen-bonded arrays listed in Table 1.4. This allows a qualitative assessment of the relative influences of hydrogen bonding and non-directional interactions in determining the supramolecular structure. KAP stages that lack a hydrogen bond vector along its axis are instead supported by non-directional interactions and packing effects (Perlstein, *et al.*, 1996).

Table 1.4 The 16 possible hydrogen-bonded vector types and subtypes as determined by the application of Kitaigorodskii's Aufbau Principle (Perlstein, *et al.*, 1996).

Type	KAP Stages	Subtype Notation	H-Bond description
0		0	No hydrogen bonds present
1			H-bond vector present in one stage only
	0	1 ₀	Intramolecular H-bond or intermolecular H-bond for a finite group of molecules.
	1	1 ₁	H-bond occurs in chain structure (intrachain), typically with translation, screw, glide or inversion symmetry.
	2	1 ₂	A vector which couples stage 1 chains (interchain) to make a layer, usually one of seven layer types.
	3	1 ₃	H-bond occurs between layers only (interlayer)
2			H-bond vector present only in two stages
	0,1	2 ₀₁	Simultaneous intramolecular and intrachain vectors
	0,2	2 ₀₂	Intramolecular and interchain vectors making layers
	0,3	2 ₀₃	Intramolecular and interlayer vectors only
	1,2	2 ₁₂	Only intrachain and intralayer vectors present
	1,3	2 ₁₃	Only intrachain and interlayer vectors present
	2,3	2 ₂₃	Only intralayer and interlayer vectors present
3			H-bond vectors occurring in three stages
	0,1,2	3 ₀₁₂	Intramolecular H-bonds and intrachain and intralayer vectors
	0,1,3	3 ₀₁₃	Intramolecular H-bonds and intrachain and interlayer vectors
	0,2,3	3 ₀₂₃	Intramolecular H-bonds and intralayer and interlayer vectors
	1,2,3	3 ₁₂₃	No intramolecular H-bonds but H-bonds in all other stages
4	0,1,2,3	4 ₀₁₂₃	H-bond vector occurring in all four stages

1.4.4 Other anisotropic interactions

Short non-bonded interactions are formed between halogen atoms such as Cl, Br and I with distinctive geometries from symmetrical (Cl-Cl) to asymmetric (Cl-Br) as a result of atomic polarisation. There is debate as to whether the interaction is a result of anisotropy (Price, *et al.*, 1994) or a unique type of intermolecular interaction between the atoms in the crystal (Desiraju and Parthasarathy, 1989).

In aromatic systems, the C-H bonds are slightly polarised to produce a small positive charge on the hydrogen atom and a corresponding negative charge on the π -bonded core. This results in dispersion effects from π - π interactions between aromatic groups on neighbouring molecules with a directional electrostatic component because the polarisation makes the interaction anisotropic.

1.5 pKa and ionisation state

The pKa of an acid is the negative logarithm of the dissociation constant and is commonly used as a predictor of the ionisation states of molecules in the solid state (Stanton and Bak, 2008). The generally accepted principle is that salt formation will occur for acid-base combinations with ΔpKa ($\text{pKa}_{\text{base}} - \text{pKa}_{\text{acid}}$) > 3 as both species will exist predominantly as ions at the equilibrium pH (Black *et al.*, 2007). Cocrystal formation is expected for acid-base combinations where $\Delta\text{pKa} \approx 0$, in effect making salts and cocrystals two extremes of a continuum for the position of ionisable protons in the solid state. There are several examples of proton migration on changing temperature altering the ionisation state of both cocrystals and salts (Steiner, *et al.*, 2001; Wilson, 2001). As measured pKa values relate to species at equilibrium in aqueous solutions they can be altered by several factors including temperature and solvent. As changing the solvent can increase the pKa of an acid this has a more marked effect on ΔpKa for systems with weak acids than strong acids (Black *et al.*, 2007).

For acid-base combinations where $0 < \Delta\text{pKa} < 3$ the pKa difference does not reliably predict the ionisation state of the crystalline system, in this case a salt, cocrystal or disordered solid can be formed with the position of the acidic proton determined by the crystal packing environment (Mohamed, *et al.*, 2009a). Ionisation state can be dependent on acid-base stoichiometry in the solid state, for example 2,3-lutidine and fumaric acid can crystallise as a 2:1 cocrystal or 1:1 salt (Haynes, *et al.*, 2006), or the chain length of aliphatic dicarboxylic acid counterions (Braga, *et al.*, 2003).

1.6 Crystal engineering

Crystal engineering is the rational design of molecular solids with desired physical properties for specific applications based on “*the understanding of intermolecular interactions in the context of crystal packing and in the utilisation of such understanding in the design of new solids with desired physical and chemical properties*” (Desiraju, 1989). Supramolecular synthesis is the construction of such assemblies and is based on the philosophy that the relationship between a supermolecule and its constituent molecules is analogous to the relationship between an intermolecular interaction and a covalent bond (Lehn, 1988). The understanding and control of intermolecular interactions is as important in this case as that of the covalent bond in traditional chemical synthesis (Dunitz, 1991). In covalent synthesis, the products are kinetically stable and their bonds are characterised by their enthalpies. In supramolecular synthesis the structures of the products reflect a necessary balance between enthalpic and entropic contributions (Whitesides, *et al.*, 1995). The structures are based on supramolecular synthons that incorporate the intermolecular interactions and molecular structure that describe the supermolecule that can be treated as approximations of the overall crystal structure (Desiraju, 2007).

The supramolecular structure of a crystalline solid cannot be predicted from the molecular structure of its constituent molecules, nor can its properties as these are an emergent feature on crystallisation (Desiraju, 2005). It is instead necessary to identify supramolecular synthons that will occur reliably in a structure if its constituent molecules feature a particular functional group, ideally even if the molecule contains other functionalities. In practice, the correspondence between molecular and crystal structure is not obvious due to several factors. These include the disproportionately large increase in possible synthons that can result from a small increase in the functionality of a molecule; unpredictable and unreliable interference from remote functional groups on the intermolecular interactions of the synthon and the interference of the hydrocarbon core of molecules with the directional interactions from polar functional groups (Desiraju, 2007). The examination of large libraries of related crystal structures is therefore necessary to identify robust supramolecular synthons (Kuduva, *et al.*, 1999).

1.6.1 Growth synthons and crystal nucleation

The relationship between supramolecular synthons observed in crystal structures and the growth unit of crystal nucleation has only recently become an area of active research. Davey *et al* have used the examination of recurrent supramolecular interactions in related crystal structures as an approach to understanding the structural elements of the assembly process in crystallisation and the factors controlling them. The effect of solvent properties and solution behaviour on the crystallisation of several systems was examined (Davey, *et al.*, 2002).

For example, twinned crystals are the frequent result of the crystallisation of saccharin from low supersaturations in acetone but are rare for high supersaturations in ethanol. In acetone solution, the saccharin exists as solvated monomers while in ethanolic solutions a mixture of monomers and dimers was observed. All the twins were symmetric, indicating that twinning occurred only at the point of nucleation and was favoured by the presence of monomeric saccharin in solution. This observation was rationalised by the different functional groups accessible on the crystal nucleus. The crystallisation of monomers was shown to leave exposed hydrogen bonding groups while dimers crystallised to leave non-polar phenyl rings at the surface, inhibiting the formation of the twin.

Sulfathiazole is a chiral molecule that crystallises in five polymorphic forms. Form I, the least stable, is based on racemic R₂,2(8) α -dimers while forms II–IV contain enantiomeric R₂,2(8) β -dimers and V is based on R₃,3(10) rings. In aqueous suspensions, sulfathiazole sequentially transforms from form I to form IV in 24 hours whereas in propanol form I is stable for at least one year. In water, both the α -dimer and β -dimer can build nuclei but in propanol, the solvent molecules bind to the dimers and sterically hinder the formation of the β -dimer.

These examples illustrate the applicability of the information that can be derived from the study of supramolecular synthons to understanding the nucleation and growth processes of crystals. In the above case, the important factors in determining the viability of the crystal structures were the flexibility of dimeric units as building blocks and the effect of solvent-solute interactions.

1.6.2 Crystal engineering and the design of pharmaceutical cocrystals

The generation of cocrystals of pharmaceutically active molecules offers a potential route to optimising their physicochemical properties in a manner analogous to salt formation and is an area of active research (Almarsson and Zaworotko, 2004). A key difference between the design parameters for cocrystals and salts for molecules containing an ionisable group is that there is no ΔpK_a criterion for cocrystal formation as a neutral hydrogen bonded system is targeted. The relative acid and base strengths of the components in cocrystal systems may determine their relative stabilities, for example in a series of carboxylic acid cocrystals of caffeine those formed with the strongest and weakest acids were found to be the most and least stable towards hydration. A polymorph of the weakest acid cocrystal had intermediate stability, indicating that structural factors also determined the cocrystal stability (Trask, *et al.*, 2005).

The design strategy for pharmaceutical cocrystals is based on the identification of potential hydrogen bonded supramolecular synthons that can be formed between the pharmaceutical molecule and the cocrystal formers. A good cocrystallising agent is one that will form stronger and more stable heteromeric hydrogen bonds to the pharmaceutical molecule than the corresponding homomeric bonds in the two species. Species that are polymorphic in their native state are believed to be more effective cocrystal formers due to their flexibility in forming intermolecular hydrogen bonded synthons (Aakeroy, *et al.*, 2003).

The identification of robust synthons for combinations of functional groups and their hierarchies in a multi-functional system can enable the rational design of cocrystals. Examples include the identification of consistent hydrogen and halogen bonded synthons in the formation of *iso*-nicotinamide cocrystals with iodine and tetrafluorodiodobenzene (Aakeroy, *et al.*, 2007a) and a screen of hydroxybenzoic acid cocrystals of caffeine that generated nine novel cocrystals (Bucar *et al.*, 2009). An example of a robust heterosynthon used in cocrystal design is the carboxylic acid-pyridine heterosynthon (Du, *et al.*, 2006) and this was used in a proof-of-concept study to direct the formation of model pyridine cocrystals of ibuprofen and aspirin (Walsh, *et al.*, 2003).

1.6.3 Issues confronting salt systems

Salt formation is analogous to the formation of cocrystals but the proton transfer results in the replacement of a neutral bond by its charge-assisted equivalent. For example, the formation of a strong neutral hydrogen bond between a carboxylic acid and an N-heterocyclic acceptor is a key interaction in cocrystal formation (Aakeroy, *et al.*, 2006) but proton transfer can occur to form a salt (Banerjee, *et al.*, 2005).

In a study by Aakeröy *et al* the “expected outcome” of cocrystallisation of two species was the likely stoichiometric ratio from the number of mutually complementary hydrogen bonding groups present on the molecules. Of 61 cocrystals the expected stoichiometry was observed in 58 with the remaining three forming cocrystal solvates. In contrast, only 13 of 24 salts displayed the expected stoichiometry with replacement of the neutral O-H \cdots N interaction with a charge-assisted O \cdots H-N⁺ hydrogen bond. Two of the salts were ethanol solvates and the remaining nine incorporated a free carboxylic acid molecule into the crystal lattice. This significantly alters the intermolecular interactions, making the estimation of the composition and structure of the salt unreliable (Aakeroy, *et al.*, 2007b).

As discussed previously the formation of a salt as opposed to a cocrystal can be unpredictable and dependent on the reaction conditions. The acid-base stoichiometry can determine if a cocrystal or salt is formed (Wiechert and Mootz, 1999) and the stoichiometry of a salt can vary depending on the preparation method used (Andre, *et al.*, 2009). However, the creation and analysis of systematic series of molecular salts has enabled the identification of robust structural features for specific types of molecule. A recent and pertinent example is the systematic study of dicarboxylic acid salts of imidazolium derivatives initiated by MacDonald *et al* (MacDonald, *et al.*, 2001) with the characterisation of four dicarboxylic acid salts of imidazoles. This has been greatly expanded by studies by Callear *et al* (Callear, *et al.*, 2010) of substituted imidazolium salts with aliphatic dicarboxylic counterions. In these studies, the crystalline salts formed three types of hydrogen-bonded substructure (acid-base or acid-acid chains or no chains). As expected, the degree of diprotonation of the acid was not determined solely by ΔpK_a and the stoichiometry of the multi-component system was independent of the initial ratio of the species in solution.

1.7 Systematic structural analysis

The identification of robust and reproducible solid-state architectures is necessary to develop an understanding of the relationship between molecular structure and properties and the supramolecular structures of the crystalline systems. The reduction in data collection times offered by area detectors in modern single-crystal X-ray diffractometers has enabled the rapid characterisation and compilation of large libraries of structures. These afford a resource for knowledge generation that will lead to new approaches to understanding the factors that influence supramolecular structure. Numerous cheminformetric approaches have been developed to extract meaningful information from these libraries.

1.7.1 The Cambridge Structural Database System

The Cambridge Structural Database was established in 1965 to provide a comprehensive database of structural information on small-molecule crystal structures containing a maximum of 500 non-hydrogen atoms including organic and metal-organic systems. (Allen, 2002) It has become an important resource for investigations into organic chemistry and crystal chemistry (Allen and Motherwell, 2002), inorganic chemistry (Orpen, 2002) and drug design (Taylor, 2002).

Numerous studies have been undertaken using the information contained in the database to examine different aspects of crystal formation and structure pertinent to crystal engineering. These include solvate and hydrate formation (Gillon, *et al.*, 2003); the variation in molecular conformations of molecules in different crystal environments (Weng, *et al.*, 2008) and the probabilities of formation of hydrogen bonded contacts for functional groups (Infantes and Motherwell, 2004), synthon competition (Haynes, *et al.*, 2004) and the effect of hydrogen bonding contacts on molecular packing arrangements (Pidcock and Motherwell, 2005).

1.7.1.1 Associated software

PreQuest is used to incorporate structures into both the main CSD and “in-house” databases and generates the two-dimensional diagrams used by the ConQuest search program. The diagrams are generated automatically from the three-dimensional information in the CIF file or created by the user using a 2-D drawing program. The crystal data is checked against the specified chemical formula and the connectivity in the two-dimensional diagram is verified against that calculated from the three-dimensional data (Motherwell, *et al.*, 2009).

Database searches are performed via a graphical user interface by the ConQuest program. A drawing tool is used to construct searches for two- and three-dimensional molecular substructures and non-bonded contacts and several queries can be combined into a single search. Geometric features including torsion angles and non-bonded contacts can be defined and used in the search. The search results are viewed using a three-dimensional visualiser including basic functions such as atom labelling, the display of unit cell contents and geometric parameters. The data can be output to Vista or Microsoft Excel for statistical analysis (Bruno, *et al.*, 2002).

A visualisation program with increased functionality, Mercury, can interface directly with the CSD database. An important function is the location and expansion of hydrogen bonded contacts to visualise hydrogen-bonded networks in crystal structures. The criteria for detecting hydrogen bonds are user-defined and include amine-carboxylate contacts, intramolecular hydrogen bonds and Cl...O contacts (Bruno *et al.*, 2002). Updates improved the graphical display and enabled the overlay of multiple structures and calculation of powder diffraction patterns (Macrae, *et al.*, 2006). The Mercury CSD 2.0 release incorporates a Materials Module allowing searches for specified intermolecular interactions between functional groups (motifs) and crystal packing features defined as atomic arrangements (Macrae, *et al.*, 2008). A packing similarity calculation function derived from the COMPACK program (Chisholm and Motherwell, 2005) has also been incorporated to enable the comparison of molecular packing arrangements in structures. This module was employed to study the hydrogen bonding motifs and packing arrangements of 50 crystal structures containing carbamazepine (Childs, *et al.*, 2009).

1.7.2 XPac

The XPac program was developed by Gelbrich and Hursthouse to identify sub-components of crystal structures that consist of similar types of molecules with a common spatial arrangement. This allows the identification of assemblies of molecules that are a result of more diffuse interactions than hydrogen bonds, entities such as close packing that are difficult to detect specifically in the structure. These common molecular assemblies have been termed “*supramolecular constructs*” and can indicate preferences in crystal nucleation and growth, with robust assemblies providing a potential starting point for the directed assembly of particular structures (Gelbrich and Hursthouse, 2005).

The program identifies similarities between components of two or more crystal structures as a function of the geometrical similarity of the configuration of atoms in each structure rather than by considering similar intermolecular connectivity. The method is independent of conventional crystallographic descriptors such as space groups, asymmetric units and number of crystallographically independent molecules to enable the direct comparison of molecular arrangements in the structures. A brief outline is derived here from the more detailed explanation by Gelbrich and Hursthouse (Gelbrich and Hursthouse, 2005).

1.7.2.1 Principle of the method

Each molecule in the crystal structure is surrounded by a sphere of closest neighbour molecules, forming a cluster centred on the kernel molecule surrounded by the shell molecules. The numbers of crystallographically independent clusters in the structure is therefore the same as the number of crystallographically independent molecules in the structure and are generated from the symmetry operators, unit cell parameters and atomic coordinates. Any crystal structure can be considered a combination of sub-assemblies of molecules that can range from discrete combinations of molecules to three-dimensional assemblies, each of which can be represented by a cluster containing the kernel molecule in combination with one or more shell molecules to give the seed of any particular arrangement. Two crystal structures contain a similar

molecular sub-assembly therefore contain similar seeds that can be identified by comparing the clusters in the two structures. (Gelbrich and Hursthouse, 2005)

The geometry of a molecule can be described by set of three or more ordered points, p , corresponding to the positions of atoms P_i in the structure:

$$p = \{P_1, P_2, P_3, \dots, P_n\}$$

a second ordered set of points, p' , can describe a molecule with a similar structure,

$$p' = \{P'_1, P'_2, P'_3, \dots, P'_n\}$$

if p and p' represent two sets of points in the same order they are regarded as a **corresponding ordered set of points** (COSP) and the consistency between two structures tested by comparison of a representative list of internal coordinates including distances, angles and torsion angles. The mean difference δ for the intramolecular angles generated by N pairs of corresponding points x_i and x'_i can be calculated to give an indication of the consistency of the COSPs:

$$\delta = \frac{1}{N} \sum_{i=1}^N |x_i - x'_i|$$

If the points selected are suitable COSPs then δ will be close to 0° and is used by XPac as a consistency check for the COSPs under investigation.

A cluster of molecules centred on one OSP representing kernel molecule p surrounded by k OSPs for the shell molecules generated by applying symmetry operations on p can be compared with a cluster in a second structure of OSP p' with k' symmetry generated OSPs when p and p' are COSPs. By identifying similar cluster sub-units in two or more structures centred on the kernel molecules with s shell molecules the seed of a supramolecular construct can be generated. Each seed is composed of **triple sub-units** comprising one kernel and two shell molecules and a common supramolecular construct is observed in structures where the corresponding triple sub-unit seeds are similar.

The search method first compares two clusters for similar *double sub-units* formed by the kernel molecule and one shell molecule that are then combined to form triple sub-units and their similarity between the two structures is evaluated. Similar triple sub-units are the seeds of the supramolecular construct characterised using the crystallographic information contained in the seed.

The similarity of double and triple sub units can be established by comparing lists of intermolecular angles, dihedral angles and torsion angles to detect similarity based on the preservation of angular relationships between molecules instead of distance. The mean absolute difference in intermolecular angles δ_{ang} , dihedral angles δ_{dhd} and torsion angles δ_{tor} for each pair of lists is calculated using equation (3) and compared to a set of filter parameters f_{ang} , f_{dhd} and f_{tor} that can be set according to the desired sensitivity of the similarity search as shown in Table 1.5.

Table 1.5 The three tolerance limits for the filter parameters in the intermolecular angles, dihedral angles and torsion angles in XPac.

Tolerance	f_{ang}	f_{dhd}	f_{tor}
Low	7	13	13
Medium	10	18	18
High	12	25	25

When the geometry of supramolecular constructs is nearly identical δ_{dhd} is usually 2.5 times the size of δ_{ang} and δ_{tor} is 2 times the size of δ_{ang} while δ_{ang} is 1.6 times the size as the consistency index δ_{con} . These relative magnitudes can be used to calculate a dissimilarity index Δ between two isostructural supramolecular constructs (Fabbiani, *et al.*, 2009; Hursthouse, *et al.*, 2010).

$$\Delta = 1/3 (\bar{\delta}_{\text{ang}} + \bar{\delta}_{\text{dhd}}/2.5 + \bar{\delta}_{\text{tor}}/2)$$

The dissimilarity index can give a convenient quantitative assessment of the effect of changing aspects of molecular structure on the degree of isostructurality between pseudoisostructural structures, with a larger dissimilarity index indicating a greater perturbation from isostructurality (Hursthouse, *et al.*, 2010).

1.7.2.2 Case examples

A case study of 25 crystal structures of carbamazepine and two analogues including 19 multi-component systems gave new information on the importance of molecular shape and packing patterns in defining the supramolecular structures of these systems. 24 of the 25 structures were shown to be based on one of two dominant motifs that were alternative close-packing arrangements of the V-shaped azepine ring moiety. Four primary supramolecular constructs were identified, three of which were stacks of molecules related by translation and one was a hydrogen-bonded dimer. Two stacks were based on the close-packing motifs and as a result were mutually exclusive. The packing arrangements did not contain hydrogen bonds but were preserved within different hydrogen bonded networks, demonstrating the importance of molecular packing in determining crystal structure (Gelbrich and Hursthouse, 2006).

An examination of five polymorphs of the antimicrobial compound sulfathiazole was performed to complement previous studies on the interrelationships between the polymorphs that focused on hydrogen bonding arrangements. Seven picryl-*p*-toluidine polymorphs and solvates were shown to be based on a common 1-dimensional chain of molecules that was not correlated to a significant intermolecular interaction and had a high degree of variability in the length of the translation vector between the molecules in the chain (Braun, *et al.*, 2008a).

Conformational flexibility in molecules can pose a challenge for the method as changes in molecular geometry prevents the selection of COSPs, in these cases a rigid substructure of the molecules may be selected for comparison. One example was a study of nine crystal structures of apiprazole, due to flexible molecular structure only three structures could be compared using a “whole molecule” set of COSPs. One part of the molecule containing functional groups that direct intermolecular hydrogen bond formation were selected instead, in contrast to the carbamazepine study the two groups of structures identified were based on intermolecular hydrogen bonds rather than packing effects (Braun, *et al.*, 2009).

1.7.3 Hirshfeld surface analysis: Crystal Explorer

Crystal Explorer was developed to allow the simultaneous examination of all the interactions between molecules in a crystal structure to enable the visualisation and comparison of the intermolecular interactions and crystal packing in different structures (Spackman and McKinnon, 2002). The method uses an extension of the Hirshfeld stockholder partitioning scheme to divide the crystalline electron density into molecular fragments (Spackman and Byrom, 1997). The original partitioning scheme was developed to extract molecular fragments from the electron density of the crystal through adapting the application of the molecular weight function originally proposed by Hirshfeld.

$$\omega(\mathbf{r}) = \rho_{\text{promolecule}}(\mathbf{r}) / \rho_{\text{procrystal}}(\mathbf{r}) = \frac{\sum_{i \in \text{molecule}} \rho_i(\mathbf{r})}{\sum_{i \in \text{crystal}} \rho_i(\mathbf{r})}$$

The Hirshfeld surface is defined as the point at which the weight function $\omega(\mathbf{r}) = 0.5$, where $\omega(\mathbf{r})$ is the sum of the spherical electron densities of the atoms in the molecule under examination ($\rho_{\text{promolecule}}$) divided by the sum for the surrounding crystal ($\rho_{\text{procrystal}}$). In effect inside the Hirshfeld surface, the spherical atomic electron distribution $\rho_i(\mathbf{r})$ for the i th nucleus has a greater contribution from the promolecule than from the surrounding molecules in the crystal structure. At each point on the surface the distance to the closest atoms internal (d_i) and external (d_e) to the surface can be easily defined (McKinnon, *et al.*, 2004).

Crystal Explorer uses this method to generate a two-dimensional fingerprint plot of the interactions between a promolecule and the surrounding crystal structure. First, the Hirshfeld surface is calculated from the information contained in the CIF file and both d_i and d_e are calculated for each surface point as shown in Figure 1.7.

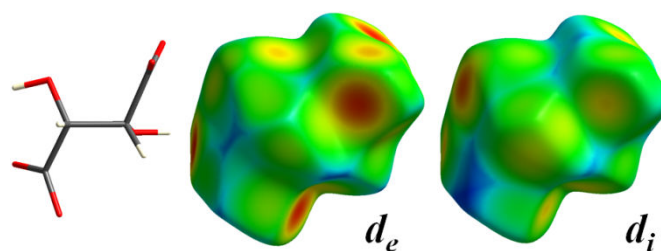


Figure 1.7 Hirshfeld surfaces for the L-tartrate anion in 1-methylpiperazinium L-tartrate monohydrate with d_i and d_e mapped in colours corresponding to the closeness of the contacts with the atoms. Red areas show the closest contacts and the most distant contacts are coloured blue.

In order to enable a visual evaluation of the Hirshfeld surface d_i and d_e are calculated simultaneously for each surface point and then binned into intervals of d_i and d_e with a width of 0.01\AA and plotted as a 2-D graph as shown in Figure 1.8. The graph can also be set to highlight contacts to defined atom types both internal and external to the surface.

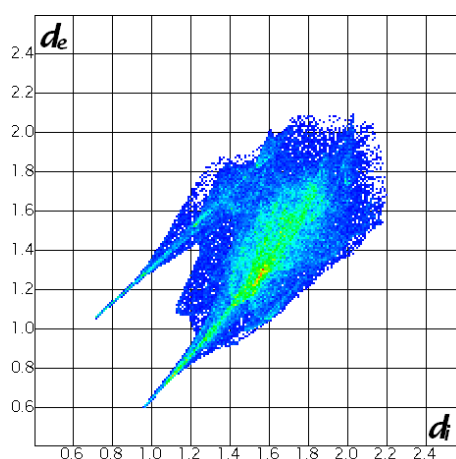


Figure 1.8 A 2-D fingerprint plot produced for the L-tartrate anion in 1-methylpiperazinium L-tartrate monohydrate from the d_i and d_e surfaces shown above in Figure 1.7. Each point corresponds to a 0.01\AA bin width of both d_i and d_e and are coloured according to the number of points in each bin from relatively few points (blue) to many points (red).

Particularly notable features of Hirshfeld fingerprint plots are the sharp features corresponding to short d_i and d_e contacts that are indicative of hydrogen bonds, with the point where $d_i > d_e$ and $d_e > d_i$ corresponding to hydrogen bond acceptors and donors respectively (Spackman and McKinnon, 2002).

1.7.3.1 Application in crystal structure analysis

Crystal Explorer has been widely applied in the examination of intermolecular interactions in crystal structures and in some cases has been employed as a complementary technique to XPac. A comparison of the Hirshfeld surfaces of the stable Form I and metastable Form II of aprepitant showed small differences in the intermolecular interaction environments, indicating that 80% of the nearest-neighbour contacts were the same. This was consistent with the two-dimensional packing similarity identified by the XPac analysis that resulted from similar intermolecular interactions. The differences in physical properties were therefore a result of differences in the packing arrangements instead of the intermolecular interactions (Braun, *et al.*, 2008b).

In a study of nine forms of apiprazole the fingerprint plots showed common spikes corresponding to the N-H \cdots O interactions between the apiprazole molecules in the polymorphs and solvate structures, additional interactions in the solvates and different interactions in the hydrate. The information in the plots correlated to the relative stabilities of the solvates as the longer *di* and *de* for the C-H \cdots N contacts were considered to indicate weaker interactions, which was confirmed by TGA. An increased number of longer contacts in a structure indicated less efficient packing and corresponded to the calculated densities of the solvates (Braun, *et al.*, 2009).

Dendrograms showing the degree of similarity between different crystal structures can be obtained from cluster analysis of their Hirshfeld surfaces using PolySNAP. (Barr *et al.*, 2004) This technique has been termed “*structural genetic fingerprinting*” and a proof of concept study calculated a numerical correlation coefficient between the crystal structures of related molecules and enabled a quantitative comparison of their similarities (Parkin, *et al.*, 2007).

This thesis is concerned with applying some of these tools to the examination of a library of crystalline multi-component systems to identify robust hydrogen bonded synthons and packing arrangements. This information will be used to rationalise aspects of crystalline salt formation and structure as an outcome of both molecular and supramolecular structure and properties.

Chapter 2

Aims and Objectives

2.1 Aims

The aim of this project is to develop an improved understanding of the structural factors that determine the success of crystalline salt formation for acid counterions used in pharmaceutical salt selection studies. A bespoke library of related crystal structures is presented and the occurrence of supramolecular structural features is investigated to evaluate their importance in crystalline salt formation. The data generated is used to propose a novel series of structural rules geared towards enhancing understanding of salt formation and the reliability of salt selection studies for new pharmaceuticals.

2.2 Objectives

2.2.1. Crystallise a library of pharmaceutically acceptable acid counterions with a systematic series of model bases and characterise the products by single-crystal X-ray diffraction (SXRD) to generate a library of related crystalline structures.

2.2.2. Compile the structures into a searchable database and utilise structure analysis tools to identify information on supramolecular structural features including hydrogen bonding motifs, molecular packing arrangements and acid-base stoichiometry.

2.2.3. Relate the supramolecular structural features to the ionisation state of the system and correlate them with the molecular structures of the species. Rationalise crystalline salt formation as an outcome of molecular and supramolecular structures and pKa.

2.2.4. Assess the frequency of occurrence of hydrated systems in relation to the molecular structures of the acidic and basic species and investigate the role of water in defining and propagating the supramolecular structure.

2.2.5. Validate the trends and correlations observed by examining a series of salts of more complex pharmaceutically active molecules containing similar basic functional groups to the species in the initial library.

Chapter 3

Materials and Methods

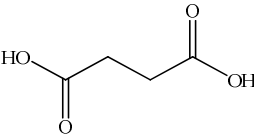
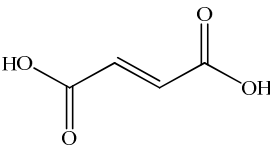
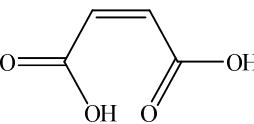
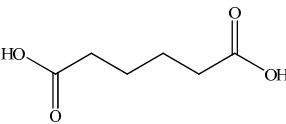
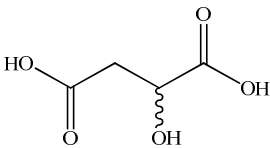
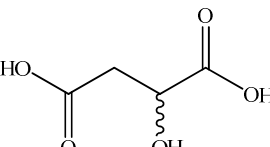
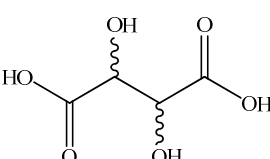
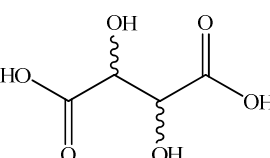
3.1 Materials

All the materials used in this work were commercially available reagents obtained from Sigma-Aldrich or Fluka and used as supplied, with the exception of the 1,4-ethanedisulfonic acid monohydrate that was obtained from Alfa Aesar. The acid counterions are listed in Table 3.1, the model bases used to construct the initial database are listed in Table 3.2 and the pharmaceutically active molecules studied are shown in Table 3.3.

With the exception of salicylic acid the counterions examined in this work satisfy the criteria to be generally regarded as safe (GRAS) for use in pharmaceutical formulations set by the US Food and Drug Administration (FDA, 2007). Crystal structures for the majority of the acids can be found on the Cambridge Structural Database (Allen, 2002) and the pKa values for the first and second ionisations were calculated using the ACD/pKa DB software to allow the ionisation states of the acid molecules in the crystalline structures to be evaluated relative to this property (ACD Labs, 1999). The acid molecules exhibit systematic changes in their molecular structures including the number and type of ionisable groups, additional hydrogen bond donor and acceptor groups, aliphatic chain length and flexibility and stereochemistry in order to investigate the effect these molecular properties have on ionisation state and supramolecular structure in the crystalline systems.

The library of simple cyclic amine bases was selected to model the functional groups found on complex pharmaceutically active molecules. With the exception of piperazine, these are all liquids at standard temperature and pressure. They have similar molecular size and geometry and vary in the pKa values, calculated using the ACD/pKa DB software, number of potential protonation sites, number of hydrogen bond donor and acceptor groups and steric bulk of substituent groups. The pharmaceutically active molecules that were used to validate the trends observed in the initial database contain a piperazinyl ring as the ionisable moiety. Six fluoroquinolone antibiotics were studied along with the antidepressant drug Amoxapine.

Table 3.1 The acidic counterions selected for examination in this work including their molecular weights (MW), melting points and pKa values calculated using ACD/pKa DB version 4.04 software.

Acid	Molecular Structure	MW	Melting Point °C	pKa ₁	pKa ₂
Succinic Acid		118.09	185-187	4.39	5.13
Fumaric Acid		116.07	287	3.15	4.79
Maleic Acid		116.07	131-139	1.83	6.07
Adipic Acid		146.12	152	4.43	5.41
L-Malic Acid		134.09	130	3.61	4.82
DL-Malic Acid		134.09	130	3.61	4.82
L-Tartaric Acid		150.09	170-172	3.07	4.35
DL-Tartaric Acid		150.09	170-172	3.07	4.35

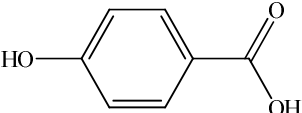
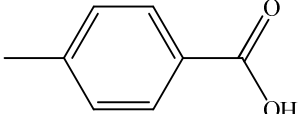
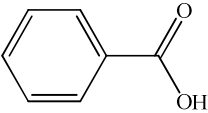
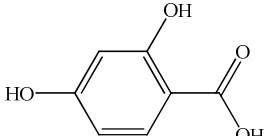
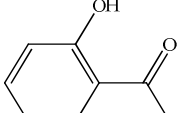
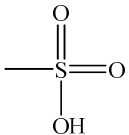
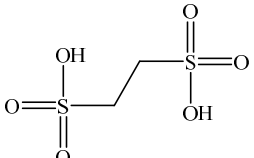
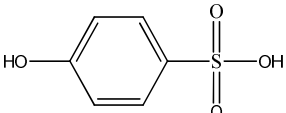
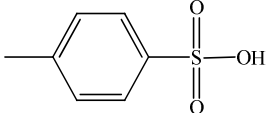
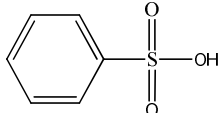
Acid	Molecular Structure	MW	Melting Point °C	pKa ₁	pKa ₂
4-Hydroxybenzoic Acid		138.12	214-217	4.57	N/A
4-Methylbenzoic Acid		136.15	177-180	4.37	N/A
Benzoic Acid		122.12	122	4.20	N/A
2,4-Dihydroxybenzoic Acid		154.12	225-227	3.32	N/A
Salicylic Acid		138.12	159	3.01	N/A
Methanesulfonic Acid		96.106	17-19	1.75	N/A
Ethanedisulfonic Acid		190.20	109-113	-2.89	-1.49
4-Hydroxybenzenesulfonic Acid		174.17	6.4	-0.23	N/A
4-Toluenesulfonic Acid		172.21	106-107	-0.43	N/A
Benzenesulfonic Acid		158.18	51	-0.60	N/A

Table 3.2 The model bases crystallised with the acidic counterions in this work including their molecular weights (MW), melting points and calculated pKa values from ACD pKa DB 4.0 software.

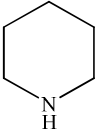
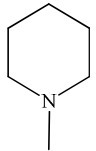
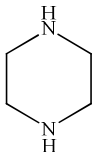
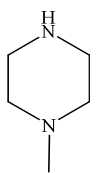
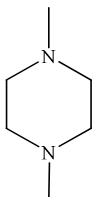
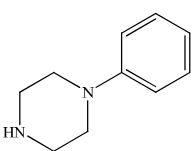
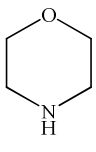
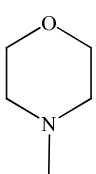
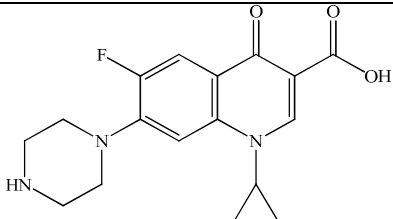
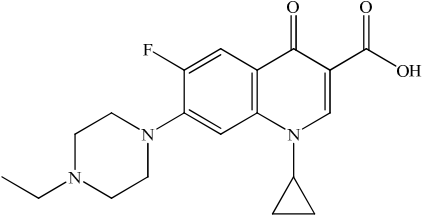
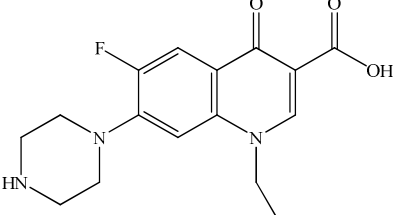
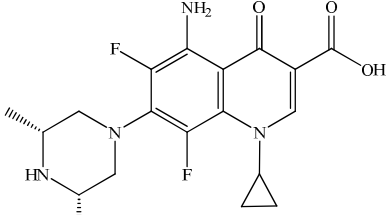
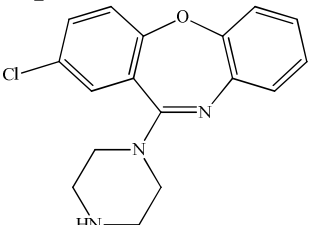
Compound	Molecular Structure	MW	Melting Point °C	pKa ₁	pKa ₂
Piperidine		85.15	N/A	11.24	N/A
1-Methylpiperidine		99.17	N/A	9.91	N/A
Piperazine		86.14	106	9.90	5.30
1-Methylpiperazine		100.16	N/A	9.65	4.35
1,4-Dimethylpiperazine		114.19	N/A	8.26	4.08
4-Phenylpiperazine		162.23	N/A	8.94	5.22
Morpholine		87.10	N/A	8.97	N/A
4-Methylmorpholine		101.15	N/A	7.41	N/A

Table 3.3 The pharmaceutically active molecules crystallised with the acidic counterions in this work including their molecular weights (MW), melting points and calculated pKa values from ACD pKa DB 4.0 software.

Compound	Molecular Structure	MW	Melting Point °C	pKa
Ciprofloxacin		331.346	255-257	8.76
Enrofloxacin		359.40	220-224	7.11
Norfloxacin		319.331	227-228	8.76
Sparfloxacin		392.41	266-269	7.16
Amoxapine		313.781	175.5	8.03

* pKa values quoted are for the secondary amine nitrogen in the piperiznyl ring moiety with the exception of enrofloxacin, in which case the value is for the equivalent tertiary amine nitrogen.

3.2 Synthesis of salts and crystal growth

3.2.1 Evaporative crystallisation

Unless otherwise stated in the text the following method was used for the crystallisation of the acid counterions with the model bases given in Table 3.2. Approximately 10g of acid was added to water at room temperature and the base added drop wise to give a 1.1:1.0 acid: base molar ratio. If a clear solution was not obtained additional water was added until the majority of the excess material had dissolved. The solution was filtered into an evaporating basin or test tube and left to stand in a fume hood at ambient temperature until crystallisation occurred. If no crystallisation was observed after 3 weeks the solution was placed in a fridge to attempt to induce crystallisation.

3.2.2 Crystallisation by slow diffusion

1-2cm³ samples of solutions that failed to give crystalline products after one month were placed in sample vials and sealed inside jars containing ethyl acetate, acetonitrile or acetone and left to stand at ambient temperature until crystallisation was observed. The morpholinium DL-malate salt was successfully crystallised using acetone as the antisolvent by this method.

3.2.3 Crystallisation of novel pharmaceutical salts

Approximately 100mg of the pharmaceutically active compound was slurried in 100ml of water and the acid added portion-wise to give a 1.1:1.0 acid: base molar ratio. The slurry was heated to approximately 50°C to dissolve the majority of the solid material and then filtered into a beaker. The solution was covered with pierced cling film to slow evaporation and allowed to cool to room temperature then left to stand in a fume hood at ambient temperature until crystallisation occurred.

3.3 Single-crystal X-ray diffraction

3.3.1 University of Strathclyde data collection

The majority of the single-crystal X-ray diffraction experiments were measured at 123K using graphite monochromated Mo K α radiation ($\lambda = 0.71073\text{\AA}$) using either a Nonius Kappa CCD, Oxford Diffraction Xcalibur S or Bruker APEX II instrument. Structures solution was carried out using direct methods in SHELXS-97 (Sheldrick, 1998) or SIR-2004 (Altomare, *et al.*, 1993). Hydrogen atom positions on hydrogen bonding and ionisable groups were located from the difference maps where possible with the remaining hydrogen atoms placed in calculated positions using a riding model. Refinement of atomic coordinates and thermal parameters was done by full-matrix least squares methods on $|F^2|$ within SHELXL-97 (Sheldrick, 1998) using all the unique data. The refined structures were viewed using PLATON (Spek, 1998) and ORTEP (Johnson, 1965) within the WinGX suite of programs (Farrugia, 1998).

3.3.2 EPSRC X-ray crystallography service data collections

Diffraction data were collected on a Bruker-Nonius Kappa CCD diffractometer using graphite monochromated Mo K α radiation ($\lambda = 0.71073\text{\AA}$) from a Nonius FR591 rotating anode X-ray generator. Data collection was performed using COLLECT (Hooft, 1998) and unit cell refinement was performed using DENZO (Otwinowski and Minor, 1997). Reflection intensities were obtained by integrating the frames and then scaled using Scalepack, absorption corrections were performed using SADABS (Sheldrick, 2003). Structure solution and refinement was carried out as described in Section 3.3.1.

3.3.3 Synchrotron data collection

Poor quality and small crystals were collected at Station 9.8 at the CCLRC synchrotron facility at Daresbury (Cernik, *et al.*, 1997) as the radiation produced was of higher intensity and flux compared to a rotating anode source (Clegg, 2000). Data was collected using APEX2 (Bruker, 2004), data reduction and cell refinement was performed using SAINT and absorption corrections made using SADABS. Structure solution and refinement was performed as described in Section 3.3.1.

3.4 X-ray powder diffraction (XRPD)

3.4.1 Fingerprint analysis

X-ray powder diffraction data for representative samples of the bulk phase of the crystallised products was collected using a Bruker D5000 diffractometer operating in transmission mode using Cu K α radiation ($\lambda = 1.54056 \text{ \AA}$), with the samples supported by foil on a multiwall plate. Data were collected at ambient temperature in the range 4.000° to $35.056^\circ 2\theta$. The samples were ground with an agate mortar and pestle to produce a homogeneous polycrystalline powder.

3.4.2 Variable temperature X-ray powder diffraction (VT-XRPD)

In-situ dehydration experiments were performed on a Bruker D8 Advance diffractometer using monochromated Cu K α_1 radiation collecting in transmission geometry, configuration details are given in Table 3.4. The samples were mounted in 0.7mm borosilicate glass capillaries and heated to 10°C above their dehydration temperatures. Data was collected and compared with the initial pattern to confirm complete transformation to the anhydrous form and the samples were returned to room temperature and held under a dry air stream. To ensure high resolution and accuracy of the data a variable-count time (VCT) method was used (typically $2\text{-}70^\circ 2\theta$, 2-24s). Indexing was performed using DICVOL-04 (Boultif and Louer, 2004) and intensity extraction was performed using the Pawley method (Pawley, 1981) as employed within the DASH software package (David, *et al.*, 2006). Structure solution was carried out using the simulated annealing method implemented in DASH.

Table 3.4 Configuration of the Bruker D8 Advance XRPD diffractometers.

Instrument	Bruker D8 Advance $\theta/2\theta$
Generator settings	50kV/ 40mA
Measuring diameter	435 mm
Radiation	Cu K α_1 , $\lambda = 1.54056 \text{ \AA}$
Monochromator	Primary, focusing curved Ge111
Detector	Bruker LynxEye
Sample holder	0.7mm borosilicate glass capillary
Alignment reference	NIST SRM 640c

3.5 Thermal analysis

DSC and TGA data for the dehydrations of the hydrated salts were collected on a Netzsch STA-449-C Jupiter instrument. Samples were placed in pierced 25 μL aluminium pans under a He atmosphere and a heating ramp set from -50 to 315 $^{\circ}\text{C}$ (or less than 315 $^{\circ}\text{C}$ when decomposition was expected) at a rate of 5 $^{\circ}\text{C}$ per minute. The data were processed using the Netzsch Proteus data analysis package.

3.6 Structure analysis

3.6.1 Analysis of hydrogen bonding interactions

3.6.1.1 Quantitative analysis of hydrogen bond motif frequencies

The strong hydrogen bonding contacts in the structures were examined using the graph set analysis function in the Materials Module of the Mercury CSD system. Hydrogen bond contacts were identified using the default definition of N, O and S donor groups and N, O, S and halogen acceptors. The contact distance range was set at VdW to (VdW – 5.0 \AA) with no restrictions on the D-H \cdots A contact angle. Both intermolecular and intramolecular contacts for donor and acceptor atoms separated by more than three covalent bonds were searched. The graph set analysis was performed for all intermolecular motif types up to and including level 4 and intramolecular motifs.

The probability of observation (**Pm**) for the hydrogen bonding motifs in the database of model systems in Chapter 1 and the structures retrieved from the CSD and the novel fluoroquinolone salts in Chapter 3 were calculated using the procedure established by Allen et al (Allen, *et al.*, 1999). **Pm** is calculated as a percentage based on the number of occurrences of a motif was divided by total number of systems containing the requisite functional groups to form the motif in either their ionised or neutral states.

3.6.1.2 Systematic analysis of hydrogen bond structures

Hydrogen bonding synthons in the model systems were compared using a method based on Kitaigorodskii's Aufbau Principle discussed in Section 1.3.3.1. A qualitative approach was adopted where the frequency of observation of a motif was equated to its favourability in stabilising crystal structure. The most common zero or one-dimensional motifs were identified and assigned as the base vector for a family of structures. The most common additional vectors to produce a two-dimensional substructure were assigned and finally any motifs linking these sheets into three-dimensional arrays were identified. The results are presented as a modified Hasse diagram where the similarity in the hydrogen bonding motifs in the structures is indicated by the level at which two structures share a common node. A simplified plot is shown in Figure 3.1.

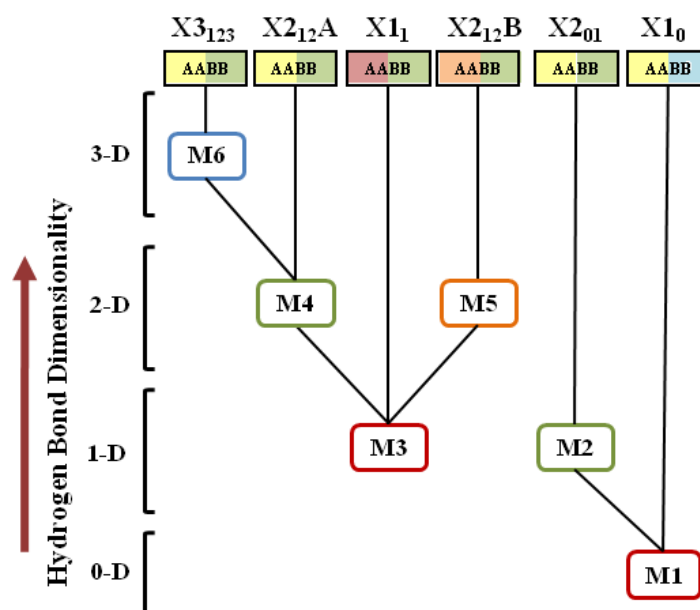


Figure 3.1 The modified Hasse plot used in Chapter 1, read in the direction of the arrow. Hydrogen bonding motifs (M) are coloured by the interacting groups: ■ acid-base; ■ hydroxyl-acid and ■ hydroxyl-hydroxyl. The motifs are placed according to the overall dimensionality of the H-bonding vectors in the structure. Structures are identified by a four-letter code where AA=acid and BB=base. Boxes are coloured by the H-bonding groups present: ■ acid group(s) only ■ one hydroxyl ■ two hydroxyl groups ■ tertiary amine ■ secondary amine. The arrays are labelled according to KAP where X identifies the counterion type (D, B or S), followed by the number of vectors in the structure with their types in subscript from Table 1.4.

3.6.2 XPac analysis

The XPac program was used to identify common packing arrangements of similar molecules in the structures using the principle described in Chapter 1. In this work the packing arrangements of the benzoic and benzenesulfonic acid counterions in the model systems were compared using the method and for the pharmaceutically active systems the pharmaceutical molecules were compared as they represented the largest component in the system. The molecules were parameterised by selection of the COSPs as indicated by the red circles in

Figure 3.2 to define the geometry of the common atomic arrangement in the molecules under comparison. The symmetrical nature of the COSPs selected for components A-C was necessitated by the requirement for the COSPs to be unaffected by conformational changes in the molecules, alternative COSP selections were attempted but were unsuccessful as a basis for comparison.

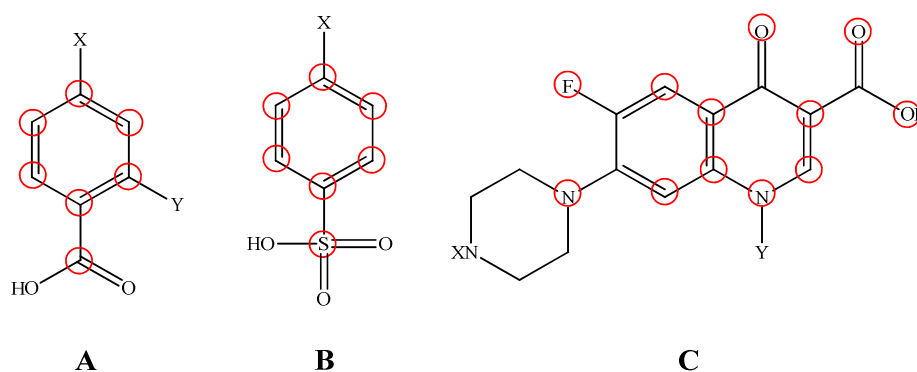


Figure 3.2 Common Ordered Sets of Points selected for the comparison of the packing arrangements of similar molecular components in the structures containing benzoic acids (A, where X= H, OH or Me and Y = H or OH), benzenesulfonic acids (B, where X= H, OH or Me) and fluoroquinolone molecules (C, where X= H, Me or Et and Y= Me, Et or Cp).

The consistency index for all the structures was checked before the analysis was performed. The analyses were carried out using the standard cut-off parameters to identify mean differences δ of 10° for δ_{ang} and 18° for δ_{dhd} and δ_{tor} . The base vectors for the constructs identified in the four analyses are given in Tables 3.5 – 3.8.

Table 3.5 Data for base vectors \boldsymbol{t} in the supramolecular constructs identified in the benzoic acid systems. The structures are identified using the four-letter codes established in Section 4.3 using the identifiers given for the acids in Figure 4.1 on page 56 and for the bases in Figure 4.2 on page 57, distances d are given in Å and angles are in degrees.

ID	t_1	d_1	t_2	d_2	t_3	d_3	t_4	d_4	t_7	d_7	t_{11}	d_{11}	$\langle(t_1, t_2)$	$\langle(t_1, t_3)$	$\langle(t_2, t_3)$
DBDM	0-10	9.5498	00-1	13.0384	-	-	-	-	-	-	-	-	92.551	-	-
DEMAI	0-10	9.0424	100	13.1872	-	-	-	-	-	-	-	-	90	-	-
HBMAI	-100	10.5124	0-10	12.3365	00-1	20.6231	-	-	-	-	-	-	90	90	90
SAMA	100	10.4717	0-10	11.9061	00-1	21.1017	-	-	-	-	-	-	90	90	90
DBPA	-	-	-	-	-	-	0-10	9.7317	-	-	-	-	-	-	-
HBMM	-	-	-	-	-	-	0-10	9.5828	-	-	-	-	-	-	-
BZPA	-	-	-	-	-	-	-	-	-100	8.2112	-	-	-	-	-
HBMD	-	-	-	-	-	-	-	-	010	8.1838	-	-	-	-	-
HBPA	-	-	-	-	-	-	-	-	001	8.6432	-	-	-	-	-
SADM	-	-	-	-	-	-	-	-	100	5.9261	-	-	-	-	-
SADMI	-	-	-	-	-	-	-	-	100	7.1441	-	-	-	-	-
SAMR	-	-	-	-	-	-	-	-	100	6.8175	-	-	-	-	-
SAPA	-	-	-	-	-	-	-	-	100	6.244	-	-	-	-	-
SAPD	-	-	-	-	-	-	-	-	100	6.9839	-	-	-	-	-
TUMD	-	-	-	-	-	-	-	-	0-10	6.4759	-	-	-	-	-
TUPP	-	-	-	-	-	-	-	-	-100	6.0256	-	-	-	-	-
BZMA	-	-	-	-	-	-	-	-	-	-	100	6.1841	-	-	-
BZPP	-	-	-	-	-	-	-	-	-	-	100	6.1245	-	-	-
TUDM	-	-	-	-	-	-	-	-	-	-	0-10	6.0425	-	-	-

Table 3.5 (cont.)

ID	t_5	d_5	t_6	d_6	t_8	d_8	t_9	d_9	t_{10}	d_{10}	$\langle(t_8, t_9)\rangle$	$\langle(t_8, t_{10})\rangle$	$\langle(t_9, t_{10})\rangle$	$\langle(t_5, t_6)\rangle$
BZPD	-100	12.7227	110	14.7501	-	-	-	-	-	-	-	-	-	149.604
DBMA	-100	12.7201	-	-	-	-	-	-	-	-	-	-	-	-
TUMA	-100	12.8453	110	14.9024	-	-	-	-	-	-	-	-	-	149.537
DBMD	-100	12.1041	-	-	-	-	-	-	-	-	-	-	-	-
DBMR	-	-	-	-	0-10	8.3414	-	-	-	-	-	-	-	-
HBMR	-	-	-	-	00-1	7.3303	0-10	16.1588	-100	11.2922	90	102.17	90	-
HBPD	-	-	-	-	001	7.4007	0-10	15.994	100	11.966	90	107.515	90	-

Table 3.6 Data for base vectors \mathbf{t} in the supramolecular constructs identified in the benzenesulfonic acid systems. The structures are identified using the four-letter codes established in Section 4.3 using the identifiers given for acids in Figure 4.1 on page 56 and for the bases in Figure 4.2 on page 57, distances d are given in Å and angles are in degrees.

ID	t_1	d_1	t_2	d_2	t_3	d_3	t_4	d_4	t_5	d_5	t_6	d_6	t_6	d_6	$\langle(t_1, t_2)\rangle$	$\langle(t_1, t_3)\rangle$	$\langle(t_2, t_3)\rangle$	$\langle(t_6, t_7)\rangle$
BSPA	100	6.1027	-	-	-	-	-	-	-	-	-	-	-	-	-	-	-	-
BSPD	100	6.2357	0-10	8.2849	00-1-	11.7028	-	-	-	-	-	-	-	90	90	88.629	90	-
HSPD	-100	6.4435	010	8.4183	001	11.67	-	-	-	-	-	-	-	90	90	88.333	90	-
HSPP	100	6.0653	-	-	-	-	-	-	-	-	-	-	-	-	-	-	-	-
HSPA	-	-	-	-	-	-	0-10	6.8246	-	-	-	-	-	-	-	-	-	-
HSPP	-	-	-	-	-	-	0-10	7.1419	-	-	-	-	-	-	-	-	-	-
T SMA	-	-	-	-	-	-	0-10	8.0783	-100	6.7471	-	-	-	-	-	-	-	-
HSMR	-	-	-	-	-	-	-	-	100	5.7204	-	-	-	-	-	-	-	-
TSDM	-	-	-	-	-	-	-	-	0-10	6.2848	-	-	-	-	-	-	-	-
TSPA	-	-	-	-	-	-	-	-	-100	6.0216	-	-	-	-	-	-	-	-
BSPP	-	-	-	-	-	-	-	-	-	-	-100	8.18	0-10	10.7536	-	-	-	90
TSPP	-	-	-	-	-	-	-	-	-	-	100	8.513	010	10.834	-	-	-	90

Table 3.7 Data for base vectors \mathbf{t} in the supramolecular constructs identified in the fluoroquinolone structures. The structures are identified using the four-letter codes established in Section 4.3 with the acids identified according to Figure 4.1 on page 56 and the fluoroquinolones identified according to Figure 6.1 on page 144, distances d are given in Å and angles are in degrees.

ID	t_1	d_1	t_7	d_7	t_8	d_8	t_9	d_9	t_{10}	d_{10}	t_{12}	d_{12}	$\langle(t_7, t_1)\rangle$	$\langle(t_1, t_8)\rangle$	$\langle(t_1, t_9)\rangle$	$\langle(t_1, t_{12})\rangle$	$\langle(t_8, t_{12})\rangle$	$\langle(t_9, t_{10})\rangle$
ADCP	100	7.2567	010	11.3826	-	-	-	-	-	-	-	-	93.07	-	-	-	-	-
SACP	-100	7.091	001	11.6265	-	-	-	-	-	-	-	-	95.806	-	-	-	-	-
TSCP	100	7.3715	-	-	0-10	11.8033	-	-	-	-	00-1	14.8389	-	94.405	-	96.229	105.443	-
TSNR	100	7.4317	-	-	0-10	11.979	-	-	-	-	00-1	14.5805	-	90.74	-	99.639	105.632	-
TSEN	100	7.1827	-	-	0-11	17.2888	-	-	-	-	-	-	-	101.317	-	-	-	-
EDNR	100	7.4513	-	-	0-10	9.8848	-	-	-	-	-	-	-	93.806	-	-	-	-
SUCP	0-10	7.4263	-	-	-	-	-	-	-	-	-	-	-	-	-	-	-	-
FUNR	-100	8.1019	-	-	-	-	-	-	-	-	-	-	-	-	-	-	-	-
SANR	100	7.0614	-	-	-	-	001	17.045	-	-	-	-	-	-	95.439	-	-	-
MECP	010	10.3206	-	-	-	-	-100	6.98	00-1	14.6768	-	-	-	-	74.329	85.985	-	90.48
VEIWIB	010	9.8742	-	-	-	-	-100	7.089	00-1	14.5854	-	-	-	-	77.063	83.543	-	92.3
RTNR	010	10.0647	-	-	-	-	-	-	-100	7.5448	-	-	-	-	-	99.563	-	-
LTNR	010	9.7874	-	-	-	-	-	-	-100	7.5462	-	-	-	-	-	103.999	-	-
FORGAU	010	9.6007	-	-	-	-	-	-	-100	6.9637	-	-	-	-	-	71.434	-	-

Table 3.7 (cont.)

ID	t_2	d_2	t_3	d_3	t_4	d_4	t_5	d_5	t_6	d_6	t_{11}	d_{11}	$\langle (t_6, t_{11}) \rangle$
JEKMOB	00-1	7.039	-	-	-	-	-	-	-	-	-	-	-
VEIWAT	100	6.8086	-	-	-	-	-	-	-	-	-	-	-
BSEN	100	6.9547	-	-	-	-	-	-	-	-	-	-	-
BZSF	010	7.0102	-	-	-	-	-	-	-	-	-	-	-
HBNR	100	7.2507	-	-	-	-	-	-	-	-	-	-	-
HSCP	010	7.0573	-	-	-	-	-	-	-	-	-	-	-
HSNR	010	7.0573	-	-	-	-	-	-	-	-	-	-	-
FUEN	100	6.9257	-	-	-	-	-	-	001	13.1625	-1-10	14.9127	1-10
SAEN	-	-	-	-	-	-	-	-	0-10	13.3514	-1/2 -1/20	14.8124	63.2125
FORGAU	-	-	-	-	-	-	110	9.90418	-	-	-	-	-
LTCP	-	-	-	-	-	-	-100	9.6055	-	-	-	-	-
MATMAV	-	-	-	-	-	-	010	10.4013	-	-	-	-	-
EDEN	-	-	-1-11	18.7459	-	-	110	9.88415	-	-	-	-	-
FUCP	-	-	0-11	13.6495	-	-	-	-	-	-	-	-	-
RTSP	-	-	-	-	-10	7.2795	-	-	-	-	-	-	-

Chapter 4
Structure correlation in salt structures

4.1 Introduction

The data-mining of structural libraries is an important aspect of developing crystal engineering approaches to control the crystal structure of materials (Chisholm, *et al.*, 2006). The Cambridge Structural Database (Allen, 2002) is widely used in such endeavours, permitting the examination of intermolecular interactions across large numbers of published crystal structures including hydrogen bonding motifs (Chertanova and Pascard, 1996) and molecular packing patterns (Pidcock and Motherwell, 2005). A number of tools have been developed to extract pertinent information from crystal structures. These include the Materials Module in the Mercury CSD system, used to identify hydrogen bonding motifs (Childs, *et al.*, 2009); XPac, a tool to identify similarities in molecular packing arrangements (Gelbrich and Hursthouse, 2006); Crystal Explorer for Hirschfeld surface analysis (Spackman and McKinnon, 2002) and PIXEL for the evaluation of intermolecular interaction energies (Gavezzotti, 2005).

Whilst such approaches have been widely applied to investigate polymorphism (Galek, *et al.*, 2009), solvate formation (Gorbitz and Hersleth, 2000) and in the development of synthon based approaches to co-crystal formation (Fleischman, *et al.*, 2003) they have not been widely employed in the development of synthon based design strategies for salt selection. In this case proton transfer from the acidic to basic species can lead to deviation from the expected stoichiometric composition in the resultant lattice as a consequence of the different hydrogen bonding requirements of ionised functional groups (Aakeroy, *et al.*, 2007b).

The focus of the work presented in this chapter is the interpretation of the crystal structures of a series of molecular salts as a function of the molecular structure of their constituent ions and the supramolecular interactions formed in the solid-state. A systematic investigation has been performed using a large bespoke library of structures for a series of small, organic acids cocrystallised with a systematic series of simple bases to identify recurring hydrogen bonding motifs and packing arrangements. Molecular structure, pKa and the numbers of hydrogen bond donor and acceptor groups on the acid and base components have been used alongside this

analysis of recurring supramolecular structural features constructs to classify salt structures according to the component molecular properties and structural type.

A *salt* is the ionic product of proton transfer by the neutralisation of an acid and base, in *molecular salts* both components are molecules instead of single atom ions. Proton transfer can be accompanied by the incorporation of a neutral molecule into the crystalline structure resulting in a *mixed system* (Aakeroy, *et al.*, 2007b). When proton transfer does not occur, the resultant crystal containing two neutral species is termed a *cocrystal* as opposed to a *solvate*. This nomenclature is adopted here as, although the majority of the bases in this work are liquids at room temperature, the intent or “element of design” in crystallising the system means the term *cocrystal* is appropriate (Bernstein, 2005). The different system types encountered in this study are shown in Figure 4.1.

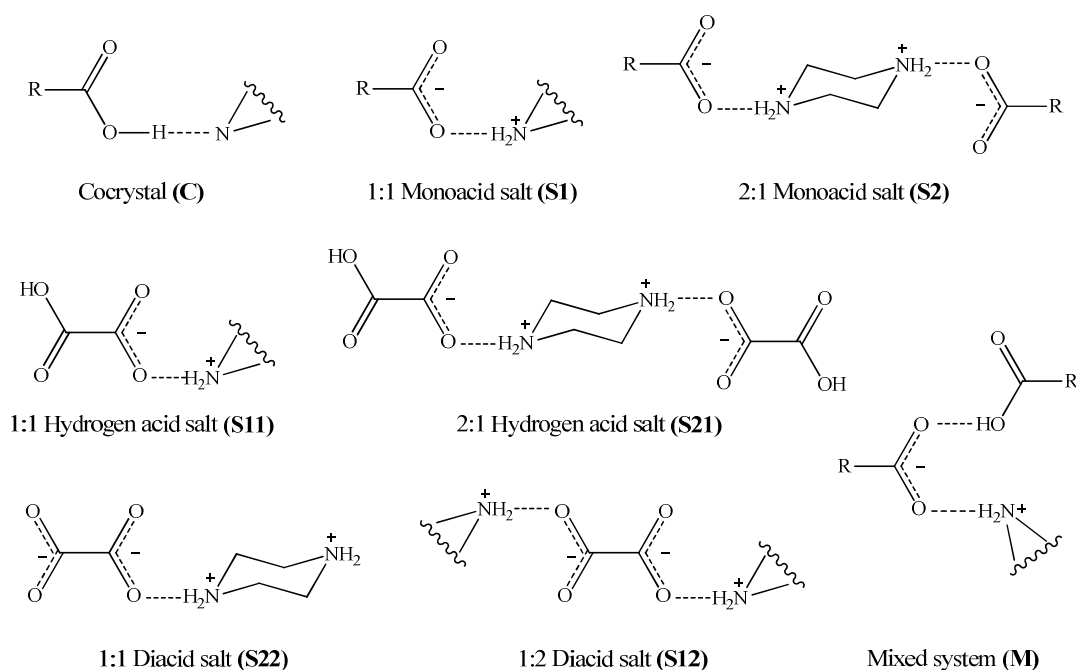


Figure 4.1 Classification of multicomponent crystalline solids characterised in this work. Salts are classified according to the acid:base stoichiometry and ionisation state of the diacid or dibasic species where applicable. Letters and numbers in brackets show codes used in subsequent diagrams to represent these system types. The classifications are applied to both carboxylic and sulfonic acids.

4.2 Method

4.2.1 Sample preparation and data collection

The library of 20 carboxylic and sulfonic acids that are used as pharmaceutical salt formers shown in Figure 4.2 was selected for this study. The acids differ in the number and type of functional groups present on the structure, enabling the intermolecular interactions that determine the crystalline structures formed to be examined in a systematic fashion. Selected chemical properties including pKa are given in Table 2.1.

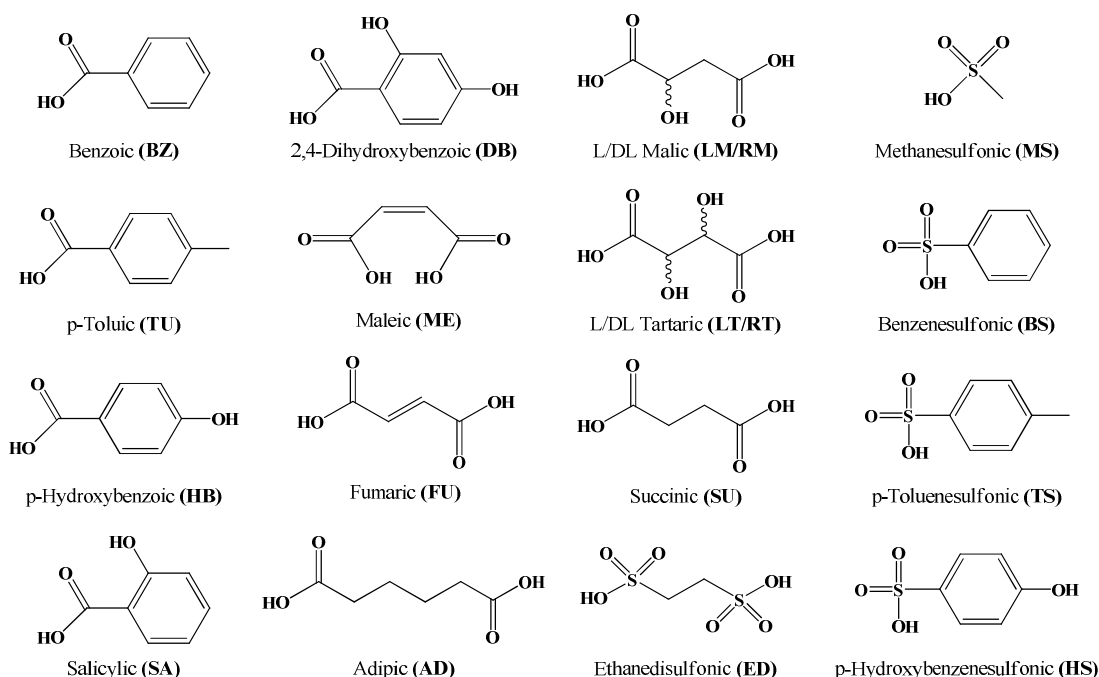


Figure 4.2 The carboxylic and sulfonic acids selected as counterions in this study. In the case of tartaric and malic acid both the L-enantiomer and racemate have been studied. The acids can be broadly grouped into three families- aliphatic dicarboxylic acids (**ME**, **FU**, **AD**, **SU**, **LM**, **RM**, **LT**, **RT**), mono-carboxylic acids (**BZ**, **TU**, **HB**, **SA**, **DB**) and sulfonic acids (**MS**, **BS**, **TS**, **HS**, **ED**). The two letters shown in bold are used to denote the acid component in the systems formed in the four letter codes used to identify the structures in the diagrams throughout this thesis.

The series of cyclic amine bases shown in Figure 4.3 was used to model functional groups present on larger pharmaceutically active molecules. They have similar molecular conformations and sizes but vary in the number and pKa of ionisable nitrogen atoms and also vary in potential hydrogen bond donor and acceptor sites. This enables the systematic examination of crystalline salt formation and structure, in relation to these features.

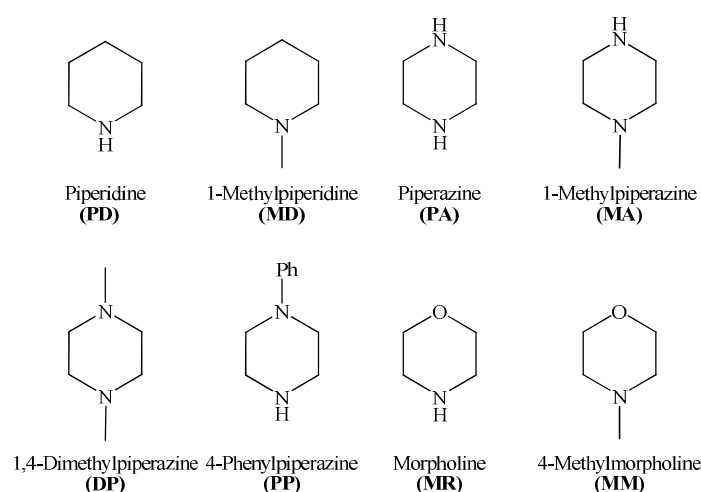


Figure 4.3 Heterocyclic bases tested as salt formers in combination with the acid counterions shown in Figure 4.1. The two letters in bold are used to identify the base molecule present in the systems characterised in subsequent diagrams. For example, a piperazinium fumarate salt will be termed FUPA.

The acids and bases were dissolved in water and mixed in a 1.1:1 molar ratio and left to evaporate slowly at ambient temperature. In cases where crystallisation did not occur, efforts were made to induce crystallisation by cyclic cooling or slow diffusion with acetone. Crystals obtained by these methods are identified in the subsequent text. The crystals were characterised by single-crystal X-ray diffraction using the data collection parameters described in Section 2.4.1.

4.2.2 Data analysis

The structures were visualised using the CSD Mercury version 2.2 and the graph set analysis function was used to identify and classify the hydrogen bond motifs present. Oxygen, nitrogen and sulphur atoms were defined as both donor and acceptor atoms with a contact distance range of VdW - 5Å to VdW + 0Å. Similar molecular arrangements (supramolecular constructs) of the acidic components of the benzoate and besylate structures were identified using XPac. The standard search radius (VdW + 1.5 Å) and the cut-off parameters as defined in Section 3.5.3 to identify low mean distances of 10° for δ_{ang} and 18° for δ_{tor} and δ_{dhd} . The total number of comparison steps, K , performed for each group of structures was related to the number of structures N by $K = [(N^2 - N)/2]$. The COSPs were selected to give geometrically identical atomic arrangements for the components in each structure, as described in Section 3.5.3, and the data for the base vectors \mathbf{t} in the supramolecular constructs are given in Tables 3.5 and 3.6.

4.3 Results and discussion

4.3.1 Outcomes of crystallisation experiments

In order to facilitate a systematic examination of solid-state structure the experimental matrix has been divided into sub-groups with dicarboxylic, monocarboxylic or sulfonic acid counterions. This division reflects expected differences in molecular structure and pKa. The outcomes of the crystallisation experiments for each group are shown in Tables 4.1 - 4.3, the acids are listed in order of increasing acidity and the bases from left to right in order of decreasing basicity with each component identified by the two-letter code given in Figures 2.1 and 2.2. The ΔpK_a values for the first proton transfer obtained from the pKas calculated with ACD Labs pKa DB are shown in the boxes. Crystalline multi-component products are denoted using the classifications established in Figure 4.1, with other outcomes given in text. The proportions of each experimental outcome observed for the three types of acid counterion are compared in Figure 4.4.

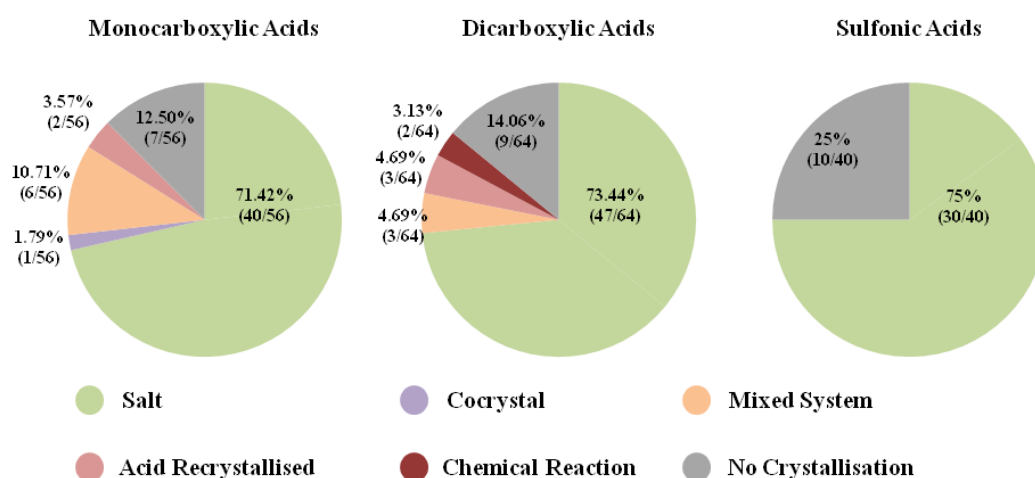


Figure 4.4 Comparison of the outcomes of the crystallisation experiments for each group of acid counterions shown as a percentage of the acid-base combinations examined with the number of each result and number of experiments given in brackets.

ΔpK_a		Base							
		PD	MD	PA	MA	MR	PP	DM	MM
Acid Counterion	AD	6.85 S11	5.52	5.50 S22	5.28 M	4.58 S11(H)	4.55 S11	4.22 M	3.02
	SU	7.00 S11	5.67	5.65 S22	5.43 S21(H)	4.73 S11	4.70 S11	4.37 S22(H)	3.17 S11
	LM	7.63	6.30 S11(H)	6.28 S21(H)	6.06 S22(H)	5.36	5.33	5.00 S21	3.80 S11(H)
	RM	7.63	6.30 S11(H)	6.28 S21	6.06 S22(H)	5.36 S11	5.33 S11(H)	5.00 S21(H)	3.80 S11(H)
	FU	8.09 S11	6.76 S11	6.74 S22	6.52	5.82 M	5.79 S11	5.46 S21	4.26 S11
	ME	8.09	6.76 S11	6.74 S21	6.52	5.82	5.79	5.46 S21	4.26 S11
	LT	8.17 S11(H)	6.84 S11(H)	6.82 S22	6.60 S22	5.90 S11(H)	5.87 S11(H)	5.54 S22(H)	4.34 S11(H)
	RT	8.17 S11(H)	6.84 S11(H)	6.82 S22	6.60	5.90 S11(H)	5.87	5.54 S21(H)	4.34 S11(H)

Table 4.1 Outcomes of crystallisation experiments for dicarboxylic acid counterions with model bases. The numerical values shown are the ΔpK_a values for the first proton transfer between acid and base. Boxes are coloured according to the product obtained (■ = salt and (H) denotes hydrate, ■ = no solid product retrieved, ■ = acid component recrystallised, ■ = acid component chemically reacted with base, ■ = mixed system) where crystalline multi-component systems are described as S = salt or M = mixed.

		Base							
		PD	MD	PA	MA	MR	PP	DM	MM
Acid Counterion	HB	6.67 S1(H)	5.54 M	5.32 S1/S2(H)	5.10 S1(H)	4.40 S1(H)	4.37 S1(H)	4.04 S2	2.84 M
	TU	6.87 S1	5.54 S1(H)	5.52 S2	5.30 S1(H)	4.60 S1	4.57 S1(H)	4.24 C	3.04 M
	BZ	7.04 S1(H)	5.71	5.69 S2	5.47 S1(H)	4.77 S1	4.74 S1(H)	4.41	3.21 M
	DB	7.92 S1	6.59 S1	6.57 S2	6.35 S1/S2(H)	5.65 S1	5.62 S1	5.29 S1	4.09 S1
	SA	8.23 S1	6.90 S1	6.88 S2	6.66 S1(H)	5.96 S1	5.93 S1	5.60 S1/S2	4.40 M

Table 4.2 Outcomes of crystallisation experiments for monocarboxylic acid counterions with model bases. The numerical values shown are the ΔpK_a values for the first proton transfer between acid and base. Boxes are coloured according to the product obtained (■ = salt and (H) denotes hydrate, ■ = acid component recrystallised, ■ = cocrystal, ■ = mixed system) where crystalline multi-component systems are described as S = salt or M = mixed followed by the acid:base stoichiometry.

		Base							
		PD	MD	PA	MA	MR	PP	DM	MM
Acid Counterion	MS	9.49 S1	8.16	8.14 S2	7.92	7.22 S1	7.19 S1	6.86 S2	5.66
	HS	11.47 S1	10.14 S1	10.12 S2	9.90 S2	9.20 S1	9.17 S1(H)	8.84 S1	7.64
	TS	11.67 S1	10.34 S1(H)	10.32 S2(H)	10.10 S1	9.40 S1	9.37 S1	9.04 S2(H)	7.84 S1(H)
	BS	11.84 S1	10.51	10.49 S1	10.27 S1	9.57 S1	9.54 S1	9.21 S1	8.01
	ED	10.53 S12	9.20	9.18 S22	8.96 S22	8.26 S12(H)	8.23 S12	7.90 S22	6.70

Table 4.3 Experimental outcomes for crystallisations of sulfonic acid counterions and model bases. The numerical values shown are the ΔpK_a values for the first proton transfer between acid and base. Boxes are coloured according to the product obtained (■ = salt and (H) denotes hydrate, □ = no solid product retrieved) where crystalline multi-component systems are described as S = salt or M = mixed followed by the acid:base stoichiometry.

Overall, a larger proportion of the sulfonic acid systems failed to crystallise (25%) compared to the mono- and dicarboxylic acid counterions (12.5 and 14 % respectively), however all of the crystalline sulfonic acid products obtained are salts. Hence, the overall frequency of salt formation across the three counterion types is similar (> 70% salt formation). This outcome differs from the frequency of successful salt formation for a series of basic drug compounds that showed high success rates for sulfonic acid counterions in comparison with dicarboxylic acids, for example 100% of mesylate salts crystallised successfully with no tartrate salts crystallising (Morissette *et al.*, 2004). However, the drug molecules in the study were weak bases and the ΔpK_a s with the fumarate, tartrate and maleate counterions were all less than 2, making salt formation unlikely. In contrast, the minimum ΔpK_a with the counterions in this study was 4.26.

Notably, for the monocarboxylic and sulfonic acid systems the majority of the salts are anhydrous (67.5 and 80% respectively), in contrast the dicarboxylic acid systems that returned approximately equal proportions of hydrated and anhydrous salts. As can be seen in Table 4.1 the majority of the hydrated salts in this family occur for systems with malic or tartaric acid as the counterion with only two examples for the simpler non-hydroxy substituted dicarboxylic acid salts. It appears that the preponderance of hydrates in this family is a result of the higher number of hydrogen

bond donor/acceptor groups on the acid molecule. The factors influencing hydrate formation within these systems will be discussed in more detail in Chapter 5.

A range of outcomes was observed for the carboxylic acid systems. Only one example of a cocrystal was observed. This was in the monocarboxylic acid group and this group of compounds was observed to form mixed systems containing free acid with approximately twice the frequency of the dicarboxylic acids. Only a small number of crystallisations (5 in total) resulted in the acid component recrystallising from the liquid base as a single component crystal. The crystallisation attempts for the dicarboxylic acid, maleic acid, and piperidine and morpholine both resulted in substituted succinic acid derivatives via Michael-type addition (Smith and March, 2003).

4.3.2 Salt formation and ΔpK_a

To evaluate the extent of correlation between ΔpK_a and the ionisation state of the species in the resultant crystalline systems, the outcomes were plotted as a function of the pK_a s of the acid and base molecules (Figure 4.5). In cases where one or both of the components contains two possible ionisation sites only the pK_a of the first ionisation is considered.

The results confirm that the “rule of three” discussed in Section 1.5 is not a reliable predictor of salt formation, as the sole cocrystal observed in this study was formed for an acid-base combination with a ΔpK_a greater than 4. Four acid-base combinations that returned unreacted acid and six that formed salts with the incorporation of a neutral acid molecule also had ΔpK_a values in excess of 3. Salt formation was the exclusive outcome for systems where $\Delta pK_a > 6$.

In the majority of piperazine and 1,4-dimethylpiperazine salts formed with monoacids, the bases are protonated on both nitrogens. For 1-methylpiperazine diprotonation occurs in two salts and 4-phenylpiperazine is exclusively monoprotonated. The protonation of the base in these cases is not dictated solely by pK_a . For example, in piperazinium besylate, where ΔpK_a is 10.49, the cation is monoprotonated whilst it is diprotonated in all of the monocarboxylic acid salts despite the lower ΔpK_a values (5.32 to 6.88). 1,4-dimethylpiperazine shows similar

behaviour, being diprotonated in the 4-hydroxybenzoate salt ($\Delta pK_a = 5.33$) whilst being monoprotated in the besylate salt in spite of having the largest ΔpK_a (10.49). This data is consistent with the argument that the ionisation states of molecules in crystalline solids are not determined solely by pK_a difference. A recent modelling study has demonstrated that despite the differences in molecular geometry of *ab initio* optimised ionic and neutral molecules in cocrystallised acid-base structures, the minimum lattice energy crystal structure is dependent on the location of the ionisable proton between the acid and base molecule (Mohamed, *et al.*, 2009a).

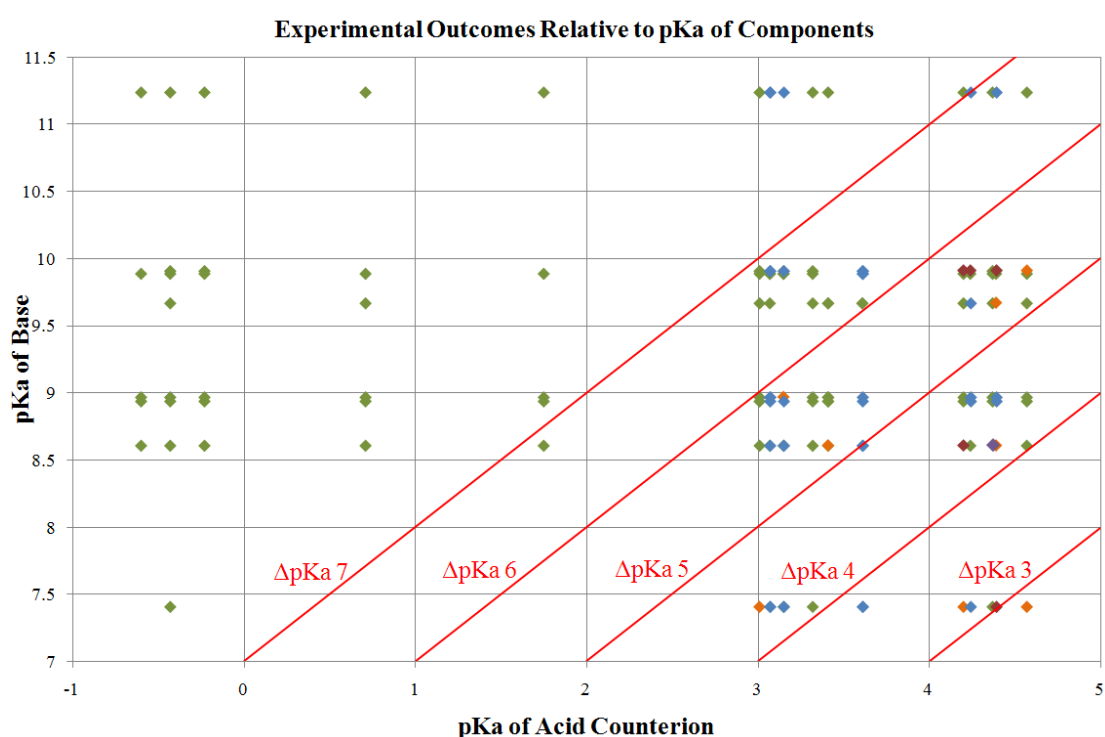


Figure 4.5 Chart showing the individual experimental outcomes according to the pK_a values of the acid and base species. Each point corresponds to a single acid-base combination and is coloured according to the system observed where ● = salt, ● = hydrogen acid salt, ● = mixed system, ● = cocrystal and ● = recrystallisation of acid component. The diagonal red lines indicate specified ΔpK_a values for acid and base combinations.

4.4 Crystal structure analysis of dicarboxylic acid systems

The hydrogen bonding interactions in the 50 structures containing a dicarboxylic acid counterion were examined. The structures for piperazinium hydrogen maleate (Jin, *et al.*, 2003); succinate (Vanier and Brisse, 1983); L-tartrate (Aakeroy, *et al.*, 1992); L-malate (Aakeroy and Nieuwenhuyzen, 1996) and DL-malate (Wang, *et al.*, 2005) as well as 1,4-dimethylpiperazinium bis(L)-malic acid and bis(DL)-tartaric acid dihydrate (Farrell, *et al.*, 2002) were retrieved from the CSD and incorporated into the study. Samples of these were crystallised in this work and confirmed to be the same form by means of a Pawley-type fit (Pawley, 1981) of the unit cell and space group of the published structure to laboratory XPRD data collected from each sample. All the other structures were determined in the experimental investigation and are provided in CIF format (Hall, *et al.*, 1991) in Appendix 1.

4.4.1 Intermolecular hydrogen bonding interactions

17 unique intermolecular hydrogen bond interactions formed by the acid and base molecules in the dicarboxylic acid structures were identified by visual inspection using Mercury 2.0 and are shown in Figure 4.6. As this was an examination of interactions between the salt formers hydrogen bonds with water molecules were ignored. To assess the relative importance the interactions in determining the supramolecular structure of the salt and their robustness, the number of structures in this library featuring each interaction (Nobs) was compared to the number of structures in which the molecules possessed the requisite functional groups to form the interaction (Nposs). The prevalence of the interactions are expressed as percentages (Pm) as described in Chapter 1 and by Allen *et al* (Allen, *et al.*, 1999). For contacts in which one or both groups are ionic, the number of possible interactions included all the structures in which those functional groups are present, irrespective of whether proton transfer had occurred. The statistics for the occurrence of each interaction are given in Table 4.4. The bifurcated contact from the secondary amine to two carboxylic acids, **8**, was not observed but is included as a contrast to the comparable ionic contacts **7** and **12**.

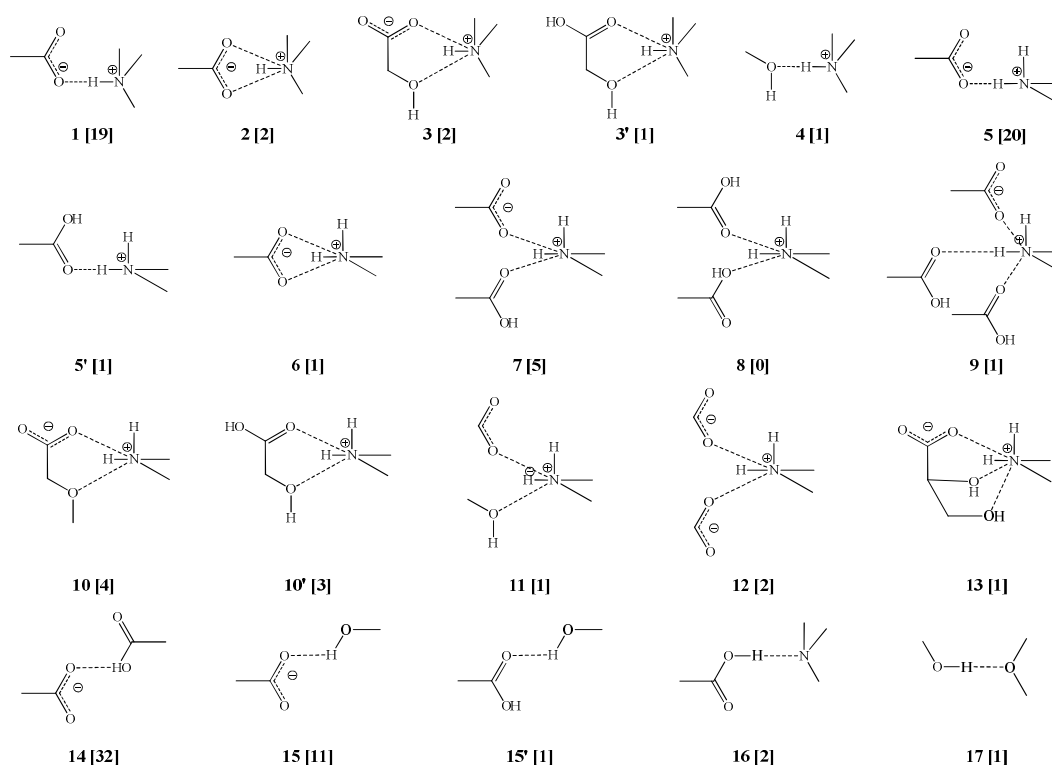


Figure 4.6 Hydrogen bond contacts with type number, seen in the dicarboxylic acid structures. The number of structures containing each interaction type is given in brackets.

Table 4.4 Frequencies of occurrence of the 17 contacts in Figure 1.6.

Bond	Donor	Acceptor	N _{poss}	N _{obs}	P _m (%)
1	<i>tert</i> -NH ⁺	CO ₂ ⁻	26	19	73
2	<i>tert</i> -NH ⁺	CO ₂ ⁻	26	2	7
3	<i>tert</i> -NH ⁺	CO ₂ ⁻ /COH	15	2	13
3'	<i>tert</i> -NH ⁺	CO ₂ H/COH	15	1	7
4	<i>tert</i> -NH ⁺	COH	15	1	7
5	<i>sec</i> -NH ₂ ⁺	CO ₂ ⁻	27	20	74
5'	<i>sec</i> -NH ₂ ⁺	CO ₂ H	27	1	4
6	<i>sec</i> -NH ₂ ⁺	CO ₂ ⁻	27	1	4
7	<i>sec</i> -NH ₂ ⁺	CO ₂ ⁻ + CO ₂ H	27	5	19
8	<i>sec</i> -NH ₂ ⁺	CO ₂ H + CO ₂ H	27	0	0
9	<i>sec</i> -NH ₂ ⁺	CO ₂ ⁻ + CO ₂ H +CO ₂ H	27	1	4
10	<i>sec</i> -NH ₂ ⁺	CO ₂ ⁻ /COH	17	4	24
10'	<i>sec</i> -NH ₂ ⁺	CO ₂ H/COH	17	3	18
11	<i>sec</i> -NH ₂ ⁺	CO ₂ H + COH	17	1	6
12	<i>sec</i> -NH ₂ ⁺	CO ₂ ⁻ + CO ₂ ⁻	27	2	7
13	<i>sec</i> -NH ₂ ⁺	CO ₂ ⁻ /COH/COH	9	1	11
14	CO ₂ H	CO ₂ ⁻	50	32	64
15	COH	CO ₂ ⁻	26	11	42
15'	COH	CO ₂ H	26	1	4
16	CO ₂ H	<i>tert</i> -N	26	2	8
17	COH	ether	12	1	8

The secondary amine donor groups exhibits the greatest number of different types of contacts to dicarboxylic acids with nine interactions identified from the 27 structures containing this group. This compares with four contacts for the tertiary amine group and two for the carboxylic acid and hydroxyl groups. Whilst there is considerable variety in the interactions formed for the four donor types, certain interactions are highly favoured and each donor type shows one dominant interaction having Nobs > 10.

For both secondary and tertiary amine donor groups the interaction with the highest probability of occurrence is a simple hydrogen bond to a carboxylate group; $\text{NH}^+\cdots\text{CO}_2^-$ contact **1** occurs for the tertiary amine donor in 73% of the structures and $\text{NH}_2^+\cdots\text{CO}_2^-$ contact **5** is formed by the secondary amine donor group in 74% of its structures. Examples of bifurcated hydrogen bonds to single carboxylate groups (**2** and **6**) have been identified for both donor groups along with two cases where a secondary amine group donates a bifurcated bond to the carboxylate groups of two cations however, these interactions are heavily disfavoured in comparison with the simple hydrogen bonds. For both donor groups a similar number of bifurcated interactions to a hydroxyl group and a neighbouring carboxylate (**3**, **10**) or carboxylic acid group (**3'**, **10'**) are formed, in both cases the incidence of ionic-ionic and ionic-neutral contacts are similar.

For neutral donor groups the formation of interactions with ionic groups is favoured over contacts to neutral acceptors. The carboxylic acid group donates hydrogen bonds to the carboxylate group of a neighbouring acid molecule to give interaction **14** almost exclusively, with only one competing neutral interaction, **16**, identified in the two structures. A similar trend is observed for the hydroxyl groups on the hydroxyacid counterions, with 11 interactions occurring to carboxylate groups (**15**) compared with a single interaction with the corresponding neutral carboxylic acid group (**15'**). The low frequency of observation of interactions from the hydroxyl group results from the formation of contacts with water molecules with comparable frequency to contacts with groups on other acid molecules. The water contacts are not considered in this section and will be discussed in detail in Chapter 5.

4.4.2 Hydrogen bond motifs

The hydrogen bond motifs formed by interactions between two functional groups were identified using the graph set calculation function in Mercury 2.0. The five different motifs formed by amine and carboxylate groups are shown in Figure 4.7 and are labelled by their graph set notation (Etter, 1990).

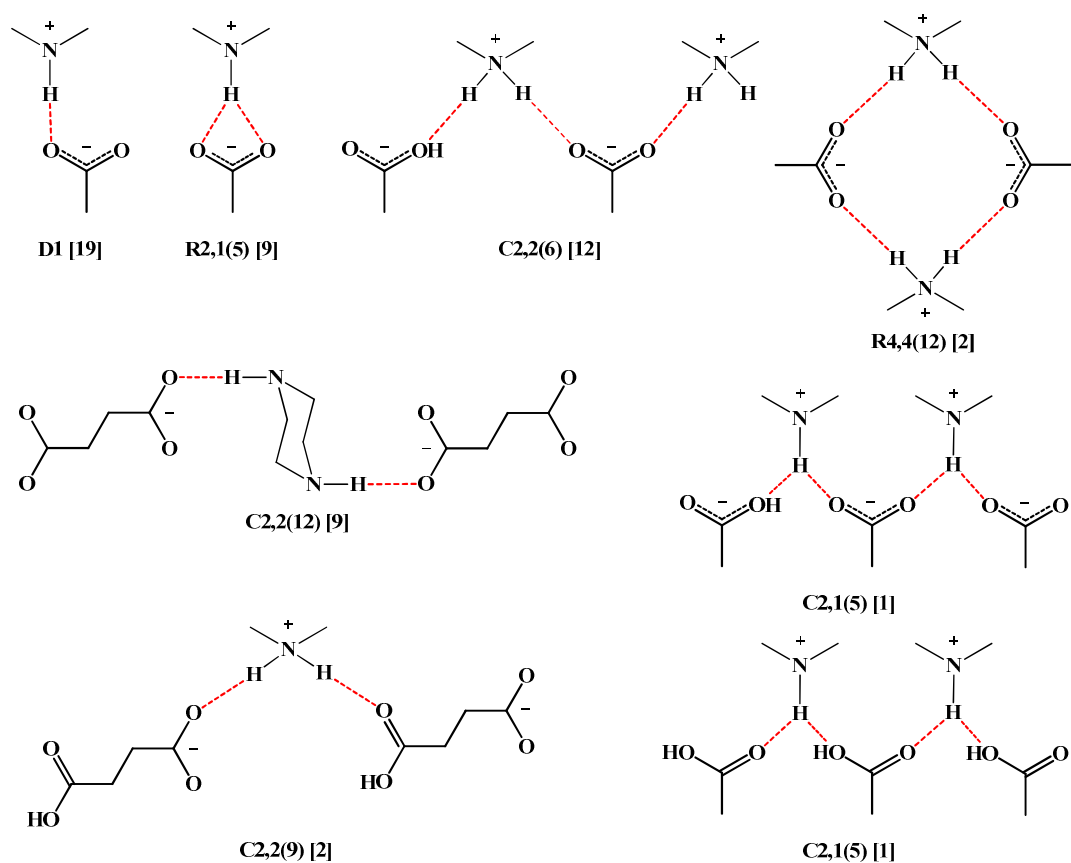


Figure 4.7 Amine-carboxylate hydrogen bond motifs identified in the dicarboxylic acid structures identified by their graph set notation. The number of structures in which each motif has been identified is shown in square brackets.

In 32 of the 37 hydrogen acid salts the anions are linked by *syn-syn* or *anti-anti* hydrogen bonds as shown in Figure 4.8, giving C1,1(7) or C1,1(9) hydrogen bonded chain motifs depending on the length of the acid molecule. The presence of hydroxyl groups on the malic and tartaric acid molecules enables the formation of additional acid-acid hydrogen bonds resulting in one of the four motifs shown in Figure 4.9.

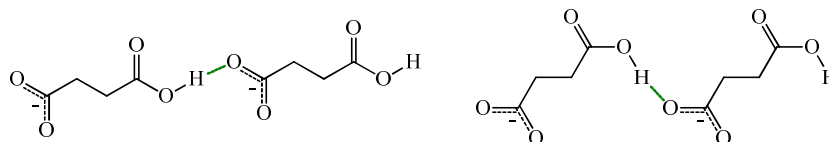


Figure 4.8 *Syn-syn* and *anti-anti* hydrogen bonded acid molecules that form the basis of the C1,1(7) and C1,1(9) hydrogen bonded chains in the dicarboxylic acid structures.

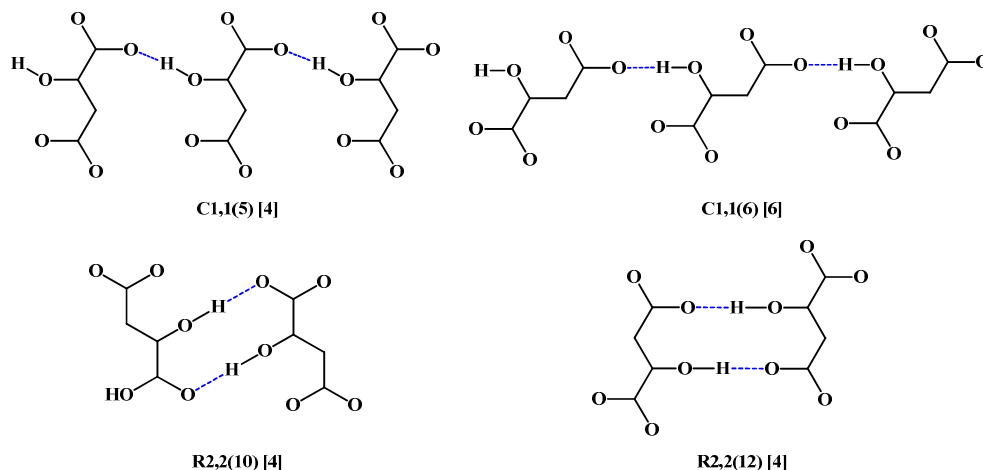


Figure 4.9 Acid to acid hydrogen bonded motifs formed in the malic and tartaric acid salt structures. The interactions are indicated by a dashed blue line and labelled according to their graph set notation. The number of structures in which each motif occurs is given in square brackets.

Statistics for the occurrence of each motif in the 50 structures are given in Table 4.5. In common with the calculations for the interactions in Table 4.4 N_{poss} is calculated as the number of structures in which the molecules contain the required functional groups to form the motif in either their ionised or neutral states to allow the examination of ionisation state as an outcome of the motifs that can be formed.

Table 4.5 Frequencies of occurrence for the 12 motifs in the structures containing dicarboxylic acids.

Donor	Acceptor	Graph Set	Nposs	Nobs	Pm (%)
<i>tert</i> -NH ⁺	CO ₂ ⁻	D1	21	14	67
		R2,1(5)	21	3	14
		C2,2(12)	7	2	29
<i>sec</i> -NH ₂ ⁺	CO ₂ ⁻	D1	29	5	17
		R2,1(5)	29	5	17
		C2,2(6)	29	11	38
		C2,2(9)	29	2	7
		C2,2(12)	18	6	33
		R4,4(12)	29	2	7
CO ₂ H	CO ₂ ⁻	C1,1(7)/ C1,1(9)	50	32	64
		C1,1(5)	27	4	15
COH	CO ₂ H / CO ₂ ⁻	C1,1(6)	27	6	22
		R2,2(10)	27	4	15
		R2,2(12)	27	4	15

There is considerable diversity in the hydrogen bonded structures with only the D1 acid-base interaction in systems containing *tert*-amine bases and the C1,1(7)/C1,1(9) carboxylic acid- carboxylate chain motifs having **Pm** > 50%. As the amine and carboxylic acid groups are the best hydrogen bond donors and acceptors on the molecules the favourability of intermolecular interactions between them is expected in accordance with Etter's rules (Etter, 1991). For secondary amine bases extended acid-base chain motifs are more common in comparison to the tertiary amine structures but no single motif is clearly favoured. The lack of robust hydroxyl-carboxylic acid motifs indicates that this interaction plays a secondary role in determining the hydrogen- bonded structures.

As these interactions are observed in more than one crystalline structure they are considered to be supramolecular synthons. Six motifs are mutually exclusive and the structures featuring these are grouped into families as shown in Figure 4.10. Structures are classed as Type 1 or Type 2 structures containing the C1,1(7)/C1,1(9) acid chain or C2,2(12) acid-base chain respectively. They are then sub-classified according to other amine to carboxylate hydrogen bond motifs and then by motifs formed by hydroxyl groups. Four structures where discrete acid - base contacts are the sole interaction have been classed as discrete ion pairs and four structures are ungrouped.

4.4.2.1 Structures featuring a C1,1(7) chain

64% of the dicarboxylic acid systems formed the C1,1(7) (or isostructural C1,1(9) motif containing adipate with 6 carbon atom backbone) hydrogen acid chain. **Pm** for this motif is approximately equal for both secondary and tertiary amine bases with 62% and 67% of the systems containing these functional groups forming this motif respectively. The motif is the base vector in nine hydrogen bonding arrays formed by the inclusion of other hydrogen bonding motifs as shown in Figure 4.11 and Figure 4.12. These figures provide more detail on the hydrogen bonded structural arrays summarised in Figure 4.10.

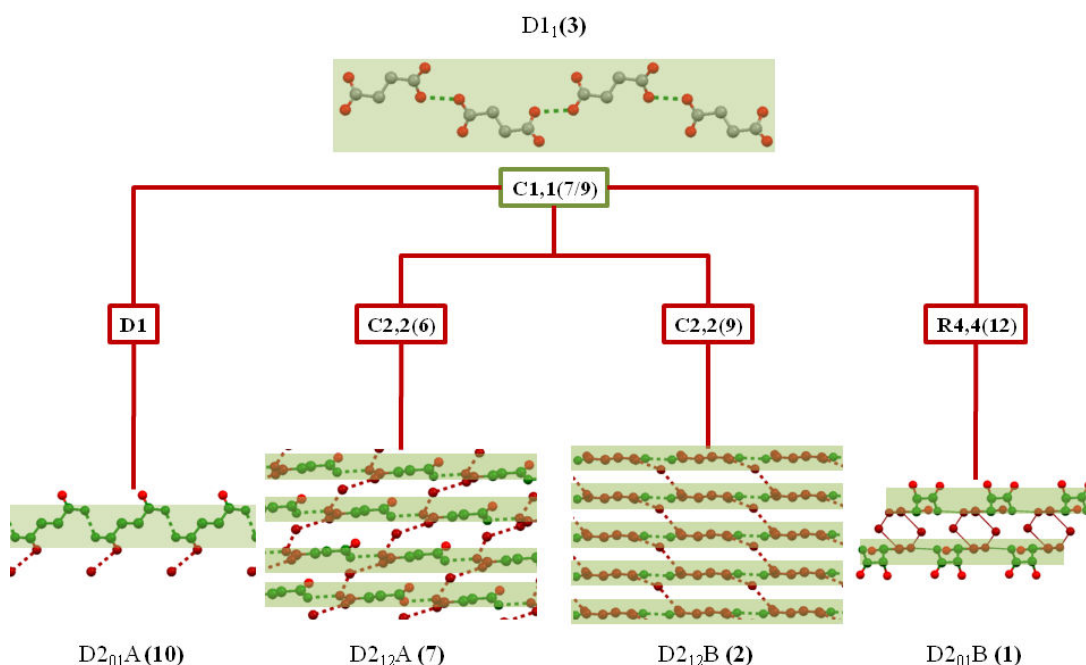


Figure 4.11 H-bonded arrays containing an $NH^+ \cdots CO_2^-$ motif in addition to the C1,1(7/9) hydrogen acid chain (highlighted in green) from Figure 4.10. Connector lines indicate additional hydrogen bonding motifs in the structure and atoms and contacts are coloured according to the motif they are part of with ■ C1,1(7/9) motif only ■ $NH^+ \cdots CO_2^-$ contacts. The $D2_{12}A$ and $D2_{12}B$ arrays are viewed perpendicular to the plane of the hydrogen bonds.

For tertiary amine bases, the formation of a discrete amine-carboxylate hydrogen bond to form a **D2₀₁A** chain occurs with a 100% probability if there are no additional functional groups on the acid molecule. In 90% of the structures containing a secondary amine base each amine proton forms a simple hydrogen bond to a carboxylate group, cross-linking the C1,1(7/9) chains to give **D2₁₂A** or **D2₁₂C** arrays with a single example of a **D2₀₁A** chain. The hydrogen-bonded structures appear highly predictable in these systems but in the secondary amine structures the C1,1(7) chain appears to dictate the hydrogen bonded topology.

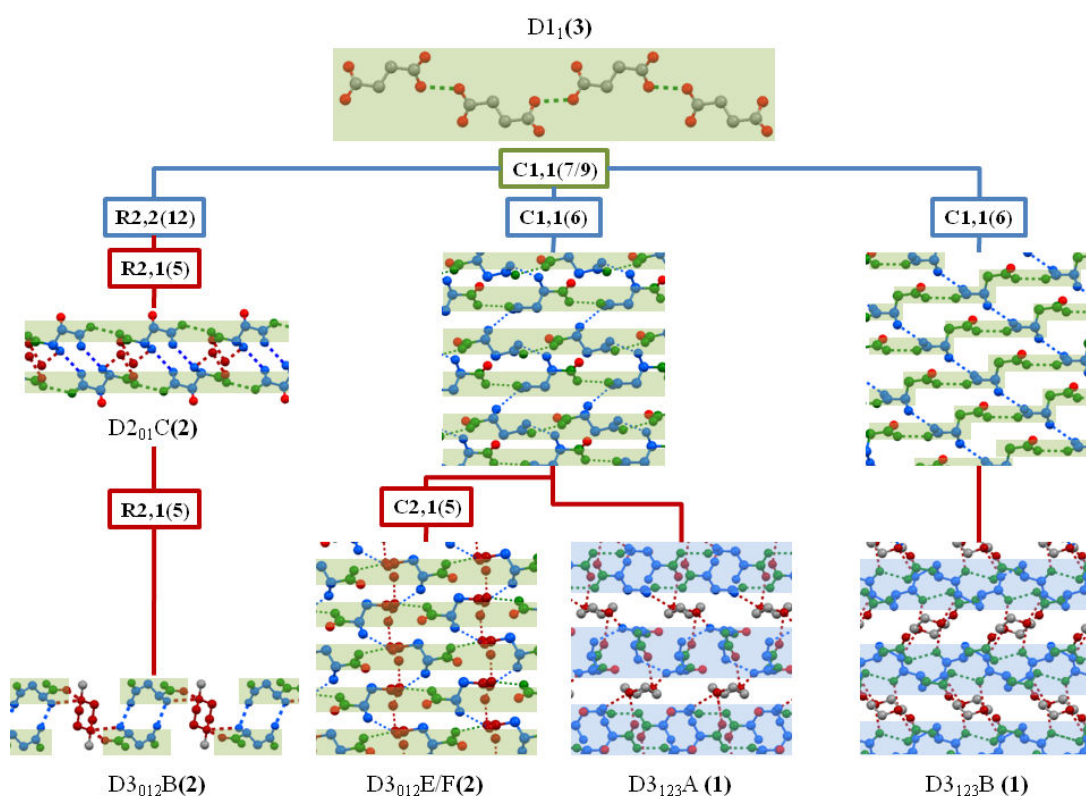


Figure 4.12 H-bond arrays containing $\text{OH}\cdots\text{CO}_2^-/\text{CO}_2\text{H}$ motifs and the C1,1(7/9) base vector (highlighted green) from Figure 4.10. Connector lines indicating additional motifs in the structure and atoms and contacts are coloured according to the motif they are part of with ■ C1,1(7/9) motif only; ■ $\text{NH}^+\cdots\text{CO}_2^-$ and ■ $\text{OH}\cdots\text{CO}_2^-$ motifs. Sheets formed by the C1,1(7/9) and $\text{OH}\cdots\text{CO}_2^-/\text{CO}_2\text{H}$ motifs are viewed perpendicularly to the H-bonds and the **D3₁₂₃A/D3₁₂₃B** arrays are viewed along the plane of the 2-dimensional sheet substructures (highlighted blue).

The structures containing hydroxyacid counterions have a much greater diversity in their intermolecular hydrogen bonding arrangements than dicarboxylic acids. For tertiary amine bases there is a 50% probability of formation of a direct acid-amine contact. In 20% of the structures a bifurcated hydrogen bond is donated to a hydroxyl and carboxylate group in an acid molecule with the R2,1(5) motif, cross-linking the hydrogen acid chains to give the two-dimensional **D3₀₁₂B** structure. In the remaining 30% of the structures no acid-base hydrogen bonds are formed, in these cases the amine donates a hydrogen bond to a water molecule and these structures will be discussed in detail in Chapter 5.

The amine-carboxylate hydrogen bonding arrangement in secondary amine hydroxyacid salts is equally unpredictable. The only extended amine-carboxylate motif formed in these cases is the C2,1(5) chain, in the **D3₀₁₂E** structure the amine donates a bifurcated hydrogen bond to one carboxylate and one carboxylic acid group and in **D3₀₁₂F** the bond is donated to two carboxylate groups. In two cases one amine hydrogen forms an R2,1(5) motif and the second donates a hydrogen bond to water to produce the **D2₀₁C** chain structure. The two remaining structures both contain the piperazinium cation and in both cases a unique pattern of hydrogen bonds to the acid anions is formed, cross-linking two-dimensional sheets of acid molecules into a three-dimensional network.

The hydroxyl-carboxylate motifs are formed in 44.4% of the structures featuring the requisite functional groups. The R2,2(12) and C1,1(6) motifs are most common, occurring in four and three structures respectively, the low incidence of these interactions is a result of competition with interactions to water molecules and this will be discussed in detail in Chapter 5. It appears from these structures that the hydroxyl-carboxylate interaction does not play a dominant role in defining the supramolecular structure of these systems and the incorporation of hydroxyacid counterions introduces significant uncertainty to the final hydrogen bonded structure.

4.4.2.2 Structures based on the C2,2(12) motif

The C2,2(12) motif is observed in 32% of systems containing dinitrogen bases, with only a slightly higher probability of formation of 33% in cases where the base contains one or two secondary amine groups than the 28% probability for 1,4-dimethylpiperazine. The motif is more common for hydroxyacids with 43% of the structures containing the required functional groups forming the interaction in comparison to 25% of the systems in which the acid molecule contains carboxylic acid groups only. Six different hydrogen-bonded arrays contain this motif as the base vector as shown in Figure 4.13.

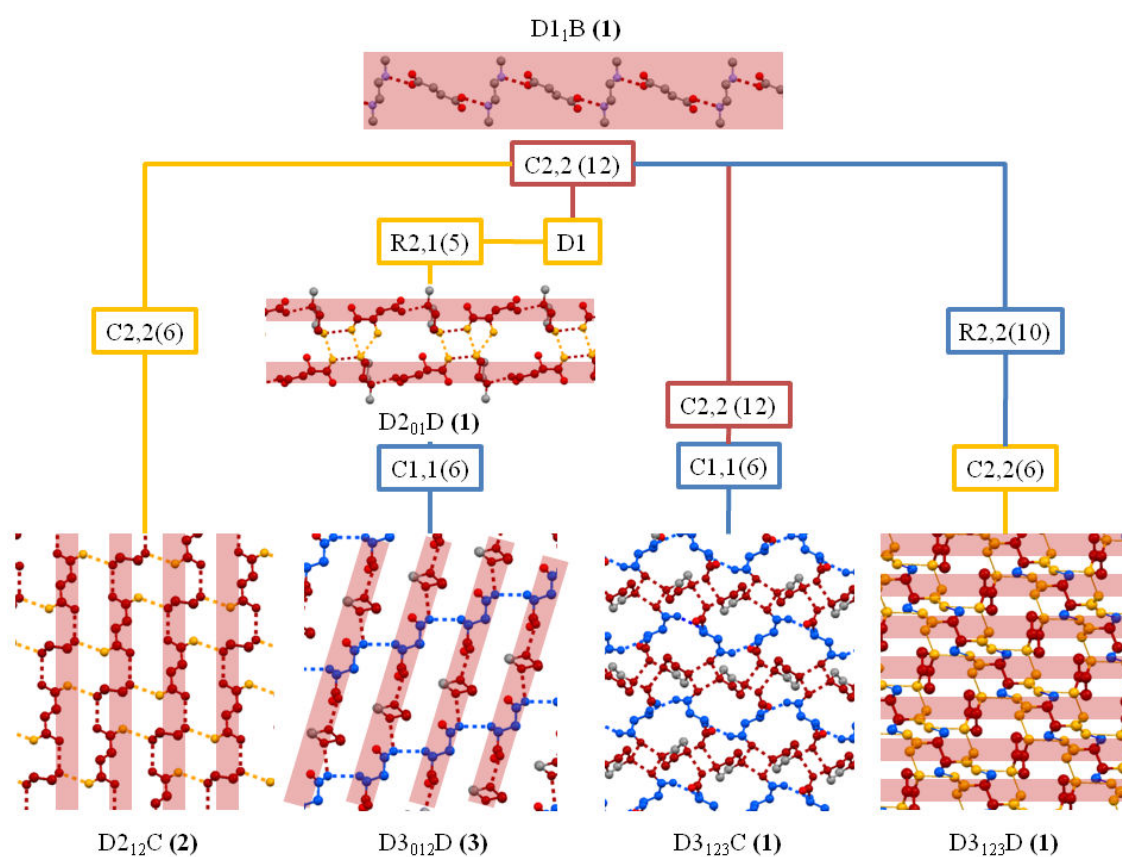


Figure 4.13 Dicarboxylic acid structures based on the C2,2(12) $\text{NH}^+\cdots\text{CO}_2^-$ motif (highlighted red). The connector lines indicate the additional hydrogen bonding motifs in the structure and the atoms in the diagrams are coloured according to the motif they are part of with ■ C2,2(12) motif only ■ additional $\text{NH}^+\cdots\text{CO}_2^-$ and ■ $\text{OH}\cdots\text{CO}_2^-$ contacts. The **D3₁₂₃C** structure is a three-dimensional network and is visualised along the axis of the C1,1(6) $\text{OH}\cdots\text{CO}_2^-$ chain.

As the majority of the structures contain a secondary amine and a hydroxyacid molecule two and three-dimensional hydrogen bond arrays are common. There is one example of a structure where the C2,2(12) motif is the sole intermolecular hydrogen bonded vector formed by the acid and base. Secondary amine bases form the C2,2(6) $\text{NH}_2^+\cdots\text{CO}_2^-$ chain motif in addition to the C2,2(12) interaction in 50% of cases. These combine to give two-dimensional hydrogen bonded sheet structures (e.g. **D2₁₂C**, Figure 4.13) when the acid has no additional hydrogen bonding groups or three-dimensional networks (e.g. **D3₁₂₃D**) with hydroxyacid counterions. It appears that, in contrast to the extended $\text{NH}_2^+\cdots\text{CO}_2^-$ motifs present in the structures based on the C1,1(7/9) motif, the C2,2(12) motif is not competitive with motifs formed by the hydroxyl groups on the acid molecule.

$\text{OH}\cdots\text{CO}_2^-$ interactions are proportionately more common than in the structures containing the C1,1(7) chain as the base vector as 80% of the hydroxyacid structures form either the C1,1(6) or R2,2(10) motif. In three cases (LMMA, LTDM and LTMA) the C1,1(6) motif extends the structure along an axis perpendicular to the C2,2(12) motif to give a two-dimensional hydrogen bonded sheet (**D3₀₁₂D**), while in two cases (LMPA and LTPA) the $\text{OH}\cdots\text{CO}_2^-$ C1,1(6) or R2,2(10) motifs extend the structures into a three-dimensional network.

4.4.2.3 Discrete structures

Eight structures within the library do not contain either the C1,1(7) or C2,2(12) motif and hence are not classified as belonging to one of the two main groups. These include four hydrogen maleate salts, three of which are arrays of hydrogen bonded discrete ion pairs (**D1₀**). In these cases the limited hydrogen bond forming potential of the tertiary amine bases and the formation of an S1,1(7) intramolecular hydrogen bond by the anion prevent the formation of extended intermolecular hydrogen bond motifs. In contrast the high hydrogen bonding potential of piperazine allows the formation of a hydrogen bonded chain structure in piperazinium hydrogen maleate (Jin, *et al.*, 2003).

Two malic acid salts feature unique intramolecular hydrogen bonds that prevent the hydroxyl groups from forming intermolecular hydrogen bonds. In morpholinium DL-

malate the hydroxyl group forms an S1,1(6) hydrogen bonded ring with the adjacent carboxylate group. Similarly in the 1,4-dimethylpiperazinium hydrogen L-malate structure reported by Farrell *et al* (Farrell, *et al.*, 2002) the carboxylic acid group forms an S1,1(7) hydrogen bond to the second carboxylate group.

Two mixed systems formed by adipic acid contain a fully deprotonated adipate anion and a neutral adipic acid molecule. In both cases, the base is monoprotated and forms intermolecular hydrogen bonds to both carboxylate groups on the adipate anions. In the structure of the salt with 1,4-dimethylpiperazine this results in what are essentially base-acid-base hydrogen bonded trimers while in the 1-methylpiperazinium structure the secondary amine group enables the formation of an acid-base hydrogen bonded chain with the molecules linked by the R4,4(12) motif. Both these substructures are interlinked by intermolecular hydrogen bond contacts formed from the carboxylic acid groups on the neutral adipic acid molecules to form the extended hydrogen bonded networks.

4.4.3 Structural rules for dicarboxylic acid counterions

From examination of the structures containing dicarboxylic acid derived counterions the following structural rules are proposed. The number of observations on which each rule is based is given in bold:

Rule D1: In systems containing a single nitrogen donor atom there is a >95% probability that a hydrogen acid salt will form that contains the C1,1(7/9) acid chain motif. **(22)**

Rule D2: When Rule D1 holds for an aliphatic dicarboxylic acid, there is a 90% probability that secondary amine bases will form two hydrogen bond contacts to carboxylate groups. In > 75% of these the C2,2(6) chain motif will form to produce a 2-dimensional hydrogen bonded sheet. **(10)**

Rule D3: When Rule D1 is observed and there are additional hydrogen bonding groups on the acid molecule the C2,2(6) motif will not form. There will always be at least one amine-carboxylate hydrogen bond contact, but the motif observed becomes unpredictable. **(4)**

Rule D4: In cases where Rule D2 is observed and the base contains a single tertiary donor nitrogen there is a >70% probability that a hydrogen bond will be formed to the carboxylate group. **(11)**

Rule D5: When the base contains two basic nitrogens the C2,2(12) motif is competitive with the C1,1(7/9) motif and will be observed twice as frequently. **(13)**

Rule D6: Hydroxyl to carboxylate/carboxylic acid interactions are not as robust as amine-carboxylate interactions. They are frequently replaced by hydroxyl-water contacts and cannot be considered a reliable structure-directing interaction. **(25)**

Rule D7: Maleic acid crystallises as the hydrogen acid with an intramolecular hydrogen bond. None of the other rules are applicable to this counterion. **(4)**

4.5 Benzoic acid counterions

4.5.1 Intermolecular hydrogen bonds

Ten intermolecular hydrogen bonded contact types involving functional groups on the acidic and basic components of the systems were identified in the 40 structures in the benzoate subgroup. All ten are types that were previously observed in the dicarboxylic acid group and as with the analysis of the dicarboxylic acid salts interactions involving water molecules have been ignored. They are shown below in Figure 4.14. The statistics for the occurrence of each interaction are given in Table 4.6.

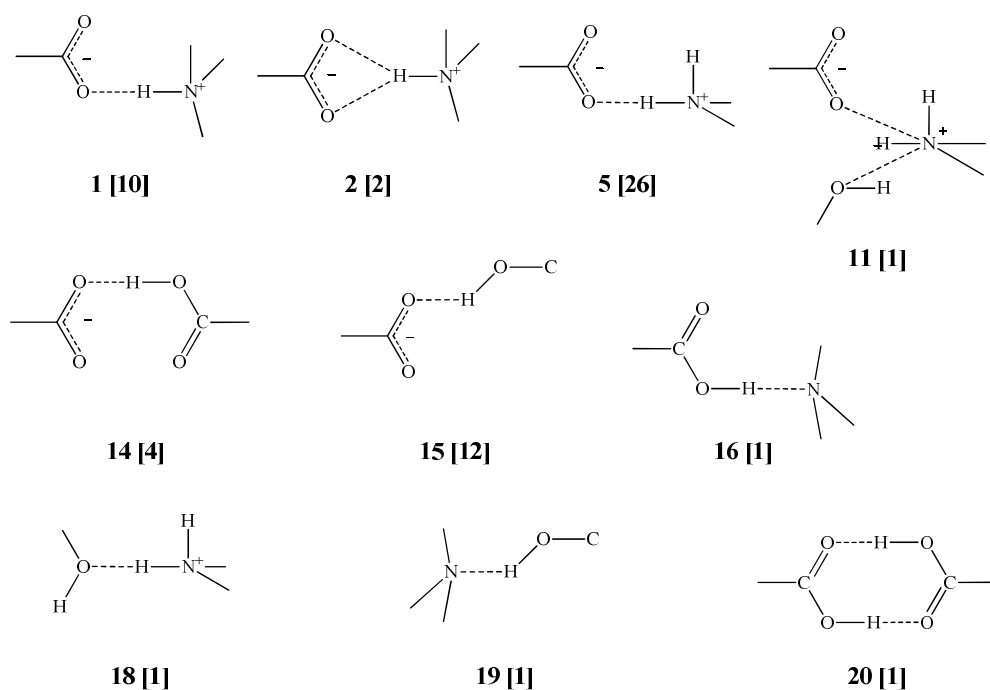


Figure 4.14 Hydrogen bonds involving only acid or base molecules in the dicarboxylic acid structures, the number of structures containing each interaction type is given in brackets.

Table 4.6 Frequencies of occurrence for the hydrogen bond contacts identified in the structures containing benzoic acids.

Bond	Donor	Acceptor	N _{poss}	N _{obs}	P _m (%)
1	<i>tert</i> -NH ⁺	CO ₂ ⁻	24	10	42
2	<i>tert</i> -NH ⁺	CO ₂ ⁻	24	2	8
5	<i>sec</i> -NH ₂ ⁺	CO ₂ ⁻	26	26	100
11	<i>sec</i> -NH ₂ ⁺	CO ₂ ⁻ + <i>o</i> -OH	10	1	10
14	CO ₂ H	CO ₂ ⁻	40	4	10
15	<i>p</i> -OH	CO ₂ ⁻	18	12	67
16	CO ₂ H	<i>Tert</i> -N	25	1	4
18	<i>sec</i> -NH ₂ ⁺	<i>o</i> -OH	10	1	10
19	<i>p</i> -OH	<i>Tert</i> -N	11	1	9
20	CO ₂ H	CO ₂ H	40	1	3

There is less variety in the interactions than in the dicarboxylic acid structures because of the reduced number of functional groups on the molecules. The low probability of formation of NH⁺⋯CO₂⁻ contacts **1** and **2** is a result of the inclusion of bases containing both tertiary and secondary amine nitrogens; with one exception these bases are protonated on the secondary amine nitrogen only. When bases with only tertiary amine nitrogens are considered the probability of these contacts being formed increases to 71% and 14% respectively. The two structures with no amine-carboxylate contacts both contain tertiary amine bases, in one this is a result of the system crystallising as a neutral cocrystal and in the other the amine donates the hydrogen bond to water.

Secondary amine bases always form NH₂⁺⋯CO₂⁻ contact **5** and there is competition between the carboxylate anion and water for the second hydrogen bond from the amine group. This results in the diversity in amine-carboxylate hydrogen bonded motifs discussed in the next section. When the acid molecule possesses a *para*-hydroxyl group there is a 67% probability that *p*-OH ⋯ CO₂⁻ contact **15** will be formed with a carboxylate group. There is a small degree of competition with *p*-OH - *tert*-N interaction **19** when the base molecule features a neutral tertiary amine nitrogen in addition to a protonated secondary amine nitrogen but the main competing interaction is the donation of a hydrogen bond to a water molecule.

The incorporation of a neutral acid molecule to yield a mixed system is more likely for systems containing benzoic acid counterions than dicarboxylic acids. The most frequent mode of contact in the mixed species is $\text{CO}_2\text{H} \cdots \text{CO}_2^-$ **14**, in which the neutral acid molecule donates a hydrogen bond to the carboxylate group. There is also one example of the formation of the traditional carboxylic acid dimer **20**. A search of the CSD database for structures containing one of the neutral acid molecules examined in this section in a system with an organic molecule returned 81 hits of which 7 contained the dimer. Thus this gives a higher probability of occurrence to this data set of 9%, however it must be noted that the CSD search contained both neutral and ionic systems.

4.5.2 Hydrogen bonded motifs

In the 40 benzoate structures characterised, four hydrogen bonding motifs involving the contacts identified in Section 4.5.1 are observed in more than one structure. These are the three amine-carboxylate motifs shown in Figure 4.15 and the hydroxyl-carboxylate motif shown in Figure 4.16. Statistical information for the occurrence of each motif is summarised in Table 4.7.

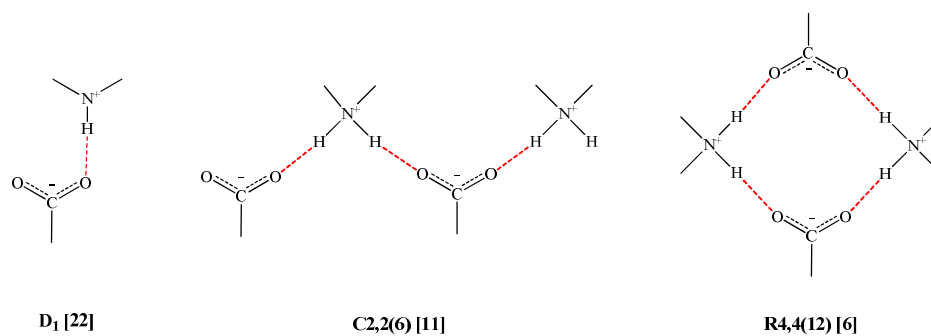


Figure 4.15 Amine-carboxylic acid hydrogen bonding motifs identified in the benzoic acid subset of structures. The number of structures containing the motif is given in square brackets.

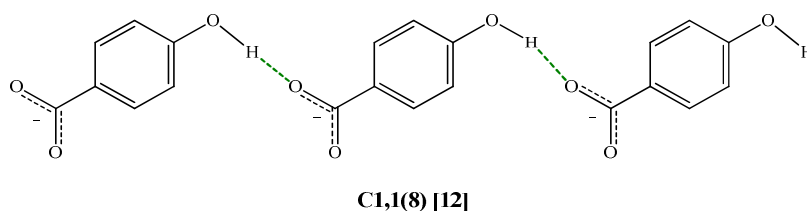


Figure 4.16 The hydroxyl to carboxylate hydrogen bonded chain motif identified in the structures containing a *para*-hydroxyl group. The number of structures containing the motif is given in square brackets.

Table 4.7 Frequencies of occurrence of the motifs in the benzoic acid structures.

Donor	Acceptor	Graph Set	N _{poss}	N _{obs}	P _m (%)
<i>tert</i> -NH ⁺	CO ₂ ⁻	D1	14	12	86
<i>sec</i> -NH ₂ ⁺	CO ₂ ⁻	D1	26	9	35
		R4,4(12)	26	6	23
<i>p</i> -OH	CO ₂ ⁻	C1,1(8)	18	12	67

The occurrence of the D1 motif in structures with tertiary amine bases has been discussed in the previous section. For clarity, both the simple and bifurcated hydrogen bond contacts are considered to be the same here as they play a similar role in determining the extended hydrogen bonded structures. In secondary amine salts, the base always donates a hydrogen bond to one carboxylate oxygen. The probability of formation of the C2,2(6) or R4,4(12) motifs is lowered by competition from water to accept the second hydrogen bond from the base instead of another carboxylate oxygen.

In all cases where contact **15** between an acid *para*-OH group and a CO₂⁻ group is present the interaction propagates the C1,1(8) hydrogen bonded acid chain. Extended motifs due to this interaction in aminopyridine salts of hydroxybenzoic acids were shown to be a consistent structural feature in a study by Sarma *et al* (Sarma *et al.*, 2009) when the salt was anhydrous, but rare for hydrated salts. The hydrogen-bonded synthons in the structures are compared in Figure 4.17. As the amine-carboxylate synthons are mutually exclusive the structures are grouped into three families based on these interactions. The neutral COOH...N contact in the DMTU cocrystal is regarded as the same as the corresponding ionic contact in the salts.

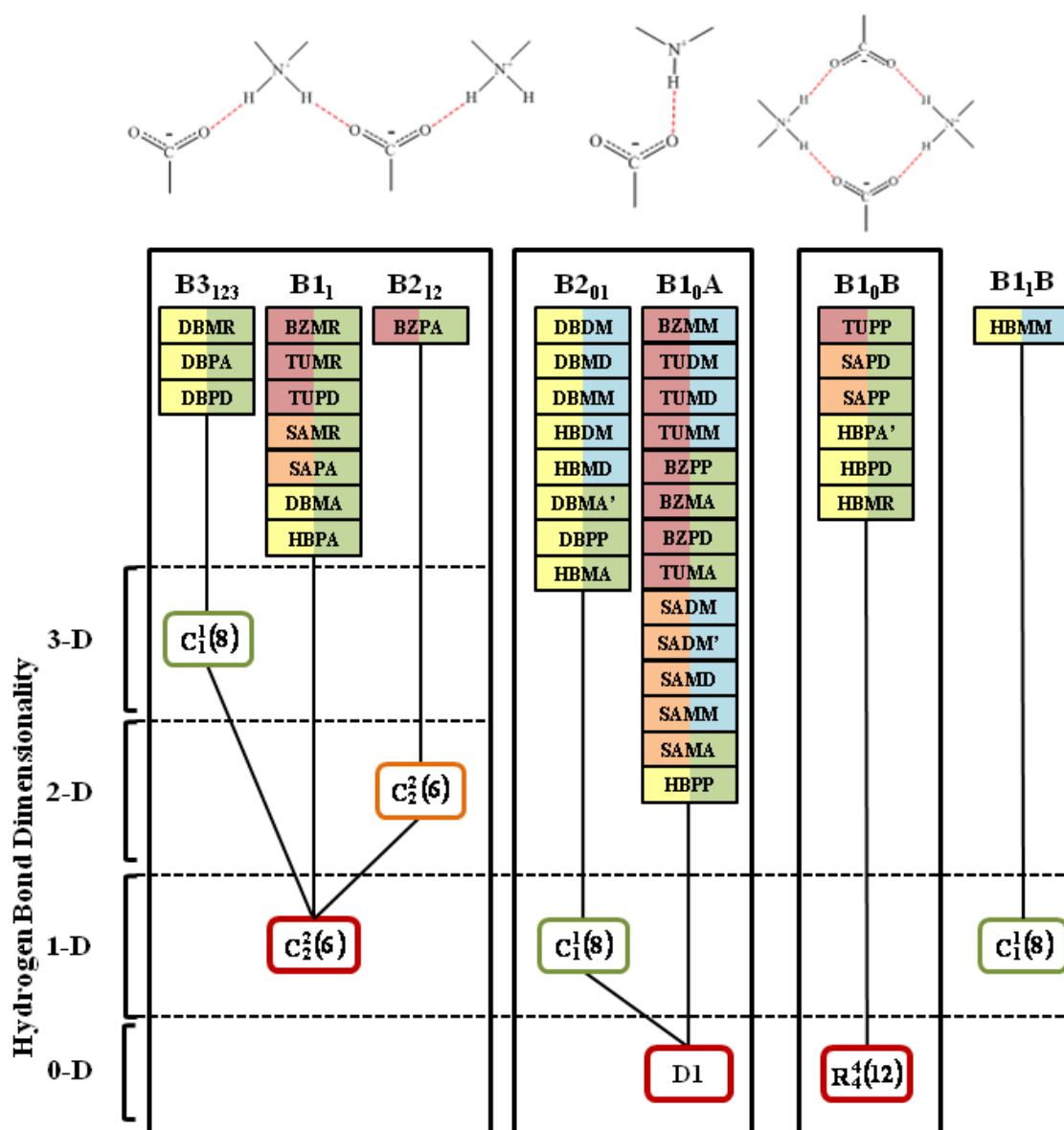


Figure 4.17 Dendrogram showing the hydrogen bond synthons present in the benzoic acid structures. Structures are represented by boxes, the acid and base components are identified by the two letter codes assigned in Section 4.1 and coloured according to the hydrogen bonding groups present on the molecules: ■ CO_2H group only; ■ CO_2H and one *ortho*-OH group; ■ CO_2H and one *para*- or one *ortho*- and one *para*- OH group; ■ NH^+ donor groups only; ■ NH_2^+ donor group available. Hydrogen bonding motifs are represented by graph set notation with outline colours according to the interaction type: — NH^+/NH_2^+ to CO_2^- bond, — *para*-OH to CO_2^- bond.

4.5.2.1 Structures based on the C2,2(6) motif

The C2,2(6) $\text{NH}_2^+\cdots\text{CO}_2^-$ motif is the most common for secondary amine salts, however it is not heavily favoured as it is observed in 42% of these salts. Due to the hydrogen bond donor and acceptor geometries required to form the C2,2(6) motif, 10 structures in this group are 1:1 salts and BZPA forms a 2:1 salt. The relationships between the three vector types in this group are shown in Figure 4.18.

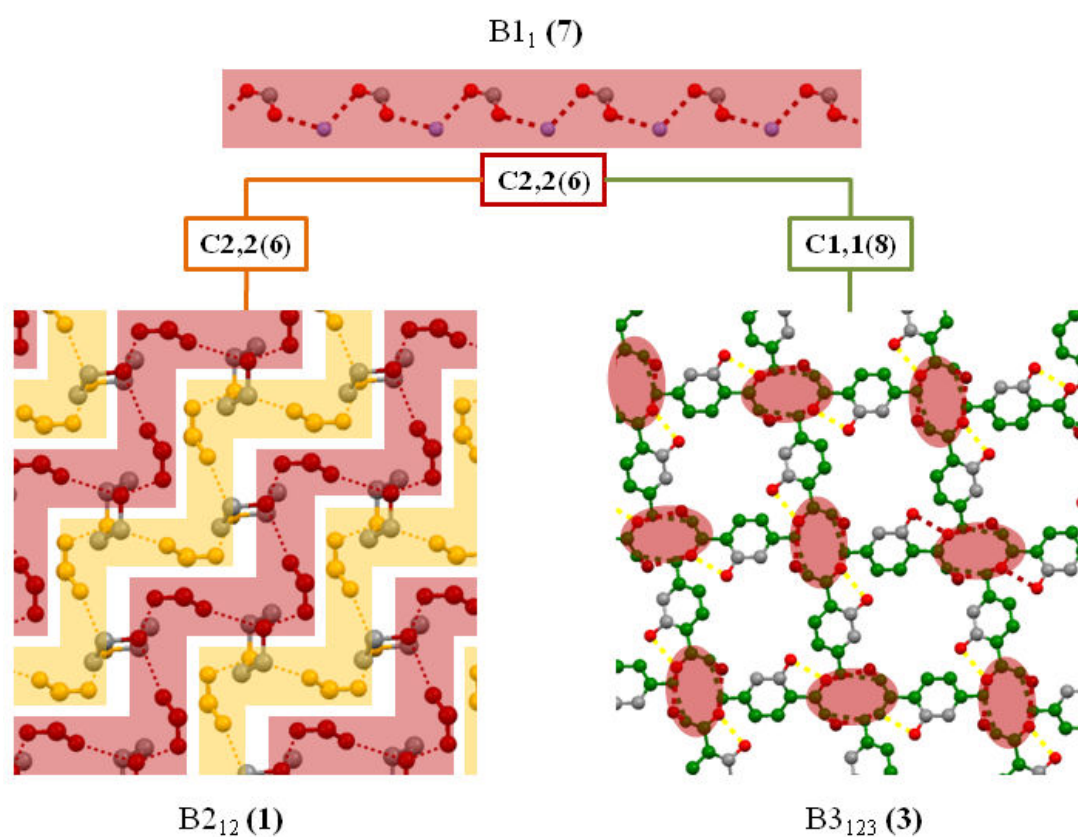


Figure 4.18 The H-bond arrays formed by structures containing the C2,2(6) $\text{NH}_2^+\cdots\text{CO}_2^-$ motif (highlighted in red). The connector lines indicate the additional hydrogen bonding motifs in the structure and the atoms in the diagrams are coloured according to the motif they are part of with ■ primary C2,2(6) motif; ■ secondary C2,2(6) motif and ■ $\text{OH}\cdots\text{CO}_2^-$ contacts. For clarity only the nitrogen atoms of the base molecules are shown in **B**₃₁₂₃, which is viewed along the axis of the C2,2(6) chains.

The most common array is the one-dimensional **B1₁** chain. Two of these are formed by acid molecules with a *para*-hydroxyl group but these groups interact with water. Two structures contain the piperazine base that forms the motif at both nitrogens along the same axis, essentially giving a pair of **B1₁** chains linked through the base molecules. In the **B2₁₂** array the C1,1(6) chains formed at each piperazinium nitrogen lie in different directions resulting in a 2-dimensional hydrogen bonded sheet. In the three anhydrous structures where the acid molecule possesses a *para*-hydroxyl group the formation of the C1,1(8) motif propagates intermolecular hydrogen bonds along all three axes to give hydrogen bonded network **B3₁₂₃**.

4.5.2.2 Structures based on the D1 motif

Structures in which the acid and base molecules are connected by discrete hydrogen bonds are the most prevalent type with the interaction occurring in all but one of the tertiary amine salts and in nine secondary amine salts. In 14 of these, there are no further acid-base interactions giving arrays of discrete hydrogen bonded pairs of ions (**B1₀**) and in eight the hydroxyl groups on the acid molecules form hydrogen bonded chain motifs. With the exception of HBPP the C1,1(8) chain is always formed when the acid molecules possess a *para*-hydroxyl group. The relationships between the structural types are shown overleaf in Figure 4.19.

As formation of the D1 motif leaves the hydrogen bond acceptor requirements of the second carboxylate oxygen unfulfilled, the stoichiometry and ionisation state of the acidic and basic components in the **B1₀A** arrays is unpredictable in comparison with systems based on the C2,2(6) and R4,4(12) motifs. The 15 **B1₀** arrays include 11 salts, 1 cocrystal and 4 mixed systems in which a neutral acid molecule is incorporated into the crystal structure. The proportion of each type of system formed by combinations of each type of acid and base are given overleaf in Table 4.8.

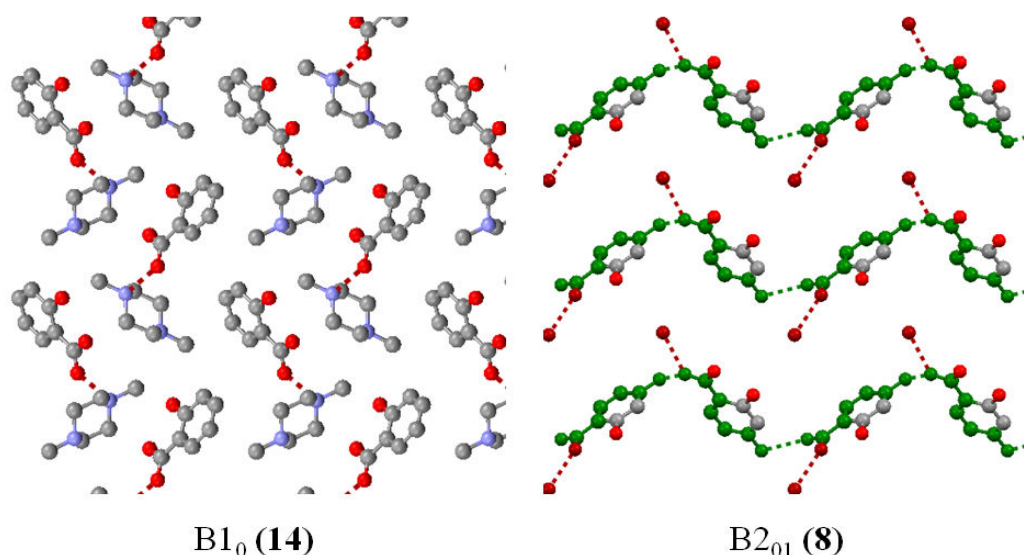


Figure 4.19 The two H-bonded arrays formed by structures containing discrete acid-base hydrogen bonds. The $\text{NH}^+\cdots\text{OC}^-$ bonds are indicated by dark red lines and in the $\mathbf{B2}_{01}$ structures the contact atoms for this interaction are also coloured dark red, for clarity only the hydrogen bonding nitrogens of the bases are shown. Atoms and contacts that make up the C1,1(8) motif are coloured green.

Table 4.8 Relative proportions of system types forming $\mathbf{B1}_0$ arrays.

Hydrogen Bonding Groups		Salt	System Type	
Acid	Base		Cocrystal	Mixed
CO ₂ H only	<i>tert</i> -NH ⁺	1/4	1/4	2/4
	<i>sec</i> -NH ₂ ⁺	4/4	0/4	0/4
CO ₂ H and <i>o</i> -OH	<i>tert</i> -NH ⁺	3/5	0/5	2/5
	<i>sec</i> -NH ₂ ⁺	1/1	0/1	0/1
CO ₂ H and <i>p</i> -OH	<i>tert</i> -NH ⁺	0	0	0
	<i>sec</i> -NH ₂ ⁺	1/1	0/1	0/1

Mixed systems are formed for tertiary amine systems where the hydrogen bonding potential of the second carboxylate oxygen is satisfied by a bond from a neutral acid molecule. In three of the benzoic acid structures, this results in trimers as shown Figure 4.20. In BZMM and TUMM there is no further intermolecular hydrogen bonding in the crystal structure. The hydrogen bonding geometry in SAMM is slightly different as the base forms a bifurcated intermolecular hydrogen bond to the carboxylate group.

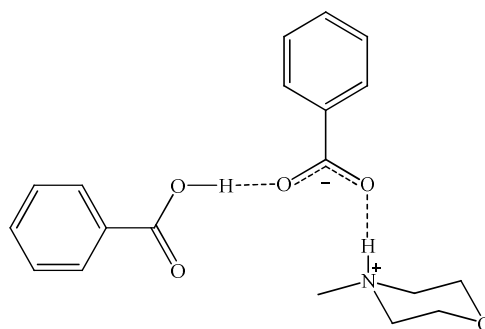


Figure 4.20 Intermolecular hydrogen bonding arrangement in 4-methylmorpholine benzoate benzoic acid (BZMM), representative of the most common type of mixed system found for the benzoic acid structures.

4.5.2.3 Structures based on the R4,4(12) motif

The seven structures based on the R4,4(12) motif are all salts with a 1:1 acid:base stoichiometry. This motif has the lowest **P_m** for secondary amine systems at 22%. It is never formed in structures with benzoic or 2,4-dihydroxybenzoic acid and the single example of a 4-toluic acid salt corresponds to an 11% probability of formation with this counterion. This motif is observed with a higher frequency in systems containing salicylic and 4-hydroxybenzoic acid, with frequencies of formation of 40% and 50% respectively. The extended structures of TUPP, SAPP and SAPD consist of arrays of tetramers with no further intermolecular hydrogen bonding. The C1,1(8) hydrogen bonded chain is not formed in structures containing 4-hydroxybenzoic acid, the hydrogen bonding requirements of the *para*-hydroxyl groups are instead satisfied by interactions with water molecules as discussed in Chapter 5.

4.5.2.4 Solvent-separated structure


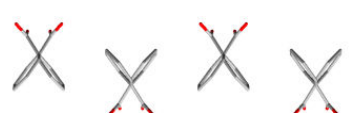
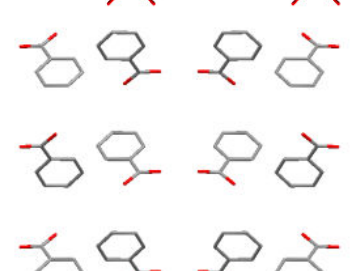
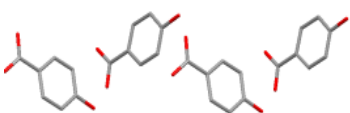
There are no direct acid-base contacts in 4-methylmorpholine 4-hydroxybenzoate 4-hydroxybenzoic acid. In this case, the base donates a hydrogen bond to a water molecule that in turn donates hydrogen bonds to the carboxylate and carboxylic acid groups of a 4-hydroxybenzoate anion and 4-hydroxybenzoic acid molecule respectively.

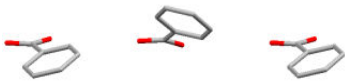
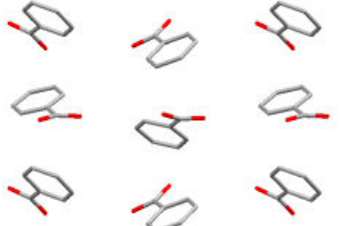
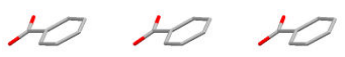
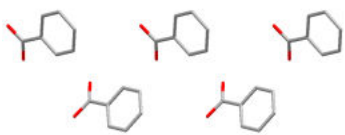
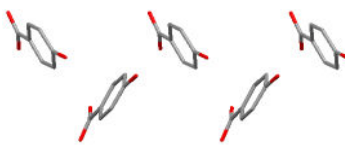
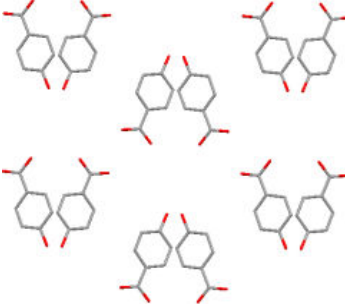
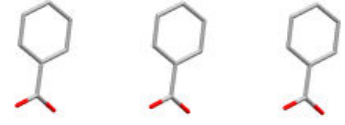
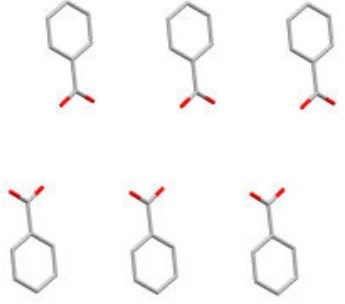
4.5.3 XPac analysis of the packing arrangements of the benzoate anions

The packing arrangements of the acid molecules, as opposed to solely the hydrogen bonding contacts, in the structures were compared using the XPac program with the parameters described in Section 2 with the benzene ring and carboxylate carbon atoms used as COSPs. Supramolecular constructs (SCs) consisting of common 1, 2 and 3-dimensional arrangements of molecules were identified in 25 of the 41 structures.

Six one-dimensional SCs were identified and as these do not contain any lower-dimensionality constructs as sub-components they are termed “*primary supramolecular constructs*”. Two further one dimensional SCs consisting of pairs of primary SCs were identified in addition to two two-dimensional and two three-dimensional SCs. The SCs are detailed overleaf in Table 4.9 including information on their dimensionality (D), the number of occurrences (#) of the construct, the number of base vectors (Base) and the dependencies between the primary, secondary and tertiary SCs.

Table 4.9 SCs in the benzoate structures. Primary SCs do not have a subscript while for secondary and tertiary SCs the subscript indicates the dimensionality of the construct.

SC	D	Description	Fig	#	Base	Dependencies
A	1	Single stack (translation)		4	t_1	
A ₂	2	Sheet		2	t_1, t_2	A ₁ → A ₂
A ₃	3	3-D Array		2	t_1, t_2, t_3	A ₁ → A ₃
B	1	Single stack (translation)		2	t_4	

SC	D	Description	Fig	#	Base	Dependencies
C	1	Single stack (translation)		3	t_5	
C ₂	2	Sheet		2	t_5, t_6	$C_1 \rightarrow C_2$
D	1	Single stack (translation)		10	t_7	
D ₁	1	Double stack (translation)		2	t_7	
E	1	Double stack (translation)		3	t_8	
E ₃	3	3-D Array		2	t_8, t_9, t_{10}	$E \rightarrow E_3$
F	1	Single stack (translation)		3	t_{11}	
F ₁	1	Double stack (translation)		2	t_{11}	$F \rightarrow F_1$

4.5.3.1 Structures containing supramolecular construct A

Supramolecular construct **A**, a one-dimensional head-to-tail chain of molecules, is found in four structures: DBDM, DBMA1, HBMA and SAMA. This construct forms the basis of two independent higher dimensionality constructs, a two-dimensional construct **A**₂ common to DBDM and DBMA1 and a three-dimensional array **A**₃ in HBMA and SAMA. Selected details for the structures containing these constructs are given in Table 4.10.

Table 4.10 Selected structural details for structures containing construct A.

Structure	SC	System	Z'	Spacegroup	H-Bonding Array
DBDM	A ₂	Salt	2	P-1	B2 ₀₁ (D1, C1,1(8))
DBMA1	A ₂	Salt	3	P21/c	B2 ₀₁ (D1, C1,1(8))
HBMA	A ₃	Salt	2	Pbca	B2 ₀₁ (D1, C1,1(8))
SAMA	A ₃	Salt	2	Pbca	B1 ₀ A (D1)

The structures containing construct **A** are all based on the D1 type acid-base hydrogen bonding motif. Three of the structures also contain the C1,1(8) acid chain motif, however the presence of the extended **A** construct in SAMA where this motif is absent due to the lack of a *para*- hydroxyl group indicates that the formation of this construct is not a result of a this particular hydrogen bonding interaction .

The packing arrangements of the one-dimensional **A** constructs in the four structures are shown in Figure 4.21 and Figure 4.22 overleaf. In all four cases, the constructs stack along a second axis to create two-dimensional sheets of acid molecules. In DBDM and DBMA1 the constructs stack antiparallel to the neighbouring constructs to give the two-dimensional construct **A**₂ while in HBMA and SAMA the constructs stack in parallel. In the latter structures these sheets are stacked along the third axis in an alternating arrangement to give the three-dimensional **A**₃ construct of acid molecules within the two structures.

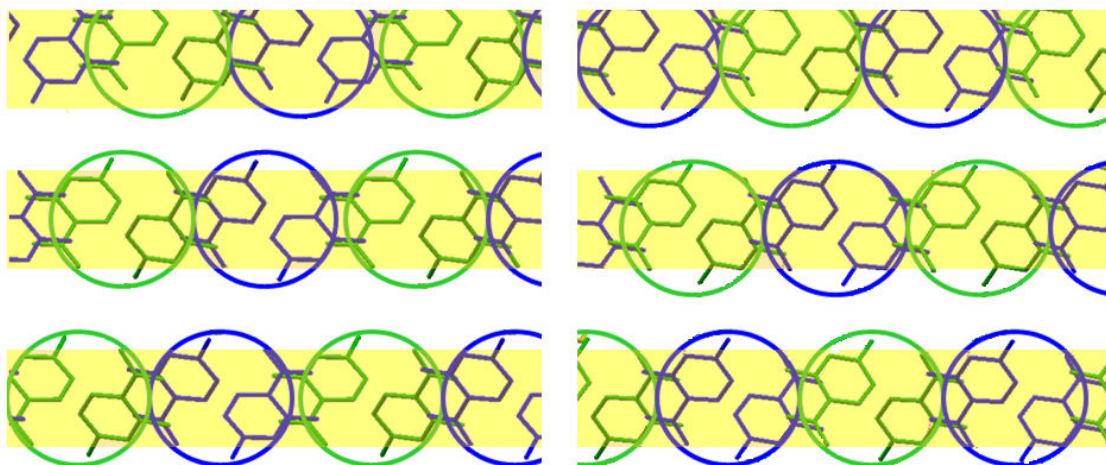


Figure 4.21 Packing arrangement of \mathbf{A} constructs in DBDM (left) and DBMA1 (right) viewed along the crystallographic b -axis. Constructs viewed along the \mathbf{t}_1 vector are coloured green and constructs viewed along the $-\mathbf{t}_1$ vector are shown in blue. The \mathbf{A}_1 constructs pack along the horizontal axis in the same arrangement in both structures to form two-dimensional \mathbf{A}_2 constructs highlighted in yellow.

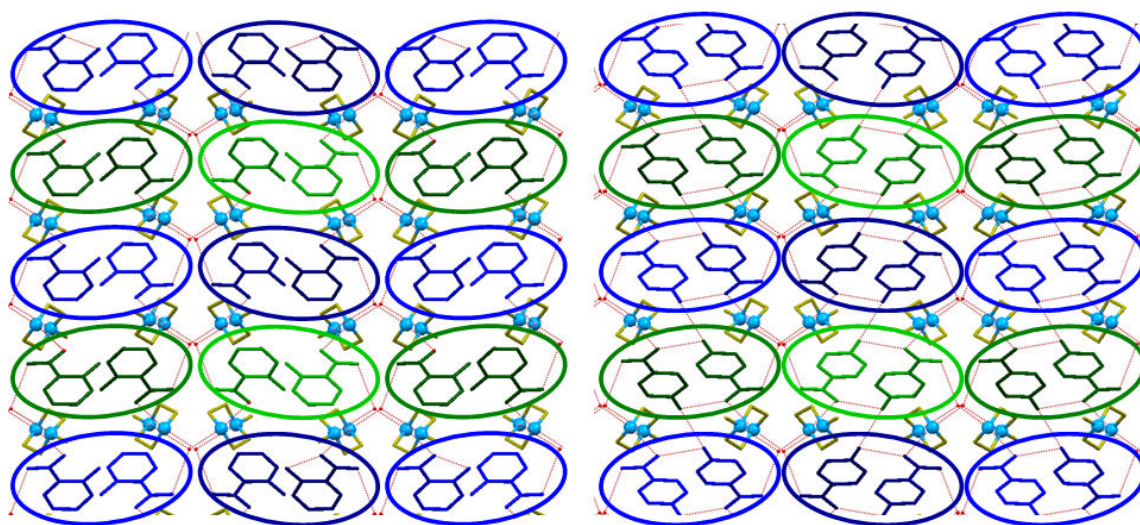


Figure 4.22 Packing arrangement of \mathbf{A} constructs in SAMA (left) and HBMA (right) viewed along the crystallographic a -axis. Constructs are viewed along the axis of the \mathbf{t}_1 vector with the same colour scheme used in Figure 4.22. The \mathbf{A}_1 constructs stack in the same arrangement along the b and c axes in both structures to give the three-dimensional \mathbf{A}_3 array of acid molecules. Neighbouring constructs lying in parallel are differentiated by light and dark shading.

4.5.3.2 Structures containing supramolecular construct B

Supramolecular construct **B**, a similar construct to **A**, is a one dimensional stack of acid molecules related by a 2_1 screw axis and is present in DBPA and HBMM. Selected details for the two structures are given in Table 4.11.

Table 4.11 Selected structural details for structures containing construct B.

Structure	SC	System	Z'	Spacegroup	H-Bonding Type
DBPA	B	Salt	2	P21/n	B3 ₁₂₃ (C2,2(6), C1,1(8))
HBMM	B	Mixed	3	C2/c	B1 ₁ B (C1,1(8))

The construct is a result of the formation of the C1,1(8) hydrogen bonded acid chains, in both structures the constructs are arranged into layers and alternate with respect to the orientation of the t_4 vectors. In HBMM the layers of constructs are linked by neutral acid molecules while in DBPA the base performs this function leading to different packing arrangements of the constructs as shown in Figure 4.23.

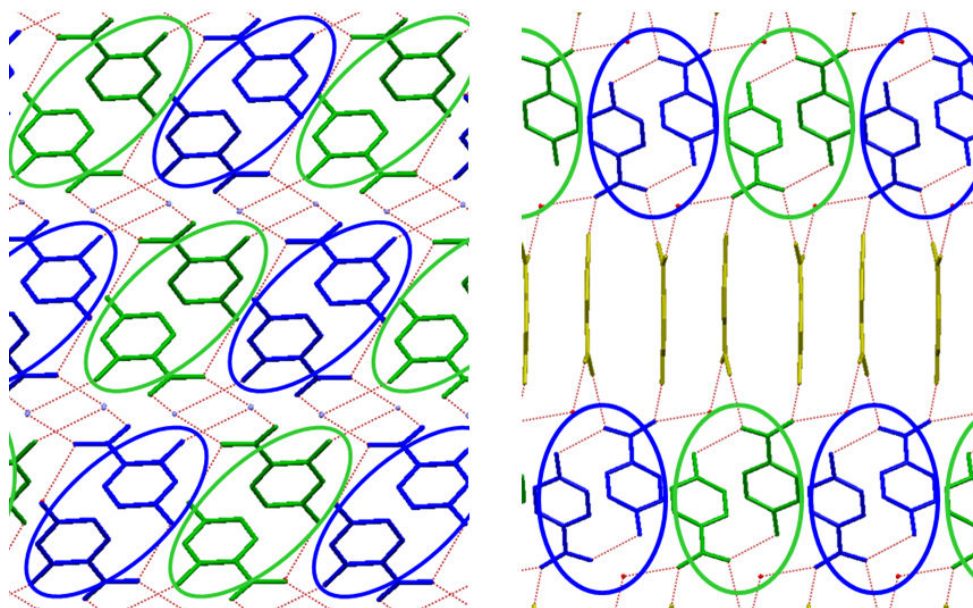


Figure 4.23 Packing of SC **B** in DBPA (left) and HBMM (right). Constructs are viewed along the t_4 vector. For clarity the base molecules in both structures have been omitted with the hydrogen bond contacts to the amine nitrogens indicated by small blue spheres.

4.5.3.3 Structures containing supramolecular construct C

Construct C, a single row of acid cations lying along a glide plane with the aromatic rings staggered in an alternating pattern, is observed in DBMA, BZPD and TUMA. Selected details for these structures are given in Table 4.12.

Table 4.12 Selected structural details for structures containing construct C.

Structure	SC	System	Z'	Spacegroup	H-Bonding Type
BZPD	C ₂	Salt	2	Pca21	B1 ₀ A (D1)
DBMA	C	Salt	2	Pna21	B1 ₁ (C2,2(6))
TUMA	C ₂	Salt	2	Pca21	B1 ₀ A (D1)

The structure of DBMA is based on the C2,2(6) acid-base hydrogen bonded chain in contrast to the discrete hydrogen bonded pairs of BZPD and TUMA. The constructs stack in parallel along the second axis of hydrogen bonding, in DBMA this axis is formed by interactions between the acid hydroxyl groups and amine nitrogens and is formed by amine-water interactions in BZPD and TUMA to give the two-dimensional C₂ construct. The different packing arrangements in the structures are shown in Figure 4.24.

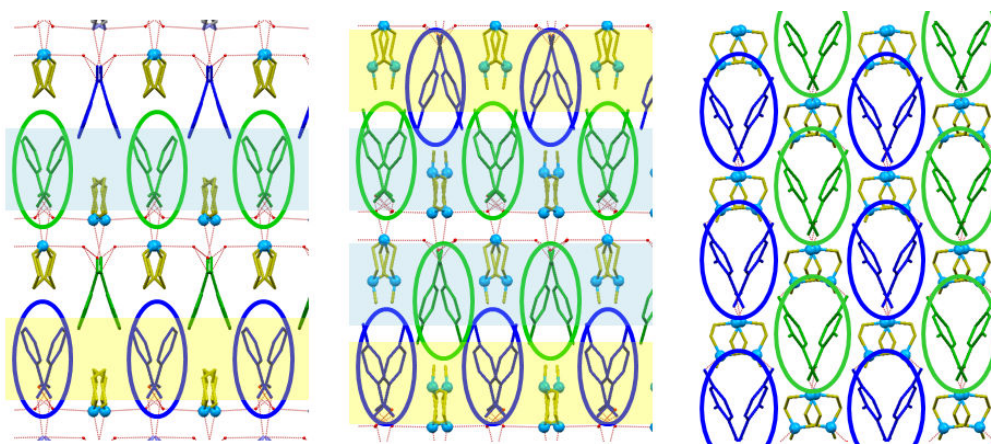


Figure 4.24 Packing arrangements of construct C₁ in BZPD (left), TUMA (centre) and DBMA (right). Constructs viewed along the t_5 vector are coloured green and constructs viewed in the $-t_5$ direction are blue. In BZPD and TUMA the horizontal layers of C₁ constructs form the two-dimensional C₂ sheet, sheets viewed along the t_5 axis are shaded yellow and those viewed along the $-t_5$ axis are shaded green, in both cases the t_6 vector runs horizontally across the page.

4.5.3.4 Structures containing supramolecular construct D

Construct **D** is a single offset face-to-face stack of acid molecules that has been identified in the ten structures listed in Table 1.13. The geometric relationships between the molecules in the construct vary considerably between the different structures as shown in Figure 4.25.

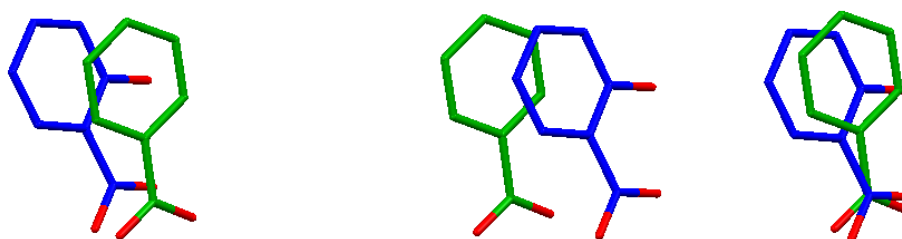


Figure 4.25 Construct **D** in SADM1 (blue) overlaid with construct **D** in BZPA (green), viewed perpendicular to the t_1 translation vector.

Table 1.13 Selected structural details for structures containing construct D.

Structure	SC	System	Z'	Spacegroup	H-Bonding Type
BZPA	D ₁	Salt	2	Pcab	B2 ₁₂ (C2,2(6), C2,2(6))
HBMD	D	Mixed	3	P2 ₁ 2 ₁ 2 ₁	B2 ₀₁ (D1, C1,1(8))
HBPA	D ₁	Salt	2	P2 ₁	B1 ₁ (C2,2(6))
SADM	D	Salt	2	P2 ₁	B1 _{0A} (D1)
SADM1	D	Salt	2	P2 ₁ /c	B1 _{0A} (D1)
SAMR	D	Salt	2	P2 ₁	B1 ₁ (C2,2(6))
SAPA	D	Salt	2	P2 ₁ /n	B1 ₁ (C2,2(6))
SAPD	D	Salt	2	P2 ₁ /c	B1 _{0B} (R4,4(12))
TUMD	D	Salt	2	P2 ₁ /c	B1 _{0A} (D1)
TUPP	D	Salt	2	P-1	B1 _{0B} (R4,4(12))

The construct has been identified in at least one structure featuring each of the common hydrogen bond motifs identified in Section 4.5.2, with an approximately equal number of structures featuring zero-dimensional (**B1_{0A}** and **B1_{0B}** types in

Figure 4.17) and one and two-dimensional acid - base hydrogen bonded arrays (**B1**₁ and **B2**₁₂ type in Figure 4.17). The absence of hydrogen bond connectivity along the same axis as the construct appears to indicate that it is a result of $\pi - \pi$ stacking interactions between the acid molecules in the structures. Due to its geometric flexibility and low dimensionality, the construct adopts a diverse range of packing arrangements as shown in Figure 4.26.

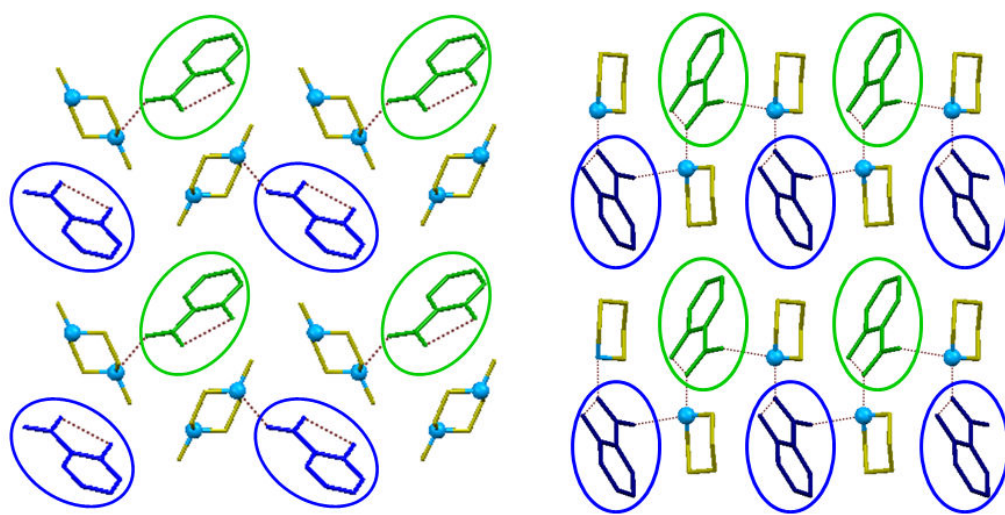


Figure 4.26 Packing arrangement of supramolecular construct **D** in SADM1 (left) and SAMR (right). Constructs viewed along the t_7 vector are coloured green and constructs viewed along the $-t_7$ vector are shown in blue.

A higher degree of similarity is observed for two of the structures containing the C2,2(6) hydrogen bonded chain motif. In BZPA and HBPA pairs of **D** constructs are aligned in parallel along a glide plane to give construct **D**₁, a double row of acid molecules. The packing arrangements of the construct in the two structures are shown in Figure 4.27.

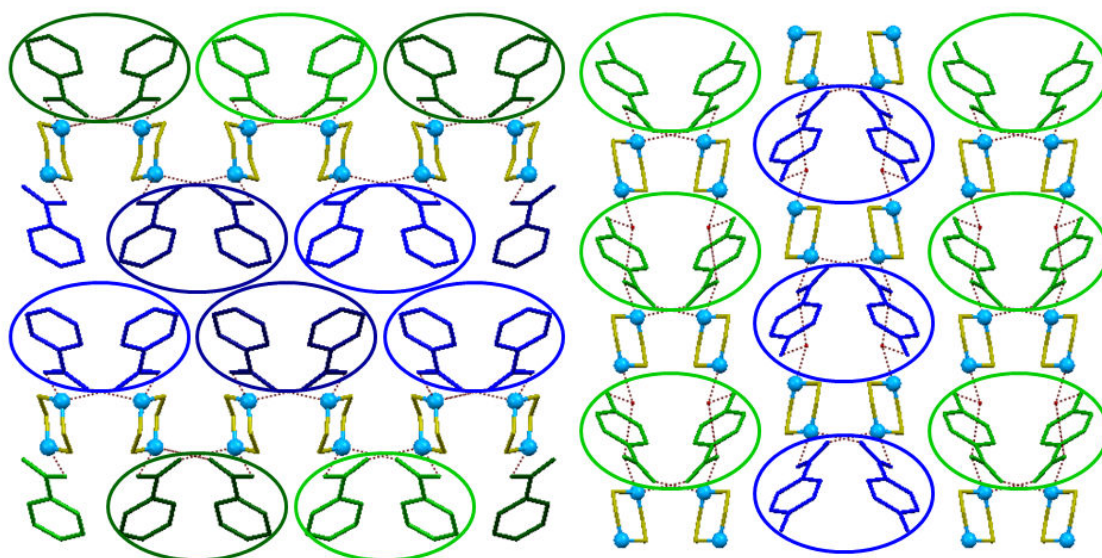


Figure 4.27 Packing arrangement of supramolecular construct \mathbf{D}_1 in BZPA (left) and HBPA (right). Constructs viewed along the t_7 vector are coloured green and constructs viewed along the $-t_7$ vector are shown in blue. Neighbouring constructs lying in parallel are differentiated by light and dark shading.

In BZPA the t_7 vector runs parallel to the a -axis while in HBPA the vector runs parallel to the b -axis. It can be seen that the construct is a consequence of the acid-base hydrogen bonding and in both cases intermolecular hydrogen bonding propagates the structure along the t_7 vector. In BZPA the constructs are stacked in parallel along the second axis of hydrogen bonding, the symmetrical piperazinium cations result in the formation of a bilayer. In HBPA the hydroxyl group propagates a different hydrogen bonding arrangement with the second piperazinium nitrogen hydrogen bonding to this group via a water molecule. As a result the second axis of hydrogen bonding connectivity runs perpendicularly to that in BZPA, resulting in the absence of the bilayer arrangement and the constructs stacking in parallel along an axis perpendicular to that in BZPA.

4.5.3.5 Structures containing supramolecular construct E

Supramolecular construct **E** is composed of two rows of acid molecules tilted towards each other with a glide plane running between them. It is found in DBMR, HBMR and HBPD. Selected details for the three structures are given in Table 4.14.

Table 4.14 Selected structural details for structures containing construct **E**₁.

Structure	SC	System	Z'	Spacegroup	H-Bonding Type
DBMR	E	Salt	2	Pbca	B3 ₁₂₃ (C2,2(6), C1,1(8))
HBMR	E ₃	Salt	2	P2 ₁ /c	B1 ₀ B (R4,4(12))
HBPD	E ₃	Salt	2	P2 ₁ /c	B1 ₀ B (R4,4(12))

In all three structures there are no direct hydrogen bond contacts between the molecules comprising the constructs but in HBMR and HBPD the packing arrangements of the constructs are the same, leading to structures that are isostructural with respect to the geometric arrangement of the acid molecules. The packing arrangements of the constructs are shown in Figure 4.28.

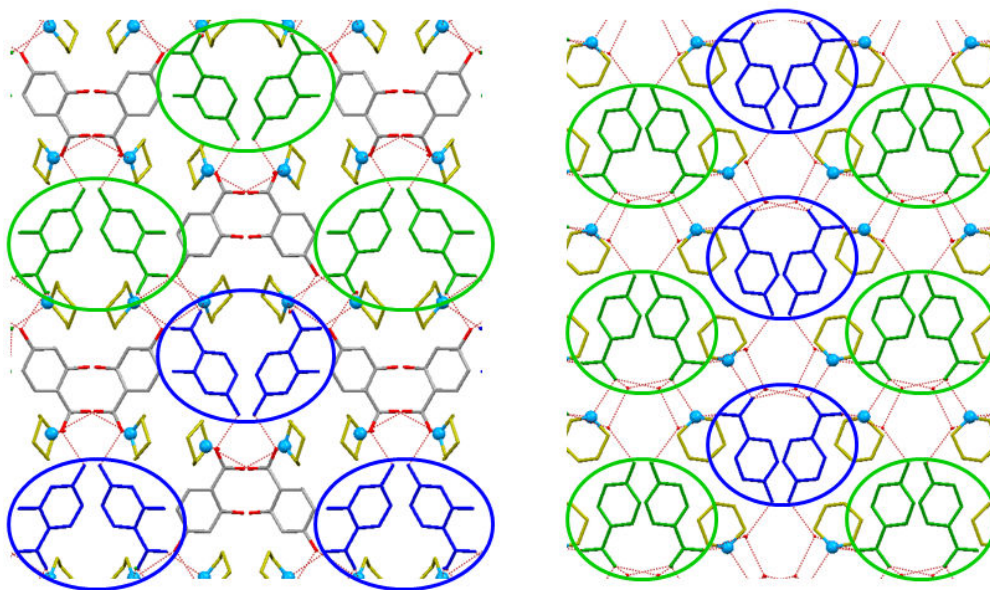


Figure 4.28 Packing arrangement of supramolecular construct **E**₁ in DBMR (left) and HBMR (right), the arrangement of **E**₁ constructs in HBPD is the same as in the latter. Constructs viewed along the **t**₈ vector are coloured green and constructs viewed along the **-t**₈ vector are shown in blue.

4.5.3.6 Structures containing supramolecular construct F

Supramolecular construct **F** is a single stack of acid molecules, in TUDM it is the sole construct and in BZMA and BZPP two **F** constructs related by an inversion operation form construct **F**₁. Selected details of the three structures are given in Table 4.15.

Table 4.15 Selected structural details for structures containing construct **F**.

Structure	SC	System	Z'	Spacegroup	H-Bonding Type
BZMA	F ₁	Salt	2	P-1	B1 ₀ A (D1)
BZPP	F ₁	Salt	2	P2 ₁ /c	B1 ₀ A (D1)
TUDM	F	Cocrystal	2	P2 ₁ /c	B1 ₀ A (D1)

Due to the lack of additional intermolecular hydrogen bonding the packing arrangement of **F** in TUDM differs substantially the other structures as shown in Figure 4.29. The symmetrical base in TUDM creates an inversion through the centre of the molecule, in contrast the inversion centres in BZMA and BZPP lie in the centre of the pseudo six-membered intermolecular hydrogen bond rings.

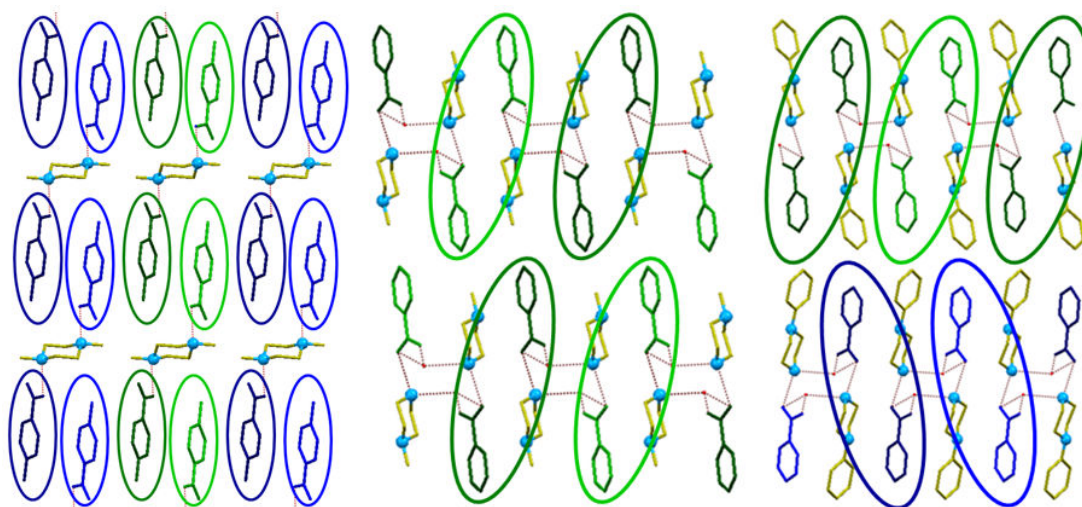


Figure 4.29 Packing arrangements of SC **F** in TUDM (left), BZMA (centre) and BZPP (right). Each benzoate represents one **F** construct, those viewed along the t_{11} vector are green and those along $-t_{11}$ are blue, with neighbouring constructs viewed along the same axis distinguished by dark and light shading. In TUDM individual **F** constructs are circled while in BZMA and BZPP pairs of **F** constructs that make up the **F**₁ construct are circled together. Hydrogen bonds are dark red lines.

4.5.3.7 Relationship between hydrogen bonding and supramolecular constructs

The numbers of structures with a particular amine-carboxylate hydrogen bonding motif that contain an SC are shown in Figure 4.30.

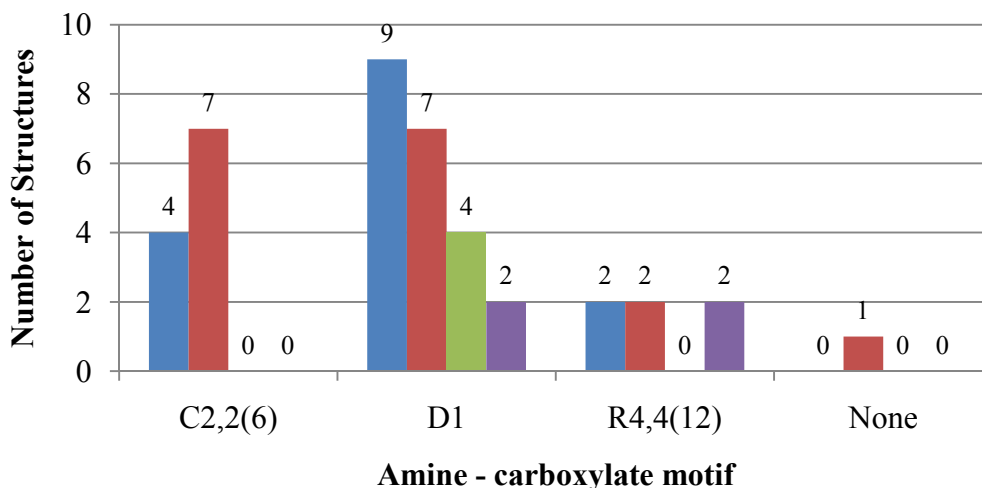


Figure 4.30 Number of structures based on each amine-carboxylate hydrogen bonding motif containing ■ no supramolecular construct or a ■ one-dimensional, ■ two-dimensional or ■ three-dimensional supramolecular construct.

As the identification of an SC in structures containing any of the acid-base hydrogen bond motifs is probable, with over 60% of the structures containing a construct, non-directional interactions and packing effects are clearly an important determinant of supramolecular structure. Higher-dimensionality constructs are formed in systems with zero-dimensional hydrogen bonded acid-base substructures, indicating that the packing arrangement in the structures based on the C2,2(6) motif is more heavily influenced by hydrogen bonded contacts than in the D1 and R4,4(12) structures.

The relationships between the structures containing the constructs are illustrated in a dendrogram in Figure 4.31. Structures with two or three-dimensional SCs have the same acid-base hydrogen bonding interaction, whereas for one-dimensional SCs there is no clear requirement for similar hydrogen bonding arrangements. The C1,1(8) interaction between the acid molecules does not appear to play a significant role in determining the packing arrangement of the acid molecules.

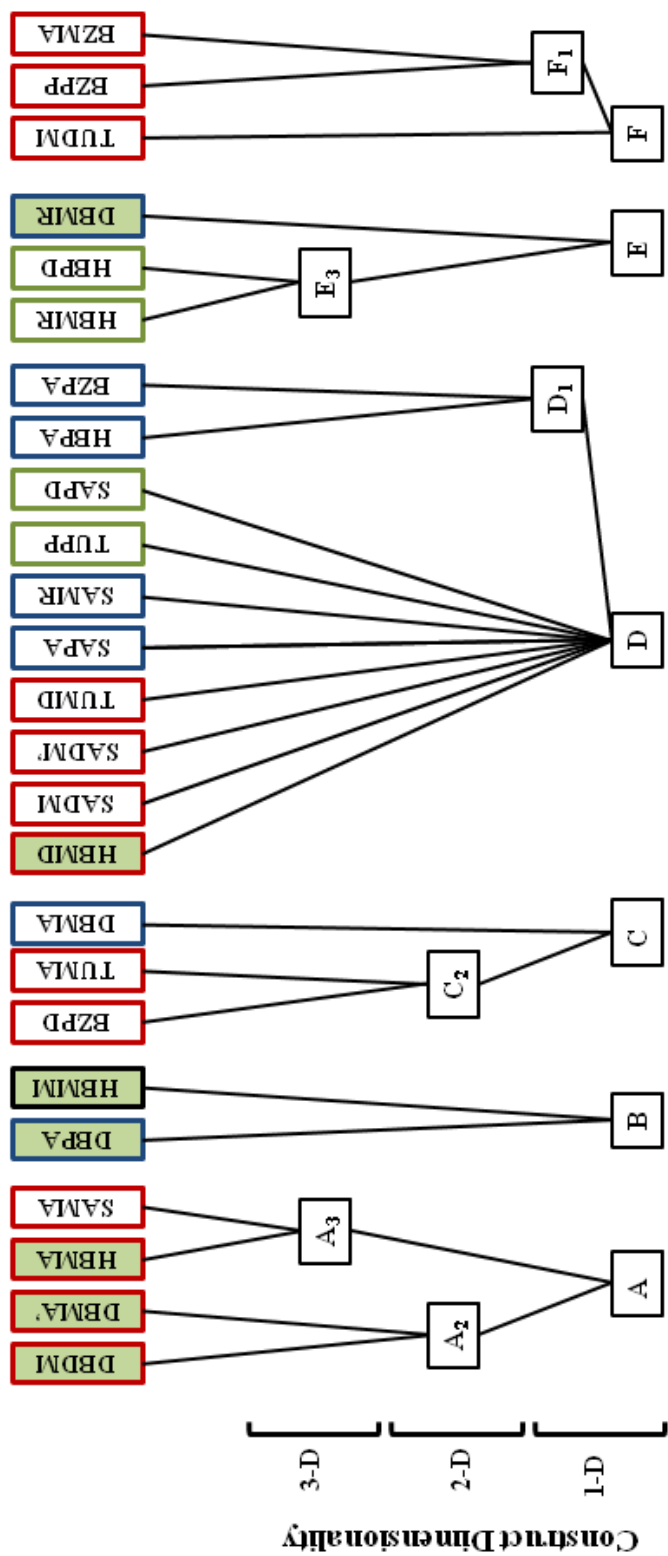


Figure 4.31 Dendrogram showing the similarity relationships between the SCs identified in the benzoic acid structures. The structures are identified by their four letter codes, tie lines indicate the constructs present in each. The constructs are arranged in levels corresponding to their dimensionality. The boxes identifying the structures are coloured according to the amine-carboxylate hydrogen bonding motif: ■ discrete D1 contact, ■ C2,2(6) chain motif, ■ R4,4(12) ring, ■ no amine-carboxylate interaction and boxes filled in green indicate the inclusion of the C1,1(8) hydroxyl-carboxylate motif.

4.5.4 Structural rules for benzoic acid counterions

From the trends observed in the benzoate structural series, the following structural rules are proposed to apply.

Rule B1: When the base molecule has a tertiary amine nitrogen there is a > 90% probability that an amine-carboxylate hydrogen bond will be formed. **(14)**

Rule B2: When Rule B1 is observed and the acid counterion has a *para*-hydroxyl group a C1,1(8) hydrogen bonded chain of acid molecules will form to give a one-dimensional hydrogen bonded structure. **(6)**

Rule B3: When the base molecule contains a secondary amine nitrogen, the most likely acid-base hydrogen bonding motif will be the C2,2(6) chain, but if the base molecule possesses a large substituent group a D1/ R4,4(12) motif may be expected. **(26)**

Rule B4: For secondary amine bases, when the acid molecule possesses a *para*-hydroxyl group there is a 60% probability that the C1,1(8) hydrogen bonded acid chain will be observed in addition to the C2,2(6) amine-carboxylate chain motif and a 75% probability that it will be observed in addition to the D1 motif but it will be absent from structures containing the R4,4(12) motif. **(12)**

Rule B5: The ionisation state of the systems based on the D1 motif is inherently unpredictable in cases where the base has a tertiary amine nitrogen, regardless of the number of available hydrogen bond donor groups on the acid molecule. **(13)**

Rule B6: The packing arrangement of the molecules is determined by non-directional interactions and similarities in packing arrangements will be observed in structures with different hydrogen bonding arrangements. However, higher degrees of similarity (2-D and 3-D SCs) are only observed between systems with the same amine-carboxylate hydrogen-bonding motif. **(25)**

4.6 Sulfonic acid structures

4.6.1 Intermolecular hydrogen bonds

Six intermolecular hydrogen bonded contact types between functional groups on the acidic and basic components of the systems were identified in the 25 structures in this subgroup. They are shown below in Figure 4.32 and their frequencies of occurrence are given in Table 4.16.

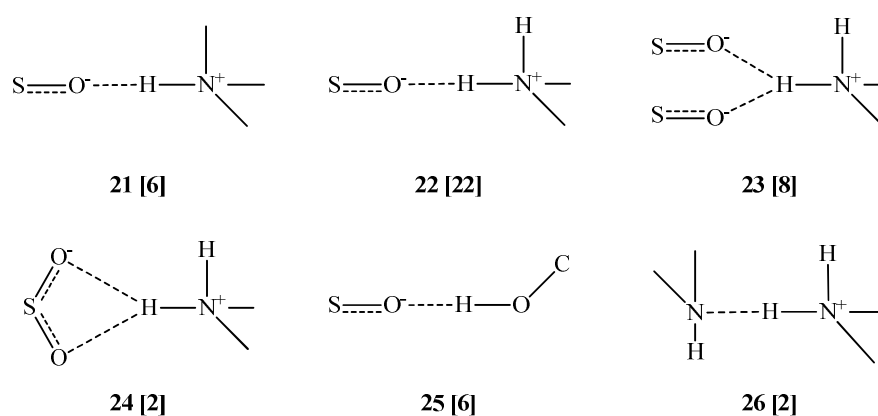


Figure 4.32 Hydrogen bond contacts involving only acid and/or base molecules in the sulfonic acid structures, the number of structures containing each interaction is given in brackets.

Table 4.16 Frequencies of occurrence of the six hydrogen bonded contacts in the sulfonate salt structures.

Bond	Donor	Acceptor	N _{poss}	N _{obs}	P _m (%)
21	<i>tert</i> -NH ⁺	SO ₃ ⁻	8	6	80
22	<i>sec</i> -NH ₂ ⁺	SO ₃ ⁻	22	22	100
23	<i>sec</i> -NH ₂ ⁺	SO ₃ ⁻ + SO ₃ ⁻	22	8	36
24	<i>sec</i> -NH ₂ ⁺	SO ₃ ⁻ / SO ₃ ⁻	22	2	9
25	COH	SO ₃ ⁻	6	6	100
26	<i>sec</i> -NH ₂ ⁺	<i>sec</i> -NH	4	2	50

In contrast to the dicarboxylic and benzoic acid structures, the interactions in this family are highly consistent. Two robust interactions can be identified in this series. Firstly, in cases where a secondary amine donor is present a hydrogen bond is always formed to a sulfonate oxygen and secondly, *para*-hydroxyl groups consistently form a contact to sulfonates as well. The second amine proton in these cases is capable of forming an amine-amine hydrogen bond, an interaction unique in this work to the sulfonate salts.

4.6.2 Hydrogen bonding motifs

Eight amine-sulfonate hydrogen bonding motifs have been identified in the structures in this matrix. In five structures containing a tertiary amine the acid and base molecules are linked by a single discrete interaction. For secondary amine bases, seven extended motifs have been identified and are shown in Figure 4.33.

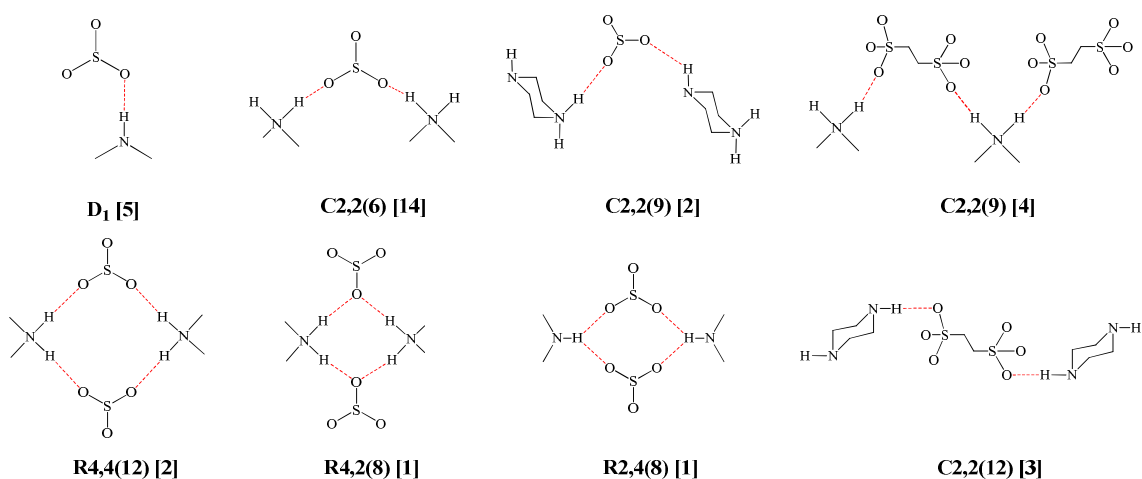


Figure 4.33 Amine-sulfonate hydrogen bond motifs identified in the sulfonic acid structures labelled by their graph set notation. The number of structures in which each motif has been identified is shown in square brackets.

The two other motifs shown in Figure 4.34 were identified, a C_{1,1(8)} chain of acid molecules hydrogen bonded through their *para*-hydroxyl groups and a C_{1,1(5)} chain of piperazinium molecules. The frequencies of occurrence for each motif are given in Table 4.17.

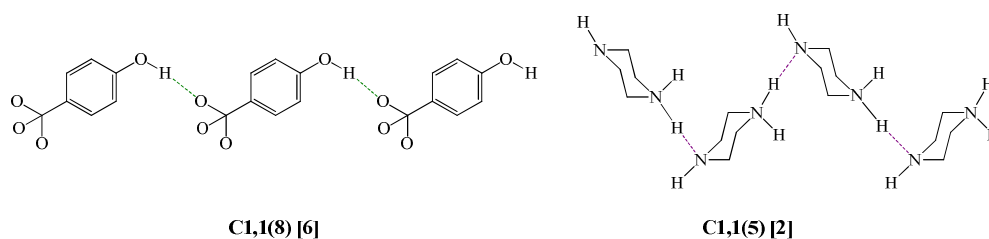


Figure 4.34 C1,1(8) and C1,1(5) hydrogen bonded chain motifs identified in the sulfonic acid structures. The number of structures containing each motif is given in the square brackets.

Table 4.17 Frequencies of occurrence for motifs in the structures containing sulfonic acids. Structures containing ethanedisulfonic acid (**ED**) are listed separately to the monosulfonic acid structures.

Donor	Acceptor	Graph Set	Nposs	Nobs	Pm (%)		
<i>tert</i> -NH ⁺	SO ₃ ⁻	D1	13	4	31		
		D1	18	1	6		
		C2,2(6)	18	14	78		
		C2,2(9)	14	2	14		
		R4,4(12)	18	2	11		
		R2,4(8)	18	1	6		
<i>tert</i> -NH ⁺	SO ₃ ⁻ (ED)	R4,2(8)	18	1	6		
		C2,2(12)	1	1	100		
		C2,2(6)	5	2	40		
		C2,2(9)	5	3	60		
		C2,2(12)	3	2	40		
<i>sec</i> -NH ₂ ⁺	SO ₃ ⁻ (ED)	R4,4(12)	5	1	20		
		Hydroxyl	6	6	100		
		<i>sec</i> -NH ₂ ⁺	<i>sec</i> -NH	C1,1(8)	6	6	100
				C1,1(5)	5	2	40

The formation of NH⁺⋯O contacts in tertiary amine salts is less frequently observed than in dicarboxylic and benzoic acid salts (57% c.f. >70%) indicating increased competition with water contacts. In secondary amine salts NH⁺⋯O contacts are always formed, indicating that the water molecules may be incorporated into the tertiary amine salts to enable the formation of extended hydrogen bonded structures. This aspect of supramolecular structure will be discussed in detail in Chapter 5.

For secondary amine salts the most common motif is the C2,2(6) acid-base chain which has a higher probability of formation than in the benzoic acid salts. The other motifs have comparatively low probabilities of observation with the rarest being observed in single structures. With the exception of the D1 and C2,2(9) motifs, these are secondary motifs formed in structures along with the C2,2(6) motif, most often to satisfy the hydrogen bond acceptor potential of the third sulfonate oxygen.

For acid molecules with a *para*-hydroxyl group formation of a C1,1(8) hydrogen bonded chain is more probable than the analogous motif observed in the hydroxybenzoic acid salts in Section 4.5. The formation of amine-amine motifs is a unique feature to this family of counterions, but the low probability of occurrence and the small molecular size of the piperazine make it unlikely that this interaction will be observed in more complex (e.g. “drug like”) systems. The structures are compared according to their hydrogen bond motifs and molecular structures in Figure 4.35. Due to the small number and diversity of structures characterised for the ethanedisulfonate salts these will be omitted.

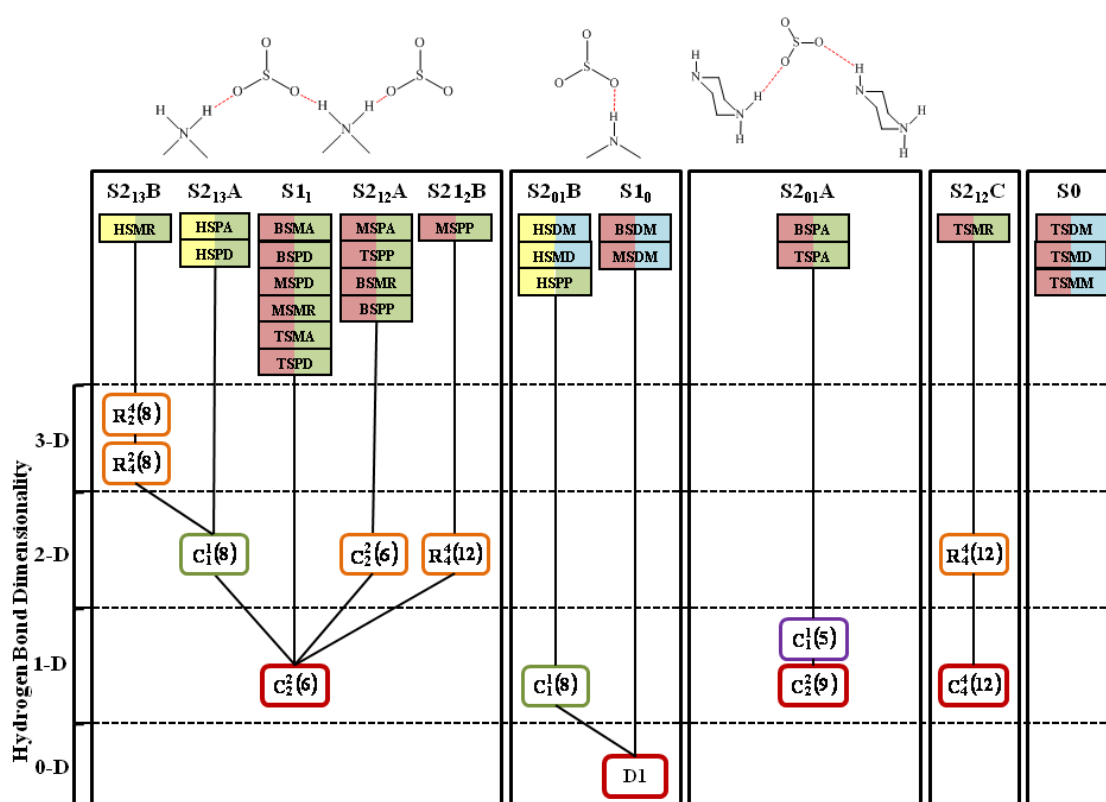


Figure 4.35 Dendrogram showing the hydrogen bond synthons present in the sulfonic acid salts. The acid and base components are identified by the codes assigned in Section 4.1 and coloured according to the hydrogen bonding groups present: ■ SO_3^- ; ■ SO_3^- and *para*-OH; ■ NH^+ donor groups only; ■ NH_2^+ donor group available. Hydrogen bonding motifs are represented by graph set notation with outline colours according to the interaction type: — $\text{NH}^+/\text{NH}_2^+\cdots\text{SO}_3^-$ motif, — second $\text{NH}^+/\text{NH}_2^+\cdots\text{SO}_3^-$ motif; — $\text{OH}\cdots\text{SO}_3^-$ motif, — $\text{NH}_2^+\cdots\text{NH}$ motif. The level at which the box describing the motif sits indicates the overall dimensionality of the hydrogen bond network in the structure due to the interaction and those below it.

4.6.2.1 Structures based on the C2,2(6) motif

The C2,2(6) amine-sulfonate motif is the most common within this class of structures and is the basis of the four extended hydrogen bonded arrays shown in Figure 4.36.

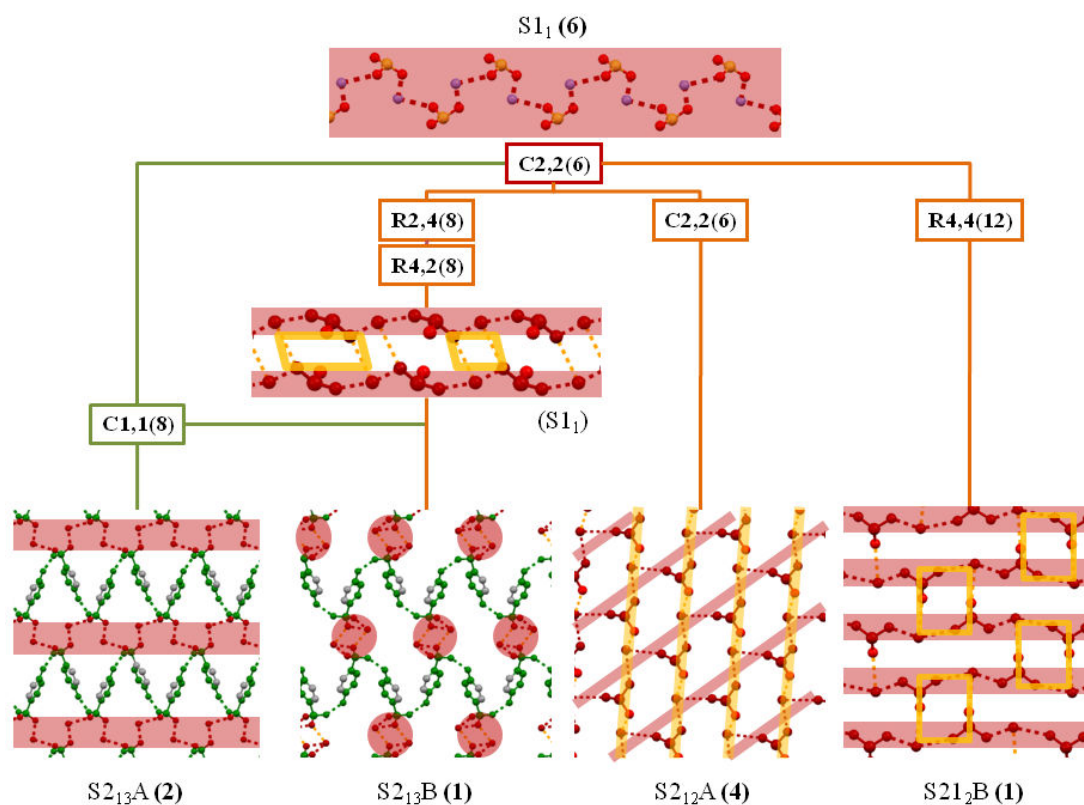


Figure 4.36 Schematic showing the relationships between the extended hydrogen bonded structures based on the C2,2(6) chain (highlighted in red). The connector lines indicate the additional hydrogen bonding motifs in the structure and the atoms in the diagrams are coloured according to the motif they are part of with ■ C2,2(6) motif only; ■ additional NH₂⁺...SO₃⁻ motifs and ■ OH...SO₃⁻ contacts. **S2₁₃B** is a three-dimensional network and is viewed along the axis of the C2,2(6) chain.

In the **S2₁₂A** and **S2₁₂B** arrays one NH₂⁺ proton forms a bifurcated hydrogen bond, creating a two-dimensional hydrogen bonded array through a second NH₂⁺...SO₃⁻ motif. In the **S2₁₃A** structure the C1,1(8) acid chain forms along the same axis as the NH₂⁺...SO₃⁻ contacts, bridging the chains into a two dimensional sheet while in the **S2₁₃B** array this C1,1(8) motif vector is along an axis perpendicular to the NH₂⁺...SO₃⁻ contacts, forming a three-dimensional network.

4.6.2.2 Structures based on other motifs

In 50% of the piperazinium salts the base is monoprotonated and forms a C2,2(9) hydrogen bonded chain (S1₁). In 57% of the tertiary amine salts a single discrete NH₂⁺⋯SO₃⁻ contact is formed, a single example of this contact type is also observed for a secondary amine base (S1₀). If the anion possesses a *para*-hydroxyl group, the C1,1(8) motif is formed to give a hydrogen bonded chain (SC2₀₁A). The three systems are shown in Figure 4.37.

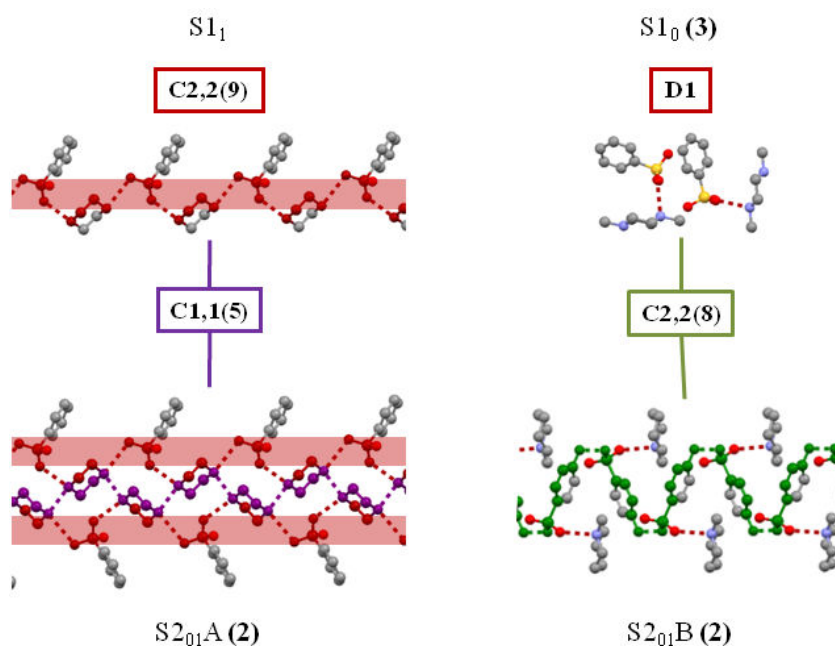


Figure 4.37 Schematic showing the structures based on the alternative amine-sulfonate hydrogen bonding motifs to the C2,2(6) chain. The connector lines indicate the additional hydrogen bonding motifs in the structure and the atoms in the diagrams are coloured according to the motif they are part of with ■ NH⁺⋯SO₃⁻ motif only; ■ NH⁺⋯NH motif and ■ OH⋯SO₃⁻ contacts.

4.6.2.3 Solvent-separated structures

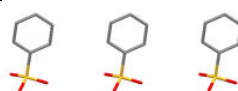
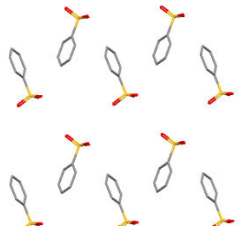
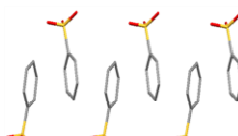

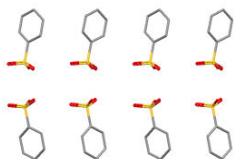
43% of the structures containing a tertiary amine base do not have any contacts between the acid and base molecules (S₀) and instead the ions are linked through hydrogen bonds to water molecules. These structures are discussed in detail in Chapter 5.

4.6.3 Examination of supramolecular constructs using XPac

The packing arrangements of the sulfonic acid anions were examined using XPac, as described in Section 4.4.2. There is a similar incidence of similarity between the structures in terms of their packing arrangements as the benzoic acid structures, with 11 of 21 structures containing a supramolecular construct. Four one-dimensional constructs were observed along with a single two-dimensional construct; finally one pair of structures has a common three-dimensional arrangement of acid anions.

The constructs are detailed below in Table 4.18 including information on their dimensionality (D), the number of occurrences (#) of the construct, the number of base vectors (Base) and the dependencies between the primary, secondary and tertiary supramolecular constructs.

Table 4.18 SCs in the benzenesulfonate structures. Primary SCs do not have a subscript while for secondary and tertiary SCs the subscript indicates the dimensionality of the construct.

SC	D	Description	Fig	#	Base	Dependencies
SA	1	Stack of molecules		4	t_1	
SA ₃	3	Array of A stacks		2	t_1, t_2, t_3	SA → SA ₃
SB	1	Stack of molecules		3	t_1	
SC	1	Stack of molecules		4	t_1	
SD	2	Layer of molecules		2	t_1, t_2	

4.6.3.1 Structures containing supramolecular construct SA

Supramolecular construct **SA** is a single row of sulfonic acid molecules and is found in the four structures detailed in Table 4.19.

Table 4.19 Selected structural details for structures containing construct **SA**.

Structure	SC	System	Z'	Spacegroup	H-Bond Array
BSPA	SA	Salt	2	P2 ₁ 2 ₁ 2 ₁	S2 ₀₁ A (C2,2(9), C1,1(5))
BSPD	SA ₃	Salt	2	P2 ₁ 2 ₁ 2 ₁	S1 ₁ (C2,2(6))
HSPD	SA ₃	Salt	2	P2 ₁ /c	S2 ₁₃ A (C2,2(6), C1,1(8))
HSPP	SA	Salt	2	P2 ₁ 2 ₁ 2 ₁	S2 ₀₁ B (D1, C1,1(8))

The packing arrangements of the constructs are compared below in Figure 4.38, in all four structures the constructs stack in parallel along a second axis to form layers of acid molecules separated by layers of base molecules. As the t_1 vector lies perpendicular to the axis of hydrogen bond connectivity it appears that the construct arises as a result of $\pi - \pi$ stacking interactions between the acid molecules aligning the hydrogen bonded chains along the t_1 axis. In BSPD and HSPD the **SA** constructs pack into a common three dimensional array **SA₃**. In HSPD the constructs are linked by a C1,1(8) motif formed by acid molecules in along an axis perpendicular to t_1 but the absence of this interaction in BSPD indicates that this interaction does not direct the packing.

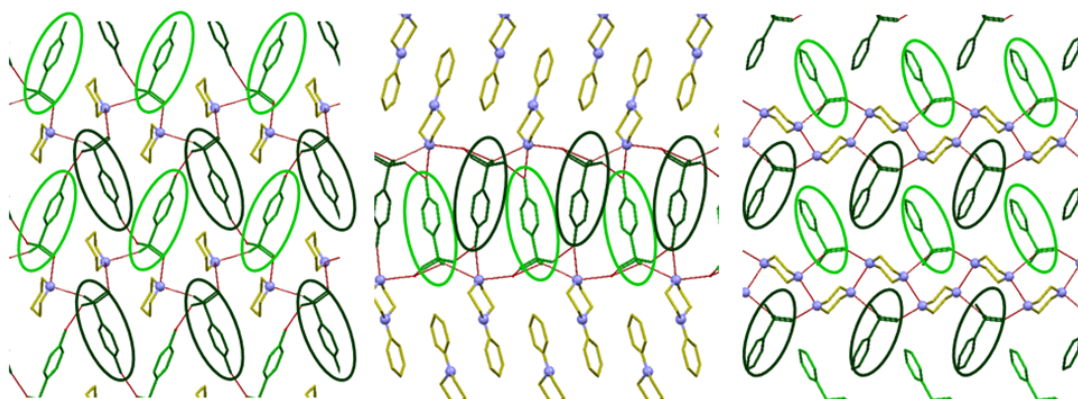


Figure 4.38 Packing arrangements of supramolecular construct **SA1** in HSPD (left) HSPP (middle) and BSPA (right). All constructs are viewed along the t_1 translation vector with each circled molecule corresponding to a single **SA₁** construct.

4.6.3.2 Structures containing construct supramolecular SB

Supramolecular construct **SB** is a double stack of molecules related by a 2_1 screw axis found in the three structures detailed in Table 4.20.

Table 4.20 Selected structural details for structures containing construct **SB**.

Structure	SC	System	Z'	Spacegroup	H-Bond Array
HSPA	SB	Salt	2	P2 ₁ 2 ₁ 2 ₁	S2 ₁₃ A (C2,2(6), C1,1(8))
HSPB	SB	Salt	2	P2 ₁ 2 ₁ 2 ₁	S2 ₀₁ B (D1, C1,1(8))
TSMA	SB	Salt	2	P2 ₁ /c	S1 ₁ (C2,2(6))

The packing arrangements of the constructs are compared in Figure 4.39, in all structures the **SB** constructs align in parallel along a second axis to give a structure consisting of alternating acidic and basic layers with the acid layers alternating with respect to the orientation of the t_1 vector. In HSPA and HSPB the acid molecules in each **SB** construct are linked by the C1,1(8) hydrogen bonded chain motif, but the absence of the required *para*-hydroxyl group in TSMA indicates that this interaction does not determine the molecular arrangement in the construct.

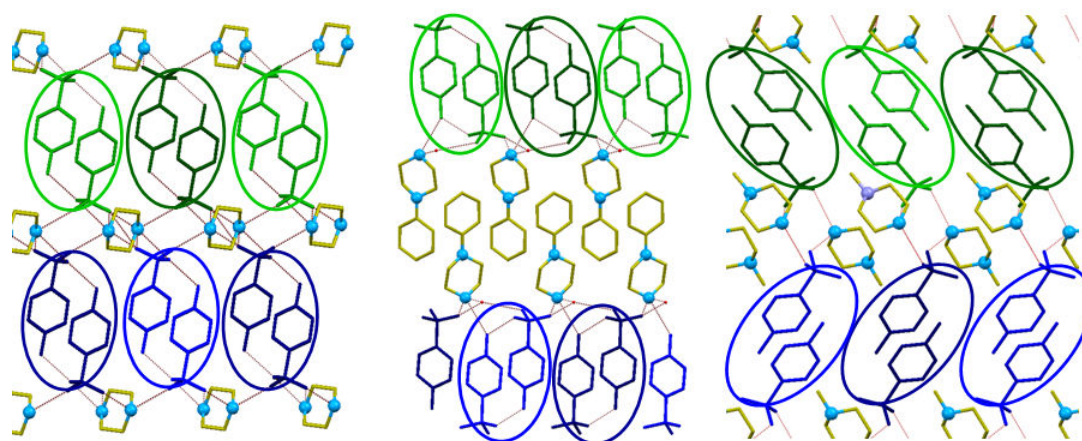


Figure 4.39 Packing arrangement of supramolecular construct **SB** in HSPA (left) HSPB (centre) and TSMA (right). Constructs viewed along the t_4 vector are coloured green and constructs coloured blue are viewed along the $-t_4$ direction. Neighbouring constructs lying in parallel are differentiated by light and dark shading.

4.6.3.3 Structures containing construct SC

Supramolecular construct **SC** is a single row of acid molecules and is found in the four structures detailed in Table 4.21.

Table 4.21 Selected structural details for structures containing construct **SC**.

Structure	SC	System	Z'	Spacegroup	H-Bond Array
HSMR	SC	Salt	2	P2 ₁ 2 ₁ 2 ₁	S2 ₁₃ B (C2,2(6), C1,1(8), R2,4(8))
TSDM	SC	Salt	2	P2 ₁ 2 ₁ 2 ₁	S0
TSMA	SC	Salt	2	P2 ₁ /c	S1 ₁ (C2,2(6))
TSPA	SC	Salt	2	P2 ₁ /c	S2 ₀₁ A (C2,2(9), C1,1(5))

The packing arrangement of the construct in the four structures is compared in Figure 4.40. In all four cases the constructs stack along an axis perpendicular to the t_5 vector to form a bilayer of acid molecules separated by layers of base molecules. In the four salts the axis of the extended hydrogen bonding motif is also perpendicular to the t_5 translation vector.

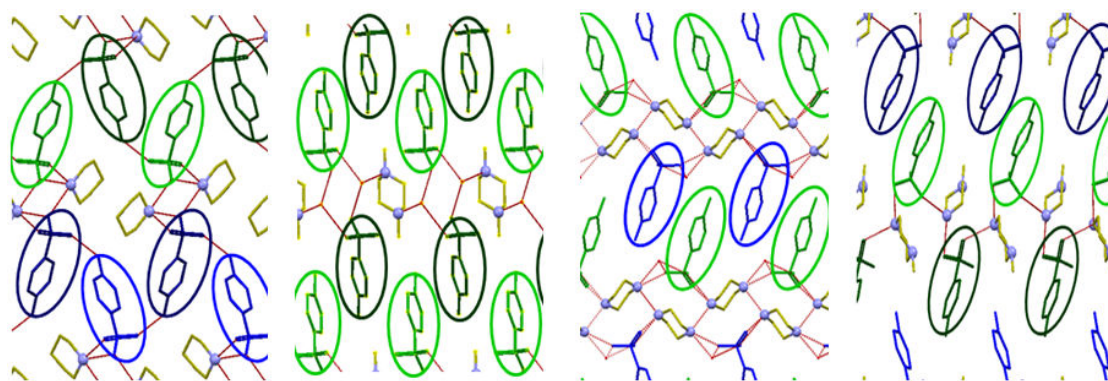


Figure 4.40 Packing arrangements of supramolecular construct **SC** in HSMR (far left), TSDM (middle left), TSPA (middle right) and TSMA (far right). Constructs coloured green are viewed along the t_5 translation vector and blue constructs are viewed in the $-t_5$ direction. Neighbouring constructs lying in parallel are differentiated by light and dark shading.

4.6.3.4 Structures containing construct SD

Supramolecular construct **SD** is a two-dimensional bilayer of acid molecules related by a 2_1 screw axis along one axis and simple translation along the second axis. It is found in the two structures detailed in Table 4.22.

Table 4.22 Selected structural details for structures containing construct **SD**.

Structure	SC	System	Z'	Spacegroup	H-Bond Array
BSPP	SD	Salt	2	$P2_12_12_1$	$S1_1$ (C2,2(6))
TSPP	SD	Salt	2	$P2_1$	$S21_2B$ (C2,2(6), C2,2(6))

The packing arrangement of the construct in both structures is compared in Figure 4.41, in both cases the construct is part of an acid-base hydrogen bonded layer. In BSPP each layer is composed of parallel stacked hydrogen bonded chains as opposed to the two-dimensional sheet in TSPP, indicating that π - π stacking interactions are responsible for determining the observed structure. The constructs stack in parallel in TSPP and are antiparallel in BSPP restricting the structures to two-dimensional similarity.

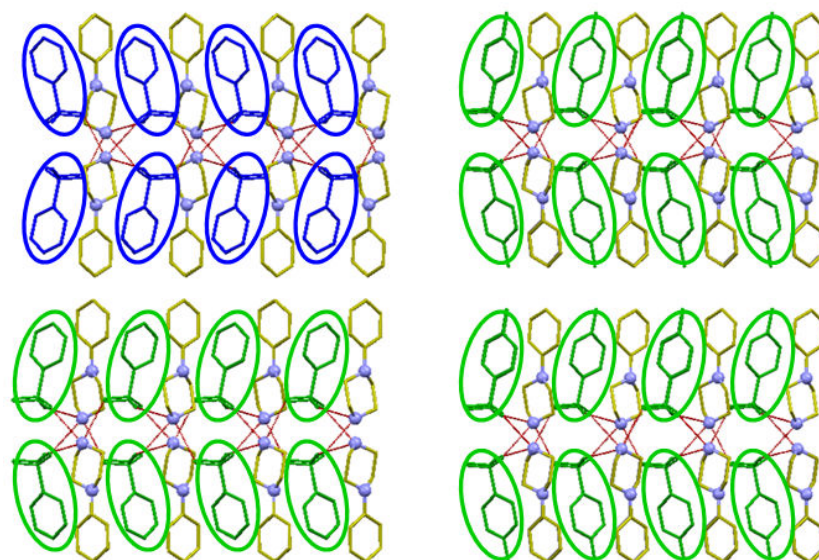


Figure 4.41 Packing arrangement of supramolecular construct **SD** in BSPP (left) and TSPP (right). Constructs coloured green are viewed along t_6 translation vector and constructs coloured blue are viewed in the $-t_6$ direction.

4.6.3.5 Relationship between hydrogen bonding and supramolecular constructs

The relationships between the structures containing supramolecular constructs is shown by the dendrogram in Figure 4.42. It can be seen that, in common with the supramolecular constructs in the benzoic acid structures, similar one-dimensional arrangements of acid molecules are found in systems based on different amine-sulfate hydrogen bonding motifs. Common two and three-dimensional constructs only occur in cases where the primary amine-sulfonate hydrogen bonding motif is the same in both the structures. This suggests that the one dimensional constructs are a consequence of favourable stacking interactions between the phenyl rings on the acid molecules and the necessary alignment of these constructs to form common two and three-dimensional arrangements is dictated by the hydrogen bonding interactions.

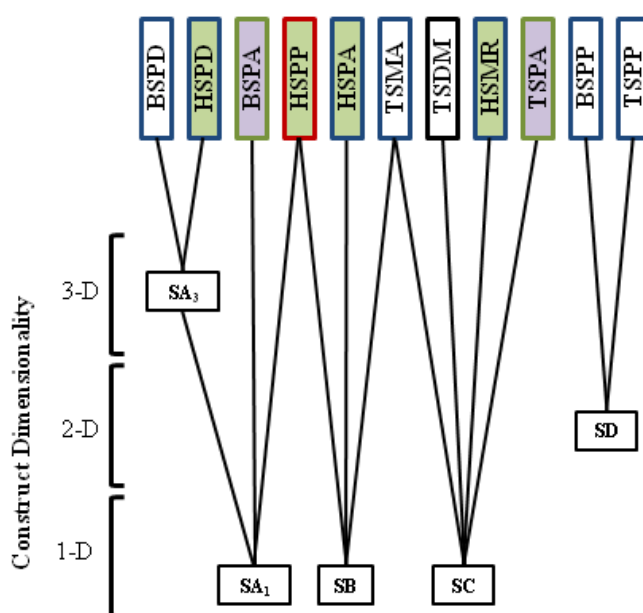


Figure 4.42 Dendrogram showing the similarity relationships between the supramolecular constructs identified in the benzenesulfonic acid structures. The structures are identified by their four letter codes, tie lines indicate the constructs present in each. The constructs are arranged in levels corresponding to their dimensionality. The boxes identifying the structures are bordered according to the amine-carboxylate hydrogen bonding motif- ■ discrete D1 contact, ■ C2,2(6) chain motif, ■ C2,2(9) chain, ■ no amine-carboxylate interaction, boxes filled in green indicate the inclusion of the C1,1(8) hydroxyl-carboxylate motif and purple indicates the inclusion of the C1,1(5) amine-amine motif.

4.6.4 Structural rules for benzenesulfonic acid counterions

From examination of the structures in this subgroup the following structural rules are proposed for salts formed with benzenesulfonic acid counterions. The number of observations on which each rule is based is given in bold:

Rule S1: For tertiary amine bases there is a 57% probability that an amine-sulfonate contact will form. The competition from formation of contacts to water also makes hydrate formation likely. **(7)**

Rule S2: When the base molecule is a secondary amine, both basic protons will form amine-sulfonate bonds with formation of the C2,2(6) motif the most probable outcome. Even in the absence of additional hydrogen bonding groups, there is a 50% probability that additional hydrogen bond contacts will form to the third sulfonate oxygen. **(18)**

Rule S3: For acids with *para*-hydroxyl groups, formation of the C1,1(8) acid chain always occurs. Where there is an extended amine-sulfonate motif the C1,1(8) chain propagates in an unpredictable direction relative to this axis resulting in two and three-dimensional hydrogen bonded arrays. **(6)**

Rule S4: The formation of amine-amine contacts appears moderately likely for secondary amine dinitrogen bases. This results in the formation of the C2,2(9) amine-sulfate motif to accommodate this arrangement. However, increasing the size of the base will probably preclude formation of this motif. **(4)**

Rule S5: The amine-sulfonate hydrogen bonding arrangement does not appear to determine if similar one-dimensional packing arrangements are formed, however two and three-dimensional similarity is only observed when the structures have the same hydrogen bonding motif. **(11)**

4.7 Summary

In this chapter the results from structural analyses on 127 multi-component crystals containing dicarboxylic, benzoic and sulfonic acid counterions with simple model bases have been presented. These observations have been used to propose a series of rules highlighting the most likely supramolecular structural features that will be observed upon co-crystallisation of these acids and molecular entities with similar basic functional groups. The size of the library allows a confident assessment of trends relating to major structural features such as the number and type of ionisable groups. Observations relating other functionalities such as hydroxyl groups are based on smaller numbers of structures and so must be treated with caution. Nevertheless, the observed trends can form a useful tool in anticipating the most likely ionisation state and structural features for a multi-component system formed with one of the counterions in the library.

The rules will be extended to take into account the influence of hydrate formation on molecular structure in Chapter 5. The structural rules will be refined and their applicability to complex systems validated against a library of multi-component systems with pharmaceutically active molecules in Chapter 6. There is evidence from the benzoic and benzenesulfonic acid systems that non-directional interactions play an important role in determining the supramolecular structures adopted by small benzoic and benzenesulfonic acid molecules and this is likely to become more pronounced as molecular size increases. A consequent reduction in the number and type of hydrogen bonding interactions may also be expected in line with the decreasing number of possible molecular packing arrangements.

4.7.1 Case example of the application of the structural rules

As an example of the applicability of the structural rules derived thus far, predictions that can be made for Amoxapine are discussed. This is a tetracyclic antidepressant with a known crystal structure (Cosulich and Lovell 1977) shown in Figure 4.43. As it has a piperazinyl ring with a calculated pKa of 8.03 the structural rules suggest the following outcomes on cocrystallisation with the counterions shown in Figure 4.2 would not be unexpected:

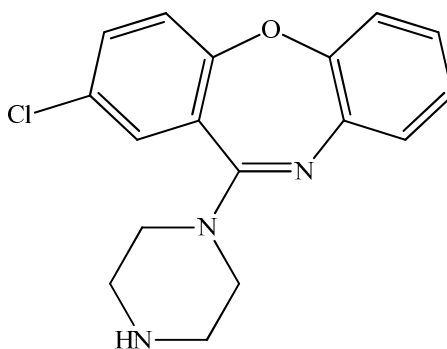


Figure 4.43 Chemical structure of the tetracyclic antidepressant Amoxapine.

(i) The probability of crystalline salt formation with all types of counterion shown in Figure 4.2 is $> 70\%$ and is the sole outcome when a crystalline product is formed with a sulfonic acid counterion. For the dicarboxylic and benzoic acid counterions, other crystalline products including mixed systems and cocrystals are also possible.

(ii) Cocrystallisation with a dicarboxylic acid can be expected to result in the hydrogen acid salt with a one-dimensional hydrogen bonded structure based on the C1,1(7/9) hydrogen bonded chain of acid molecules. If the acid counterion has hydroxyl groups additional contacts between the acid molecules may be formed but the overall intermolecular hydrogen bond connectivity can be expected to be one-dimensional.

(iii) Cocrystallisation with a benzoic acid is equally likely to result in formation of a single direct amine-carboxylate interaction or an R4,4(12) motif as observed for the structures containing 4-phenylpiperazine. If the acid counterion incorporates a *para*-hydroxyl group then a C1,1(8) hydrogen bonded acid chain can be expected.

(iv) Cocrystallisation with a sulfonic acid will result in the formation of a salt based on the C2,2(6) amine-sulfonate chain with additional amine-sulfonate contacts propagating the hydrogen bonded structure along a second axis. When the acid counterion possesses a *para*-hydroxyl group a C1,1(8) hydrogen bonded acid chain will be formed.

Chapter 5
Hydration in salt structures

5.1 Introduction

In a survey of organic structures in the CSD 8.1% were found to be hydrates, making water the solvent molecule most commonly incorporated into crystalline lattices (Gorbitz and Hersleth, 2000). This frequency results from the ubiquity of water in crystallization environments, its small molecular size and its ability to form hydrogen bonds in multiple directions. The presence of charged groups in salt systems increase the probability of hydrate formation (Infantes, *et al.*, 2003) with the type of counterion affecting this probability, for example sulfate salts have been shown to form hydrates more frequently than carboxylate or carbonate salts of NH^+ containing molecules (Haynes, *et al.*, 2005).

The probability of hydrate formation has been linked to several aspects of molecular structure. It is more common when the molecules possess charged or polar groups and when they have higher aqueous solubility (Infantes, *et al.*, 2003). It has been posited that a low ratio of hydrogen bond donor to acceptor groups increases the probability of hydrate formation (Desiraju, 1991), however this point is in debate as an extensive study of structures in the CSD found no correlation between hydrate formation and donor/acceptor ratio (Infantes, *et al.*, 2007). The same survey did demonstrate a positive correlation between the overall number of hydrogen bonding groups and the probability of forming a hydrate.

In this chapter, the structural database discussed in Chapter 4 is employed as a resource for the examination of hydrate formation in crystalline salt structures. Aspects of salt hydration examined included the probability of formation for different classes of counterion; relationships between hydrate formation and the structural rules established in Chapter 4 and the hydrogen bonding of the water in the structures. Variable-temperature X-ray powder diffraction (VT-XRPD) was employed to access the anhydrous structures of selected hydrates. These pairs of structures were used to examine the competition between interactions in crystalline salts to water and other functional groups to rationalise further the formation of hydrates and their structure.

5.2 Method

The dehydration temperatures of the hydrated salts were identified using DSC and TGA. Samples of the hydrates were ground with an agate mortar and pestle to produce a homogenous powder with no visible sparkling and loaded into a 0.7mm borosilicate glass capillary. Diffraction data was collected on a Bruker AXS D8 Advance diffractometers equipped with a LynxEye PSD. The samples were heated to 10°C above the dehydration temperature using an Oxford Cryosystems Cryostream Series 700 Plus temperature control device and returned to room temperature. XRPD data were collected over the range 3-70° 2 θ (2kW, Cu K α 1.54056Å, step size 0.0017° 2 θ) using a variable count time scheme (Madsen and Hill 1994).

The diffraction data were indexed to obtain the unit cells of the anhydrous salts using DICVOL (Boultif and Louer, 2004) and the structures refined by rigid-body Rietveld refinement (Rietveld, 1969) in the program TOPAS Academic v4.1 (Coelho, 2007). The data sets were background subtracted and truncated for Pawley fitting (Pawley, 1981). The simulated annealing component of DASH (David, *et al.*, 2006) was used to optimise the anhydrous crystal structures. Internal coordinate descriptions were derived from the single-crystal structures of the hydrated salts. Crystallographic data and data collection/solution parameters for the structures are given overleaf in Table 5.1.

Topas-type rigid body descriptions of the molecules were then constructed using the single-crystal structures of the hydrated forms. X-H distances were normalised to normal neutron diffraction values and torsion angles checked using Mogul (Bruno, *et al.*, 2004). Rotatable H-atoms were placed manually in positions that satisfied the local hydrogen bonding requirements. Rigid-body descriptions were mapped onto the molecules of the SA global minimum, using a distance minimisation procedure within Topas. Thereafter, the SA coordinates were deleted and Rietveld refinement against all the data proceeded in terms of the rigid bodies only. A 4th order spherical harmonics based preferred orientation correction (Jarvinen, 1993) was applied with Topas during the refinement. The CIF files are given for the anhydrous systems in Appendix 2.

Table 5.1 Crystallographic data and SDPD refinement parameters for the anhydrous salts generated by VT-XRPD.

Salt	LTMR	LTPD	LTMA	HBMA
Chemical formula	C ₈ H ₁₅ N ₁ O ₇	C ₉ H ₁₇ N ₁ O ₆	C ₉ H ₁₈ N ₂ O ₆	C ₁₂ H ₁₈ N ₂ O ₃
Formula mass	237.19	236.02	250.25	238.28
Crystal system	Orthorhombic	Orthorhombic	Monoclinic	Monoclinic
Space group	P2 ₁ 2 ₁ 2 ₁	P2 ₁ 2 ₁ 2 ₁	P2 ₁	P2 ₁ /a
<i>a</i> (Å)	16.23430(13)	7.20558(8)	8.734665(88)	12.59379(16)
<i>b</i> (Å)	9.111888(63)	8.48491(6)	10.54423(11)	10.14947(16)
<i>c</i> (Å)	7.252436(56)	19.02139(18)	6.210480(78)	9.87809(14)
α (°)	90	90	90	90
β (°)	90	90	96.6803(9)	97.6104(5)
γ (°)	90	90	90	90
Cell volume (Å ³)	1072.817(14)	1162.894(20)	568.104(11)	1251.498(31)
Z	4	3	2	4
Temperature (K)	298	298	298	298
VCT collection range (2 θ)	2 - 70°	2 - 70°	2 - 70°	2 - 70°
Step size (°)	0.017	0.017	0.017	0.017
Radiation wavelength (Å)	Cu K α 1 (1.5450 Å)	Cu K α 1 (1.5450 Å)	Cu K α 1 (1.5450 Å)	Cu K α 1 (1.5450 Å)
Degrees of freedom	15	15	15	13
Data range (2 θ)	2 - 45°	2 - 55°	2 - 55°	2 - 70°
Number of reflections (SA)	98	176	124	247
Profile χ^2 / Pawley χ^2	1.880	3.456	3.866	2.256
Number of reflections	143	176	124	247
R _{wp}	0.040	0.046	0.044	0.034
R _{ietveld}	0.017	0.018	0.017	0.018
R _p	0.035	0.046	0.034	0.028
S	2.382	2.627	2.493	1.871

5.3 Occurrence of hydrate formation by cation and anion type

41 of the 115 salts characterised in this work were hydrates, giving an overall incidence of hydrate formation of 35.7%. The occurrence of hydrate formation for secondary and tertiary amine salts with the counterions classified by the number and type of acid groups is summarised in Table 5.2.

Table 5.2 Occurrence of hydrates in salts in experimental matrix as no. of hydrates / total structures; frequency as a percentage in parentheses.

	<i>Tert</i> -Amine		<i>Sec</i> -Amine	
	Anhydrous	Hydrate	Anhydrous	Hydrate
Monocarboxylic	7/9 (78%)	2/9 (22%)	16/26 (62%)	10/26 (39%)
Dicarboxylic	7/20 (35%)	13/20 (65%)	15/28 (54%)	13/28 (47%)
Monosulfonic	4/7 (57 %)	3/7 (43%)	17/19 (90%)	2/19 (11%)
Disulfonic	1/1	0/1	4/5	1/5

The occurrence of hydrates in salts of monocarboxylic acids is more likely for secondary amines than tertiary amines with 39% of secondary amines and 22% of tertiary amine salts crystallising as hydrates. For dicarboxylic and monosulfonic acid counterions the reverse is the case, 46% of secondary amine salts and 65% of tertiary amine salts of dicarboxylic acids are hydrates and the corresponding occurrences for monosulfonic acid counterions are 10% and 43% for respectively. Hydrate formation is most likely for a dicarboxylic acid salt of a tertiary amine base and least likely for a monosulfonic acid salt of a secondary amine.

A CSD survey of hydrate formation in NH^+ -containing salts of pharmaceutically acceptable anions by Haynes *et al* (Haynes, *et al.*, 2005) found a comparable occurrence of hydrates in secondary and tertiary amine salts of each type of acid. In this case 17.4% of secondary amine and 16.7% of tertiary amine carbonate and carboxylate salts were hydrates and higher occurrences of 29.3% for secondary amine and 25% for tertiary amine sulfate and sulfonate salts. These findings are in contrast to this work where the occurrence of hydrated salts of secondary amines is significantly lower for sulfonate salts than for either type of carboxylic acid counterion, while the occurrence of hydrates is higher for tertiary amine salts of dicarboxylic acids than sulfonic acids.

5.3.1 Hydrate occurrence and number of H-bonding groups

5.3.1.1 Hydrate formation and basic nitrogens

To assess if the chemical functional groups on the molecules favour hydrate formation the water affinity, defined as “*the likelihood of incorporating water molecules*” by Infantes *et al* (Infantes, *et al.*, 2003) was calculated as the number of hydrate structures divided by the number of structures containing the same number of functional groups per molecule. As the ionisation state of an acidic or basic group can alter its tendency to form hydrates, ionised and neutral groups were considered separately. The variation of water affinity with the number, type and protonation state of amine nitrogens on the base molecules is shown in Figure 5.1.

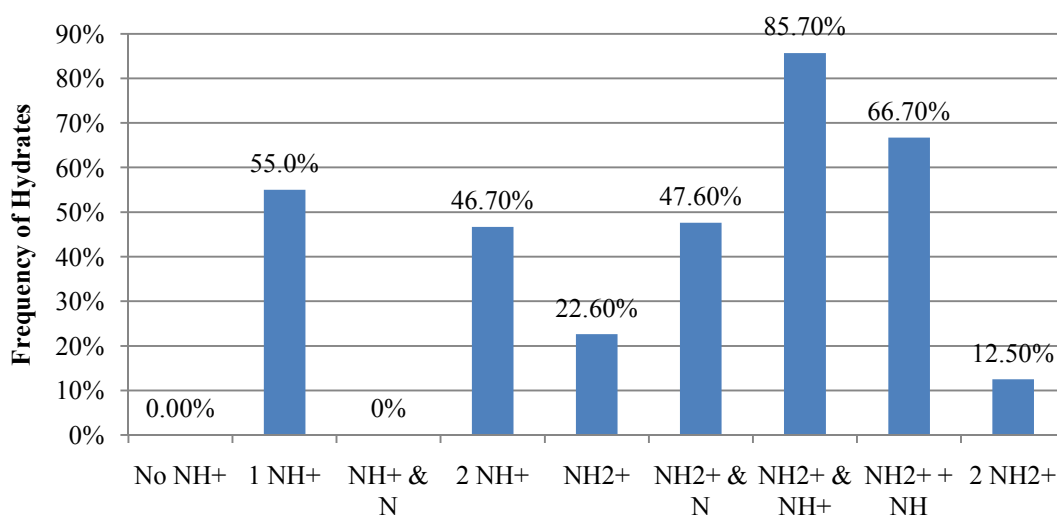


Figure 5.1 Variation of water affinity with the number, type and protonation states of amine nitrogens in the basic molecules across the experimental matrix.

There is no clear correlation between the number of nitrogen atoms and the frequency of hydrate formation for bases with single tertiary amine donor nitrogens is similar to those with two protonated tertiary nitrogens or one protonated secondary and one neutral nitrogen. Hydrate formation is most common in systems containing 1-methylpiperazine with protonated secondary and tertiary amine nitrogens. There is also no correlation between the number of ionised groups and hydrate formation as the fully ionised piperazinium base has the lowest water affinity.

5.3.1.2 Hydrate formation and carboxylic acid groups

The variation in water affinity in structures containing carboxylic acid counterions with the number and ionisation state of the acid groups present on the counterions is shown in Figure 5.2.

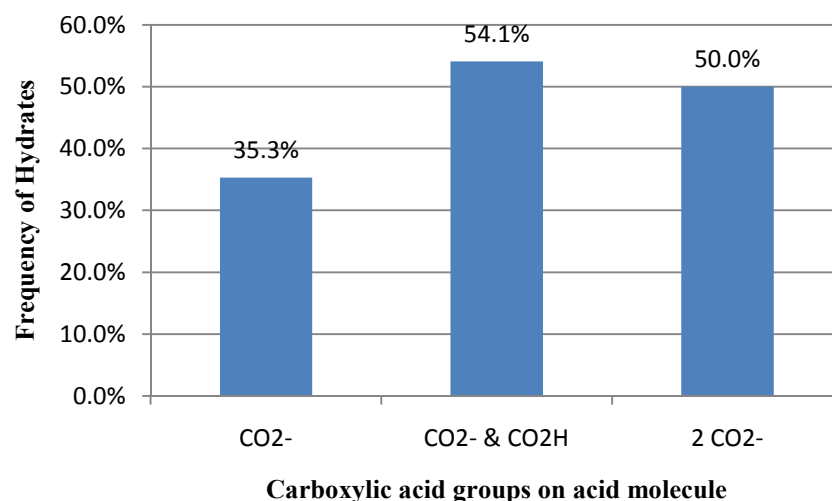


Figure 5.2 Variation in water affinity with the number of neutral and ionized carboxylic acid groups present on the acid molecule.

Hydrate formation is more common in systems where the acid molecule contains two carboxylic acid functional groups, consistent with the previously reported affinity of the carboxylate group for hydrate formation. In these structures the number and not the ionisation state of the acid groups appears to be the determining factor as there is no significant difference in the frequency of hydrate formation for systems containing two ionised groups compared to those containing one ionized and one neutral.

The system in which there are no ionised carboxylic acid groups, the 1,4-dimethylpiperazine 4-methylbenzoic acid cocrystal, was also anhydrous but as this is the single example no firm conclusions can be drawn. It should be noted that as the monocarboxylic acids are all benzoic acid derivatives they have lower water solubility than the dicarboxylic acids, a factor that has been demonstrated to reduce the probability of hydrate formation (Infantes, *et al.*, 2003).

The effect of the presence of hydroxyl groups on the water affinity of the resultant system is shown in Figure 5.3.

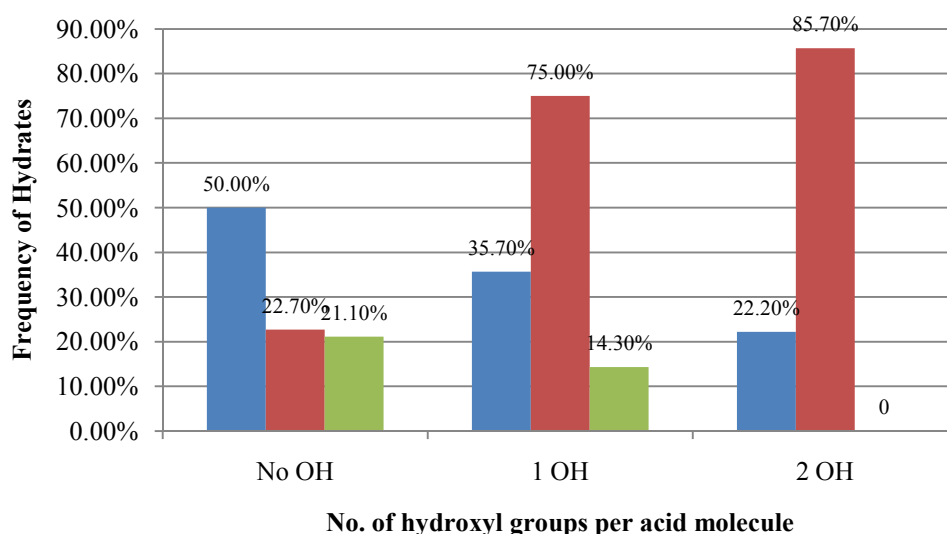


Figure 5.3 Variation in water affinity with the number of hydroxyl groups present on the acid molecule for ■ monocarboxylic, ■ dicarboxylic and ■ monosulfonic counterions.

In the case of the monocarboxylic and monosulfonic counterions the inclusion of hydroxyl groups on the acid molecule reduces the affinity for water of the system, with the addition of two hydroxyl groups on the monocarboxylic acids causing a greater reduction than the presence of a single group. This appears consistent with the principle that hydrate formation is partly the result of an imbalance in the donor/acceptor ratio in the structure and contradicts the view that increasing the number of polar groups favours hydrate formation.

However, in the case of the dicarboxylic acid counterions the inclusion of hydroxyl groups has the opposite effect with a significant increase in the water affinity for these systems. It should be noted that the increase in water affinity for systems containing two hydroxyl groups per acid molecule compared with those containing one is less significant than the increase from systems containing no hydroxyl groups. This is consistent with the increased frequency reported in the CSD survey, albeit here the affinity is much higher than the survey's reported 10-15%.

5.4 Hydrogen bonding interactions of water

Three contact environments were observed for the water molecules in these structures, significantly fewer than the eight found in the CSD survey by Gillon *et al* (Gillon, *et al.*, 2003). The three environments shown in Figure 5.4 are the most common identified in the CSD survey and their frequencies of observation are compared in Table 5.3.

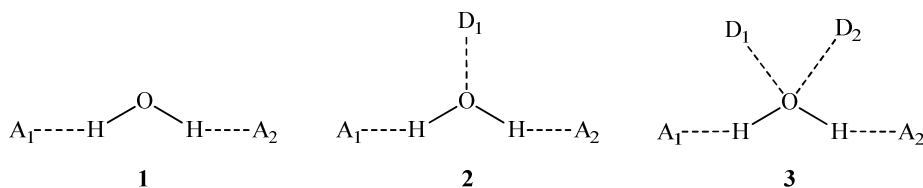


Figure 5.4 The three hydrogen bonding environments for water molecules in the hydrate structures. A_1 and A_2 represent hydrogen bond acceptor atoms and D_1 and D_2 represent hydrogen bond donor atoms.

Table 5.3 Comparison of the frequencies of occurrence of water environments in this work and the CSD survey (Gillon *et al.* 2003).

Environment (CSD survey)	This Work		CSD Survey	
	Number/Total	Frequency (%)	Number/Total	Frequency (%)
1 (2)	11/71	15.5%	471/3159	14.9%
2 (5)	51/71	71.8%	1273/3159	40.3%
3 (6)	4/71	5.6%	910/3159	28.8%

In both datasets the Type 2 environment is the most common, but the frequency of occurrence in this work is considerably higher than in the CSD survey. The rank orders of the remaining two environments are different, with the Type 1 interaction being the second most common of the three interactions in this work but the least common of the three in the CSD survey. It is however notable that the frequency of occurrence for Type 1 is similar in the two datasets. The CSD survey included all types of organic crystal systems and so the smaller molecular size and prevalence of charged groups in the structures in this work are the most likely reasons for the differences in the relative frequencies of the water environments.

5.4.1 Hydrogen bonding interactions of water in dicarboxylic acid salts

22 of the 50 dicarboxylic acid salts are hydrated with the majority forming Type 2 hydrates. Selected structural details for the systems are given in Table 5.4.

Table 5.4 Structural details for the dicarboxylic acid hydrates.

Structure		Acid - Base H-bond Motif	H ₂ O Environment	Water Contacts					
Acid	Base			A ₁	D ₁	A ₂	A ₁ '	D ₁ '	A ₂ '
AD	MR	C2,2(6)	2 x 2	CO ₂ ⁻	H ₂ O	H ₂ O	CO ₂ H	H ₂ O	H ₂ O
LM	MA	C2,2(12)	1x 1	CO ₂ ⁻	-	CO ₂ ⁻	-	-	-
LM	MD	D1	1 x 2	CO ₂ ⁻	OH	OH	-	-	-
LM	MM	D1	1 x 2	CO ₂ ⁻	OH	CO ₂ H/ OH	-	-	-
LM	PA	C2,2(12)	1 x 1	CO ₂ ⁻	-	OH	-	-	-
LT	DM	C2,2(12)	1 x 1	CO ₂ ⁻	-	OH	-	-	-
LT	MA	C2,2(12)	1 x 1	CO ₂ ⁻	-	CO ₂ ⁻	-	-	-
LT	MD	D1	2 x 2	CO ₂ H	OH	OH	CO ₂ ⁻	OH	CO ₂ H/ OH
LT	MM	None	1 x 2, 1x 3	CO ₂ ⁻	OH	CO ₂ ⁻	CO ₂ ⁻	OH	CO ₂ H/ OH
LT	MR	C2,1(5)	1 x 2	OH	NH ₂ ⁺	CO ₂ H/ OH	-	-	-
LT	PD	C2,1(5)B	1 x 2	CO ₂ ⁻	NH ₂ ⁺	OH	-	-	-
RM	DM	R2,1(5)	1 x 2, 1 x 3	CO ₂ ⁻	-	H ₂ O	CO ₂ ⁻	H ₂ O	OH
RM	MA	C2,2(12)	2 x 2	CO ₂ ⁻	OH	OH	CO ₂ ⁻	OH	CO ₂ ⁻
RM	MD	D1	1 x 2	CO ₂ ⁻	OH	OH	CO ₂ ⁻	OH	CO ₂ ⁻ /OH
RM	MM	D1	1 x 2	CO ₂ ⁻	OH	OH	-	-	-
RM	PP	R2,1(5)	1 x 2	CO ₂ ⁻	NH ₂ ⁺	CO ₂ ⁻	-	-	-
RT	DM	R2,1(5)	1 x 2	CO ₂ ⁻	OH	OH	-	-	-
RT	MD	None	2 x 2	CO ₂ ⁻	OH	CO ₂ ⁻ /OH	CO ₂ ⁻	OH	CO ₂ H
RT	MM	None	1 x 2	CO ₂ ⁻	OH	OH	-	-	-
RT	MR	R2,1(5)	1 x 2	CO ₂ ⁻	NH ₂ ⁺	OH	-	-	-
RT	PD	R4,4(12)	1 x 2	CO ₂ H	OH	OH	-	-	-
SU	MA	D1	1 x 3	CO ₂ ⁻	NH ₂ ^{+/} NH ₂ ⁺	CO ₂ H	-	-	-

Hydrate formation is observed in structures with a variety of acid-base hydrogen bonding motifs described in Section 4.4.2, with the most common types being the C2,2(12) chain and single discrete acid-base contacts. The majority of the salts contain hydroxyacid counterions and tertiary and secondary amine bases are observed with approximately equal frequency.

The carboxylate group is the most common acceptor of hydrogen bonds from water and the hydroxyl groups are the most common donors. As no hydrogen bonds are accepted by water molecules from the carboxylic acid groups in the hydrogen acid

salts it can be concluded that this interaction is heavily disfavoured relative to the carboxylate-carboxylic acid interactions forming the C1,1(7) and C1,1(9) motifs in the majority of the hydrogen acid salts as discussed in Chapter 4.

Of the 11 structures containing a secondary amine base only 6 feature a hydrogen bond interaction between the amine group and a water molecule, the 5 structures that do not contain this interaction are dinitrogen secondary amine base salts based on the C2,2(12) chain motif. Hydrogen bond interactions between water molecules are rare, indicating a lack of water clusters in the structures.

5.4.2 Hydrogen bond interactions of water in substituted benzoate salts

15 of the 35 structures containing benzoic acid counterions are hydrated with the majority forming Type 5 hydrates. Selected structural details for the systems are given in Table 5.5.

Table 5.5 Structural details for the benzoic acid hydrates.

Structure		Acid - Base H-bond Motif	H ₂ O Environment	Water Contacts					
Acid	Base			A ₁	D ₁	A ₂	A ₁ '	D ₁ '	A ₂ '
BZ	MA	D1	1 x 2	CO ₂ ⁻	NH ₂ ⁺	CO ₂ ⁻	-	-	-
BZ	PD	D1	2 x 2	CO ₂ ⁻	NH ₂ ⁺	CO ₂ ⁻	CO ₂ ⁻	NH ₂ ⁺	CO ₂ ⁻
BZ	PP	D1	1 x 2	CO ₂ ⁻	NH ₂ ⁺	CO ₂ ⁻	-	-	-
DB	MA	D1	1 x 2	CO ₂ ⁻	NH ₂ ⁺	<i>o</i> COH	-	-	-
HB	DM	D1	2 x 1	CO ₂ ⁻	-	CO ₂ ⁻	CO ₂ ⁻	-	CO ₂ ⁻
HB	MA	D1	1 x 2	CO ₂ ⁻	NH ₂ ⁺	<i>tert</i> -N	-	-	-
HB	MR	R4,4(12)	2 x 2	CO ₂ ⁻	<i>p</i> OH	H ₂ O	CO ₂ ⁻	H ₂ O	CO ₂ ⁻
HB	PA	C2,2(6)	1 x 2	CO ₂ ⁻	<i>p</i> OH	<i>Sec</i> -N	-	-	-
HB	PA	R4,4(12)	1 x 2	CO ₂ ⁻	<i>p</i> OH	CO ₂ ⁻	-	-	-
HB	PD	R4,4(12)	2 x 2	CO ₂ ⁻	<i>p</i> OH	H ₂ O	CO ₂ ⁻	H ₂ O	CO ₂ ⁻
HB	PP	D1	2 x 2	CO ₂ ⁻	<i>p</i> OH	CO ₂ ⁻	CO ₂ ⁻	NH ₂ ⁺	<i>p</i> OH
SA	MA	D1	1 x 2	CO ₂ ⁻	NH ₂ ⁺	<i>tert</i> -N	-	-	-
TU	MA	D1	2 x 2	CO ₂ ⁻	NH ₂ ⁺	CO ₂ ⁻	CO ₂ ⁻	NH ₂ ⁺	CO ₂ ⁻
TU	MD	D1	2 x 2	CO ₂ ⁻	H ₂ O	H ₂ O	CO ₂ ⁻	H ₂ O	H ₂ O
TU	PP	R4,4(12)	1 x 1	CO ₂ ⁻	-	CO ₂ ⁻	CO ₂ ⁻	-	CO ₂ ⁻

Hydrated benzoic acid structures most frequently have a simple hydrogen bond connecting the acid and base molecule in the structure. There is only one example of a structure containing the C2,2(6) acid-base hydrogen bond motif forming a hydrate. Hydrate formation common for structures containing the R4,4(12) acid-base motif, with four hydrates from six structures.

The carboxylate group is the most common acceptor of hydrogen bonds from water molecules and the second amine proton on the NH_2^+ group is the most common donor. The second most common hydrogen bond donor to water molecules is the para-hydroxyl group of the acid although the number of occurrences of this interaction is comparable to the number of interaction between water molecules. Hydrogen bond interactions between water molecules are comparatively rare and the majority of the structures in this group are isolated site hydrates.

5.4.3 Hydrogen bonding interactions of water in sulfonate salts

Only 6 of the 32 sulfonic acid salts are hydrates, with hydrate formation in systems containing secondary amine bases a particularly rare occurrence. In the morpholinium edisylate salt water crystallises as hydronium cations and will not be discussed further. Selected structural details for the remaining hydrates are given in Table 5.6.

Table 5.6 Structural details for the benzenesulfonic acid hydrates.

Structure		Acid - Base H-bond Motif	H ₂ O Environment	Water Contacts					
Acid	Base			A ₁	D ₁	A ₂	A ₁ '	D ₁ '	A ₂ '
BS	PP	D1	1 x 2	SO ₃ ⁻	NH ₂ ⁺	SO ₃ ⁻	-	-	-
TS	DM	D1	1 x 2	SO ₃ ⁻	NH ⁺	SO ₃ ⁻	-	-	-
TS	MD	None	2 x 2	SO ₃ ⁻	NH ⁺	SO ₃ ⁻	SO ₃ ⁻	NH ⁺	SO ₃ ⁻
TS	MM	None	1 x 2	SO ₃ ⁻	NH ⁺	SO ₃ ⁻	-	-	-
TS	PA	D1	1 x 2	SO ₃ ⁻	NH ⁺	SO ₃ ⁻	-	-	-

5.5 Guidelines for counterion selection to minimise hydrate formation

Some guidelines can be derived to assess the likelihood of hydrate formation in salts of a pharmaceutically active molecule possessing tertiary or secondary amine functional groups.

5.5.1.1 Tertiary amines

For tertiary amine bases salts with monocarboxylic acids have the lowest probability of hydrate formation and as shown in Figure 5.1 this is not increased by additional protonated tertiary amine groups on the molecule. In the hydrated benzoate salts the water molecules donate hydrogen bonds to the acid anions but do not accept hydrogen bonds from the base, indicating that this interaction is not competitive with the acid-base contact and instead the water molecules are incorporated to allow the formation of extended hydrogen bonded structures.

5.5.1.2 Secondary amines

For secondary amine bases sulfonic acid salts are the least likely to form hydrates, however in contrast to the tertiary amine bases the probability of hydrate formation increases if there are additional nitrogen atoms on the molecule. As shown in Figure 5.1 additional tertiary amine nitrogens on the base molecule result in an approximately twofold increase in the water affinity of the system relative to molecules with only one protonated secondary amine nitrogen and an almost four-fold increase when this additional nitrogen is protonated.

5.5.1.3 General guidelines

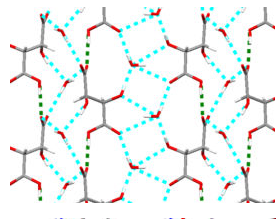
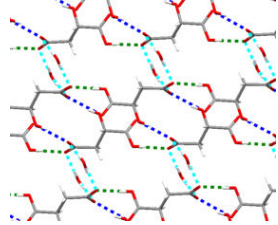
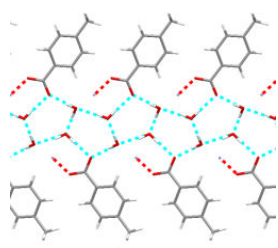
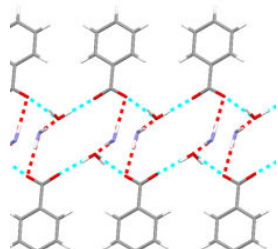
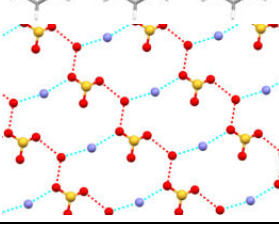
Dicarboxylic acid salts have the highest probability of hydrate formation for tertiary and secondary amine salts; with tertiary amines the formation of a hydrate is more likely, at 65%, than the formation of an anhydrous salt. As shown in Table 5.4 interactions between acid hydroxyl groups and water occur in all eleven hydrated tertiary amine salts and five of the eleven secondary amine salts, indicating that water may be incorporated to satisfy the hydrogen bonding requirements of the acid.

5.6 Structural aspects of salt hydration

5.6.1 Extended motifs from water and functional groups

Several motifs formed by water molecules and the functional groups on the acid or base molecules were identified. The most common motifs are shown in Table 5.7 and are considered likely to occur in salts with the three classes of counterion:

Table 5.7 Most common hydrogen bonding arrangements observed for secondary and tertiary amine salts of the major types of acid counterion examined in this work. Pm is calculated as the percentage of hydrate structures with the acid-base combination featuring the motif.

Base	Counterion	Acid-Water Motif	Pm (%)	Most common substructure
<i>tert</i> -NH ⁺	Dicarboxylic	C2,2(6) chain	36.3%	
<i>sec</i> -NH ₂ ⁺	Dicarboxylic	R4,4(12) ring or C2,2(10) chain	45.4%	
<i>tert</i> -NH ⁺	Benzoate	Ribbon of R5,5(10) rings	50%	
<i>sec</i> -NH ₂ ⁺	Benzoate	C2,2(6) chain	46.2%	
<i>tert</i> -NH ⁺	Sulfonate	C2,2(6) chain	100%	
<i>sec</i> -NH ₂ ⁺	Sulfonate	C2,2(6) chain	100%	

5.6.2 Extended motifs in dicarboxylic acid salts

As shown in Table 5.7 hydrated hydrogen acid salts are the most common type observed for both secondary and tertiary amine bases. The water molecules interact exclusively with the anions, forming two-dimensional hydrogen bonded sheets with the basic components bonding to the anions above and below the plane of these sheets. In most cases the water molecules bridge the C1,1(7) hydrogen acid chains through contacts to the carboxylate groups to form the two-dimensional sheet structures and incorporation of water molecules into malate salts has been shown to perform a similar role in malate (2-) salts (Aakeroy and Nieuwenhuyzen, 1996).

5.6.3 Extended motifs in benzoic acid salts

The most common motifs formed by water in hydrated salts of benzoic acids are one-dimensional water-carboxylate chains that are cross-linked by the amine or are independent of the amine-carboxylate contacts. This is consistent with the established rationale for the role of water in crystalline hydrates of monocarboxylic acids as supporting the formation of catemeric structures by spacing the aromatic rings, hence reducing the repulsive forces, and increasing the donor : acceptor ratio (Desiraju, 1991). It should be noted that for both these and the dicarboxylic acid salts, the most common extended structures are observed in a minority of structures, indicating that the structural consequences of hydrate formation are unpredictable.

5.6.4 Extended motifs in sulfonic acid salts

In contrast to the dicarboxylic and benzoic acid salts, water plays a consistent structural role in hydrated sulfonic acid salts of both secondary and tertiary amine bases. As can be seen in Table 5.7 the water molecules form C2,2(6) chains with the sulfonate groups on the acid molecules, in secondary amine salts these chains are cross-linked by the base to give two-dimensional hydrogen bonded sheets, in the tertiary amine bases the amines-sulfonate contact is missing. Water molecules appear to have a similar function as in the majority of the benzoic acid salt hydrates, increasing the dimensionality of the accessible hydrogen-bonded networks.

5.7 Comparison of Hydrated and Anhydrous Structures

As noted in Section 5.6 the incorporation of water into a salt results in an unpredictable anion-water substructure being formed for both dicarboxylic and benzoic acid salts. To investigate the structural consequences of hydrate formation and rationalise the incorporation of water six novel anhydrous salts were formed from hydrates and characterised as described in Section 5.2. Structures were characterised for primary and tertiary amine salts of dicarboxylic acids and secondary amine salts of benzoic acids. To examine the role of water molecules in the structures the hydrogen bond contacts and molecular packing arrangements in the six anhydrous salts were compared to their corresponding hydrates.

5.7.1 Changes to hydrogen bond interactions

The hydrogen bond contacts in the anhydrous salts are compared to the parent hydrate structures in the matrix in Figure 5.5. For each pair of structures the number and type of contacts between the acid and base molecules are calculated as the number of donated and accepted contacts. For example, a molecule that accepts two $\text{OH}\cdots\text{O}_2\text{C}$ contacts and donates two $\text{OH}\cdots\text{O}_2\text{C}$ contacts is assigned four $\text{OH}\cdots\text{O}_2\text{C}$ contacts.

5.7.1.1 Hydrogen bond interactions in hydrogen tartrate salts

This comparison confirms the importance of the major motifs identified in Chapter 4. In dicarboxylic hydrogen acid salts this was the C1,1(7) acid-acid chain and as shown in Figure 5.5 this contact is preserved on dehydration. In the tertiary amine salt (RTMD) the acid - base contacts are preserved whereas for the secondary amine salts (LTMR and LTPD) an additional acid-base contact is formed to compensate for the loss of water contact with the rearrangement of the bifurcated acid-base contact. This appears to confirm that acid-base contacts are highly probable in these systems but play a secondary role in directing the structures to the acid- acid contacts. Contacts including the acid hydroxyl groups were not found to be structure-directing interactions in Chapter 4, a view apparently confirmed by their general absence from the hydrate structures or loss on dehydration.

Contact																			Δ
	HY	AH	HY	AH	HY	AH	HY	AH	HY	AH	HY	AH	HY	AH	HY	AH	HY	AH	
LTMR	2	2	2	0	0	1	1	0	0	1	0	1	0	1	0	0	0	0	0
LTPD	2	2	2	0	1	2	0	1	0	1	0	1	0	1	0	0	0	0	0
LTMA	N/A	N/A	4	4*		2	2									2	0	0	0
RTMD	2	2	0	4							1	1							+4
HBMR	N/A	N/A	0	2		2	2*						N/A						+2
HBPD	N/A	N/A	0	2		2	2*						N/A						+2
HBMA	N/A	N/A	2	2		1	2						N/A						+1

*Number of contacts per acid and base molecule remains the same but motif changes.

Figure 5.5 Changes in hydrogen bond contacts between the acid and base molecules upon dehydration of the hydrate (HY) structures to form the anhydrate structures (AH). The number of each type of contact donated and accepted by each acid and base molecule is given with the contacts coloured according to whether the contact is maintained in upon dehydration, the contact is lost on dehydration or the contact is formed on dehydration to a group previously interacting with water. The number of contacts per acid and base molecule in each case is given; N/A denotes contacts for which the requisite functional groups are not present in the structure and are therefore not relevant, Δ is the change in the number of acid-base contacts.

5.7.1.2 Hydrogen bond contacts in bitartrate salts

The single example of a bitartrate salt, LTMA, confirms the established importance of the C2,2(12) acid-base chain in determining the structures of salts of diamine bases as this contact is preserved on dehydration. The contact environment of the equatorial secondary amine proton does change slightly from a trifurcated to bifurcated contact, indicating that this proton most likely stabilises the arrangement of the chains formed by the contacts with the axial amine protons. In contrast to the hydrogen acid salts hydroxyl-carboxylate contacts are observed in the hydrate and anhydrate, however they are rearranged on dehydration from an R2,2(10) motif to a C1,1(6) chain as the relative positions of the acid molecules in the neighbouring C2,2(12) chains shift on dehydration.

5.7.1.3 Hydrogen bond contacts in benzoate salts

The hydrogen bonding motifs in the benzoic acid salts are far more flexible and change more significantly on dehydration. This is reflective of the greater number of structure-directing motifs established in Chapter 4 for salts of this type of counterion (three amine-carboxylate motifs and one hydroxyl-carboxylate motif) and indicates that hydrogen bonds play a less significant role in determining the structures than in the dicarboxylic acid salts.

5.7.1.4 Overall trends on dehydration

It is also notable that on dehydration of the hydrogen tartrate and bitartrate salts of secondary amines results the number of hydrogen bond contacts is essentially unchanged and in the other cases the number of hydrogen bond contacts increases. This indicates that in at least some cases the incorporation of water is not driven by the need to satisfy excess hydrogen bond potential or even simply increase the number of hydrogen bond contacts in the structure. An examination of the changes in the packing arrangements of the major structure-directing motifs will assess the importance of these factors in directing hydrate formation.

5.7.2 Comparison of hydrate and anhydrous hydrogen tartrate salts

5.7.2.1 Secondary amine hydrogen tartrate salts

The packing arrangements of the molecules in the hydrated and anhydrous piperidinium and morpholinium hydrogen tartrate salts were compared by visual inspection of the spacefill crystal structures using Mercury shown in Figure 5.6.

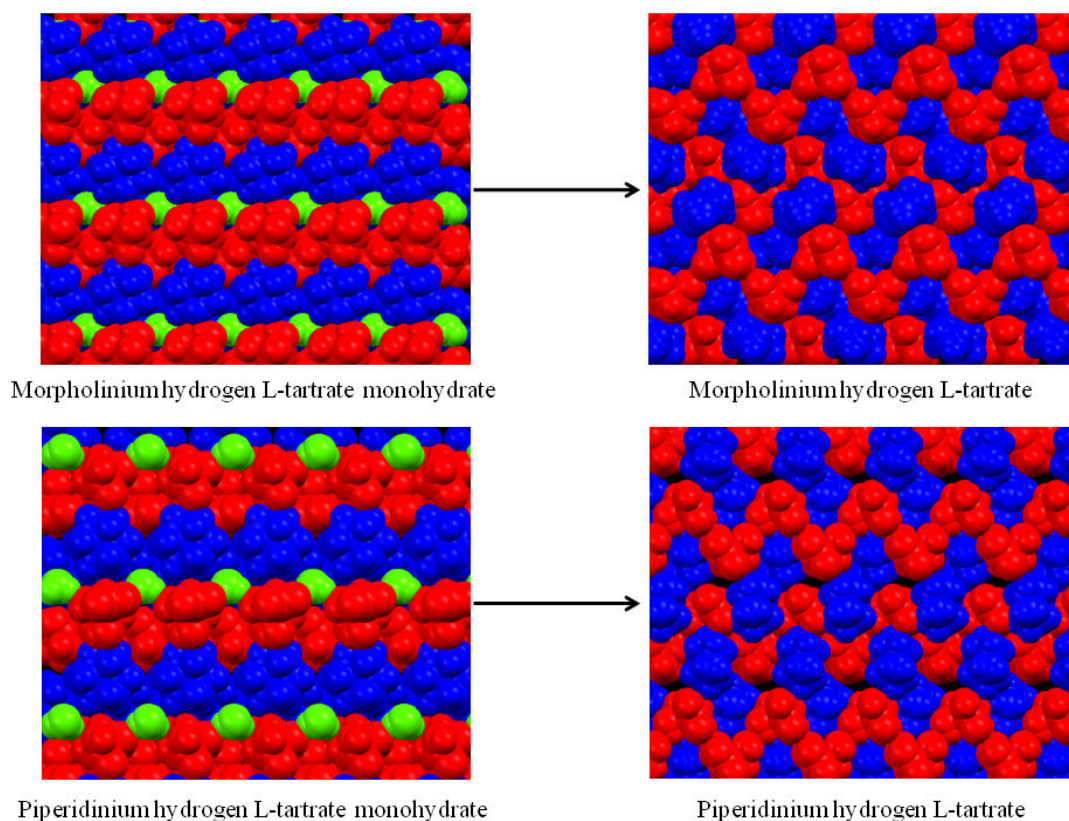


Figure 5.6 Comparison of the molecular packing arrangements in the monohydrate structures of morpholinium (top left) and piperidinium (bottom left) hydrogen L-tartrate with their corresponding anhydrous structures (top and bottom right). The structures are viewed along the axis of the C1,1(7) hydrogen acid chain motifs, acid molecules are coloured red, base molecules are blue and water molecules are green. In each case the axes of hydrogen bond connectivity are through the plane of the paper for the C1,1(7) acid chains and along the horizontal axis for the acid-water and acid-acid layers. The base layers are interdigitated between anion-water and anion layers and are not hydrogen bonded.

In both cases the hydrate structures contain well defined anion-water layers separated by layers of base molecules that dehydrate to form corrugated layers of acid molecules with the base molecules rotating to occupying voids rather than forming separate layers. This substantial rearrangement is driven by the change in the orientation of the anion chains required to form the contacts between the hydroxyl groups and the acid molecules of the neighbouring chains to compensate for the loss of the water molecules.

As discussed in Section 5.5.1.3 this rearrangement is not accompanied by a change in the degree of acid-acid and acid-base hydrogen bonding within the structure. In any case, it is clear from the anhydrous structures that the acid and base molecules contain sufficient hydrogen bond donor and acceptor groups to satisfy their hydrogen bonding potential in the absence of water molecules. The water molecules may be included in order to satisfy the hydrogen bonding potential of the acid hydroxyl groups whilst maintaining the more favourable layered acid-base packing arrangement. Hydrogen succinate and hydrogen fumarate salts of secondary amines adopt similar layered arrangements to the monohydrated hydrogen tartrate salts as shown in Figure 5.7. In these cases the lack of acid hydroxyl groups removes the requirement for acid-acid hydrogen bonding along an axis perpendicular to the C1,1(7) chain and hence the need to incorporate water to maintain the layered structure.

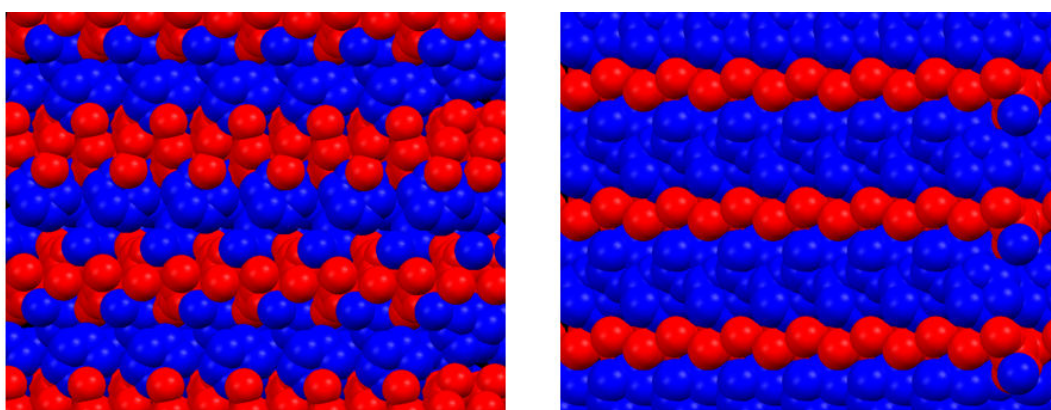


Figure 5.7 Layered packing arrangement of the anions (red) and cations (blue) in piperidinium hydrogen fumarate (left) and morpholinium hydrogen succinate (right). Both structures are viewed along the axis of the C1,1(7) hydrogen acid chains.

5.7.2.2 Tertiary amine hydrogen tartrate salt

The dehydrated 1-methylpiperidinium DL-tartrate salts is based on the C1,1(7) hydrogen acid chain and as with the secondary amine salts this is preserved on dehydration. In the hydrate the C1,1(7) hydrogen acid chain are also cross-linked by water into two-dimensional hydrogen bonded sheets with the base molecules bonded above and below the plane. The additional anion-anion hydrogen bonds formed on dehydration result in their rearrangement into a three-dimensional network with base molecules filling the voids as shown in Figure 5.8.

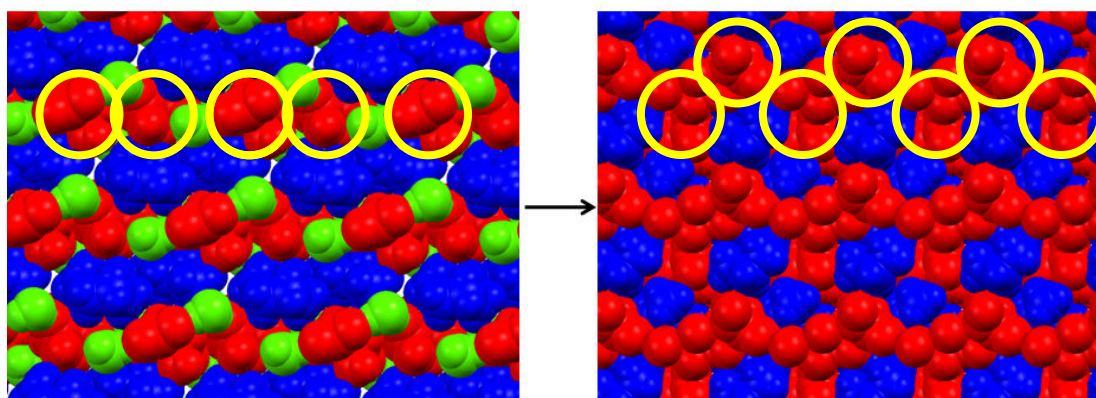


Figure 5.8 Packing arrangements in the dihydrated 1-methylpiperidinium hydrogen DL-tartrate (left) compared with the anhydrate structures (right). The structures are viewed along the axis of the C1,1(7) hydrogen acid chain. Acid anions are coloured red, base molecules are blue and water molecules are green. In both structures the C1,1(7) chains are circled in yellow, in the 1,4-dimethylpiperazinium salt these pairs of these chains are linked via hydroxyl-carboxylate contacts.

5.7.3 Secondary amine bitartrate salts

1-Methylpiperazinium hydrogen L-tartrate is the sole example of a bitartrate salt examined in this work. As discussed in Section 5.7.1.2 the main structure-directing hydrogen bond motif is the C2,2(12) acid-base chain, which is preserved on dehydration. The major structural change is the rearrangement of the hydroxyl-carboxylate contacts from an R2,2(10) ring in the hydrate to the C1,1(5) chain in the anhydrate. The overall change is relatively modest in comparison to the other structures as demonstrated by the comparison of the packing arrangements of the molecules in the two structures as shown in Figure 5.9.

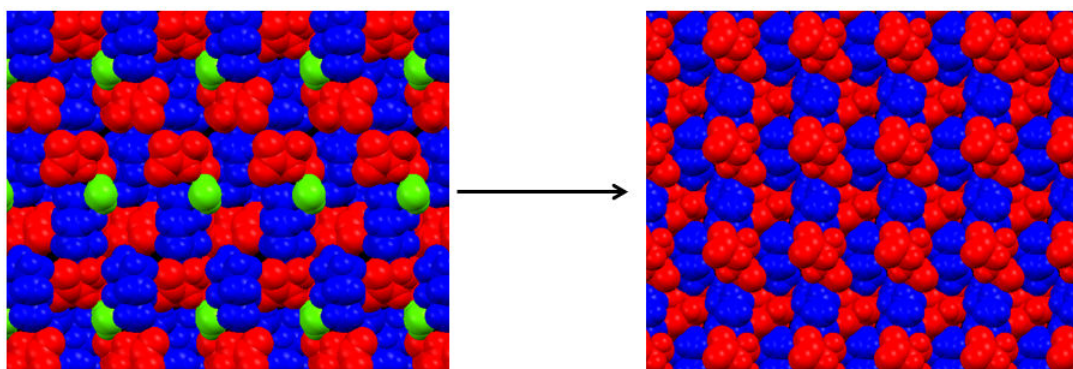


Figure 5.9 Comparison of the molecular packing arrangement in 1-methylpiperazinium L-tartrate monohydrate (left) with the anhydrous structure (right). Acid molecules are coloured red, base molecules are blue and water molecules are green. The structures are viewed perpendicular to the axes of the C2,2(12) anion-cation chains.

In contrast to the hydrogen tartrate salts there is minimal rearrangement of the structure on dehydration in this case, both structures are quite similar to those of other anhydrous salts based on the C2,2(12) motif such as piperazinium DL-tartrate and piperazinium succinate. It is also notable that the piperazinium DL-tartrate salt contains the R2,2(10) hydroxyl-carboxylate motif in common with the hydrated 1-methylpiperazinium tartrate salt, indicating that this may be a more strongly favoured motif in relation to the primary amine-carboxylate motif than the analogous interactions in the hydrogen tartrate salts to the C1,1(7) acid chain.

5.7.4 Secondary amine benzoate salts

5.7.4.1 Piperidinium and morpholinium 4-hydroxybenzoate

The structures of morpholinium and piperidinium 4-hydroxybenzoate dihydrate have isostructural packing and hydrogen bonding arrangements and are R4,4(12) hydrogen bonded acid-base rings connected into a 3-D hydrogen bonded network through contacts to water. As discussed in Section 5.7.1.3 the hydrogen bond contacts undergo significant rearrangement on dehydration to form C2,2(6) anion-cation chains with hydroxyl-carboxylate contacts between the acid molecules. In both cases this results in the formation of C1,1(8) anion chains and a substantial structural rearrangement as shown in Figure 5.10.

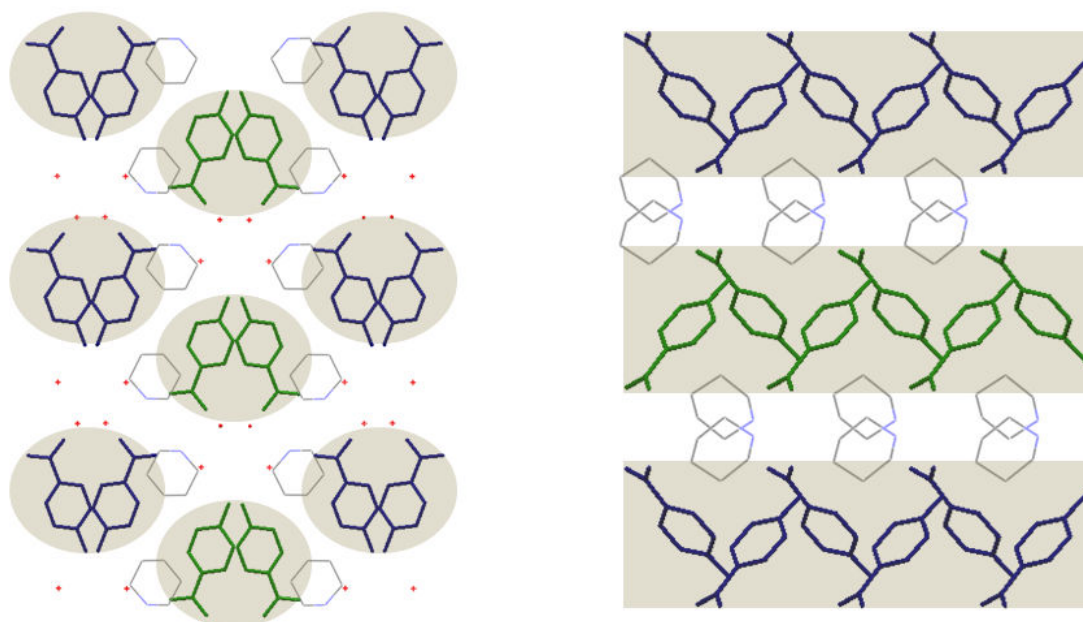


Figure 5.10 Comparison of the packing arrangements of the stacks of acid anions in piperidinium 4-hydroxybenzoate dihydrate (left) and the layers in the anhydrate (right) (Fukuyama, Kashino and Haisa 1973). The packing arrangement of the stacks of anions in morpholinium 4-hydroxybenzoate dihydrate is isostructural with the piperidinium dihydrate salt. In both anhydrates the anions form isostructural layers of C1,1(8) acid chains along the crystallographic *ac* plane, highlighted by the grey bands in the structure above. The stacking of these layers along the *b* axis differs between the morpholinium and piperidinium structures and an XPac analysis did not identify the two anhydrate structures as isostructural.

5.7.4.2 1-Methylpiperazinium 4-hydroxybenzoate monohydrate

The C1,1(8) anion chain is preserved on dehydration of 1-methylpiperazinium 4-hydroxybenzoate monohydrate, in which a hydrogen bond is accepted from a base by one carboxylate oxygen while the other accepts a hydrogen bond from water. This water molecule in turn forms hydrogen bonds to two base molecules, once as a donor and once as an acceptor. Dehydration results in the formation on an additional amine-carboxylate contact to compensate for the loss of the amine-water contact with the formation of an R2,2(12) amine-carboxylate ring motif analogous to that observed in the hydrates piperidinium and morpholinium salts. This results in rearrangement of the C1,1(8) acid chains with translation and rotation along the *a*-axis as shown in Figure 5.11.

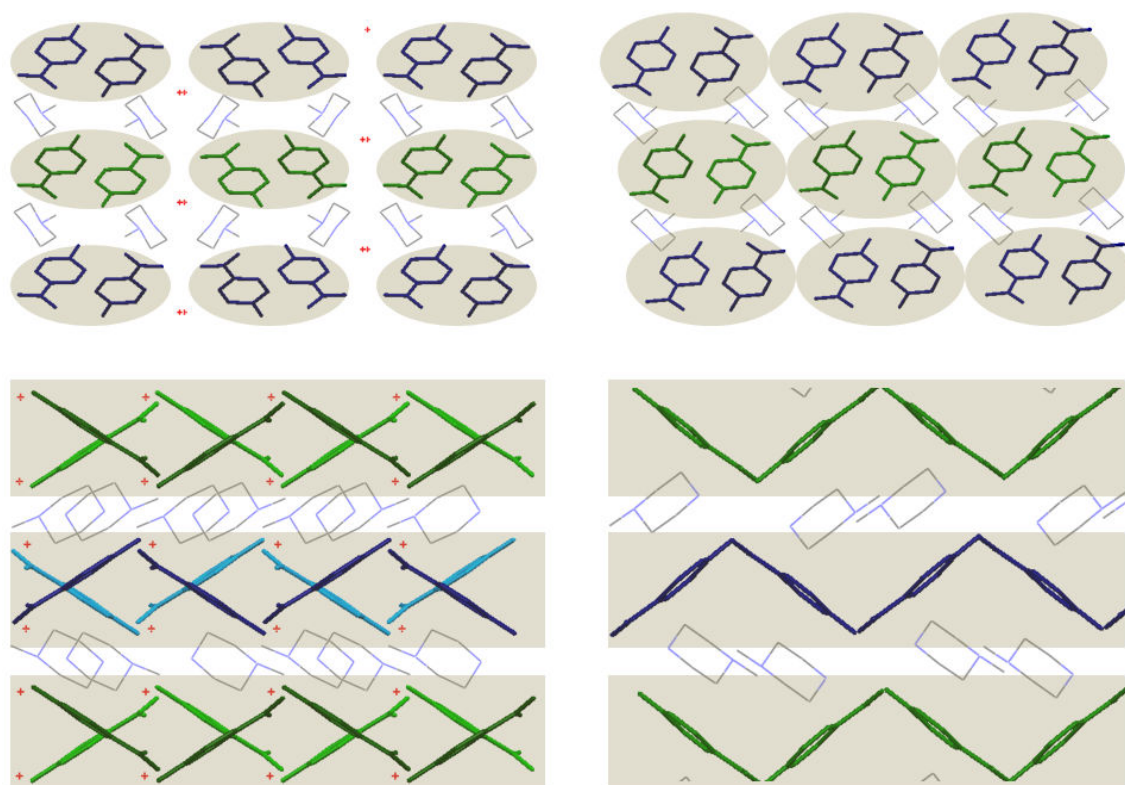


Figure 5.11 Rearrangement of the C1,1(8) acid chains on dehydration of 1-methylpiperazinium 4-hydroxybenzoate monohydrate (right top along *a*-axis and bottom along *c*-axis) to the anhydrate (left top along *a*-axis and bottom along *c*-axis). The C1,1(8) chains are coloured according to their orientation, in the view of the monohydrate along *c* dark or light coloration is used to distinguish adjacent offset chains in each layer.

5.7.5 Conclusions from the dehydration experiments

Variable-temperature X-ray powder diffraction (VT-XRPD) and structure-determination from powder diffraction data (SDPD) readily enabled the expansion of a small library of pairs of hydrated and anhydrous salts that had been obtained serendipitously from replicated crystallization experiments. The changes in hydrogen bond connectivity and packing arrangements between the hydrated and anhydrous states provided an insight into the structural role played by water in the hydrates and further confirmation of the importance of the structure-directing hydrogen bonded motifs identified in Chapter 4.

Although the conformational flexibility of the tartrate anions prevented the application of the XPac method considerable information was gained by the examination of the hydrogen bond contacts and general packing arrangements using Mercury. Although the rearrangement of both the hydrogen bonded contacts and packing arrangements on dehydration were considerable it is notable that the two main motifs identified in Chapter 4, the C1,1(7) hydrogen acid chain and C2,2(12) acid-base chain, are consistently preserved. This confirms of the importance of these two synthons in determining the supramolecular structure of the crystalline salts.

Also of interest is the similarity of the well-defined acid/water-base layers in the packing arrangements of the hydrates to those of corresponding anhydrous systems containing fumaric or succinic acid. As the tartrate anions can satisfy their hydrogen bonding potential in the anhydrous systems, albeit with significant changes in the packing arrangements, it can be postulated that the inclusion of water in these cases is to support the formation of the preferred layered structure. Three guidelines can be proposed for application to similar systems:

- (i) Hydrate formation may occur regardless of whether the anions and cations can satisfy their intermolecular hydrogen bonding potential in the absence of water.
- (ii) The most robust acid-base hydrogen bonded motifs expected for the anhydrous acid-base combination will also be observed in the hydrate.

- (iii) The structure of the hydrate will allow the packing of these motifs into a preferred arrangement that is similar to that of related anhydrous structures.

The XPac method proved to be of considerable utility in the comparison of the packing arrangements of the 4-hydroxybenzoate salts. The hydrogen bond connectivity of the isostructural dihydrated piperidinium and morpholinium salts, with their single acid-base hydrogen bond, increases on dehydration with the formation of the C1,1(8) hydroxyacid and C2,2(6) acid-base chains. This confirms the identification of these motifs as robust synthons in Chapter 4. The anhydrates are not isostructural, suggesting that the packing arrangement is determined by the hydrogen-bonded structure. In contrast, the lower acid-base hydrogen bond connectivity in the dihydrates indicates that non-directional interactions play a much more important role in determining their structures. However, the packing arrangements of the anhydrous structures differ in the positions of two-dimensional anion sheets along an axis and are essentially similar.

Modification of the 1-methylpiperazinium 4-hydroxybenzoate salt is much less pronounced. There is rearrangement of the acid-base hydrogen bonding motif to form an additional acid-base contact with the formation of the R4,4(12) motif, again identified as a robust synthon in Chapter 4. Similarly, the C1,1(8) acid chain is also preserved on dehydration, with rearrangement of neighbouring chains to produce parallel layers of anions and a more pronounced rearrangement of the cations. From the comparison of the three 4-hydroxybenzoate structures the following guidelines are proposed:

- (i) The structures of hydrates with a low degree of acid-base or acid-acid hydrogen bonding will rearrange significantly on dehydration to form at least one of the robust synthons.
- (ii) Similar or isostructural hydrates will have similar anhydrate structures.
- (iii) Structures in which the hydrate features one of the robust synthons will preserve this feature on dehydration with the minimum change in packing arrangement required to enable the satisfaction of all hydrogen bond donor and acceptor groups.

5.8 Summary

In this chapter the structural library developed as part of this work (Chapter 4) has been used to examine the probability of hydrate formation in salts formed with the three classes of counterion. The large number of closely related structures in the database enabled a highly systematic investigation into the influence of molecular structural features on the probability of hydrate formation. This has allowed some general guidelines to minimise the probability of hydrate formation in pharmaceutical salt selection to be derived as detailed in Section 5.5.

VT-XRPD and SDPD were successfully applied to generate four anhydrous structures from hydrates and the examination of these structures gave an insight into the structural role of water and enabled a rationalisation of hydrate formation in terms of the accessible supramolecular structures. In addition to confirming the importance of some of the hydrogen bonding motifs that are the basis of the structural rules in Chapter 4 the guidelines can be used to refine and expand these structural rules to include hydrate formation when applied to counterion selection for a novel pharmaceutical.

5.8.1 Case example of the application of the guidelines

In Section 4.7.1 the structural rules were used to describe the most likely salt structures for amoxapine, a pharmaceutical molecule with a piperazinyl ring. The guidelines derived in this chapter can be employed to explore the likelihood of hydrate formation and probable structural features.

(i) Based on the water affinity of salts containing a single secondary amine nitrogen base (Figure 5.1), the overall probability of hydrate formation for amoxapine salts is expected to be over 22% (i.e. at least one fifth of crystalline salts would be expected to be hydrates). As previously discussed (Infantes *et al.*, 2007) the probability of hydrate formation increases with molecular size and so the water affinity of salts of amoxapine may be higher than suggested by the small molecule salts examined in this chapter.

(ii) As the most probable intermolecular hydrogen bonded motif for a dicarboxylic acid salt is the C1,1(7) hydrogen acid chain this is expected to be the main structural feature regardless of whether a hydrate is formed. Hydrate formation can be minimised by using a dicarboxylic acid counterion such as succinic or fumaric acid (Figure 5.3), the water affinity of this type of counterion is comparatively low at 22%. If a hydroxyacid is used the probability of hydrate formation increases to >70 %, making it the most likely outcome. As discussed in Section 4.5.7 this inclusion is most likely to satisfy the hydrogen bonding requirements of the anion while allowing a preferred structural arrangement, indicated by an anhydrous salt, to be adopted.

(iii) Formation of a benzoate salt will result in a ca. 50% probability of hydrate formation, based on the water affinities shown in Figure 5.3. The higher water affinity of benzoate salts with no hydroxyl groups in comparison to the analogous dicarboxylic acid salts indicates that the inclusion of water is driven by space-filling requirements or to increase the intermolecular hydrogen bond connectivity of the structure beyond that achievable by the single acid group. The likelihood of hydrate formation can be reduced by using a 4-hydroxybenzoate anion, in this case the C1,1(8) anion chain is likely to be the major structure-directing motif with the acid-base connectivity remaining unpredictable.

(iv) Sulfonic acid salts have the lowest likelihood of hydrate formation, as shown in Figure 5.3. As the most likely acid-base motif with this class of counterion is the C2,2(6) chain if water molecules are incorporated they are most likely to cross-link these chains into a two-dimensional hydrogen bonded sheet.

Chapter 6

**Validation of structural rules:
Application to novel fluoroquinolone salts**

6.1 Introduction

The salts used to derive the structural rules for systems formed with secondary and tertiary amine bases in Chapter 4 and the associated guidelines for hydrate formation in Chapter 5 were a series of small molecules with no additional functional groups present on the base. Guides to intermolecular hydrogen bond contacts in crystalline solids such as Etter's rules are not always applicable to large molecules as steric effects and the relative locations of hydrogen bonding groups prevent all the otherwise probable contacts from forming (Byrn, *et al.*, 1994). Hydrate formation also becomes more probable with increasing molecular size as the water performs a space-filling role in the structure (Infantes, *et al.*, 2007). Therefore, it is necessary to validate the applicability of the structural rules and guidelines developed in Chapters 4 and 5 to systems containing larger and more complex molecules that are more representative of pharmaceutically active species.

The CSD can be used as a resource to examine published structures containing the counterions of interest to assess how representative the interactions observed in the structural database are of those found in systems containing additional functional groups. However, the lack of systematic series of structures limits the understanding of the relationships between molecular and supramolecular structure that can be achieved and so a systematic database analogous to the one examined in Chapters 4 and 5 is required.

A limited number of studies have systematically evaluated the role of different interactions in determining the crystal structures adopted by a series of salts of a pharmaceutically active molecule. These have demonstrated that competition between the interactions due to the hydrophilic and hydrophobic components of the molecules determine the structures of salts of molecules such as remacemide (Lewis, *et al.*, 2005) and ephedrine (Collier, *et al.*, 2006). The role of non-directional interactions and packing patterns in determining the crystal structure is expected to increase in systems with larger molecules than those in the model database. XPac can detect the similar molecular arrangements that indicate common non-directional

interactions and packing effects in systems with similar molecular species (Gelbrich and Hursthouse, 2006).

Fluoroquinolone antibiotics, which function by inhibiting bacterial DNA replication (Shen, *et al.*, 1989), were selected for this study. These are derivatives of the antimicrobial compound nalidixic acid with broader spectrums of action and improved bioavailability (King, *et al.*, 1984, Inoue, *et al.*, 1980, Miyamoto, *et al.*, 1990). Four compounds were cocrystallised with the counterions under investigation to generate a library of novel multi-component systems. These were norfloxacin, ciprofloxacin, enrofloxacin and sparfloxacin. The supramolecular chemistry of these molecules has been extensively studied including polymorphism (Llinas, *et al.*, 2008), hydrate structure (Florence, *et al.*, 2000), organic cocrystals (Sun, *et al.*, 2004), transition metal coordination complexes (Ruiz, *et al.*, 2007) and salts with organic acid (Prasanna and Row, 2001) and alkali metal counterions (Fabbiani, *et al.*, 2009). The structures of the fluoroquinolone molecules are shown in Figure 6.1.

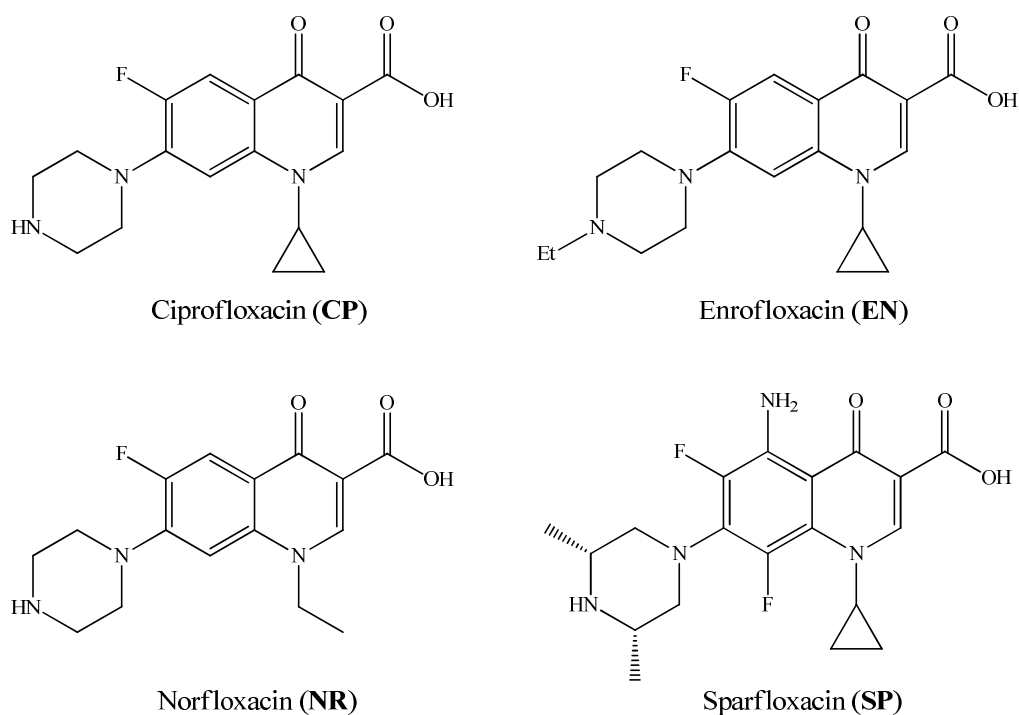


Figure 6.1 Structures of the fluoroquinolone antibacterial compounds examined in this work. The letters in bold type refer to the descriptor used in the codes in the discussions throughout this chapter.

These molecules contain a piperazine moiety, one of the bases examined in Chapter 4, with either one secondary and one tertiary or two tertiary amine nitrogens depending on the structure of the molecule. They are generally rigid molecules with limited scope for conformational variability in the orientation of the piperazine ring and alkyl side chains (Nangia, 2008). The aromatic rings result in face-to-face π - π stacking, producing layers of fluoroquinolones that is a dominant feature of the crystal structures of both single and multi-component systems containing these molecules (Basavoju, *et al.*, 2006; Prasanna and Row, 2001). In this work, 29 novel multi-component systems are presented for these molecules with the acidic counterions under investigation and the consistency of these structures with the rules derived in the previous chapters is evaluated in detail.

In common with the structural database discussed in Chapter 4 aspects of structure that will be discussed include hydrogen bonding, molecular packing arrangements, ionisation state and hydrate formation and type. The results will be used in combination with the data on the observed interaction retrieved from the CSD to refine the structural rules derived from the database of model systems to improve their general applicability to complex pharmaceutically active species.

6.2 Materials and Methods

6.2.1 CSD Database Searches

Version 5.30 of the CSD database with the November 2008 update was searched for structures containing each of the counterions in their ionised state in addition to an organic molecule using the following search parameters:

- (i) No metal atoms
- (ii) 3-D coordinates determined
- (iii) R-Factor < 10%
- (iv) No powder structures
- (v) Only organic structures
- (vi) No errors

The retrieved structures were collated and inspected visually to select structures that comply with the following criteria:

- (i) The base must feature an ionised secondary or tertiary amine nitrogen.
- (ii) The transferred protons must be explicitly located on the base nitrogen.
- (iii) The structure must contain either an ionised acid and base only or there may be an additional neutral acid molecule or water.

Structures meeting these criteria were included in the validation data sets along with the novel salt structures characterised in this work and visualised using CSD Mercury v2.2. The frequencies of observation of the hydrogen-bonded contacts between the functional groups of interest were calculated by the same method as those in the initial database.

6.2.2 Crystallisation of Novel Pharmaceutical Salts

Aqueous mixtures of the acid counterions and pharmaceutically active molecules in a 1.1:1 molar ratio were heated to 50°C and sufficient water added to dissolve the majority of the solid material. The solutions were filtered and allowed to evaporate slowly at ambient temperature to form crystals suitable for characterisation by SXRD using the data collection parameters described in Section 2.4.1 and are attached as CIF files in Appendix 3.

6.3 Validation of hydrogen bonding motifs with CSD structures

To verify that the hydrogen bonding motifs used to derive the structural rules in Chapter 4 are generally representative of crystalline salts with similar basic molecules their frequencies of observation in the model systems (**Pm**) are compared with their frequencies of observation in structures retrieved from the CSD (**Pmo**). The CSD structures were selected according to the parameters in Section 6.2.1.

6.3.1 Comparison of Pm and Pmo for motifs in dicarboxylic acid salts

The **Pm** of each of the motifs identified in the model systems in Section 4.4.3 are compared with their corresponding **Pmo** in the CSD structures in Table 6.1.

Table 6.1 Frequencies of occurrence for motifs (**Pmo**) in the CSD structures containing dicarboxylic acids compared with their frequencies in the database of model systems described in Chapter 4 (**Pm**). Major synthons identified in Chapter 4 are highlighted in bold and the difference between **Pmo** and **Pm** has been calculated as a percentage of **Pm**.

Donor	Acceptor	Graph Set	N _{poss}	N _{obs}	Pmo(%)	Pm (%)	ΔPm
<i>tert</i> -NH ⁺	CO ₂ ⁻	D1	56	46	82	67	+ 22%
		R2,1(5)	56	2	4	14	- 79%
		C2,2(12)	56	0	0	2	- 100%
<i>sec</i> -NH ₂ ⁺	CO ₂ ⁻	D1	46	16	24	17	+ 41%
		R2,1(5)	46	0	0	17	- 100%
		C2,2(6)	46	10	22	38	- 42%
		C2,2(9)	46	4	9	7	+ 28%
		C2,2(12)	46	0	0	33	- 100%
		R4,4(12)	46	3	7	7	0%
CO ₂ H	CO ₂ ⁻	C1,1(7)/(9)	102	76	75	64	+ 17%
OH	CO ₂ H/ CO ₂ ⁻	C1,1(5)	70	11	16	15	+ 6%
		C1,1(6)	70	17	24	22	+ 9%
		R2,2(10)	70	8	11	15	-27%
		R2,2(12)	70	0	0	15	- 100%

As **Pmo** > **Pm** for three of the major motifs identified in Chapter 4 their robustness as synthons is validated. In contrast **Pmo** < **Pm** for the C2,2(6) amine carboxylate chain and here the D1 contact has the highest **Pmo** for secondary amine salts. Also significant is the absence of the C2,2(12) acid-base chain that is the basis of the Type 2 salt structures with fully deprotonated counterions.

6.3.2 Comparison of **Pm** and **Pmo** for motifs in benzoic acid salts

The **Pm** of each of the motifs identified in the model systems in Section 4.5.3 are compared with their corresponding **Pmo** in the in the CSD structures in Table 6.2.

Table 6.2 Frequencies of occurrence for motifs (**Pmo**) in the validation set of structures containing benzoic acids compared with their frequencies in the database of model systems described in Chapter 4 (**Pm**). Major synthons identified in Chapter 4 are highlighted in bold and the difference between **Pmo** and **Pm** has been calculated as a percentage of **Pm**.

Donor	Acceptor	Graph Set	Nposs	Nobs	Pmo(%)	Pm (%)	ΔPm
<i>tert</i> -NH ⁺	CO ₂ ⁻	D1	13	13	100	86	+ 16%
<i>sec</i> -NH ₂ ⁺	CO ₂ ⁻	D1	15	2	13	35	- 63%
		C2,2(6)	15	6	40	42	- 5%
		R4,4(12)	15	6	40	23	+ 74%
OH	CO ₂ ⁻	C1,1(8)	5	4	80	67	+ 19%

In contrast to the dicarboxylic acid salts in Table 6.1 all the hydrogen bonding motifs in the model systems are observed in the CSD structures. As **Pmo** > **Pm** for the tertiary amine-carboxylate and hydroxyl-carboxylate motifs these appear to be reliable synthons. In the secondary amine salts **Pmo** < **Pm** for the D1 contact and **Pmo** > **Pm** for the R4,4(12) motif, making its **Pmo** equal to the C2,2(6) chain.

6.3.3 Comparison of **Pm** and **Pmo** for motifs in monosulfonic acid salts

The frequencies of observation for the motifs in the model systems (**Pm**) are compared with those in the CSD structures and novel pharmaceutical salts (**Pmo**) in Table 6.3. As **Pmo** > **Pm** for the most frequent amine-sulfonate motifs in the secondary and tertiary amine salts these are shown to be robust structure-directing interactions. The only motif for monosulfonic acid salts with **Pm** > 50% that has a lower **Pmo** is the C1,1(8) hydroxyl - sulfonate chain, although the small number of available structures containing this counterion make the evaluation of this motif unreliable. Only one suitable secondary amine salt structure was retrieved for ethanedisulfonic acid and no tertiary amine salts were found, therefore **Pm** for the hydrogen bonding motifs for the salts of this counterion cannot be compared with the CSD structures.

Table 6.3 Frequencies of observation for H-bond motifs in the CSD sulfonate salts (**Pmo**) and the database of model systems from Chapter 4 (**Pm**). Structures containing ethanedisulfonic acid (**ED**) are listed separately to the monosulfonic acid structures. Major synthons identified in Chapter 4 are highlighted in bold and the difference between **Pmo** and **Pm** has been calculated as a percentage of **Pm**.

Donor	Acceptor	Graph Set	Nposs	Nobs	Pmo (%)	Pm (%)	ΔPm
<i>tert</i> -NH ⁺	SO ₃ ⁻	D1	30	21	70	57	+ 23%
<i>sec</i> -NH ₂ ⁺	SO ₃ ⁻	D1	19	1	5	6	- 17%
		C2,2(6)	19	18	95	78	+ 22%
		C2,2(9)	1	1	100	14	+ 714%
		R4,4(12)	19	3	16	11	+ 45%
		R2,4(8)	19	0	0	6	- 100%
		R4,2(8)	19	1	5	6	- 17%
<i>tert</i> -NH ⁺	SO ₃ ⁻ (ED)	C2,2(12)	1	1	100	100	0%
<i>sec</i> -NH ₂ ⁺	SO ₃ ⁻ (ED)	C2,2(6)	2	1	50	40	+ 25%
		C2,2(9)	2	0	0	60	-100%
		C2,2(12)	2	0	0	40	-100%
		R4,4(12)	2	0	0	20	-100%
OH	SO ₃ ⁻	C1,1(8)	4	1	25	67	- 63%
<i>sec</i> -NH ₂ ⁺	<i>sec</i> -NH	C1,1 (5)	1	0	0	40	-100%

6.3.4 Summary of comparisons of Pm and Pmo

Based on the **Pmos** of the hydrogen bonding motifs used to derive the structural rules in Chapter 4 in the CSD structures the majority of the interactions used to derive the rules appear representative of those found in secondary and tertiary amine salts of the counterions under investigation. It is particularly encouraging that the motifs used to assign the major structural families are generally observed with comparable or significantly higher frequency in the CSD structures than in the database described in Chapter 4. The exceptions are the C2,2(12) acid-base chain motif for the tertiary amine salts of dicarboxylic acids and the C1,1(8) anion and C1,1(5) cation chains in the sulfonic acid salts. The unsystematic nature of the CSD structures makes a detailed rationalisation of the absence of these motifs impossible but based on the findings it can be expected that the corresponding structural rules for these three interactions are unlikely to be applicable to the fluoroquinolone salts examined in the subsequent part of this chapter.

6.4 Novel pharmaceutical salt systems

The fluoroquinolone antibiotics shown in Figure 6.1 were cocrystallised with the library of counterions as described in Section 6.2.2. The 25 novel structures characterised by X-ray diffraction will be used in Section 6.5 for a systematic examination of the applicability of the structural rules from Chapter 4 and hydrate guidelines from Chapter 5 to systems containing large molecules.

6.4.1 Novel dicarboxylic acid salts

11 novel fluoroquinolone salts were crystallised with the dicarboxylic acids under investigation along with hydrogen maleate and bisuccinate salts of norfloxacin consistent with the those reported by Basavoju (Basavoju, *et al.*, 2006). Information on the composition of the novel systems characterised is given below in Table 6.4.

Table 6.4 Novel dicarboxylic acid salts of pharmaceutically active molecules characterised in this work. Calculated pKa values for the components of the systems are taken from Chapter 2. The salts are identified by the codes for the acid component from Figure 4.1 and the fluoroquinolone from Figure 6.1.

ID	Composition	Type	pKa ₁		ΔpKa ₁
			Base	Acid	
ADCP	Bis(Ciprofloxacin) adipate dihydrate	1:2 Salt	8.76	4.39	4.37
ADNR	Norfloxacin adipate adipic acid	Mixed	8.76	4.39	4.37
FUCP	Ciprofloxacin hydrogen fumarate hydrate	1:1 Salt	8.76	3.15	5.61
FUEN	Enrofloxacin fumarate fumaric acid	Mixed	7.11	3.15	3.96
FUNR	Norfloxacin hydrogen fumarate dihydrate	1:1 Salt	8.76	3.15	5.61
LTCP	Bis(Ciprofloxacin) L-tartrate trihydrate	2:1 Salt	8.76	3.07	5.69
LTNR	Norfloxacin hydrogen L-tartrate	1:1 Salt	8.76	3.07	5.69
MECP	Ciprofloxacin hydrogen maleate hydrate	1:1 Salt	8.76	1.83	6.93
RTNR	Norfloxacin hydrogen L-tartrate dihydrate	1:1 Salt	8.76	3.07	5.69
RTSP	Sparfloxacin hydrogen DL-tartrate trihydrate	1:1 Salt	7.16	3.07	4.09
SUCP	Ciprofloxacin hydrogen succinate tetrahydrate	1:1 Salt	8.76	4.54	4.22

6.4.2 Novel benzoic acid salts

Six novel substituted benzoic acid salts of fluoroquinolones crystallised as hydrates in a 1:1 acid:base stoichiometry and are listed in Table 6.5. The exclusivity of crystalline salt formation, even for systems where $\Delta pK_a < 3$, contrasts with the model systems in Chapter 4 where mixed systems and cocrystals were also observed.

Table 6.5 Novel benzoic acid salts of fluoroquinolones characterised in this work. Calculated pKa values for the components of the systems are taken from Chapter 2. The salts are identified by the codes for the acid component from Figure 4.1 and the fluoroquinolone from Figure 6.1.

ID	Composition	Type	pKa		Δ pKa
			Base	Acid	
BZSP	Sparfloxacin benzoate hydrate	1:1 Salt	7.16	4.20	2.96
HBNR	Norfloxacin 4-hydroxybenzoate sesquihydrate	1:1 Salt	8.76	4.57	4.19
SACP	Ciprofloxacin salicylate monohydrate	1:1 Salt	8.76	3.01	5.75
SAEN	Enrofloxacin salicylate	1:1 Salt	7.11	3.01	4.10
SANR	Norfloxacin salicylate dihydrate	1:1 Salt	8.76	3.01	5.75
ENTU	Enrofloxacin 4-toluate tetrahydrate	1:1 Salt	7.11	4.37	2.74

6.4.3 Pharmaceutical salts with sulfonic acid counterions

Eight novel salts of fluoroquinolones were formed by cocrystallisation with the library of sulfonic acids under investigation. Information on the composition of the systems characterised is given in Table 6.6.

Table 6.6 Novel sulfonic acid salts of fluoroquinolones characterised in this work. Calculated pKa values for the components of the systems are taken from Chapter 2. The salts are identified by the codes for the acid component from Figure 4.1 and the fluoroquinolone from Figure 6.1.

ID	Composition	Type	pKa		Δ pKa
			Base	Acid	
BSEN	Enrofloxacin besylate hydrate	1:1 Salt	7.11	-0.60	7.76
EDEN	Enrofloxacin edisylate dihydrate	1:2 Salt	7.11	-2.89	10.00
EDNR	Norfloxacin edisylate dihydrate	1:2 Salt	8.76	-2.89	11.65
HSCP	Ciprofloxacin 4-hydroxybesylate monohydrate	1:1 Salt	8.76	-0.23	8.99
HSNR	Norfloxacin 4-hydroxybesylate monohydrate	1:1 Salt	8.76	-0.23	8.99
TSCP	Ciprofloxacin tosylate dihydrate	1:1 Salt	8.76	-0.43	9.19
TSEN	Enrofloxacin tosylate monohydrate	1:1 Salt	7.11	-0.43	7.54
TSNR	Norfloxacin tosylate tetrahydrate	1:1 Salt	8.76	-0.43	9.19

The exclusive formation of salts is consistent with the library in Chapter 4 where all the sulfonic acid systems crystallised as salts. These outcomes are unsurprising in light of the large Δ pKa values for the acid – base combinations and indicate that this class of counterions are a generally reliable salt former. In contrast to the model systems, all the salts crystallised as hydrates regardless of the type of basic functionality present in the structure.

6.5 Application of structural rules to novel pharmaceutical salts

6.5.1 Structural rules for dicarboxylic acid salts

The seven structural rules for dicarboxylic acid counterions from Chapter 4 are compared against the novel salts listed in Section 6.4.1 and the maleic and succinic acid salts of norfloxacin characterised by Basavoju (Basavoju, *et al.*, 2006).

6.5.1.1 Structural rules applicable to all dicarboxylic acid salts

Two rules, D1 and D5 (Section 4.4.3) are potentially relevant to all of the structures in the series presented in this chapter with the exception of the two hydrogen maleate salts. Each structure was scrutinised to determine whether the rules are actually obeyed in each case and the results are provided in Table 6.7.

Rule D1 states: For bases with a single nitrogen donor atom there is a >95% probability that a hydrogen acid salt will crystallise with the C1,1(7) hydrogen acid chain.

Rule D5 states: Where the base contains a piperazinyl ring the C2,2(12) acid-base chain is favoured over the C1,1(7/9) hydrogen acid chain and will be observed twice as frequently.

Table 6.7 Agreement of the novel dicarboxylic acid salts with structural rules D1 and D5. The salts are identified by the four-letter codes established in Chapter 2.1.

System	System Type	Major motif	Rule D1	Rule D5
ADCP	Biadipate (2-) salt	Water-separated ion pairs	No	No
ADNR	Mixed system	C1,1(9) dianion-acid chain	No	No
FUCP	Hydrogen acid salt	C2,2(9) acid-base chain	Partial	No
FUEN	Mixed system	C1,1(7) dianion-acid chain	No	No
FUNR	Hydrogen acid salt	C1,1(7) hydrogen acid chain	Yes	No
LTCP	Bitartrate (2-) salt	Water-separated ion pairs	No	No
LTNR	Hydrogen acid salt	C1,1(7) hydrogen acid chain	Yes	No
RTNR	Hydrogen acid salt	C1,1(7) hydrogen acid chain	Yes	No
RTSP	Hydrogen acid salt	C1,1(7) hydrogen acid chain	Yes	No
SUCP	Hydrogen acid salt	C1,1(7) hydrogen acid chain	Yes	No
VETWAT	Bisuccinate (2-) salt	R4,4(12) acid-base ring	No	No
			Pm:	95%*
			Pmo:	55%
				66%[†]
				0%

* Assuming only one protonated nitrogen atom per base available as a donor.

[†] Based on the expected 2:1 C2,2(12) : C1,1(7) ratio with diprotonated bases.

As all the base molecules featured the piperazinyl ring moiety both Rule D1 and Rule D5 were probable outcomes based on the examination of the model structures in Chapter 4. Six (54%) conformed at least partially with Rule D1 in that a hydrogen acid salt was formed and five of these (46%) were in full agreement with the rule as their structures were based on the C1,1(7/9) hydrogen acid chain. If only four-carbon dicarboxylic acids are considered, these probabilities increase to 67% and 56% respectively.

In three structures, the anion is fully deprotonated and crystallises with two monoprotonated bases. As the low pKa of the piperazinyl nitrogen adjacent to the quinolone ring prevents the required protonation to allow formation of the C2,2(12) acid-base chain this motif is never observed. Consequently, Rule D5 is not applicable to salts of this type of molecule.

6.5.1.2 Structural rules applicable to aliphatic dicarboxylic acid salts

Three rules, D2, D4 and D7 (Section 4.4.3) are potentially relevant to the salts with hydrogen acid counterions that lack additional hydrogen bonding groups. Two of these rules (D2 and D4) are for salts with the C1,1(7) hydrogen acid chain and one is for salts formed with maleic acid. The lack of appropriate acid-base combinations in the novel structures prevented the direct validation of Rule D4 and Rules D2 and D7 each applied to two structures as detailed in Table 6.8.

Rule D2 states: For a C1,1(7) hydrogen acid salt with no additional hydrogen bonding groups on the acid molecule there is a 90% probability that secondary amine bases will form two hydrogen bond contacts to carboxylate groups. In > 75% of these the C2,2(6) chain motif will form to produce a 2-dimensional hydrogen bonded sheet.

Rule D4 states: For a C1,1(7) hydrogen acid salt of tertiary amine bases there is a >70% probability that a hydrogen bond will be formed to the carboxylate group.

Rule D7 states: Maleic acid crystallises as the hydrogen acid with an intramolecular hydrogen bond. None of the other rules are applicable to this counterion.

Table 6.8 Structural features observed in the dicarboxylic acid salts in comparison to those expected from Rules D2 and D7. The acid-base combinations are identified by the codes established in Chapter 2.1. The expected (Pm) and observed (Pmo) occurrences of each rule are given.

System	Expected Motif	Observed Motif	Rule D2	Rule D7
FUNR	C2,2(6) NH ₂ ⁺ ⋯CO ₂ ⁻ motif	C3,3(7) H ₂ O ⋯NH ₂ ⁺ ⋯CO ₂ ⁻	No	N/A
MECP	Intermolecular H-bond	Intermolecular H-bond	N/A	Yes
SUCP	C2,2(6) NH ₂ ⁺ ⋯CO ₂ ⁻ motif	R3,3(8) CO ₂ ⁻ ⋯NH ₂ ⁺ ⋯CO ₂ H	No	N/A
VETWAT	Intermolecular H-bond	Intermolecular H-bond	N/A	Yes
			Pm:	68%*
			Pmo:	100%

* Calculated as 75% probability of the formation of this motif by the 90% of the secondary amine bases expected to donate two NH⁺⋯OC hydrogen bonds.

SUCP is a monohydrate with the base donating hydrogen bonds to a succinate carboxylate group and a water molecule. In FUNR, also a monohydrate, the base donates hydrogen bonds to a carboxylic acid and a carboxylate group of two anions in the same C(1,1)7 chain. Rule D2 does not appear to be applicable to salts of pharmaceutically active molecules. In contrast, Rule D7 appears to be a reliable predictor of the ionisation state and hydrogen bonding arrangement of maleic acid when cocrystallised in these systems.

Although a direct validation of Rule D4 was not possible as none of the structures featured the requisite C1,1(7) hydrogen acid motif in addition to a tertiary amine base the examination of the structures in the CSD detailed in Table 6.1 indicates that the amine-carboxylate contact is a robust synthon in systems containing this type of base. It is therefore likely that Rule D4 will be applicable to pharmaceutically active molecules.

6.5.1.3 Structural rules applicable to hydroxyacid salts

Two structural rules, D3 and D6 (Section 4.4.3) potentially apply to salts with hydroxyacid counterions. The diversity in the observed intermolecular hydrogen bonding motifs prevented a quantitative assessment of the relative probabilities of them forming on crystallisation and these rules are therefore qualitative. The agreement of the pertinent structural features of the four fluoroquinolone salts with those expected from the rules is assessed in Table 6.9.

Rule D3 states: For structures featuring the C1,1(7) hydrogen acid chain with additional hydrogen bonding groups on the acid molecule the C2,2(6) motif will not form. There will always be at least one amine-carboxylate hydrogen bond contact, but the motif observed becomes unpredictable.

Rule D6 states: Hydroxyl to carboxylate/carboxylic acid interactions are not as robust as amine-carboxylate interactions. They are frequently replaced by hydroxyl-water contacts and cannot be considered a reliable structure-directing interaction.

Table 6.9 Structural features observed in the hydroxyacid acid salts in comparison to those expected from Rules D3 and D6. The acid-base combinations are identified by the codes established in Chapter 2.1.

System	NH ₂ H-bond acceptors*	OH H-bond acceptors	Rule D3	Rule D6
LTCP	COO ⁻ or H ₂ O	H ₂ O and base CO ₂ H	N/A	Yes
LTNR	CO ₂ ⁻ (ax.), CO ₂ ⁻ /CO ₂ H (eq.)	CO ₂ ⁻ (inter), CO ₂ H (intra) [†]	Yes	Yes
RTNR	H ₂ O (ax.), COH (eq.)	CO ₂ ⁻ (inter), H ₂ O	No	Yes
RTSP	H ₂ O (ax.), H ₂ O (eq.)	CO ₂ ⁻ (inter), H ₂ O	No	Yes

* For all structures except LTCP (ax.) denotes the acceptor for the hydrogen bond from the axial amine proton and (eq.) denotes the acceptor for the equatorial proton. LTCP is a Z'=4 structure with different hydrogen bond acceptors for each amine proton in the asymmetric unit.

[†] Inter denotes an intermolecular contact to another anion, intra indicates an intramolecular bond.

Of the four hydrogen acid salts, only the anhydrous LTNR salt features an amine-carboxylate hydrogen bond. The other three hydrogen acid salts are hydrates and amine-water or amine-hydroxyl contacts are formed instead. It therefore appears that rule D3 is not applicable to salts of larger pharmaceutically active molecules, particularly hydrates where competing interactions with water molecules can be formed. In contrast, rule D6 postulates that hydroxyl-carboxylate contacts are less robust than amine-carboxylate contacts with this type of counterion, however in the validation structures this contact is observed in two of the hydrated salts and the anhydrous LTNR salt. It appears that this interaction is more robust for larger molecular systems than indicated by the database of model salts.

6.5.2 Structural rules for benzoic acid counterions

The five structural rules relating to hydrogen bonding motifs for benzoic acid salts listed in Section 4.5.4 can be directly applied to the seven novel salts listed in Table 6.5. As rule B6 refers to packing arrangements of the benzoic acid counterions, the smallest molecular components in the structures, this rule cannot be directly applied to these systems.

6.5.2.1 Structural rules applicable to tertiary amine salts

Structural rules B1 and B5 in Section 4.5.4 are potentially applicable to tertiary amine salts with benzoic acid counterions and can be assessed against the two enrofloxacin salts listed in Table 6.5. One other rule, B2, relates to salts formed by counterions with a *para*-hydroxyl group and could not be directly evaluated.

Rule B1 states: When the base molecule has a tertiary amine nitrogen there is a > 90% probability that an amine-carboxylate hydrogen bond will be formed.

Rule B5 states: The ionisation state of the systems based on the D1 motif is inherently unpredictable in cases where the base has a tertiary amine nitrogen, regardless of the number of available hydrogen bond donor groups on the acid molecule.

Direct amine-carboxylate contacts are observed in the hydrated and anhydrous enrofloxacin salts, therefore rule B1 is applicable to these systems. In contrast, rule B5 is not as both systems are 1:1 salts, indicating that formation of mixed systems is less probable for these molecules than suggested by the model salts in Chapter 4.

6.5.2.2 Structural rules applicable to secondary amine salts

Structural rules B3 and B4 in Section 4.5.4 are potentially applicable to the four secondary amine salts listed in Table 6.5. The correspondence of the observed supramolecular structural features with those anticipated from the rules is assessed in Table 6.10.

Rule B3 states: The most likely amine-carboxylate motif is the C2,2(6) chain, but as the base possesses a large substituent group the D1 or R4,4(12) motifs may be expected.

Rule B4 states: There is a 60% probability that the C1,1(8) hydrogen bonded acid chain will be observed in addition to the C2,2(6) amine-carboxylate motif and a 75% probability that it will be observed in addition to the D1 motif but it will be absent from structures with the R4,4(12) motif.

Table 6.10 Occurrence of the structural features predicted for the dicarboxylic acid systems formed with pharmaceutically active molecules from structural rules D1 and D5. The acid-base combinations are identified by the four-letter codes established in Chapter 2.1. The expected (Pm) and observed (Pmo) occurrences of each rule are given.

System	NH ₂ ⁺ ...CO ₂ ⁻ motif	C1,1(8) anion chain	Rule B3	Rule B4
BZSP	R4,4(12)	Not Applicable	Yes	N/A
HBNR	R4,4(12)	No	Yes	Yes
SACP	D1	Not Applicable	Yes	N/A
SANR	D1	Not Applicable	Yes	N/A
			Pm:	67.5%
			Pmo:	100%
				0%

The effect of increasing steric size on the likely amine-carboxylate hydrogen bonding motif postulated from the 4-phenylpiperazine structures in Chapter 4 appears to be confirmed by the formation of the R4,4(12) and D1 acid-base contacts here, despite the lack of a significant reduction in **Pmo** for this interaction in the aggregate validation set. As all the structures are hydrates, the water contacts do not appear to determine the motif observed, although it should be noted that anion-water chains are observed in both D1 structures. The incompatibility of the C1,1(8) chain with the R4,4(12) acid-base ring motif is confirmed by the norfloxacin 4-hydroxybenzoate structure.

6.5.3 Structural rules for sulfonic acid salts

In order to increase the number of validation structures for monosulfonic acid salts of fluoroquinolones two mesylate salts of pefloxacin, a tertiary amine fluoroquinolone, were retrieved from the CSD. The salts, FORGAU (Toffoli, *et al.*, 1987) and MATMAV (Parvez, *et al.*, 2000), are a dihydrate and 0.1 hydrate respectively that crystallised with a 1:1 acid-base stoichiometry.

6.5.3.1 Structural rules applicable to tertiary amine salts

Rule S1 from Section 4.6.4 is potentially applicable to the five tertiary amine fluoroquinolone salts and the correlation of the observed supramolecular structural features with those anticipated from this rule are summarised in Table 6.11.

Rule S1 states: There is a 57% probability that an amine-sulfonate contact will form, competition from formation of contacts to water makes hydrate formation likely.

Table 6.11 Hydrogen bond acceptor for the amine nitrogen in the six tertiary amine sulfonate salts. The salts are identified by the four-letter codes established in Chapter 2.1. The expected (Pm) and observed (Pmo) occurrences of the interaction are given.

System	System Type	NH ⁺ hydrogen bond contact	Rule S1
BSEN	1:1 salt hydrate	Simple to sulfonate oxygen	Yes
EDEN	1:2 salt hydrate	Simple to sulfonate oxygen	Yes
TSEN	1:1 salt hydrate	Bifurcated to sulfanoate oxygens	Yes
FORGAU	1:1 salt hydrate	Simple to sulfonate oxygen	Yes
MATMAV	1:1 salt hydrate	Bifurcated to sulfonate oxygen and water	Yes
			Pm: 57%
			Pmo: 100%

In four of the five salts there is a direct NH⁺...OS⁻ contact, in four of these a simple NH⁺...OS⁻ hydrogen bond is formed and in TSEN a bifurcated bond is formed to give an R2,1(4) ring motif. In the remaining structure, MATMAV a bifurcated hydrogen bond is donated from the amine nitrogen to a mesylate oxygen and a water oxygen. Although all the fluoroquinolone salts are hydrates competition between water for the amine hydrogen is significantly lower than in the model salts. Rule S1 is more reliable for systems containing large molecules than suggested by the model systems, even with the inclusion of water molecules in the crystal structure.

6.5.3.2 Structural rules applicable to secondary amine salts

The five salts of the secondary amine molecules ciprofloxacin and norfloxacin were used to evaluate the applicability of Rule S2 from Section 4.6.4. The correlation of the observed supramolecular structural features with those anticipated from Rule S2 is examined in Table 6.12

Rule S2 states: both amine protons will form $\text{NH}_2^+ \cdots \text{OS}$ contacts with formation of the C2,2(6) motif most probable. There is a 50% probability that additional hydrogen bond contacts will form to the third sulfonate oxygen.

Table 6.12 Consistency of the amine-sulfonate hydrogen bond motifs in the novel secondary amine pharmaceutical sulfonic acid salts with structural rules S2.

System	$\text{NH}_2^+ \cdots \text{OS}$ motif		SO_3^- contacts			Rule S2
EDNR	D1	O1: NH_2^+	O2: H_2O	O3: 2 x H_2O	Partial	
HSCP	C2,2(6)	O1: NH_2^+	O2: NH_2^+	O3: H_2O	Yes	
HSNR	C2,2(6)*	O1: $\text{NH}_2^+ / \text{H}_2\text{O}$	O2: $\text{NH}_2^+ / \text{H}_2\text{O}$	O3: NH_2^+	Yes	
TSCP	C2,2(6)	O1: NH_2^+	O2: NH_2^+	O3: H_2O	Yes	
TSNR	C2,2(6)	O1: NH_2^+	O2: NH_2^+	O3: H_2O	Yes	

*Equatorial proton forms a simple hydrogen bond to O3 on counterion A, the axial proton donates a bifurcated hydrogen bond to O1 and O2 of counterion B to form an R2,1(5) ring.

In five salts the axial proton on the fluoroquinolone NH_2^+ group donates a direct hydrogen bond to a sulfonate oxygen, the exception being HSNR where the proton forms a bifurcated hydrogen bond to the sulfonate oxygen. With the exception of EDNR the equatorial proton forms a hydrogen bond to a sulfonate oxygen, making an extended C2,2(6) chain the most probable motif for sulfonate salts of secondary amines.

In all the salts the third sulfonate oxygen accepts a hydrogen bond from a water molecules. This represents a significant increase in the probability of formation of additional contacts with the sulfonate oxygens in comparison with the model salts. In the majority of the salts the water molecules are disordered within the structure with partial occupancies of sites surrounding the sulfonate anions and the carboxylic acid moieties. This may indicate that the water fulfils a space-filling role in the structures in the hydrophilic regions created by the sulfonate and carboxylic acid groups.

6.5.3.3 Structural rules applicable to 4-hydroxybesylate salts

The applicability of Rule S3, derived from the analysis of six model 4-hydroxybesylate salts in Section 4.6.2, can be assessed against the two secondary amine 4-hydroxybesylate salts. The rule states that:

When the acid molecule contains a *para*-hydroxyl group, formation of the C1,1(8) acid chain always occurs and the amine-sulfonate contacts propagate along a single axis. The direction the C1,1(8) chain propagates in relative to the axis of the amine-sulfate motif is unpredictable and will result in two and three-dimensional hydrogen bonded arrays.

The C1,1(8) motif is not observed in the 4-hydroxybesylate fluoroquinolone salts, in both the *para*-hydroxyl group donates its hydrogen bond to the water molecules of the C2,2(6) acid-water chain. This is most likely a result of the increasing steric size of the basic component making the formation of the C1,1(8) chain incompatible with the formation of the acid-amine and acid-water contacts. The two 4-hydroxybesylate salts retrieved from the CSD (PICWUU and ABERAB) in Table 6.3 appear to confirm this hypothesis. One is a polymorph of piperazinium 4-hydroxybesylate that features the C1,1(8) chain (Marchewka and Pietraszko, 2008) while the other is a monohydrate salt of dicyclohexylammonium in which a hydroxyl-water contact is formed to the acid-water chain (Jin, *et al.*, 2004).

6.5.4 Summary

The structural rules that are most valid for each of the three classes of counterion are those that describe the motifs used to classify the major structure types. For the dicarboxylic acid counterions the C1,1(7) hydrogen acid chain motif, intramolecular hydrogen bonds and hydroxyl-carboxylate contacts are the structural features most likely to be observed in the pharmaceutical salts, indicating that the favourable hydrogen bonding arrangements for the acid component are the main factor in determining supramolecular structure. The low occurrence of the C2,2(6) motif could be expected for salts based on the C1,1(7) motif as the steric size of the base molecule would make the two motifs mutually exclusive. Similarly, the pKa of the tertiary piperazinyl nitrogen is too low for the requisite protonation for the formation of the C2,2(12) motif to occur.

For the benzoic and sulfonic acid salts, the most reliable interactions are the acid-base motifs, corresponding with the importance of these motifs in defining the supramolecular structures of the model salts. In neither case is the C1,1(8) anion chain observed for acids featuring a 4'-hydroxyl group. This motif has a **Pmo** of 80% for the CSD structures and its absence from the norfloxacin 4-hydroxybenzoate salt is not unexpected due to its established incompatibility with the R4,4(12) amine-carboxylate motif. In contrast, it has a low **Pmo** for 4-hydroxybenzyl salts and its absence in the two pharmaceutical salt structures indicates that the molecular orientations required for the requisite contact is disfavoured in systems containing larger molecules.

It was observed in both the benzoate and benzenesulfonate salts that the packing arrangements of the anions were largely independent of the acid-base hydrogen bonding motifs in Chapter 4 and that the inclusion of water molecules in the structures was partly driven by the need to stabilise the favourable packing arrangements in Chapter 5. It can be postulated that the adoption of favourable packing arrangements by the large fluoroquinolone molecules will be an important determinant of these structural features. A detailed examination of the coordination environments of water and the occurrence of supramolecular constructs will be used to refine the structural rules and adapt them for application to larger molecules.

6.6 Hydrate formation and structure in fluoroquinolone salts

6.6.1 Consistency with guidelines to minimise hydrate formation

Some general guidelines for counterion selection to minimise hydrate formation were derived from the database of model structures and are presented in detail in Section 5.5. In general, salts with dicarboxylic acid counterions are most likely to give hydrates while benzoate salts have the lowest probability for tertiary amine bases and sulfonic acids have the lowest probability for secondary amines. The salts crystallised with pharmaceutically active molecules deviated considerably from these guidelines, all the sulfonate salts and five of the six benzoate salts crystallised as hydrates. In this case, the dicarboxylic acid salts were marginally less likely to crystallise as hydrates than the other types of counterion with nine hydrated salts from the eleven novel structures.

6.6.2 Water contact environments in the fluoroquinolone salts

Details of the coordination environments of the water molecules in the three types of salt are summarised in Table 6.13 to 6.15. Due to the high incidence of disorder and partial occupancy of water positions, the analyses are limited to the hydrate type and the functional groups that contact water as either a donor or acceptor.

Table 6.13 Water coordination environments in the dicarboxylic acid salts of fluoroquinolones.

Structure	Acid - Base H-bond Motif	Hydrate Type	Water Contacts						
AD CP	D1	2 x 2	CO ₂ ⁻	NH ₂ ⁺	H ₂ O	CO ₂ ⁻	H ₂ O	CO ₂ H	
FU CP	C2,2(9)	1 x 2	CO ₂ ⁻	CO ₂ H	CO ₂ ⁻	-	-	-	
FU NR	D1	2 x 2	CO ₂ ⁻	H ₂ O	CO ₂ H	H ₂ O	NH ₂ ⁺	CO ₂ H	
LT CP	R4,2(8)								
ME CP	D1	1 x 2	CO ₂ ⁻	NH ₂ ⁺	CO ₂ ⁻	-	-	-	
ME NR*	D1	1 x 2	CO ₂ ⁻	NH ₂ ⁺	CO ₂ H	-	-	-	
RT NF	None	1 x 2	CO ₂ ⁻	NH ₂ ⁺	CO ₂ H	-	-	-	
RT OF	None	1 x 2	CO ₂ ⁻	OH	CO ₂ ⁻	-	-	-	
RT SP	None		CO ₂ ⁻	OH/ H ₂ O	OH	CO ₂ ⁻	NH ₂ ⁺	H ₂ O	
SU CP	D1		CO ₂ ⁻	NH ₂ ⁺	H ₂ O	CO ₂ ⁻	H ₂ O	H ₂ O	
SU NR*	R4,4(12)	1 x 1	CO ₂ ⁻	-	CO ₂ ⁻	-	-	-	

* From Basavajou *et al.*

Table 6.14 Water coordination environments in the novel benzoate salts of pharmaceuticals characterised in this work.

Structure		Acid - Base H-bond Motif	Hydrate Type	Water Contacts
BZ	SP	R4,4(12)	Channel	Acid CO ₂ ⁻ ; fluoroquinolone NH ₂ ⁺ and CO ₂ H; water
HB	NR	R4,4(12)	Isolated site	Acid CO ₂ ⁻ and OH
SA	CP	D1	Isolated site	Acid CO ₂ ⁻ and fluoroquinolone NH ₂ ⁺
SA	NR	D1	Isolated site	Acid CO ₂ ⁻ and fluoroquinolone NH ₂ ⁺
TU	EN	D1	Channel	Acid CO ₂ ⁻ ; fluoroquinolone CO ₂ H; water

Table 6.15 Water coordination environments in the novel fluoroquinolone sulfonate salts characterised in this work.

Structure		Acid - Base H-bond Motif	Hydrate Type	Water Contacts
BS	EN	D1	Channel	Fluoroquinolone CO ₂ H; water
ED	EN	D1	D2 chain	Acid SO ₃ ⁻ ; fluoroquinolone OH and CO ₂ H; water
ED	NR	C2,2(6)	Isolated site	Acid SO ₃ ⁻ ; fluoroquinolone NH ₂ ⁺ and CO ₂ H
HS	CP	C2,2(6)	Isolated site	Acid SO ₃ ⁻ and OH
HS	NR	C2,2(6)	Isolated site	Acid SO ₃ ⁻ and OH
TS	CP	C2,2(6)	D2 chain	Acid SO ₃ ⁻ ; fluoroquinolone OH; water
TS	EN	D1	Channel	Acid SO ₃ ⁻ ; water
TS	NR	C2,2(6)	Channel	Acid SO ₃ ⁻ ; fluoroquinolone NH ₂ ⁺ , OH CO ₂ H; water

6.6.3 Consistency with guidelines established in Chapter 5

It is clear from the above results that the guidelines to minimise hydrate formation derived from the small molecular systems in Chapter 5 are not applicable to the fluoroquinolone systems. The increasing molecular size and presence of additional hydrogen bonding groups on the fluoroquinolone molecules are undoubtedly key factors in increasing the probability of hydrate formation. The increased prevalence of channel hydrates with extended water motifs indicate that water is more likely to fulfil a space-filling role in these structures as opposed to a role in determining or maintaining a particular hydrogen bonding motif or molecular arrangement.

6.7 Study of Fluoroquinolone packing arrangements using XPac

6.7.1 General

The packing arrangements of the fluoroquinolone molecules in the 29 multi-component systems and ciprofloxacin and sparfloxacin were compared using XPac as described in Section 2.3. The analysis showed that 28 structures contain SC **A**, a face-to-face pair of molecules as shown in Figure 6.2.

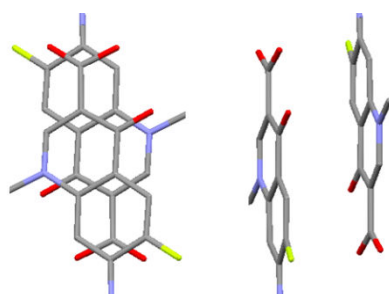


Figure 6.2 Face and side views of the 0-dimensional primary supramolecular construct **A**, found in 28 of the 31 fluoroquinolone structures.

Six one-dimensional SCs were identified and are shown in Figure 6.3. The **A** pairs stack in four unique one 1-dimensional arrangements, giving SCs **A**₁₁ to **A**₁₄. Two single rows of fluoroquinolone molecules, **B**₁₁ and **B**₁₂, were also identified. Each of these constructs are the basis of the 2- and 3-dimensional SCs detailed in Table 6.16.

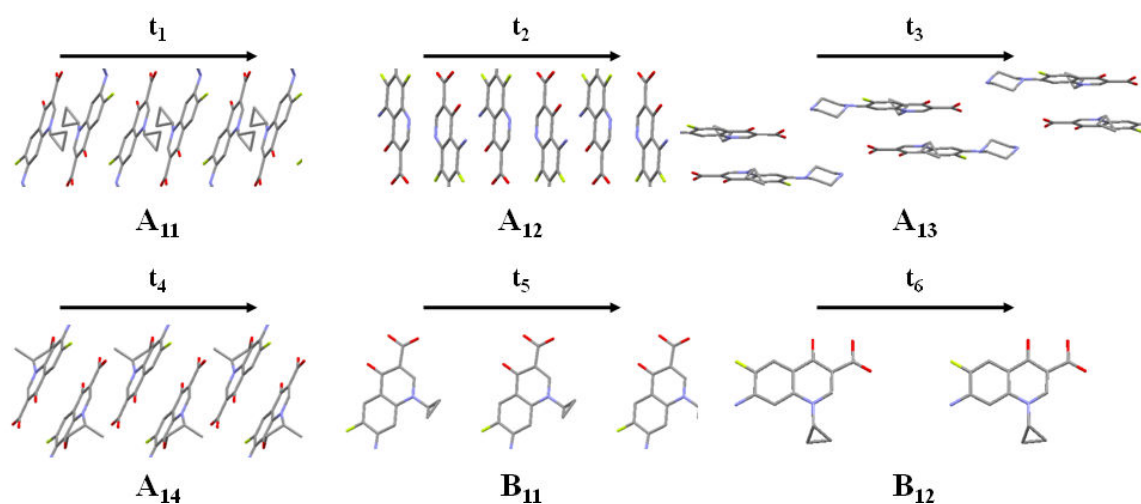


Figure 6.3 The six one-dimensional SCs identified in the fluoroquinolone structures. The directions of the translation vectors are indicated.

Table 6.16 Similarity relationships between the supramolecular constructs identified in the fluoroquinolone salt structures (D = dimensionality, # = number of structures).

SC	D	Description	Figs.	#	Base	Dependencies
A	0	Face-to-face pair of molecules	6.3	31	None	Primary SC
A ₁₁	1	Stack of molecules (translation)	6.4	14	t ₁	A → A ₁₁
A ₁₂	1	Stack of molecules (translation)	6.4	10	t ₂	A → A ₁₂
A ₁₃	1	Chain of molecules (translation)	6.4	2	t ₃	A → A ₁₃
A ₁₄	1	Stack of molecules (translation)	6.4	1*	t ₄	A → A ₁₄
B ₁₁	1	Row of molecules (translation)	6.4	7	t ₅	Primary SC
B ₁₂	1	Row of molecules (translation)	6.4	3	t ₆	Primary SC
A ₂₁	2	Layer of A ₁₁ stacks	6.7	2	t ₁ , t ₇	A ₁₁ → A ₂₁
A ₂₂	2	Layer of A ₁₁ stacks	6.8	4	t ₁ , t ₈	A ₁₁ → A ₂₂
A ₂₃	2	Layer of A ₁₁ stacks	6.9	4	t ₁ , t ₉	A ₁₁ → A ₂₂
A ₂₄	2	Layer of A ₁₁ stacks	6.9	5	t ₁ , t ₁₀	A ₁₁ → A ₂₂
B ₂₁	2	Layer of B ₁₂ rows	6.4	2	t ₆ , t ₁₁	B ₁₂ → B ₂₁
A ₃₁	3	Array of A ₁₁ stacks	6.8	2	t ₁ , t ₈ , t ₁₂	A ₂₂ → A ₃₁
A ₃₂	3	Array of A ₁₁ stacks	6.9	2	t ₁ , t ₉ , t ₁₀	A ₂₃ × A ₂₄ → A ₃₂

*Observed in two systems, one is not reported due to the poor quality of the data. It is included here to show the diversity in stacking arrangements of the A dimer.

The relationships between the 28 structures containing one or more of the SCs listed in Table 6.16 are shown in the Hasse diagram in Figure 6.4. It can be seen that all of the one-dimensional SCs based on A are mutually exclusive. 16 of the structures contain higher dimensionality SCs with the group of structures containing SC A₁₁ exhibiting the highest degrees of similarity.

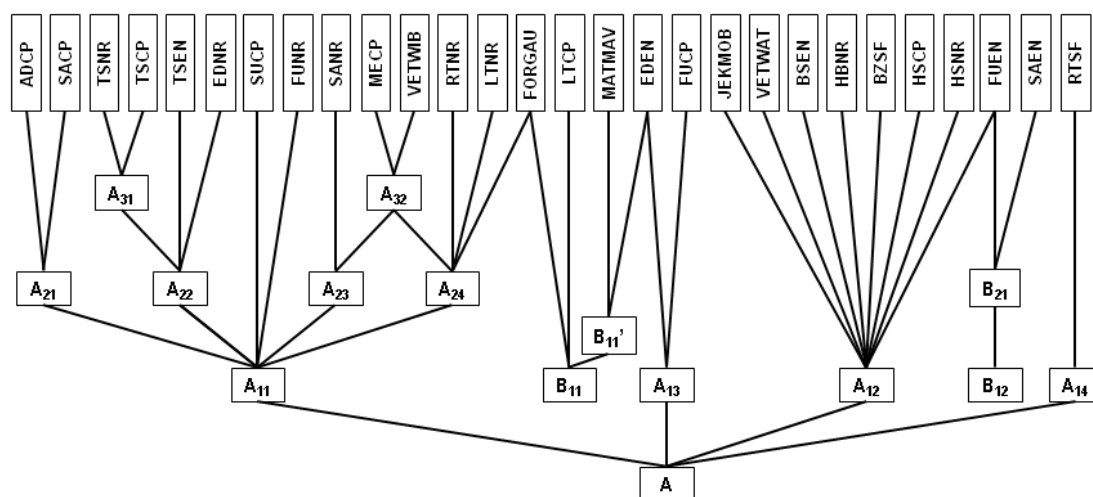


Figure 6.4 The relationships between the 18 structures with the SCs listed in Table 6.16. Novel structures are labelled according to their composition as described in Section 6.2 and published structures are denoted by their CSD reference codes.

6.7.2 Structures containing construct A_{11}

The eleven unique packing arrangements of SC A_{11} are shown in Figure 6.5. The constructs are viewed parallel to the t_1 translation vector of A_{11} with each pictured molecule representing a single stack.

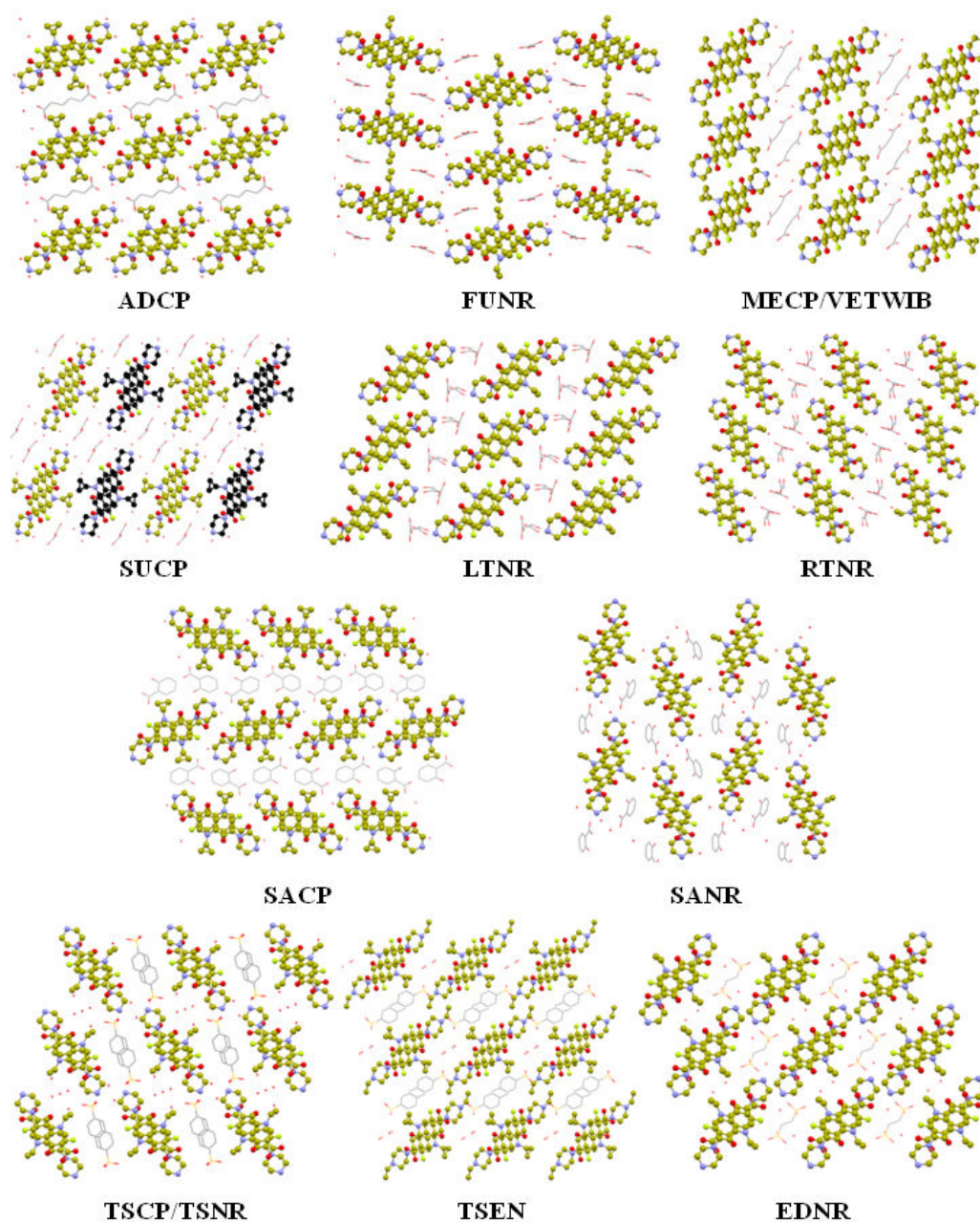


Figure 6.5 The 11 unique packing arrangements of SC A_{11} . Structures are viewed along the axis of the t_1 vector with the fluoroquinolone stacks viewed along t_1 coloured yellow and those viewed along $-t_1$ coloured black. Counterion molecules are shown as wireframes and the positions of the water molecules are indicated by the red spheres

Figure 6.5 illustrates the diversity in the 11 different packing arrangements that are adopted by the A_{11} stacks. The most common general arrangements are alternating layers of fluoroquinolone molecules and anions, observed in the dicarboxylic acid salts with the exceptions of FUNR and SUCP. These two salts are similar to the three sulfonic acid salts where channels of anions are surrounded by A_{11} stacks, however in contrast to the sulfonic acid salts the packing of the A_{11} stacks is unique. The third structure type is SANR with corrugated layers of A_{11} stacks and anion-water layers. As shown in Figure 6.5 this groups of structures includes four common two-dimensional arrangements of A_{11} stacks and two pseudoisomorphous arrays and these structures will be compared in detail.

6.7.2.1 Structures containing supramolecular construct A_{21}

In the salicylate and adipate salts of ciprofloxacin the A_{11} constructs stack along an axis perpendicular to the t_1 vector to give a two-dimensional construct A_{21} . The stacking arrangement of the sheets to form the three-dimensional structure differs in the two cases, in the salicylate salt the A_{11} constructs in neighbouring sheets lie along a 2_1 screw axis perpendicular to the plane of the sheet while in the adipate salt the sheets are related to each other through inversion centres. The two packing arrangements are compared in Figure 6.6.

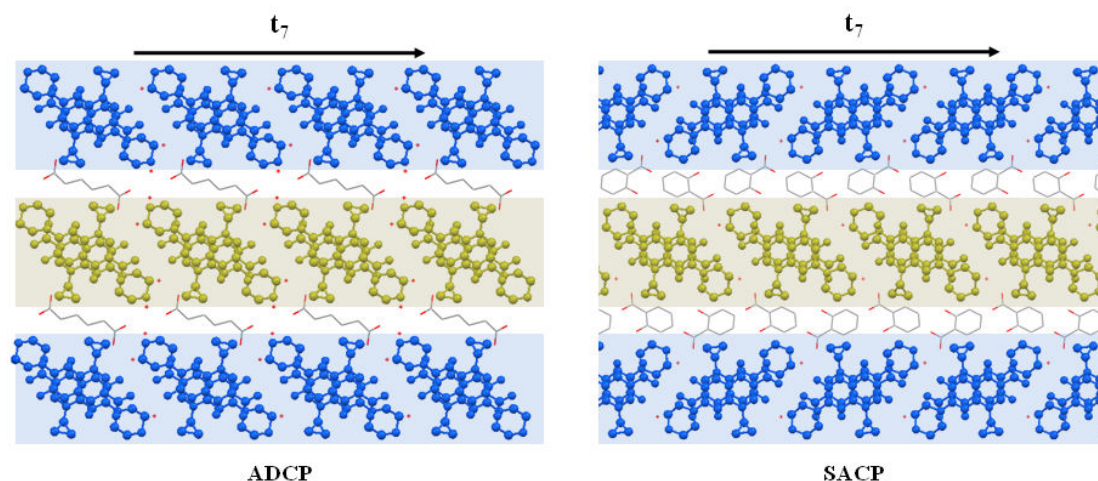


Figure 6.6 Comparison of the stacking of the two-dimensional A_{21} construct in ciprofloxacin adipate dihydrate (right) and ciprofloxacin salicylate monohydrate (left). Alternate A_{21} sheets are coloured blue and yellow and are viewed along the t_1 translation vector with each molecule representing an A_{11} stacks.

6.7.2.2 Structures containing supramolecular constructs A_{22} and A_{31}

In four salts common layers of A_{11} stacks form SC A_{22} as shown in Figure 6.7. In EDNR the formation of A_{22} is supported by a direct hydrogen bonded contact from the equatorial amine proton of the fluoroquinolone molecules in one A_{11} stack to the carboxylic acid groups of fluoroquinolones in the neighbouring stacks in the sheet. In TSCP and TSNR this contact is replaced by an amine- water- carboxylic acid contact and the A_{22} layers stack in a common arrangement to form the A_{31} array. The occurrence of A_{22} in TSEN is notable as the tertiary amine group lacks the requisite equatorial proton and there are no hydrogen bond contacts between the A_{11} stacks.

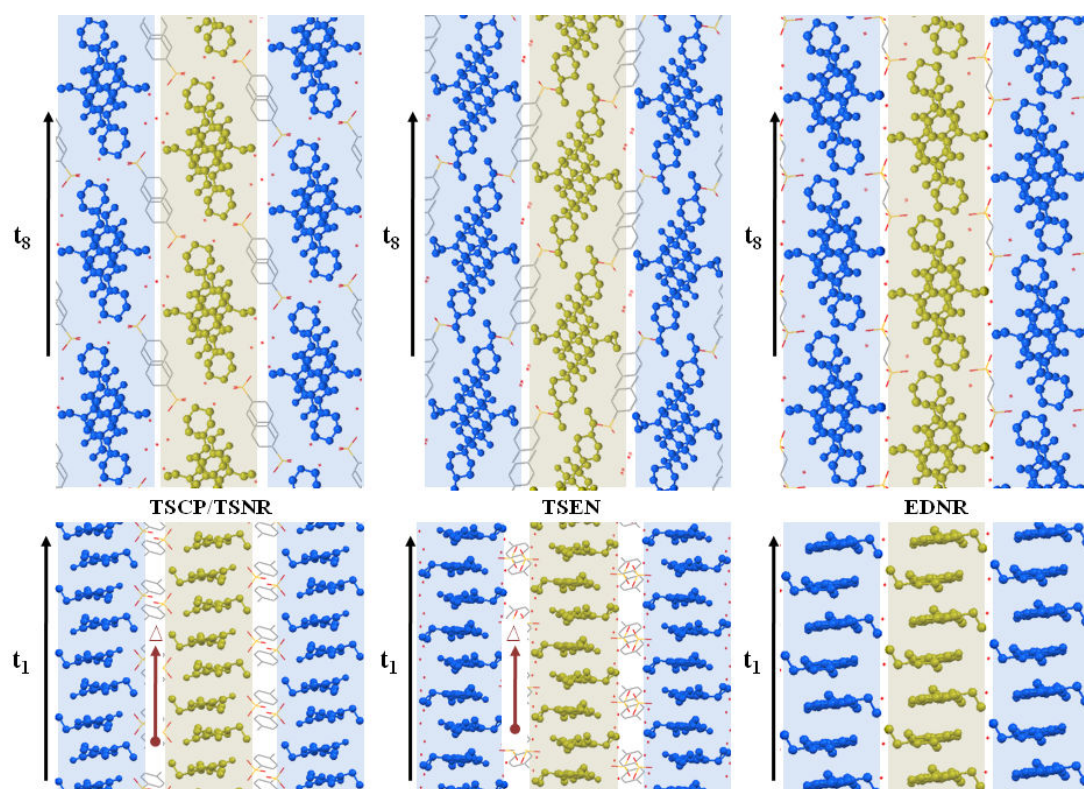


Figure 6.7 Comparison of the stacking of the two-dimensional A_{22} construct in the pseudoisomorphous TSCP and TSNR salts (left), TSEN (centre) and EDNR (right). Three constructs are shown in each structure (blue and yellow), viewed parallel to the t_1 (top) and t_8 (bottom) translation vectors. The most significant difference between the packing arrangements of the constructs in TSCP/NR and TSEN is the shift along the t_8 axis indicated by the red arrow. The packing arrangement of A_{22} in EDNR shifts along all three axes relative to the constructs in TSCP/NR and TSEN.

6.7.2.3 Structures containing supramolecular constructs A_{23} , A_{24} and A_{32}

The A_{11} stacks align along a second axis to give two different supramolecular constructs A_{23} and A_{24} . These were identified in three and six structures respectively, with the pseudoisostuctural MECP and VETWIB containing both to give the three-dimensional A_{32} array as shown in Figure 6.8. The stacking arrangement of the A_{11} constructs to give the A_{23} layers is determined by a common hydrogen bonded synthon, an R4,4(12) water-carboxylate ring with the fluoroquinolone molecules connecting to these rings via amine-water and amine-carboxylate contacts through the axial and equatorial hydrogen respectively. In contrast there are no extended hydrogen bond contacts along the t_{10} in FORGAU and MECP, indicating that the packing arrangement to form the A_{24} layers is not determined by hydrogen bonding connectivity.

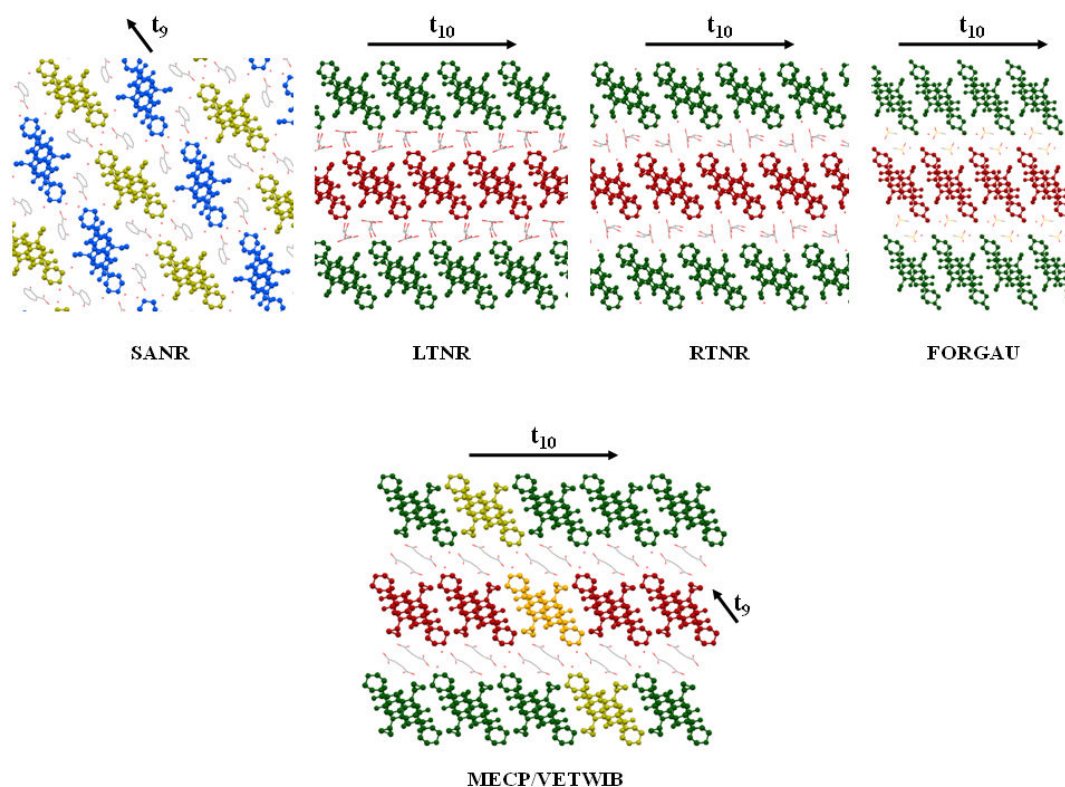


Figure 6.8 Packing arrangements of SCs A_{23} and A_{24} viewed along the t_1 vector of the A_{11} stacks. The second translation vectors in the two-dimensional constructs are shown by the arrows. In SANR alternating A_{23} layers are coloured gold and blue. In LTNR, RTNR and FORGAU the A_{24} layers, coloured red and green, differ in their relative positions along the t_{10} axis. The A_{32} array, shown by MECP, consists of A_{24} layers (green and red) aligned along the third axis by the A_{23} construct (gold).

6.7.3 Structures containing supramolecular construct A_{12}

The variety in the eleven unique packing arrangements of SC A_1 is shown in Figure 6.9. The constructs are viewed parallel to the t_1 translation vector of A_1 so that each molecule represents a single stack.

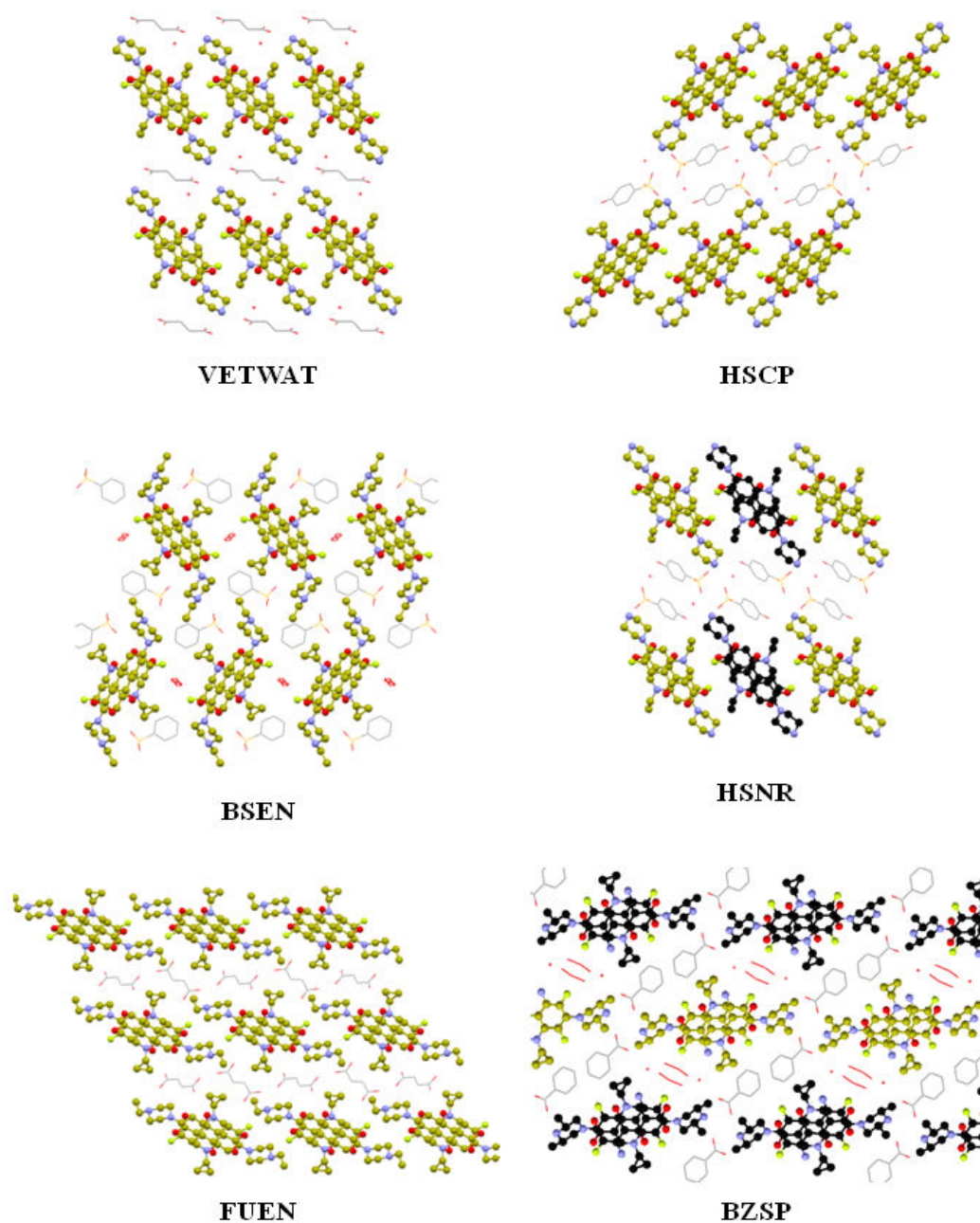


Figure 6.9 The six unique packing arrangements of SC A_{12} . Each structure is viewed along the axis of the t_1 vector with the fluoroquinolone molecules of stacks viewed along t_1 coloured yellow and those viewed along $-t_1$ coloured black.

The overall molecular arrangements of the structures containing construct \mathbf{A}_{12} are similar to those containing \mathbf{A}_{11} with examples of anion-water layers and channels. As can be seen in Figure 6.3 the difference between \mathbf{A}_{11} and \mathbf{A}_{12} is limited to the relative orientations of \mathbf{A} dimers along the axis of the stacks and it is arguable that these represent three conformations of the same construct. As a result the face-to-face stack of fluoroquinolone molecules can be considered to be the major structure-directing feature of this class of molecular salts.

6.7.4 Structures containing construct \mathbf{B}_{11}

Supramolecular construct \mathbf{B}_{11} , a one-dimensional row of fluoroquinolone molecules, was identified in the four structures as shown overleaf in Figure 6.10. **LTCP** is the unique example of a dicarboxylic acid salt in this group and the arrangement of the fluoroquinolone molecules along the t_5 axis to form the \mathbf{B}_{11} construct is a result of the amine-carboxylate contacts that form a C2,2(9) chain along this axis. In FORGAU and MATMAV there are no extended hydrogen bond contacts to align the molecules along the t_5 axis while in EDEN the contacts between these molecules are from water molecules to the hydroxyl and carboxylic acid groups of the fluoroquinolone rings. The lack of consistent hydrogen bonding connectivity indicates that this construct is not a result of directional interactions.

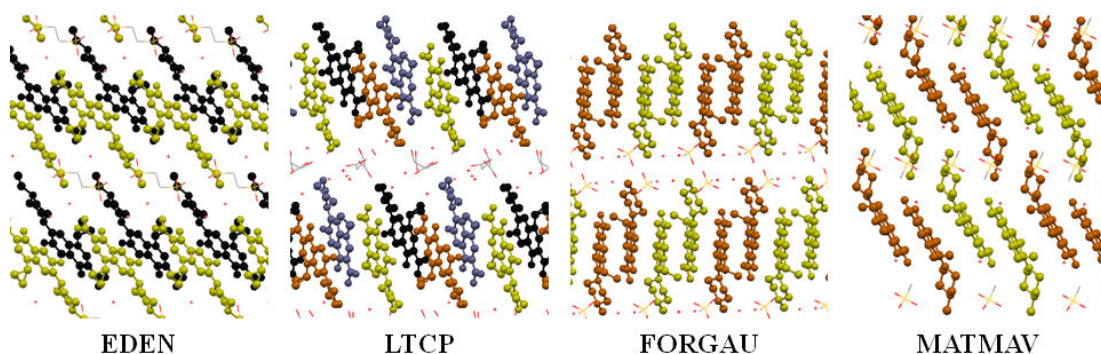


Figure 6.10 The four unique packing arrangements of construct \mathbf{B}_{11} . In each case the constructs are viewed along the axis of the t_5 vector so each molecule represents a single \mathbf{B}_{11} row. Constructs lying in the t_5 are coloured gold and dark gold and those lying in the $-t_5$ direction are coloured black and dark grey. In FORGAU and MATMAV the \mathbf{B}_{11} constructs are composed of rows of \mathbf{A} dimers instead of single molecules to form the \mathbf{B}_{11}' construct.

6.7.5 Structures containing construct B_{12}

Supramolecular construct B_{12} is a similar one-dimensional row of molecules to B_{11} that propagates approximately along the long axis of the fluoroquinolone molecules. It has been identified in the two structures shown in Figure 6.11. In both FUEN and SAEN face-to-face pairs of these constructs, similar to A , align along a second axis to produce the two-dimensional B_{21} sheet. In contrast to FUEN, there are no extended hydrogen bond motifs along any of the axes in SAEN, indicating that this construct is entirely independent of hydrogen bonding environment.

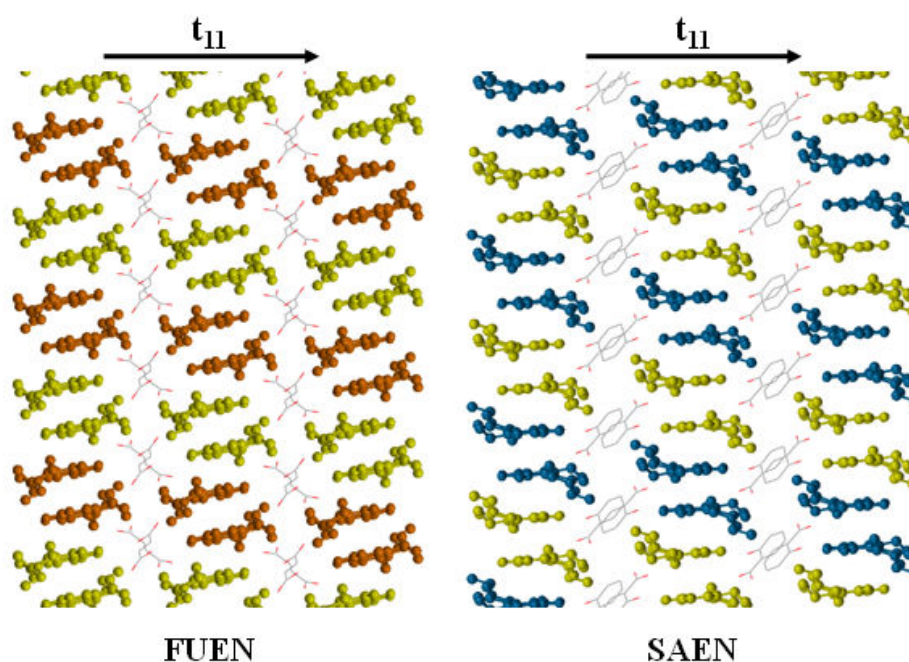


Figure 6.11 The packing arrangements of supramolecular construct B_{12} in FUEN (left) and SAEN (right). The constructs are viewed along the axis of the t_6 translation vector with each molecule representing a single B_{12} chain. In FUEN and SAEN double rows of B_{12} constructs pack along the axis of the t_{11} vector to produce the B_{21} layers. In FUEN these layers have a common orientation along the t_6 axis and are indicated by dark and light gold colouring while in SAEN the layers alternate with respect to their orientation along the t_6 axis and layers lying along t_6 are coloured gold and those lying along $-t_6$ are coloured blue..

6.7.6 Summary of the XPac analysis of the fluoroquinolone salts

The XPac analysis of the fluoroquinolone salts revealed a higher degree of structural similarity than in the model benzoic and benzenesulfonic acid salts examined in Chapter 4. It is notable that the additional hydrogen bonding potential introduced by the hydroxyl and carboxylic acid groups has not resulted in a concomitant increase in the diversity of the supramolecular structures. The near-ubiquity of the face-to-face **A** pairs of molecules; the similarity of the two most common one-dimensional SCs **A₁₁** and **A₁₂** and the general lack of correlation between hydrogen bond connectivity, hydration state and counterion identity with the SCs indicate that non-directional interactions and packing effects dominate the supramolecular structure that will be adopted by the salt. The identification of the **A₁₂** stack in the structure of anhydrous sparfloxacin, JEKMOB, is added evidence for a hypothesis that the dominant determinant of salt structure is the favourable packing of arrays of molecules determined by such non-directional interactions, rather than individual molecules, into hydrogen bonded networks.

6.8 Case example of the application of the structural rules

The anticipated outcome of the crystallisations of amoxapine with the three classes of counterion based on the structural rules was discussed in Chapter 4. The information developed in this chapter enables a qualitative re-assessment of these expectations based on the increased molecular size with amendments in italics.

(i) The probability of crystalline salt formation with all types of counterion shown in Figure 4.2 is > 70% and is the exclusive outcome when a crystalline product is formed in combination with a sulfonic acid counterion. For the dicarboxylic and benzoic acid counterions the formation of other crystalline products including mixed systems and cocrystals is also possible. *No significant amendments required.*

(ii) Cocrystallisation with a dicarboxylic acid can be expected to result in the hydrogen acid salt with a one-dimensional hydrogen bonded structure based on the C1,1(7/9) hydrogen bonded chain of acid molecules. If the acid counterion has hydroxyl groups additional contacts between the acid molecules may be formed but

the overall intermolecular hydrogen bond connectivity can be expected to be one-dimensional. *The increased molecular size may make the satisfaction of the hydrogen bond donor and acceptor potentials by the salt formers impossible due to steric interference. The possibility of hydrate formation will consequently increase unless additional hydrogen bond donor and acceptor groups are available. In the case of the acid counterion the potential axis of these contacts must be perpendicular to the main hydrogen bonding motif. Because the single anhydrous fluoroquinolone salt was formed with tartaric acid this type of counterion is recommended.*

(iii) Cocrystallisation with a benzoic acid is equally likely to result in formation of a single direct amine-carboxylate interaction or an R4,4(12) motif as observed for the structures containing 4-phenylpiperazine. If the acid counterion incorporates a *para*-hydroxyl group then a C1,1(8) hydrogen bonded acid chain can be expected. *The C1,1(8) anion chain is unlikely to form in these systems due to its incompatibility with the steric bulk of the amoxapine molecules. Similarly to (ii) the formation of hydrates is highly probable.*

(iv) Cocrystallisation with a sulfonic acid will result in the formation of a salt based on the C2,2(6) amine-sulfonate chain with additional amine-sulfonate contacts propagating the hydrogen bonded structure along a second axis. When the acid counterion possesses a *para*-hydroxyl group a C1,1(8) hydrogen bonded acid chain will be formed. *The greater molecular size of the pharmaceutical molecule relative to the acid counterion makes the formation of the C1,1(8) chains in (iii) and (iv) unlikely. A more likely consequence of the use of these counterions is the formation of a hydrate to satisfy the hydrogen bonding potential of the 4-hydroxyl group. In this case the use of counterions possessing such a group is not recommended.*

Due to the established inconsistency of the guidelines for hydrate formation in Chapter 5 with the fluoroquinolone salts the expectation for salts of amoxapine is that hydrate formation should be considered a likely outcome with all three classes of counterion. It is most probable that the water molecules will form acid-water layers in the structure or fill voids to give channel hydrates.

Novel hydrogen fumarate and benzoate salts of amoxapine were crystallised and their structures can be compared with the outcomes expected from the structural rules. The paucity of amoxapine structures deposited on the CSD prevented the identification of common molecular packing arrangements that could be used as a guide to the probable packing arrangement of the molecules in the salts. Both salts crystallised as hydrates and both featured direct amine-carboxylate contacts as expected from the structural rules. The benzoate salt consisted of acid-base pairs linked by D1 contacts with the second carboxylate oxygen and amine proton interacting with water molecules. This outcome is consistent with the expectations given in (ii) above.

The fumaric acid cocrystallisation yielded the hydrogen fumarate salt as expected from (i), however this did not feature the expected C1,1(8) hydrogen acid chain. Instead, acid-base pairs linked by a D1 contact were linked via waters to form a one-dimensional hydrogen bonded structure.

6.9 Summary

In this chapter, the structural rules derived in Chapter 4 and the guidelines for hydrate formation established in Chapter 5 were applied to a library of 32 multi-component systems containing fluoroquinolone antibiotics. The structures characterised were broadly consistent with those expected from the guidelines in Chapter 4 with respect to the major hydrogen bonding motif established for salts of each class of counterion, however several hydrogen bonding motifs observed with high frequency in the model salts were absent from the fluoroquinolone salt structures. In contrast, the hydrate guidelines established in Chapter 5 proved to be of little use in anticipating hydrate formation.

In both these cases the deviations from the structures anticipated on the basis of the Chapter 4 and 5 guidelines can arguably be anticipated *a priori* by due consideration of the molecular properties of the fluoroquinolone molecules and the supramolecular structural features of the crystalline “native” structures of the molecules in question. For instance, formation of the C2,2(12) acid-base chain with the dicarboxylic acid molecules is precluded by the low pK_a of the second piperazinyl nitrogen. The steric

width of the quinolone ring moiety precludes concurrent formation of the C1,1(8) hydrogen acid chain and C2,2(6) amine-carboxylate chain as the two axes of the motifs must be perpendicular and cannot be accommodated in the structure. Similarly, the increased number of hydrogen bonding groups on the fluoroquinolone molecule and the reduction in possible packing arrangements because of the increased molecular size appears to be the primary drivers of the increased probability of hydrate formation.

The analysis of the structures using the XPac method allowed a qualitative assessment of the relative importance of directional and non-directional interactions in determining the supramolecular structure. It was frequently demonstrated that common supramolecular arrangements were not dependent on either counterion identity, hydrogen-bonding interactions or hydration state and the identification of a robust supramolecular construct can give a reliable basis for an assessment of the likely supramolecular structure. Therefore the structural rules established in Chapter 4 must be applied with due consideration of their compatibility with these factors.

Chapter 7

Conclusions and further work

7.1 Conclusions

In this study 102 novel salts, one co-crystal and eight mixed salt/co-crystal systems were prepared and characterised for a library of 18 pharmaceutically acceptable organic acid salt formers by cocrystallisation with eight simple model bases. In combination with eight published salts, a systematic examination of the supramolecular structural features of the structures was performed using Mercury and XPac. Systems formed with similar types of counterion (dicarboxylic, benzoic or monosulfonic acids) were found to exhibit recurrent hydrogen bonding motifs and these observations were used to derive structural rules specific to each type of counterion. These rules give a probabilistic guide to the most likely supramolecular structural features that will be observed upon crystallisation of a novel pharmaceutical molecule containing either a secondary or tertiary amine base with these counterions.

Although the crystallisation of a multi-component system was a more likely outcome for dicarboxylic and benzoic acids than sulfonic acids the likelihood of salt formation was shown to be approximately equal for the three types of counterion. The products of the cocrystallisation of monosulfonic acids with the simple model bases were exclusively salts whereas the carboxylic acid systems displayed a higher incidence of crystallisation but with cocrystals, mixed systems and the recrystallisation of the acid being possible outcomes. In common with previous studies on multi-component systems containing these types of counterion (Callear, *et al.*, 2010, Mohamed, *et al.*, 2009b) the pKa differences between the components was found to be unreliable in predicting the ionisation state of the crystalline products, even in systems where $\Delta \text{pKa} > 3$.

Examination of the hydrogen bond motifs in the dicarboxylic acid systems showed that the structures can be grouped into two major families based on the most common one-dimensional hydrogen bond motifs, namely hydrogen acid salts containing a hydrogen bonded anion chain and acid salts containing a C2,2(12) cation-anion chain. These structures are observed for both secondary and tertiary amine salts with the C2,2(12) motif being the most likely for salts of dinitrogen bases. The other acid-base motifs appear to play a secondary role in determining the

structure, while the interactions involving hydroxyl groups do not appear to have a structure-directing role.

The structures of the monoacid salts differ in that the major structure-directing motifs appear to be the acid-base contacts. Here there is an obvious difference from the dicarboxylic acid salts in that the type of amine group on the base is a key determinant of the hydrogen bonded structure adopted whereas the acid-acid motif, here limited to the C1,1(8) anion chain, is secondary. There is a high degree of commonality between the structural types adopted by the sulfonic and benzoic acid salts as the two most common structural types in each case were based on the D1 and C2,2(6) amine-carboxylate motifs.

These outcomes indicate that the ionisation states of the crystalline systems are at least partly determined by the proton transfer required to support the formation of one of the preferred hydrogen bonding motifs. Salt formation is a more reliable outcome for secondary amine bases as protonation gives them the ability to donate hydrogen bonds to at least two other molecules, enabling the formation of an extended hydrogen-bonding motif. Tertiary monoamine bases cannot donate sufficient hydrogen bonds to stabilise an extended motif with monoacid counterions, requiring the incorporation of neutral acid molecule to satisfy the hydrogen-bonding requirement of the anion. The use of counterions with additional hydrogen bonding groups allowing the formation of extended structures can fulfil this requirement and allow the crystallisation of salts.

In addition to robust hydrogen bonding motifs non-directional interactions were shown to be an important determinant of supramolecular structure. Analysis of the benzoic and benzenesulfonic acid counterions using XPac identified several supramolecular constructs that indicate similar non-directional interactions in these cases. Interestingly, there was little correlation between the formation of particular hydrogen-bonding motifs and supramolecular constructs in these structures. This emphasises the importance of a holistic approach to the assessment of probable supramolecular structures for a given system as opposed to focusing on a single type of interaction.

The database of model systems also provided a resource for a highly systematic examination of the relative probabilities of hydrate formation for secondary and tertiary amine salts of the different counterions. There was no demonstrable correlation between either the number of hydrogen bonding groups present on the molecules or the ratio of donors to acceptors and the likelihood of hydrate formation. The hydrogen-bonded motifs formed by contacts to water were inherently unpredictable for the acid-base combinations examined with the exception of the sulfonate salts in which a C2,2(6) water-sulfonate chain was the sole motif observed.

The use of VT-XRPD in combination with SDPD proved to be a useful and informative for the investigation of the factors influencing hydrate structure. The generation and characterisation of the anhydrous phases of salts that had crystallised as hydrates revealed that the incorporation of water molecules appears to be driven by the stabilisation of a favourable packing arrangement that cannot be maintained if the acid and base components are required to satisfy their own hydrogen bonding requirements. The degree of structural rearrangement appeared to be linked to the number and dimensionality of robust hydrogen bonding synthons observed in the hydrate structure. In cases where the majority of synthons expected for the anhydrate were observed in the hydrate the rearrangements in structure were relatively minor.

The 32 novel salts of fluoroquinolone molecules crystallised to provide a validation set of structures exhibited considerable deviation from the structures expected from the application of the structural rules and hydrate guidelines. These deviations were most common when the expected motif was either chemically impossible due to the relative pKas of the ionisable groups on the molecules or the incompatibility of the motifs with the steric bulk of the molecules. As such, it can be argued that the structural rules do give a useful estimation of the probabilities of formation of the structural features provided that due consideration is given to the molecular structure and properties of the pharmaceutical.

7.2 Further Work

An obvious area of further investigation is the completion of the “missing” structures in the database of model systems. Of particular interest is the exploration of other crystallisation methods and conditions, including the use of different solvent systems and temperatures using the automated screening methods developed for the systematic crystallisation of organic systems (Florence, *et al.*, 2006). This would not only enable an assessment of the robustness of the structural features observed in the systems crystallised from water but also the factors preventing the crystallisation of the “missing” systems from aqueous solutions. A detailed assessment of the physical properties to develop comprehensive information regarding aqueous solubility, melting point and hygroscopicity would provide additional information of interest to pharmaceutical salt selection.

Likewise, the number of model hydrate/anhydrate pairs should also be increased with variable temperature X-ray powder diffraction and structure determination from powder diffraction data. A study of this type on the fluoroquinolone salts may also yield valuable information on the structural effects of hydration in systems with complex molecules.

The use of the pK_{HB} scale developed by Taft *et al* (Joris, *et al.*, 1972) to predict the preferred hydrogen bonding site in drug molecules has been demonstrated by Laurence and Berthold (Laurence, *et al.*, 2009). As they demonstrated, the lack of a direct correlation between pK_{HB} and pK_a the extension and application of the pK_{HB} scale to the systems studied in this work may provide additional insights into salt and cocrystal formation in the carboxylic acid systems.

Both the Materials Module of the Mercury CSD program and XPac have demonstrated their utility and mutually complementary nature in the examination of the supramolecular structural features of organic salt systems. The use of Crystal Explorer to assess the total interaction environments of molecules in the crystal structures was not examined in sufficient detail to warrant inclusion in this work. However, the combination of Hirschfeld surface analysis with the multivariate data analysis program PolySNAP to undertake “structural genetic fingerprinting” (Parkin,

et al., 2007) offers an alternative methodology for the assessment of similarities between the structures and should be explored as a complementary technique to the methods employed in this thesis.

The application of new analysis techniques to the data generated by the crystallisation of large libraries of systems offers a potential tool for identifying correlations between molecular properties, crystallisation conditions and experimental outcomes. Random forest classification of solvent properties, crystallisation conditions and experimental outcomes was successfully employed to target the crystallisation of three novel solvates of the antipsychotic drug carbamazepine (Johnston, *et al.*, 2008). Similar methodologies have also been applied to the crystallisation of novel polymorphs of this compound and allow the optimisation of crystallisation experiments to produce a desired outcome (McCabe, 2010). The use of the CASTEP program to generate of atomic-level descriptions of the component molecules in the crystallisation experiments using density functional theory (Clark, *et al.*, 2005) may enable a clearer correlation between the molecular properties and supramolecular structures of the systems examined in this work.

References

- Aakeroy, C. B., Beatty, A. M., Helfrich, B. A. and Nieuwenhuyzen, M. (2003). Do polymorphic compounds make good cocrystallizing agents? A structural case study that demonstrates the importance of synthon flexibility. *Crystal Growth and Design*, **3**, 159-165.
- Aakeroy, C. B., Desper, J., Helfrich, B. A., Metrangolo, P., Pilati, T., Resnati G. and Stevenazzi, A. (2007a). Combining halogen bonds and hydrogen bonds in the modular assembly of heteromeric infinite 1-D chains. *Chemical Communications*, 4236-4238.
- Aakeroy, C. B., Desper, J. and Scott, B. M. T. (2006). Balancing supramolecular reagents for reliable formation of co-crystals. *Chemical Communications*, 1445-1447.
- Aakeroy, C. B., Fasulo M. E., and Desper, J. (2007b). Cocrystal or salt: does it really matter? *Molecular Pharmaceutics*, **4**, 317-322.
- Aakeroy, C. B., Hitchcock, P. B. and Seddon, K. R. (1992). Organic Salts Of L-Tartaric Acid - Materials For 2nd Harmonic-Generation With A Crystal-Structure Governed By An Anionic Hydrogen-Bonded Network. *Journal Of The Chemical Society-Chemical Communications*, 553-555.
- Aakeroy, C. B. and Nieuwenhuyzen, M. (1996). Hydrogen bonding and structural motifs in organic L-malate(2-) salts. *Chemistry of Materials*, **8**, 1229-1235.
- Aakeroy, C. B. and Salmon, D. J. (2005). Building co-crystals with molecular sense and supramolecular sensibility. *CrystEngComm*, **7**, 439-448.
- Abdul, S. and Poddar, S. S. (2004). A flexible technology for modified release of drugs: multi layered tablets. *Journal of Controlled Release*, **97**, 393-405.
- Agharkar, S., Lindenbaum, S. and Higuchi, T. (1976). Enhancement of solubility of drug salts by hydrophilic counterions - properties of organic salts of an antimalarial drug. *Journal of Pharmaceutical Sciences*, **65**, 747-749.
- Allen, F. H. (2002). The Cambridge Structural Database: a quarter of a million crystal structures and rising. *Acta Crystallographica Section B-Structural Science*, **58**, 380-388.
- Allen, F. H. and Motherwell W. D. S. (2002). Applications of the Cambridge Structural Database in organic chemistry and crystal chemistry. *Acta Crystallographica Section B-Structural Science*, **58**, 407-422.
- Allen, F. H., Motherwell, W. D. S., Raithby, P. R., Shields, G. P. and Taylor, R. (1999). Systematic analysis of the probabilities of formation of bimolecular hydrogen-bonded ring motifs in organic crystal structures. *New Journal of Chemistry*, **23**, 25-34.
- Almarsson, O. and Zaworotko, M. J. (2004). Crystal engineering of the composition of pharmaceutical phases. Do pharmaceutical co-crystals represent a new path to improved medicines? *Chemical Communications*, 1889-1896.
- Altomare, A., Cascarano, G., Giacovazzo, C. and Guagliardi, A. (1993). Completion and refinement of crystal structures with SIR92. *Journal of Applied Crystallography*, **26**, 343-350.

- Amidon, G. L., Lennernas, H., Shah, V. P. and Crison, J. R. (1995). A theoretical basis for a biopharmaceutical drug classification - the correlation of in-vitro drug product dissolution and in-vivo bioavailability. *Pharmaceutical Research*, **12**, 413-420.
- Andre, V., Braga, D., Grepioni, F. and Duarte, M. T. (2009). Crystal Forms of the Antibiotic 4-Aminosalicylic Acid: Solvates and Molecular Salts with Dioxane, Morpholine, and Piperazine. *Crystal Growth and Design*, **9**, 5108-5116.
- Apperley, D. C., Basford, P. A., Dallman, C. I., Harris, R. K., Kinns, M., Marshall, P. V. and Swanson, A. G. (2005). Nuclear magnetic resonance investigation of the interaction of water vapor with sildenafil citrate in the solid state. *Journal of Pharmaceutical Sciences*, **94**, 516-523.
- Authelin, J. R. (2005). Thermodynamics of non-stoichiometric pharmaceutical hydrates. *International Journal of Pharmaceutics*, **303**, 37-53.
- Banerjee, R., Bhatt, P. M., Ravindra, N. V. and Desiraju, G. R. (2005). Saccharin salts of active pharmaceutical ingredients, their crystal structures, and increased water solubilities. *Crystal Growth and Design*, **5**, 2299-2309.
- Barr, G., Dong, W. and Gilmore, C. J. (2004). PolySNAP: a computer program for analysing high-throughput powder diffraction data. *Journal of Applied Crystallography*, **37**, 658-664.
- Basavoju, S., Bostrom, D. and Velaga, S. P. (2006). Pharmaceutical cocrystal and salts of norfloxacin. *Crystal Growth and Design*, **6**, 2699-2708.
- Bastin, R. J., Bowker, M. J. and Slater, B. J. (2000). Salt selection and optimisation procedures for pharmaceutical new chemical entities. *Organic Process Research and Development*, **4**, 427-435.
- Bauer, J., Spanton, S., Henry, R., Quick, J., Dziki, W., Porter, W. and Morris, J. (2001). Ritonavir: An extraordinary example of conformational polymorphism. *Pharmaceutical Research*, **18**, 859-866.
- Berge, S. M., Bighley, L. D. and Monkhouse, D. C. (1977). Pharmaceutical salts. *Journal of Pharmaceutical Sciences*, **66**, 1-19.
- Bernstein, J. (2005). Cultivating crystal forms. *Chemical Communications*, 5007-5012.
- Bettinetti, G., Mura, P., Sorrenti, M., Faucci, M. T. and Negri, A. (1999). Physical characterization of picotamide monohydrate and anhydrous picotamide. *Journal of Pharmaceutical Sciences*, **88**, 1133-1139.
- Black, S., Collier, E., Davey, R. and Roberts, R. (2007). Structure, solubility, screening, and synthesis of molecular salts. *Journal of Pharmaceutical Sciences*, **96**, 1053-1068.
- Bond, A. D. (2007). What is a co-crystal? *CrystEngComm*, **9**, 833-834.
- Boultif, A. and Louer D. (2004). Powder pattern indexing with the dichotomy method. *Journal of Applied Crystallography*, **37**, 724-731.

- Braga, D., L. Maini, G. de Sanctis, K. Rubini, F. Grepioni, M. R. Chierotti and R. Gobetto (2003). Mechanochemical preparation of hydrogen-bonded adducts between the diamine 1,4-diazabicyclo 2.2.2 octane and dicarboxylic acids of variable chain length: An X-ray diffraction and solid-state NMR study. *Chemistry-A European Journal*, **9**, 5538-5548.
- Braun, D. E., Gelbrich, T., Jetti, R. K. R., Kahlenberg, V., Price, S. L. and Griesser, U. J. (2008a). Colored polymorphs: thermochemical and structural features of N-picryl-p-toluidine polymorphs and solvates. *Crystal Growth and Design*, **8**, 1977-1989.
- Braun, D. E., Gelbrich, T., Kahlenberg, V., Laus, G., Wieser, J. and Griesser U. J. (2008b). Packing polymorphism of a conformationally flexible molecule (aprepitant). *New Journal of Chemistry*, **32**, 1677-1685.
- Braun, D. E., Gelbrich, T., Kahlenberg, V., Tessadri, R., Wieser, J. and Griesser U. J. (2009). Stability of solvates and packing systematics of nine crystal forms of the antipsychotic drug aripiprazole. *Crystal Growth and Design*, **9**, 1054-1065.
- Brock, C. P. and Dunitz J. D. (1994). Towards a grammar of crystal packing. *Chemistry of Materials*, **6**, 1118-1127.
- Bruker (2007). APEX2 and SADABS, Bruker AXS Inc., Madison, Wisconsin, USA.
- Bruno, I. J., Cole, J. C., Edgington, P. R., Kessler, M., Macrae, C. F., McCabe, P., Pearson, J. and Taylor R. (2002). New software for searching the Cambridge Structural Database and visualizing crystal structures. *Acta Crystallographica Section B-Structural Science*, **58**, 389-397.
- Bruno, I. J., Cole, J. C., Kessler, M., Luo, J., Motherwell, W. D. S., Purkis, L. H., Smith, B. R., Taylor, R., Cooper, R. I., Harris, S. E. and Orpen A. G. (2004). Retrieval of crystallographically-derived molecular geometry information. *Journal of Chemical Information and Computer Sciences*, **44**, 2133-2144.
- Bucar, D. K., Henry, R. F., Lou, X. C., Duerst, R. W., MacGillivray, L. R. and Zhang, G. G. Z. (2009). Cocrystals of caffeine and hydroxybenzoic acids composed of multiple supramolecular heterosynthons: screening via solution-mediated phase transformation and structural characterization. *Crystal Growth and Design*, **9**, 1932-1943.
- Byrn, S. R. and Lin, C. T. (1976). Effect of crystal packing and defects on desolvation of hydrate crystals of caffeine L-(-)-1,4-cyclohexadiene-1-alanine. *Journal of the American Chemical Society*, **98**, 4004-4005.
- Byrn, S. R., Pfeiffer, R. R., Stephenson, G., Grant, D. J. W. and Gleason, W. B. (1994). Solid-state pharmaceutical chemistry. *Chemistry of Materials*, **6**, 1148-1158.
- Callar, S. K., Hursthouse, M. B. and Threlfall, T. L. (2010). A systematic study of the crystallisation products of a series of dicarboxylic acids with imidazole derivatives. *CrystEngComm*, **12**, 898-908.
- Carstensen, J. T., Attarchi, F. and Hou, X. P. (1985). Decomposition of aspirin in the solid-state in the presence of limited amounts of moisture. *Journal of Pharmaceutical Sciences*, **74**, 741-745.

- Cernik, R. J., Clegg, W., Catlow, Bushnell, C. R. A., Wye, G., Flaherty, J. V., Greaves, G. N., Burrows, I., Taylor, D. J., Teat S. J. and Hamichi, M. (1997.) A new high-flux chemical and materials crystallography station at the SRS Daresbury .1. Design, construction and test results. *Journal of Synchrotron Radiation*, **4**, 279-286.
- Chen, L. R., Young, V. G., Lechuga-Ballesteros, D. and Grant, D. J. W. (1999). Solid state behavior of cromolyn sodium hydrates. *Journal of Pharmaceutical Sciences*, **88**, 1191-1200.
- Chertanova, L. and Pascard, C. (1996). Statistical analysis of noncovalent interactions of anion groups in crystal structures .1. Hydrogen bonding of sulfate anions. *Acta Crystallographica Section B-Structural Science*, **52**, 677-684.
- Childs, S. L., Wood, P. A., Rodriguez-Hornedo, N., Reddy, L. S. and Hardcastle, K. I. (2009). Analysis of 50 Crystal Structures Containing Carbamazepine Using the Materials Module of Mercury CSD. *Crystal Growth and Design*, **9**, 1869-1888.
- Chisholm, J., Pidcock, E., Van De Streek, J., Infantes, L., Motherwell, S. and Allen, F. H. (2006). Knowledge-based approaches to crystal design. *CrystEngComm*, **8**, 11-28.
- Chisholm, J. A. and Motherwell, S. (2005). COMPACK: a program for identifying crystal structure similarity using distances. *Journal of Applied Crystallography*, **38**, 228-231.
- Clark, S. J., Segall, M. D., Pickard, C. J., Hasnip, P. J., Probert, M. J., Refson, K. and Payne, M. C. (2005). First principles methods using CASTEP. *Zeitschrift Fur Kristallographie*, **220**, 567-570.
- Clarke, H. D., Arora, K. K., Bass, H., Kavuru, P., Ong, T. T., Pujari, T., Wojtas, L. and Zaworotko, M. J. (2010). Structure-stability relationships in cocrystal hydrates: does the promiscuity of water make crystalline hydrates the nemesis of crystal engineering? *Crystal Growth and Design*, **10**, 2152-2167.
- Clegg, W. (2000). Synchrotron chemical crystallography. *Journal of the Chemical Society-Dalton Transactions*, 3223-3232.
- Coelho, A. A. (2006). TOPAS user manual version 4.1, Bruker AXS GmbH, Karlsruhe, Germany..
- Collier, E., R. Davey, S. Black and R. Roberts (2006). 17 salts of ephedrine: crystal structures and packing analysis. *Acta Crystallographica Section B-Structural Science*, **62**, 498-505.
- Cosulich, D. B. and Lovell, F. M. (1977). X-ray crystal structures of loxapine (2-chloro-11-(4-methyl-1-piperazinyl)dibenz-1,4-oxazepine) and amoxapine (2-chloro-11-(1-piperazinyl)bibenz-1,4-oxazepine. *Acta Crystallographica Section B-Structural Science*, **33**, 1147-1154.
- Davey, R., Allen, K., Blagden, N., Cross, W., Lieberman, H., Quayle, M., Righini, S., Seton, L. and Tiddy, G. (2002). Crystal engineering - nucleation, the key step. *CrystEngComm*, 257-264.

- David, W. I. F., Shankland, K. and Shankland, N. (1998). Routine determination of molecular crystal structures from powder diffraction data. *Chemical Communications*, 931-932.
- David, W. I. F., Shankland, K., van de Streek, J., Pidcock, E., Motherwell, W. D. S. and Cole, J. C. (2006). DASH: a program for crystal structure determination from powder diffraction data. *Journal of Applied Crystallography*, **39**, 910-915.
- Davies, G. (2001). Changing the salt, changing the drug. *The Pharmaceutical Journal*, **226**, 322.
- Desiraju, G. R. (1989). *Crystal Engineering- The Design of Organic Solids*. Amsterdam: Elsevier.
- Desiraju, G. R. (1991). Hydration in organic crystals- prediction from molecular structure. *Journal of the Chemical Society-Chemical Communications*, 426-428.
- Desiraju, G. R. (2005). Chemistry - The middle kingdom. *Current Science*, **88**, 374-380.
- Desiraju, G. R. (2007). Crystal engineering: A holistic view. *Angewandte Chemie-International Edition*, **46**, 8342-8356.
- Desiraju, G. R. and Parthasarathy, R. (1989). The nature of halogen ... halogen interactions - are short halogen contacts due to specific attractive forces or due to close packing of nonspherical atoms. *Journal of the American Chemical Society*, **111**, 8725-8726.
- Donohue, J. (1952). Hydrogen Bond in Organic Crystals. *The Journal of Physical Chemistry*, **56**, 502-510.
- Du, M., Zhang, Z. H. Zhao, X. J. and Cai, H. (2006). Synthons competition/prediction in cocrystallization of flexible dicarboxylic acids with bent dipyrindines. *Crystal Growth and Design*, **6**, 114-121.
- Dunitz, J. D. (1991). Phase transitions in molecular crystals from a chemical viewpoint. *Pure and Applied Chemistry*, **63**, 177-185.
- Dunitz, J. D. (2003). Crystal and co-crystal: a second opinion. *CrystEngComm*, **5**, 506-506.
- Etter, M. C. (1982). A new role for hydrogen-bond acceptors in influencing packing patterns of carboxylic acids and amides. *Journal of the American Chemical Society*, **104**, 1095-1096.
- Etter, M. C. (1990). Encoding and decoding the hydrogen-bond patterns of organic compounds. *Accounts of Chemical Research*, **23**, 120-126.
- Etter, M. C. (1991). Hydrogen-bonds as design elements in organic chemistry. *Journal of Physical Chemistry*, **95**, 4601-4610.
- Fabbiani, F. P. A., Dittrich, B., Florence, A. J., Gelbrich, T., Hursthouse, M. B., Kuhs, W. F., Shankland, N. and Sowa, H. (2009). Crystal structures with a challenge: high-pressure crystallisation of ciprofloxacin sodium salts and their recovery to ambient pressure. *CrystEngComm*, **11**, 1396-1406.

- Farrell, D. M. M., Ferguson, G., Lough, A. J. and Glidewell, C. (2002). Chiral versus racemic building blocks in supramolecular chemistry: tartrate salts of organic diamines. *Acta Crystallographica Section B: Structural Science*, **B58**, 272-288.
- Farrigua, L. J. (1999). WinGX suite for small molecule single-crystal crystallography. *Journal of Applied Crystallography*, **32**, 837-838.
- FDA. (2007). <http://vm.cfsan.fda.gov/~dms/eafus.html>, FDA/CFSAN/OPA: Inventory of GRAS Notices, summary of all GRAS notices. United States Food and Drug Administration.
- Fick, A. (1855). V: On liquid diffusion. *Philosophical Magazine*, **10**, 30-39.
- Fleischman, S. G., Kuduva, S. S., McMahon, J. A., Moulton, B., Walsh, R. D. B., Rodriguez-Hornedo, N. and Zaworotko, M. J. (2003). Crystal engineering of the composition of pharmaceutical phases: Multiple-component crystalline solids involving carbamazepine. *Crystal Growth and Design*, **3**, 909-919.
- Florence, A. J., Johnston, A., Fernandes, P., Shankland, N. and Shankland, K. (2006). An automated platform for parallel crystallization of small organic molecules. *Journal of Applied Crystallography*, **39**, 922-924.
- Florence, A. J., Kennedy, A. R., Shankland, N., Wright, E. and Al-Rubayi, A. (2000). Norfloxacin dihydrate. *Acta Crystallographica Section C-Crystal Structure Communications*, **56**, 1372-1373.
- Florence, A. T. and Attwood, D. (2006). *Physicochemical Principles of Pharmacy*. Pharmaceutical Press, London.
- Forbes, R. T., York, P. and Davidson, J. R. (1995). Dissolution kinetics and solubilities of p-aminosalicylic acid and its salts. *International Journal of Pharmaceutics*, **126**, 199-208.
- Fukuyama, K., Kashino, S. and Haisa, M. (1973). Crystal structure of piperidinium Iparal-hydroxybenzoate. *Acta Crystallographica Section B-Structural Science*, **B29**, 2713-2717.
- Galek, P. T., Fabian, A. L. and Allen, F. H. (2009). Persistent hydrogen bonding in polymorphic crystal structures. *Acta Crystallographica Section B-Structural Science*, **65**, 68-85.
- Gavezzotti, A. (2005). Quantitative ranking of crystal packing modes by systematic calculations on potential energies and vibrational amplitudes of molecular dimers. *Journal of Chemical Theory and Computation*, **1**, 834-840.
- Gavezzotti, A. and G. Filippini (1994). Geometry of the intermolecular X-H...Y (X, Y=N, O) hydrogen bond and the calibration of empirical hydrogen bond potentials. *Journal of Physical Chemistry*, **98**, 4831-4837.
- Gelbrich, T. and Hursthouse, M. B. (2005). A versatile procedure for the identification, description and quantification of structural similarity in molecular crystals. *CrystEngComm*, **7**, 324-336.
- Gelbrich, T. and Hursthouse, M. B. (2006). Systematic investigation of the relationships between 25 crystal structures containing the carbamazepine molecule or a close analogue: a case study of the XPac method. *CrystEngComm*, **8**, 448-460.

- Gilli, G. (2006). Molecules and Molecular Crystals. In *Fundamentals of Crystallography*, ed. C. Giacovazzo, 585-687. New York: Oxford University Press.
- Gilli, G. and Gilli, P. (2000). Towards an unified hydrogen-bond theory. *Journal of Molecular Structure*, **552**, 1-15.
- Gilli, P., Bertolasi, V., Ferretti, V. and Gilli, G. (1994). Covalent nature of the strong homonuclear hydrogen bond- study of the O-H...O system by crystal structure correlation methods. *Journal of the American Chemical Society*, **116**, 909-915.
- Gillon, A. L., Feeder, N., Davey, R. J. and Storey, R. (2003). Hydration in molecular crystals- a Cambridge Structural Database analysis. *Crystal Growth and Design*, **3**, 663-673.
- Gorbitz, C. H. and Hersleth, H. P. (2000). On the inclusion of solvent molecules in the crystal structures of organic compounds. *Acta Crystallographica Section B-Structural Science*, **56**, 526-534.
- Gould, P. L. (1986). Salt selection for basic drugs. *International Journal of Pharmaceutics*, **33**, 201-217.
- Hall, S. R., Allen, F. H. and Brown, I. D. (1991). The crystallographic information file (CIF)- a new standard archive file for crystallography. *Acta Crystallographica Section A*, **47**, 655-685.
- Hammond R.B., Ma, C. and Roberts K.J. (2006). Grid-Based Molecular Modeling for Pharmaceutical Salt Screening: Case Example of 3,4,6,7,8,9-Hexahydro-2H-pyrimido (1,2a) Pyrimidium Acetate. *Journal of Pharmaceutical Sciences*, **95**, 2361-2372.
- Haynes, D. A., Chisholm, J. A., Jones, W. and Motherwell, W. D. S. (2004). Supramolecular synthon competition in organic sulfonates: A CSD survey. *CrystEngComm*, **6**.
- Haynes, D. A., Jones, W. and Motherwell, W. D. S. (2005). Hydrate formation in NH⁺-containing salts of pharmaceutically acceptable anions: A CSD survey. *CrystEngComm*, **7**, 342-345.
- Haynes, D. A., Jones, W. and Motherwell, W. D. S. (2006). Cocrystallisation of succinic and fumaric acids with lutidines: a systematic study. *CrystEngComm*, **8**, 830-840.
- Hooft, R. W. W. (1998) COLLECT: Data Collection Software. Nonius B.V., Netherlands.
- Huang, L. F. and Tong, W. Q. (2004). Impact of solid state properties on developability assessment of drug candidates. *Advanced Drug Delivery Reviews*, **56**, 321-334.
- Hursthouse, M. B., Montis, R. and Tizzard, G. J. (2010). Intriguing relationships and associations in the crystal structures of a family of substituted aspirin molecules. *CrystEngComm*, **12**, 953-959.
- Infantes, L., Chisholm, J. and Motherwell, W. D. S. (2003). Extended motifs from water and chemical functional groups in organic molecular crystals. *CrystEngComm*, **5**, 480-486.

- Infantes, L., Fabian, L. and Motherwell, W. D. S. (2007). Organic crystal hydrates: what are the important factors for formation. *CrystEngComm*, **9**, 65-71.
- Infantes, L. and Motherwell, W. D. S. (2004). The probable number of hydrogen-bonded contacts for chemical groups in organic crystal structures. *Chemical Communications*, 1166-1167.
- Inoue, M., Ito, A., Hirai, K., Koga, H., Suzue, S., Irikura, T. and Mitsuhashi, S. (1980) In-vitro anti-bacterial activity of AM-715 1-ethyl-6-fluoro-1,4-dihydro-4-oxo-7,1-piperazinyl-3-quinolonecarboxylic acid- a new nalidixic acid analog. *Antimicrobial Agents and Chemotherapy*, **17**, 103-108.
- Jarvinen, M., (1993). Application of symmetrized harmonics expansion to correction of the preferred orientation effect. *Journal of Applied Crystallography*, **26**, 525-531.
- Jeffrey, G. A. (1997) *An Introduction to Hydrogen Bonding*. Oxford University Press, Oxford.
- Jin, Z. M., Hu, M. L., Wang, K. W., Shen, L. and Li, M. C. (2003) Strong symmetrical intramolecular hydrogen bonds in diprotonated piperazinium bis(hydrogenmaleate). *Acta Crystallographica Section E-Structure Reports Online*, **59**, O1-O3.
- Jin, Z. M., Li, M. C., Wang, P., Li, L. and Hu, M. L. (2004) Dicyclohexylammonium 4-hydroxybenzenesulfonate monohydrate. *Acta Crystallographica Section E-Structure Reports Online*, **60**, O1633-O1635.
- Johnson, C. K. (1965) ORTEP. Oak Ridge National Laboratory, Tennessee, USA.
- Johnston, A., Johnston, B. F., Kennedy A. R. and Florence, A. J. (2008) Targeted crystallisation of novel carbamazepine solvates based on a retrospective Random Forest classification. *CrystEngComm*, **10**, 23-25.
- Jones, P. H., Rowley, E. K., Weiss, A. L., Bishop, D. L. and Chun, A. H. C. (1969) Insoluble erythromycin salts. *Journal of Pharmaceutical Sciences*, **58**, 337-and.
- Joris, L., Mitsky, J. and Taft, R. W. (1972) Effects of polar aprotic solvents on linear free-energy relationships in hydrogen-bonded complex formation. *Journal of the American Chemical Society*, **94**, 3438-3445.
- Khankari, R. K. and Grant, D. J. W. (1995) Pharmaceutical Hydrates. *Thermochimica Acta*, **248**, 61-79.
- Khankari, R. K., Law, D. and Grant, D. J. W. (1992) Determination of water content in pharmaceutical hydrates by differential scanning calorimetry. *International Journal of Pharmaceutics*, **82**, 117-127.
- Kiang, Y. H., Xu, W., Stephens, P. W., Ball, R. G. and Yasuda, N. (2009) Layered Structure and Swelling Behavior of a Multiple Hydrate-Forming Pharmaceutical Compound. *Crystal Growth and Design*, **9**, 1833-1843.
- King, A., Shannon, K. and Phillips, I. (1984) The in-vitro activity of ciprofloxacin compared with that of norfloxacin and nalidixic acid. *Journal of Antimicrobial Chemotherapy*, **13**, 325-331.

Kuduva, S. S., Craig, D. C., Nangia, A. and Desiraju, G. R. (1999) Cubanecarboxylic acids. Crystal engineering considerations and the role of C-H center dot center dot center dot O hydrogen bonds in determining O-H center dot center dot center dot O networks. *Journal of the American Chemical Society*, **121**, 1936-1944.

ACD Labs (1999). ACD/Labs pKa DB. 4.02, Advanced Chemistry Development Labs, Toronto.

Laurence, C., Brameld, K. A., Graton, J., Le Questel, J. Y. and Renault, E. (2009) The pK(BHX) Database: Toward a Better Understanding of Hydrogen-Bond Basicity for Medicinal Chemists. *Journal of Medicinal Chemistry*, **52**, 4073-4086.

Lehn, J. M. (1988) Supramolecular chemistry- scope and perspectives- molecules supermolecules and molecular devices. *Angewandte Chemie-International Edition in English*, **27**, 89-112.

Lewis, G. R., Steele, G., McBride, L., Florence, A. J., Kennedy, A. R., Shankland, N., David, W. I. F., Shankland, K. and Teat, S. J. (2005) Hydrophobic vs. hydrophilic: ionic competition in remacemide salt structures. *Crystal Growth and Design*, **5**, 427-438.

Lipinski, C. A., Lombardo, F., Dominy, B. W. and Feeney, P. J. (1997) Experimental and computational approaches to estimate solubility and permeability in drug discovery and development settings. *Advanced Drug Delivery Reviews*, **23**, 3-25.

Llinas, A., Burley, J. C., Prior, T. J., Glen, R. C. and Goodman, J. M. (2008) Concomitant hydrate polymorphism in the precipitation of sparfloxacin from aqueous solution. *Crystal Growth and Design*, **8**, 114-118.

MacDonald, J. C., Dorrestein, P. C. and Pilley, M. M. (2001) Design of supramolecular layers via self-assembly of imidazole and carboxylic acids. *Crystal Growth and Design*, **1**, 29-38.

Macrae, C. F., Bruno, I. J., Chisholm, J. A., Edgington, P. R., McCabe, P., Pidcock, E., Rodriguez-Spong, L., Taylor, R., van de Streek, J. and Wood, P. A. (2008) Mercury CSD 2.0 - new features for the visualization and investigation of crystal structures. *Journal of Applied Crystallography*, **41**, 466-470.

Macrae, C. F., Edgington, P. R., McCabe, P., Pidcock, E., Shields, G. P., Taylor, R., Towler, and van De Streek, J. (2006) Mercury: visualization and analysis of crystal structures. *Journal of Applied Crystallography*, **39**, 453-457.

Madsen, I. C. and Hill, R. J. (1994) Collection and analysis of powder diffraction data with near-constant counting statistics. *Journal of Applied Crystallography*, **27**, 385-392.

Malarski, Z., Rospenk, M., Sobczyk L. and Grech, E. (1982) Dielectric and spectroscopic studies of pentachlorophenol-amine complexes. *Journal of Physical Chemistry*, **86**, 401-406.

Marchewka, M. K. and Pietraszko, A. (2008). Crystal structure and vibrational spectra of piperazinium bis(4-hydroxybenzenesulphonate) molecular-ionic crystal. *Spectrochimica Acta Part A-Molecular and Biomolecular Spectroscopy*, **69**, 312-318.

- McCabe, J. F. (2010). Application of design of experiment (DOE) to polymorph screening and subsequent data analysis. *CrystEngComm*, **12**, 1110-1119.
- McKinnon, J. J., Spackman, M. A. and Mitchell, A. S. (2004). Novel tools for visualizing and exploring intermolecular interactions in molecular crystals. *Acta Crystallographica Section B-Structural Science*, **60**, 627-668.
- Meotner, M. and Sieck, L. W. (1986). The ionic hydrogen bond and ion solvation 5. OH...O- bonds- gas-phase solvation and clustering of alkoxide and carboxylate anions. *Journal of the American Chemical Society*, **108**, 7525-7529.
- Mimura, H., Kitamura, S., Kitagawa, T. and Kohda, S. (2002). Characterization of the non-stoichiometric and isomorphic hydration and solvation in FK041 clathrate. *Colloids and Surfaces B-Biointerfaces*, **26**, 397-406.
- Mitsky, J., Taft, R. W. and Joris, L. (1972). Hydrogen-bonded complex formation with 5-fluoroindole- applications of pK_{HB} scale. *Journal of the American Chemical Society*, **94**, 3442-3449.
- Miyamoto, T., Matsumoto, J., Chiba, K., Egawa, H., Shibamori, K., Minamida, A., Nishimura, Y., Okada, H., Kataoka, M., Fujita, M., Hirose, T. and Nakano, J. (1990) Pyridonecarboxylic acids as antibacterial agents. 14. synthesis and structure-activity relationships of 5-substituted 6,8-difluoroquinolones, including sparfloxacin, a new quinolone antibacterial agent with improved potency. *Journal of Medicinal Chemistry*, **33**, 1645-1656.
- Miyazaki S. and Nadai, T. (1981). Precaution on use of hydrochloride salts in pharmaceutical formulations *Journal of Pharmaceutical Sciences*, **70**, 594-596.
- Mohamed, S., Tocher, D. A., Vickers, M., Karamertzanis, P. G. and Price S. L. (2009a) Salt or Cocrystal? A New Series of Crystal Structures Formed from Simple Pyridines and Carboxylic Acids. *Crystal Growth and Design*, **9**, 2881-2889.
- Morissette, S. L., Almarsson, O., Peterson, M. L., Remenar, J. F., Read, M. J., Lemmo, A. V., Ellis, S., Cima, M. J. and Gardner, C. R. (2004). High-throughput crystallization: Polymorphs, salts, co-crystals and solvates of pharmaceutical solids. *Advanced Drug Delivery Reviews*, **56**, 275-300.
- Morris, K. (1999). Structural aspects of hydrates and solvates. In *Polymorphism in Pharmaceutical Solids*, ed. H. G. Brittain, 125-226. Marcel Dekker, New York:.
- Morris, K. R., Fakes, M. G., Thakur, A. B., Newman, A. W., Singh, A. K., Venit, J. J., Spagnuolo, C. J. and Serajuddin A. T. M. (1994). An integrated approach to the selection of the optimal salt form for a new drug candidate. *International Journal of Pharmaceutics*, **105**, 209-217.
- PreQuest. A Program for Crystal Structure Validation. Cambridge Crystallographic Data Centre, Cambridge.
- Nangia, A. (2008). Conformational polymorphism in organic crystals. *Accounts of Chemical Research*, **41**, 595-604.
- Noyes, A. A. and Whitney, W. R. (1897). The rate of solution of solid substances in their own solutions. *Journal of the American Chemical Society*, **19**, 930-934.

- Orpen, A. G. (2002). Applications of the Cambridge Structural Database to molecular inorganic chemistry. *Acta Crystallographica Section B-Structural Science*, **58**, 398-406.
- Otwinowski, Z. and Minor, W. (1997). Processing of X-ray diffraction data collected in oscillation mode. *Macromolecular Crystallography, Pt A*, **276**, 307-326.
- Parkin, A., Barr, G., Dong, W., Gilmore, C. J., Jayatilaka, D., McKinnon, J. J., Spackman, M. A. and Wilson, C. C. (2007). Comparing entire crystal structures: structural genetic fingerprinting. *CrystEngComm*, **9**, 648-652.
- Parvez, M., Arayne, M. S., Sultana, N. and Siddiqi, A. Z. (2000). Pefloxacinium methanesulfonate 0.10-hydrate. *Acta Crystallographica Section C-Crystal Structure Communications*, **56**, 910-912.
- Paulekuhn, G. S., Dressman, J. B. and Saal, C. (2007). Trends in active pharmaceutical ingredient salt selection based on analysis of the Orange Book Database. *Journal of Medicinal Chemistry*, **50**, 6665-6672.
- Pawley, G. S. (1981). Unit-cell refinement from powder diffraction scans. *Journal of Applied Crystallography*, **14**, 357-361.
- Perlstein, J. (1994). Molecular self-assemblies 4. using Kitaigorodskii's Aufbau Principle for quantitatively predicting the packing geometry of semiflexible organic molecules in translation monolayer aggregates. *Journal of the American Chemical Society*, **116**, 11420-11432.
- Perlstein, J., Steppe, K., Vaday, S. and Ndip, E. M. N. (1996). Molecular self-assemblies 5. Analysis of the vector properties of hydrogen bonding in crystal engineering. *Journal of the American Chemical Society*, **118**, 8433-8443.
- Pidcock, E. and Motherwell, W. D. S. (2005). Effect of intermolecular hydrogen-bonded motifs on packing pattern populations. *Crystal Growth and Design*, **5**, 2322-2330.
- Prasanna, M. D. and Row, T. N. G. (2001). Hydrogen bonded networks in hydrophilic channels: crystal structure of hydrated Ciprofloxacin Lactate and comparison with structurally similar compounds. *Journal of Molecular Structure*, **559**, 255-261.
- Price, C. P., Grzesiak, A. L., Lang, M. and Matzger, A. J. (2002). Polymorphism of nabumetone. *Crystal Growth and Design*, **2**, 501-503.
- Price, S. L., Stone, A. J., Lucas, J., Rowland R. S. and Thornley, A. E. (1994). The nature of Cl-center-dot-center-dot-center-dot-Cl⁻ intermolecular interactions. *Journal of the American Chemical Society*, **116**, 4910-4918.
- Pudipeddi, M., Serajuddin, A. T. M., Grant, D. G. W. and Stahl, P. H. (2002). Solubility and Dissolution of Weak Acids, Bases and Salts. In *Handbook of Pharmaceutical Salts: Properties, Selection and Use*, eds. P. H. Stahl and C. G. Wermuth, 19. Zurich: Verlag Helvetica Chimica Acta/ Wiley-VCH.
- Remenar, J. F., MacPhee, J. M., Larson, B. K., Tyagi, V. A., Ho, J. H., McIlroy, D. A., Hickey, M. B., Shaw, P. B. and Almarsson, O. (2003). Salt selection and simultaneous polymorphism assessment via high-throughput crystallization: The case of sertraline. *Organic Process Research and Development*, **7**, 990-996.

- Rietveld, H. M. (1969). A Profile Refinement Method for Nuclear and Magnetic Structures. *Journal of Applied Crystallography*, **2**, 65-71.
- Ruiz, P., Ortiz, R., Perello, L., Alzuet, G., M. Gonzalez-Alvarez, M. Liu-Gonzalez and F. Sanz-Ruiz (2007). Synthesis, structure, and nuclease properties of several binary and ternary complexes of copper(II) with norfloxacin and 1,10 phenantroline. *Journal of Inorganic Biochemistry*, **101**, 831-840.
- Sarma, B., Nath, N. K., Bhogala, B. R. and Nangia, A. (2009). Synthon Competition and Cooperation in Molecular Salts of Hydroxybenzoic Acids and Aminopyridines. *Crystal Growth and Design*, **9**, 1546-1557.
- Serajuddin, A. T. M. (2007). Salt formation to improve drug solubility. *Advanced Drug Delivery Reviews*, **59**, 603-616.
- Shankland, K., David, W. I. F. and Sivia, D. S. (1997). Routine ab initio structure determination of chlorothiazide by X-ray powder diffraction using optimised data collection and analysis strategies. *Journal of Materials Chemistry*, **7**, 569-572.
- Shefter, E. and Higuchi, T. (1963). Dissolution Behaviour of Crystalline Solvated and Nonsolvated Forms of Some Pharmaceuticals. *Journal of Pharmaceutical Sciences*, **52**, 781-791.
- Sheldrick, G (1997). SHELXS [includes SHELX97 and SHELXS97], Programs for Crystal Structure Analysis (Release 97-2). Institut für Anorganische Chemie der Universität.
- Shen, L. L., Mitscher, L. A., Sharma, P. N., Odonnell, T. J., Chu, D. W. T., Cooper, C. S., Rosen, T. and Pernet, A. G. (1989). Mechanism of inhibition of DNA gyrase by quinolone antibacterials- a cooperative drug-DNA binding model. *Biochemistry*, **28**, 3886-3894.
- Smith, M. B. and March, J. (2001). *March's Advanced Organic Chemistry: Reactions, Mechanisms and Structure*. New York: John Wiley and Sons, Inc.
- Spackman, M. A. and Byrom, P. G. (1997). A novel definition of a molecule in a crystal. *Chemical Physics Letters*, **267**, 215-220.
- Spackman, M. A. and McKinnon, J. J. (2002). Fingerprinting intermolecular interactions in molecular crystals. *CrystEngComm*, 378-392.
- Spek, L. (2010) PLATON, A Multipurpose Crystallographic Tool. Utrecht University.
- Stahl, P. H. and Vermuth, C. G. E. (Eds) (2002) *Handbook of Pharmaceutical Salts: Properties, Selection and Use*. Zurich: Wiley-VCH.
- Stahly, G. P. (2007) Diversity in single- and multiple-component crystals. The search for and prevalence of polymorphs and cocrystals. *Crystal Growth and Design*, **7**, 1007-1026.
- Stanton, M. K. and Bak, A. (2008). Physicochemical properties of pharmaceutical co-crystals: a case study of ten AMG 517 co-crystals. *Crystal Growth and Design*, **8**, 3856-3862.

- Steiner, T., Majerz, I. and Wilson, C. C. (2001). First O-H-N hydrogen bond with a centered proton obtained by thermally induced proton migration. *Angewandte Chemie-International Edition*, **40**, 2651-2654.
- Stephenson, G. A., Groleau, E. G., Kleemann, R. L., Xu, W. and Rigsbee, D. R. (1998). Formation of isomorphic desolvates: Creating a molecular vacuum. *Journal of Pharmaceutical Sciences*, **87**, 536-542.
- Sun, H. X., Li, Y. and Pan, Y. J. (2004). 2-Hydroxyethanaminium enrofloxacin. *Acta Crystallographica Section E-Structure Reports Online*, **60**, O1694-O1696.
- Taylor, R. (2002). Life-science applications of the Cambridge Structural Database. *Acta Crystallographica Section D-Biological Crystallography*, **58**, 879-888.
- Toffoli, P., Rodier, N., Ceolin, R. and Blain, Y. (1987). Perfloracin methanesulfonate (Peflacin DCI). *Acta Crystallographica Section C-Crystal Structure Communications*, **43**, 1745-1748.
- Trask, A. V., Motherwell, W. D. S. and Jones, W. (2005). Pharmaceutical cocrystallization: Engineering a remedy for caffeine hydration. *Crystal Growth and Design*, **5**, 1013-1021.
- Vanier, M. and Brisse, F. (1983). Structural Studies Of Compounds With Aliphatic Chains .8. Structure Of Piperazinium Succinate, $C_4H_4O_4^{2-} \cdot C_4H_{12}N_2^{2+}$. *Acta Crystallographica Section C-Crystal Structure Communications*, **39**, 912-914.
- Verma, R. K., Krishna, D. M. and Garg, S. (2002). Formulation aspects in the development of osmotically controlled oral drug delivery systems. *Journal of Controlled Release*, **79**, 7-27.
- Vippagunta, S. R., Brittain, H. G. and Grant, D. J. W. (2001). Crystalline solids. *Advanced Drug Delivery Reviews*, **48**, 3-26.
- Walsh, R. D. B., Bradner, M. W., Fleischman, S., Morales, L. A., Moulton, B., Rodriguez-Hornedo, N. and Zaworotko, M. J. (2003). Crystal engineering of the composition of pharmaceutical phases. *Chemical Communications*, 186-187.
- Wang, K. W., Jin, Z. M. and Pan, Y. J. (2005). Crystal structure of the piperazine-1,4-dium (DL-)hydrogen malate (1:2). *Journal Of Chemical Crystallography*, **35**, 413-417.
- Weng, Z. F., Motherwell, W. D. S., Allen, F. H. and Cole, J. M. (2008). Conformational variability of molecules in different crystal environments: a database study. *Acta Crystallographica Section B-Structural Science*, **64**, 348-362.
- Whitesides, G. M., Simanek, E. E., Mathias, J. P., Seto, C. T., Chin, D. N., Mammen, M. and Gordon, D. M. (1995). Noncovalent synthesis - using physical-organic chemistry to make aggregates. *Accounts of Chemical Research*, **28**, 37-44.
- Wiechert, D. and Mootz, D. (1999). Molecular beside ionic: Crystal structures of a 1/1 and a 1/4 adduct of pyridine and formic acid. *Angewandte Chemie-International Edition*, **38**, 1974-1976.
- Wilson, C. C. (2001). Migration of the proton in the strong O-H center dot center dot center dot O hydrogen bond in urea-phosphoric acid (1/1). *Acta Crystallographica Section B-Structural Science*, **57**, 435-439.

Wong, L. W. and Pilpel, N. (1990). The effect of particle shape on the mechanical properties of powders. *International Journal of Pharmaceutics*, **59**, 145-154.